Investigation into the pathogenic cyclin F^{E624K} sporadic mutation in amyotrophic lateral sclerosis and frontotemporal dementia

Maria de los Angeles Morales Villalva

B.Sc (Human Biology) (Macquarie University)

Centre for Motor Neuron Disease Research
Department of Biomedical Sciences
Faculty of Medicine and Health Sciences
Macquarie University

A thesis written and submitted in fulfilment of the requirements for the degree of Master of Research

May 2019

Principle Supervisor: Dr. Albert Lee

Table of Contents

List of Figures

List of Tables

Declaration

I declare that the content of this thesis "Investigation into the pathogenic cyclin F^{E624K} sporadic mutation in amyotrophic lateral sclerosis and frontotemporal dementia" is my own work, any work that is not my own has been appropriately referenced where applicable.

Maria de los Angeles Morales Villalva

Acknowledgements

Firstly, I would like to thank Prof. Roger Chung for welcoming me into the Chung group and providing me the opportunity to work on this research project. Secondly, I want to express my most sincere gratitude to my supervisor Dr. Albert Lee. With your expertise in the proteomic field and mentoring I have learnt many new skills, including life lessons, that I will carry throughout my science career. I am profoundly grateful for all your support and patience throughout this MRes journey, thank you.

Next, I would like to thank the members of the Chung group, especially Flora Cheng, Stephanie Rayner, Jennilee Davidson, and Alana de Luca. Your guidance and support in the lab helped me tremendously, and I would not have gone far without it.

Finally, I would like to thank my friends and family. To my friends and boyfriend for their incredible support and encouragement, my sister Juliette who made me smile and laugh in times when I needed it the most, and to my parents for always believing in me and provided me the strength during the most challenging times.

Publications

Publication I

Hedl TJ, San Gil R, Cheng F, Rayner SL, Davidson J, De Luca A, **Villalva MD**, Ecroyd H, Walker AK, Lee A. Proteomics approaches for understanding the pathogenesis of ALS/FTD. Frontiers in Neuroscience. *Manuscript under review as of 11th June 2019.*

The introductory section that included pathology and disease mechanisms of ALS and FTD, and proteostasis and protein aggregation in ALS and FTD was carried out by both Alana de Luca and the author of this thesis.

Abbreviations

ACN	Acetonitrile
ALS	Amyotrophic lateral sclerosis
ATCC	American type culture collection
ATP	Adenosine triphosphate
BCA	Bicinchoninic acid
Bis-Tris	1,3-bis(tris(hydroxymethyl)methylamino)propane
CDK	Cyclin-dependent kinase
CKII	Casein kinase II
CO_2	Carbon dioxide
Da	Dalton
DMEM	Dulbecco's modified eagle medium
DNA	Deoxyribonucleic acid
DTT	Dithiothreitol
E. coli	*Escherichia coli*
E1	Ubiquitin-activating enzyme
E2	Ubiquitin conjugating enzyme
E3	Ubiquitin ligase complex
ER	Endoplasmic reticulum
ERAD	Endoplasmic reticulum associated degradation
EV	Empty vector
FA	Formic acid
fALS	Familial amyotrophic lateral sclerosis
FBS	Foetal bovine serum
FT	Flow through
FTD	Frontotemporal dementia
GO	Gene ontology
GTP	Guanosine-5'-triphosphate
HEK293	Human Embryonic Kidney 293 cells
IAA	Iodoacetamide
IP	Immunoprecipitation
IPA	Ingenuity pathway analysis
K48	Lysine-48
K63	Lysine-633
kDa	Kilodalton
LB	Luria broth
LC	Liquid chromatography
LDS	Lithium dodecyl sulfate
MND	Motor neuron disease
MOPS	3-(N-morpholino)propanesulfonic acid
MS	Mass spectrometry
MW	Molecular weight
NLS	Nuclear localisation signal
NP40	Nonidet P-40
PBS	Phosphate buffered saline
PBS-T	Phosphate buffered saline + tween 20
PCR	Polymerase chain reaction
PD	Proteome discoverer
PPI	Protein-protein interaction
PTEN	Phosphate tensin homolog

RCF	Relative centrifugal force
RPM	Revolutions per minute
sALS	Sporadic amyotrophic lateral sclerosis
SCF	Skp1-Cul1-F-Box
SDS-PAGE	Sodium dodecyl sulfate polyacrylamide gel electrophoresis
siRNA	Small interference Ribonucleic acid
SM	Starting material
TBS	Tris-buffered saline
TBS-T	Tris-buffered saline + tween 20
TDP-43	Transactive response DNA binding protein 43
UPR	Unfolded protein response
UPS	Ubiquitin proteasome system
V	Volts
WT	Wild type

Abstract

Motor neuron disease (MND) is an umbrella term for many neurodegenerative disorders that are characterised with a range of symptoms and signs, from dysfunction to an individual's locomotion to abnormalities in cognitive functions. Two fatal neurodegenerative diseases that share molecular and pathogenic characteristics are amyotrophic lateral sclerosis (ALS) and frontotemporal dementia (FTD), which have been shown to present dysfunction in mechanisms that regulate protein homeostasis (proteostasis). Dysfunction of proteostasis may arise due to the presence of aggregated protein inclusions, potentially an underlying cause of ALS/FTD pathology. Recently, the *CCNF* gene has been identified to present various ALS/FTD mutants, that have been discovered in both familial and sporadic cases. The *CCNF* gene encodes for cyclin F, a protein involved in cell-cycle processes and ubiquitylation, specifically a module of the Skp1-Cul1-F-Box (SCF) E3 ubiquitin ligase complex, which is involved in quality control mechanisms that regulate proteostasis levels.

Recent studies have focused on the familial cyclin F^{S621G} mutation, demonstrating hyper-ubiquitylation due to autophagy pathway dysfunction and impairment of regulatory phosphorylation. However, further research is needed to identify whether other *CCNF* mutants, such as the sporadic cyclin F^{E624K} mutant presents with similar or different familial ALS/FTD pathogenesis. For this thesis, the aim is to generate and characterise the cyclin F^{E624K} mutant in HEK293 cells and investigate whether it causes any perturbations to cellular pathways as well as perturbed protein-protein interactions that may be shared or unique to the familial cyclin F^{S621G} mutant and cyclin F wild-type. Expression of sporadic cyclin F^{E624K} mutant revealed a decrease in phosphorylation and no change in K48-ubiquitylation of proteins. Global proteomic analysis revealed inhibition of pathways involved in actin cytoskeleton regulation. Proteomic analysis of immunoprecipitated cyclin F^{E624K} identified proteins that clustered within a ubiquitin- and proteasome-associated protein network and proteins that clustered within the oxidative stress response. Perturbed cyclin F^{E624K} protein interactors involved in these networks suggests dysregulation may lead to cellular proteostasis impairments and ultimately lead to neurodegeneration. Comparative analysis with the familial cyclin F^{S621G} mutant elucidates differences in cellular mechanisms between sporadic and familial mutations that govern ALS/FTD pathology.

1. Introduction

Motor neuron disease (MND) is an umbrella term for many neurodegenerative disorders that are characterised with a range of symptoms and signs, from dysfunction to an individual's locomotion to abnormalities in cognitive functions. Two fatal neurodegenerative diseases that share molecular and pathogenic characteristics are amyotrophic lateral sclerosis (ALS) and frontotemporal dementia (FTD) (1, 2).

1.1. Amyotrophic Lateral Sclerosis (ALS) background and epidemiology

ALS (or Lou Gehrig's disease in the US, named after the renowned 1930s American baseball player who was diagnosed with the disease) was first described between 1865 to 1869 by the "Father of Neurology", Professor Jean-Martin Charcot (3-5). Professor Charcot made significant ALS history by using thorough clinical observation and made histological recordings to distinguish the pathophysiology of ALS from other neurological diseases (5). He highlighted the pathological link between limb spasticity and lateral columns lesions in the spinal cord (4). It was not until 1874 that Professor Charcot termed the disease "Amyotrophic lateral sclerosis", "amyotrophic" referring to muscle weakness and atrophy, and "lateral sclerosis" referring to tissue stiffening in the lateral columns (5, 6). Although, over the years the understanding of ALS pathology has advanced, the original descriptions of ALS pathophysiology still remains unchanged (4).

ALS presents as a rapidly aggressive neurodegenerative disease that is characterised with upper and lower motor neuron death in the brain and spinal cord (8). It affects more than 2,000 individuals within the Australian population, with ~60% being male and 40% being female (7). The average expected survival after onset is between 3-5 years but there are rare cases where patients have survived longer (8). The prevalence of familial ALS (fALS) is ~10%, whilst ~90% of ALS cases occur sporadically (sALS) or have an unknown cause (3). The phenotypic symptoms of familial and sporadic ALS in patients is clinically indistinguishable. Genetic mutations are highly useful to recapitulate features of ALS, that has enabled the development of models to allow researchers to distinguish the causative mechanisms that underlie familial and sporadic ALS pathogenesis.

1.2. Frontotemporal Dementia (FTD) history and epidemiology

FTD is the second leading cause of young onset dementia, behind Alzheimer's disease (9). It was first identified by Arnold Pick in 1892, in which clinical features were described as behavioural alterations, progressive aphasia, and progressive apraxia, together with lobar atrophy (10). The histopathology of FTD was identified in 1911 by Alois Alzheimer, where he reported aggregates of argyrophilic neuronal inclusions in the frontal and temporal lobes of the brain, naming them "Pick's bodies" (11).

FTD is characterised by neurodegeneration in the frontal and temporal lobes of the brain presenting alterations in patient's behaviour and personality, as well as language difficulties (12). FTD can be distinguished into three distinct subtypes: behavioural and language variant; semantic dementia; and progressive non-fluent aphasia. Patients can present with either one subtype or an overlap of subtypes as the disease progresses (13). Survival after onset does vary as it reflects whether the patient presents with any other underlying pathologies (12). In addition, ~15% of ALS patients are also diagnosed with FTD, which can shorten the survival rate to a three-year average (14).

1.3. Overlap of genetic mutations associated with ALS and FTD

In ALS research, the primary gene that has been focused on extensively is the antioxidant enzyme superoxide dismutase 1 gene (*SOD1*), where mutations within this gene account for more than 20% of fALS (15). *SOD1* mutants have reported structural instability within neuronal cells, as mutations discovered within this gene causes the enzyme to mis-fold and aggregate within neurons and glial cells in the central nervous system (16). Some of the proposed hypotheses for the underlying cause of ALS in mutant *SOD1* cases include oxidative stress, axonopathy, and mitochondrial abnormalities (17-19). However, what stands out in mutant *SOD1* pathophysiology of ALS-causative cases is the presence of protein aggregates, promoting an imbalance in protein homeostasis (proteostasis). This underlying causative mechanism proposes a toxic gain-of-function as transgenic mouse models with mutant *SOD1* displayed motor dysfunction with the presence of cytoplasmic aggregated protein inclusions (20).

Other mutated genes associated with ALS and/or FTD pathology, such as *FUS*, *TARDBP* and *CCNF*, also present with cytoplasmic protein aggregates, elucidating such aggregations as a potential pathological hallmark for ALS/FTD (14, 21, 22). Interestingly, in almost all cases of ALS and in ~40% of FTD cases, transactive response DNA binding protein 43 (TDP-43),

encoded by the *TARDBP*, is present in protein aggregates - a breakthrough discovery that links the disease mechanisms for both neurodegenerative diseases (1, 23).

TDP-43 is a 414 amino acid protein that acts as a highly conserved predominant nuclear factor involved in RNA metabolism (24). Under normal conditions, TDP-43 is localised in the nucleus, however in the majority of ALS and FTD cases TDP-43 is mis-localised to the cytoplasm of affected neurons (2). Notably, only 1-2% of fALS and sALS are caused by variants in *TARDBP* (25). Both normal and abnormal TDP-43 aggregated protein inclusions were identified in motor neurons. Abnormal TDP-43 consisted of characteristics such as phosphorylation, ubiquitylation, or truncations (2). The presence of cytoplasmic aggregated protein inclusions suggests proteostasis impairment, a common theme that underlies the causative mechanism behind ALS/FTD pathology. Although it is unclear the linkage between the development of proteostasis dysfunction and ALS/FTD pathogenesis, recent studies in models recapitulating genetic mutations have provided some insight into the mechanisms.

1.4. Proteostasis

Proteins are part of the highly complex network known as the proteome, essential for regulating various major cellular processes to maintain optimal functioning and cell viability (26). The proteome maintains optimal cellular health by relying on the highly controlled systems that synthesise and degrade proteins. This is particularly important for neuronal cells (post-mitotic cells) where the cells cannot undergo mitosis to generate new healthy cells to counteract irreversible neurotoxic affects such as the formation of aggregates protein inclusions (27). Therefore to maintain optimal neuronal cell survival, proteostasis is essential (28).

Proteostasis is defined as the balance of proteins levels that have efficiently been synthesised and folded correctly for their designated roles, as well as the regulatory degradation of impaired and unwanted proteins (29). Proteins perform various functions to regulate a wide range of cellular processing systems. Thus, they continuously turn over at different rates which naturally leads to misfolding and generation of toxic insoluble aggregates (30, 31). In normal cellular conditions, proteins are folded correctly in their native conformation, this usually consists of an external hydrophilic surface and an internal hydrophobic core. However, during protein translation ~30% of proteins are misfolded, which can result in altered conformational changes in proteins (e.g. their hydrophobic cores are exposed) (28, 32). This can generate aberrant protein-protein interactions (PPIs) between proteins and create the toxic insoluble aggregates that can compromise cell viability and survival. The rise in toxic cytoplasmic aggregated protein inclusions in neurons is not only identified in ALS/FTD but is also prominent across

other various neurodegenerative diseases such as Alzheimer's disease, Huntington's disease, and Parkinson's disease (33-35). To prevent a build-up of such aggregates, protein quality control systems are enforced to regulate the production and degradation of proteins for cells to function efficiently (31).

1.4.1. Protein quality control systems

Protein quality control systems are particularly important for neuronal cells as they limit the irreversible neurotoxic damage that misfolded protein aggregates can cause (27). This system involves three main pathways that consists of molecular chaperones and protein degradation clearance mechanisms to maintain proteostasis (26, 30). These pathways are the endoplasmic reticulum associated degradation (ERAD) pathway, the autophagy-lysosomal pathway, and the ubiquitin proteasome system (UPS).

1.4.1.1. Endoplasmic Reticulum Associated Degradation (ERAD) pathway

The endoplasmic reticulum (ER) organelle is involved in three different major processes: protein folding and secretion; calcium storage and release; and, lipid biogenesis (36). It is where one third of the human proteome is synthesised for compartmentalisation or secretion (37). Together with chaperone systems, proteins are folded into their conformational state, followed by post-translational modifications, to be released for their specialised biological function (38). Under pathophysiological conditions, where an accumulation of misfolded proteins may arise, an ER stress signal is activated via the stress sensors *ATF6*, *PERK*, *IRE1* (39). The activation of any of the ER stress sensors induces a complex signalling network that counteracts the excessive load capacity of misfolded proteins in the ER, referred to as the unfolded protein response (UPR) (38). This response mediates the ERAD pathway, in which misfolded proteins are re-directed to the cytoplasm for protein degradation via the UPS (40). However, if proteostasis is not restored by the ERAD pathway, the ER stress signalling complex can then trigger apoptosis, thus consequently leading to neuronal cell death, as seen in various neurodegenerative diseases (38).

1.4.1.2. The Ubiquitin Proteasome System (UPS)

The UPS begins with the ubiquitin cascade, a three-step system of enzymes that conjugates ubiquitin to specific protein substrates prior to protein degradation. The ubiquitin cascade begins with the activation of the ubiquitin molecule. Ubiquitin is activated by binding to the

ubiquitin-activating enzyme (E1) at the C-terminal glycine residue via the transfer of ATP. The activated ubiquitin molecule is then transferred to the ubiquitin-conjugating enzyme (E2) on a cysteine residue, generating a thioester intermediate. The E2 acts as a carrier for the activated ubiquitin molecule as it is then recruited by the ubiquitin ligase complex (E3) (41). For example, the Skp1-Cul1-Fbox (SCF) ubiquitin ligase complex is one of many E3s that catalyses ubiquitin molecules to specific substrates (42). Within this SCF E3 complex, mono- or poly- ubiquitin chains, depending on substrate specificity, is transferred from E2 to the target substrate, which is recruited to the E3 via a substrate adaptor (43). Substrate specificity and the binding of mono- or poly- ubiquitin chains arises from the covalent attachment of ubiquitin to a specific lysine residue (K) on the protein substrate. Different lysine residues attach to specific ubiquitin chain types in which results in distinct functional outcomes. For example, substrates that are K48 ubiquitylated are more often directed to the proteasome degradation pathway, whereas substrates that are K63 ubiquitylated are directed to the autophagy-lysosomal pathway (42, 44). However, it is important to note that the cell's compensatory system can allow either K48/K63-specific ubiquitylated substrates to follow either degradation pathway (45-47).

In the UPS, proteins are degraded by the 26S proteasome, a sophisticated complex that consists of multiple subunits that make up its barrel-like structure (48). Primarily this proteolytic machinery is arranged with a 20S proteasome consisting of a catalytic core particle and two terminal 19S regulatory particles, driven by adenosine triphosphate (ATP) energy (49). Once protein substrates are ubiquitylated, they are transferred to the 26S proteasome. The regulatory particle recognises the ubiquitylated proteins and processes them to be de-ubiquitylated, so that the ubiquitin molecules are recycled. Proteins are then unfolded and translocated to the catalytic core particle of the proteasome (Figure 1-1). The arrangement of the core particle includes two outer *alpha*-rings and two inner *beta*-rings. Proteolytic activity occurs within the catalytic core where the proteins are degraded (30).

Studies have demonstrated that the 26S proteasome is a crucial component associated with neurodegeneration. A Cre/loxP ATPase knock-out mouse model revealed neuronal protein inclusions that caused extensive neurodegeneration in the mice (50). Similarly, a conditional knock-out mouse model for the proteasome subunit (Rpt3) specific to motor neurons displayed phenotypic locomotor dysfunction and progressive motor neuron loss. In addition, it was accompanied with TDP-43 rich protein aggregates mis-localised in the cytoplasm of motor neurons (51). As demonstrated with mouse models, dysfunction to the UPS can lead to the formation of cytoplasmic protein aggregates that seed biological processes leading to neurodegeneration.

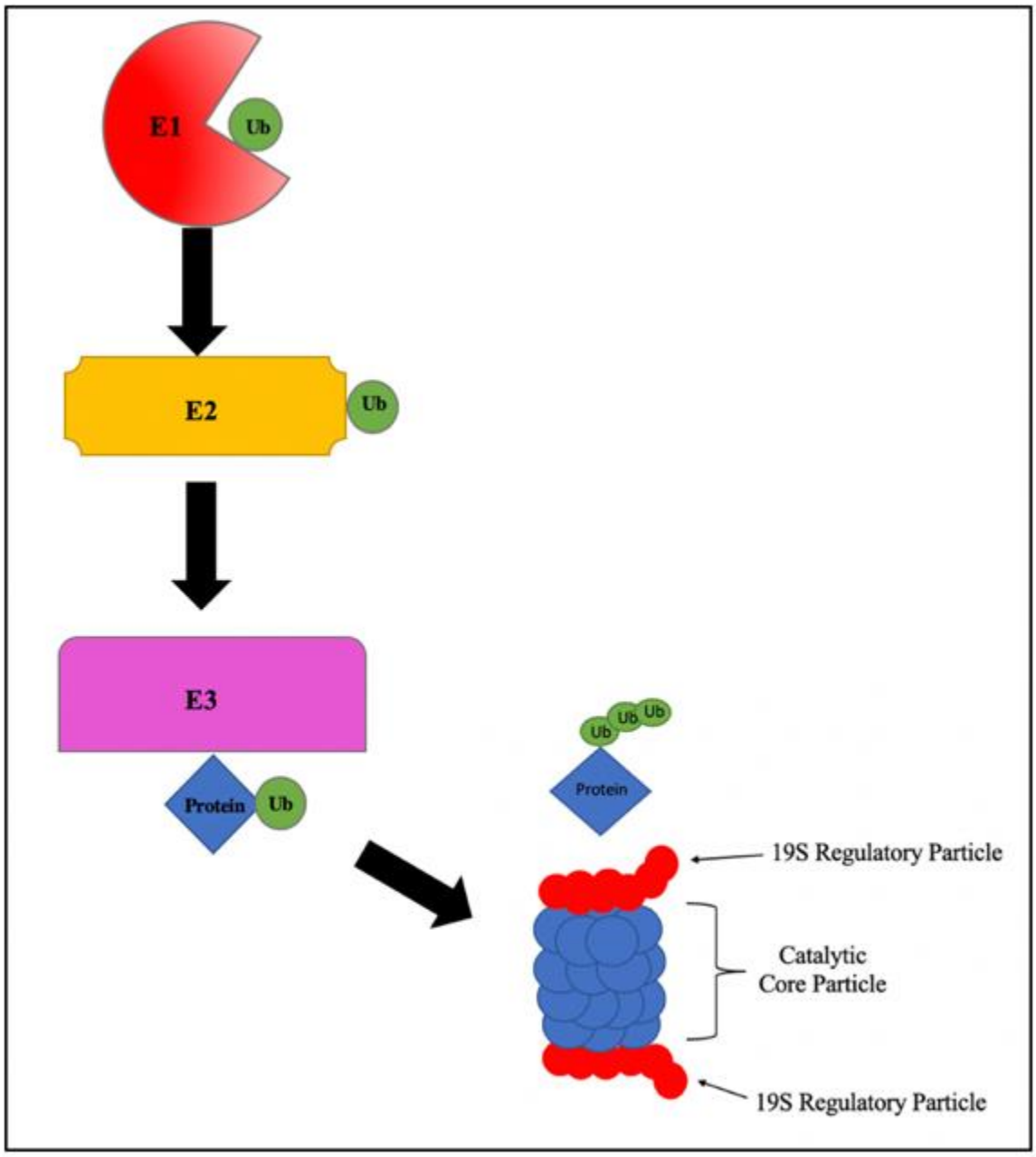

Figure 1-1. Schematic diagram of the UPS.
The UPS is initiated with the ubiquitin cascade and ubiquitylated proteins are transferred to the 26S proteasome. Proteins are unfolded and ubiquitin molecules are recycled followed by the degradation of the protein substrates.

1.4.1.3. Autophagy-lysosomal pathway

The autophagy-lysosomal pathway is the second major degradative process where selective proteins and other dysfunctional components are removed from the cell (52). The three autophagy pathways include macro-autophagy, micro-autophagy, and chaperone-mediated autophagy. Although each type of autophagy has mechanistic differences, they all play the same role delivering unwanted and dysfunctional cellular contents to the membrane-bound organelles

known as lysosomes via the double-membrane phagophore. The phagophore fuses with the lysosome, which consists of hydrolytic enzymes for proteolytic degradation (53).

Recent studies have suggested that defective autophagy is linked to the pathogenesis of cytoplasmic protein aggregates in the presence of ALS/FTD-causative gene mutations, such as *p62/SQSTM1* and *CCNF (54, 55)*. The *p62/SQSTM1* gene encodes a 440 amino acid protein that acts as a crucial component for the autophagy pathway. Its role is to target and bind to ubiquitylated protein substrates and deliver it to autophagic machinery (56). In a zebrafish *p62/SQSTM1* knock-down model, zebrafish displayed phenotypic dysfunction in motor locomotion, indicating defective autophagic machinery results in neurodegeneration (55). Moreover, a recent study showed that a mutation in the *CCNF* gene, which encodes cyclin F, a key component to the SCF E3 ligase complex in the ubiquitin cascade, displayed abnormal hyper-ubiquitylation of protein aggregates associated with impairment of the autophagy pathway. This suggests mutations in the *CCNF* gene may cause proteostasis dysfunction that contributes to ALS/FTD pathology (54).

1.5. Cyclin F

The *CCNF* gene consists of 17 exons and encodes cyclin F, a 786 amino acid protein first reported in 1994 by Bai *et al* (57). Cyclin F consists of a cyclin box, PEST region, a F-box, and two nuclear localisation signals (NLS) (Figure 1-2). The structural components of cyclin F designates its two primary functional properties: cell-cycle regulation and mediating ubiquitin-degradation systems.

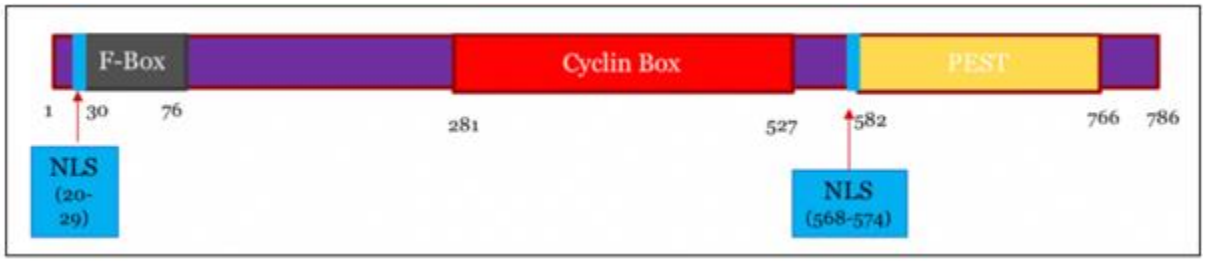

Figure 1-2. Schematic diagram of the Cyclin F protein.
The *CCNF* gene consisting of a 786 amino acid protein, that consists of two nuclear localisation signals (NLS), a F-box motif, cyclin box, and a PEST region.

1.5.1. Cyclin box

Cyclins are important regulators for the cell division cycle, as they act as regulatory subunits for cyclin-dependent kinases (CDKs). Essentially, the cell cycle is controlled by the sequential

activation and inhibition of CDKs at different checkpoints during the cell cycle (58). As cyclin F consists of the conserved cyclin box region, it is part of the cyclin family that regulates cell-cycle events, such as genome stability and maintenance of DNA replication and repair (57, 59). Like most other cyclins, cyclin F produces oscillating characteristics during the cell-cycle, where it is expressed during the S phase and peaks at the G2 phase (57). However, cyclin F differs to other cyclins as it is CDK-independent, meaning it does not rely on kinases for protein phosphorylation in the regulation of cell-cycle transitions (60). Instead it relies on independent-cell cycle kinases to regulate ubiquitylation when acting as the substrate adaptor for the E3 $SCF^{cyclin\ F}$ ligase complex (61).

1.5.2. The Proline-Glutamic Acid-Serine-Threonine (PEST) region

The PEST region in cyclin F (582-766) is a structural element that is located at the C terminus of the protein (Figure 1-3) (62). It was first described by Rogers *et al* in 1986 as a proteolytic signal peptide for rapid protein degradation as well as a region that provides stability, proposing the "PEST hypothesis" (63). However, the mechanism behind this hypothesis is still unclear as not all PEST regions in proteins are required for rapid proteolytic degradation, as seen with calpain-mediated proteolysis of the proto-oncogene c-fos (64). It is also believed to be a regulatory phosphorylated area as most serine and threonine amino acid residues are localised in this region (65). Notably, cyclin F contains five phosphorylation sites within the PEST region, that may contribute to its hypothesised functional properties in maintaining protein stability and acting as a protein degradation signal (Figure 1-3). The phosphorylation sites include: theronine-588, theronine-590, serine-621, serine-709, serine-713, and serine-754 (61).

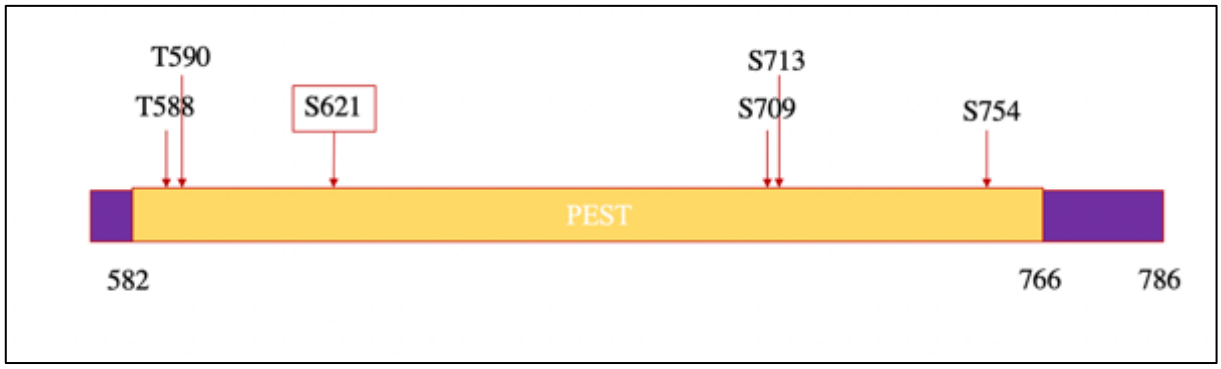

Figure 1-3. Phosphorylation sites on the PEST region.
Five phosphorylation sites within the PEST region (582–766) of the cyclin F protein were discovered. The phosphorylation sites include: theronine-588, theronine-590, serine-621, serine-709, serine-713, and serine-754. Adapted from reference (61).

1.5.3. F-box domain and the SCF^{cyclinF} E3 ubiquitin ligase complex

Another important cyclin F feature is the F-box domain, which is one of 69 substrate adaptors that are part of the F-box protein family (57). This F-box domain is essential for the binding of Skp1, a component that takes part in the E3 ligase complex known as SCF$^{cyclin\ F}$ E3 ubiquitin ligase. The SCF$^{cyclin\ F}$ E3 ligase is a multi-protein enzyme complex that formulates the last step of the ubiquitin cascade (43). Cyclin F is one of many protein adaptors that specifically bind to Skp1 to form this E3 ubiquitin ligase complex. Skp1 also binds to Cul1 with Rbx1, which acts as a loading station for E2 to initiate ubiquitylation of proteins (Figure 1-4) (66). Within the SCF$^{cyclin\ F}$ complex, the proteins recruited by cyclin F are ubiquitylated to either form mono- or poly- ubiquitylated chains to signal for degradation (43). The ubiquitin molecule is a highly conserved 76 amino acid polypeptide that is mainly known for mediating protein degradation via the ubiquitin cascade (Figure 1-5) (67).

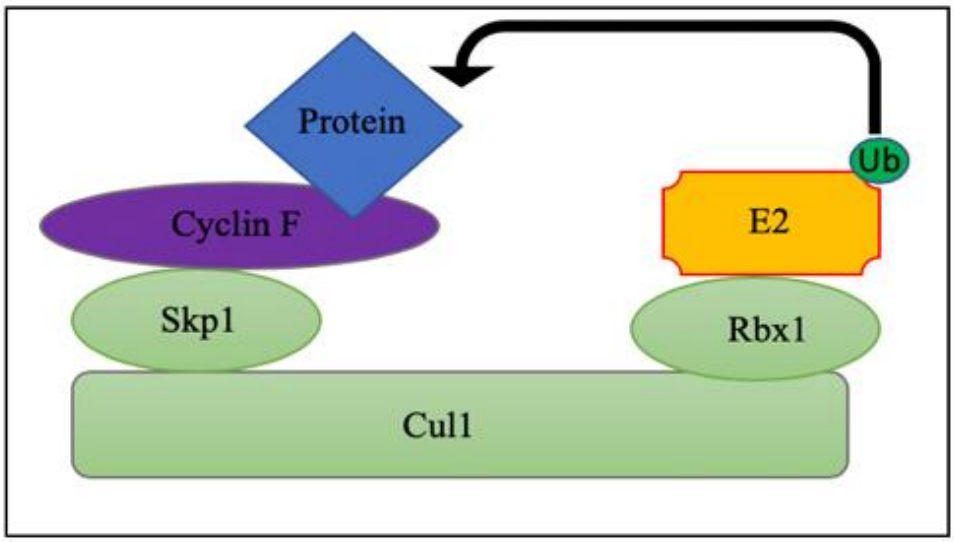

Figure 1-4. Schematic diagram of the SCF$^{cyclin\ F}$ E3 ligase complex.

The SCF$^{cyclin\ F}$ E3 ligase complex is a multi-protein complex that acts as a loading station for the E2 subunit. It consists of the Rbx1, Cul1, Skp1 and cyclin F protein. This complex initiates the binding between ubiquitin molecules and the target protein leading to degradation. Adapted from reference (43).

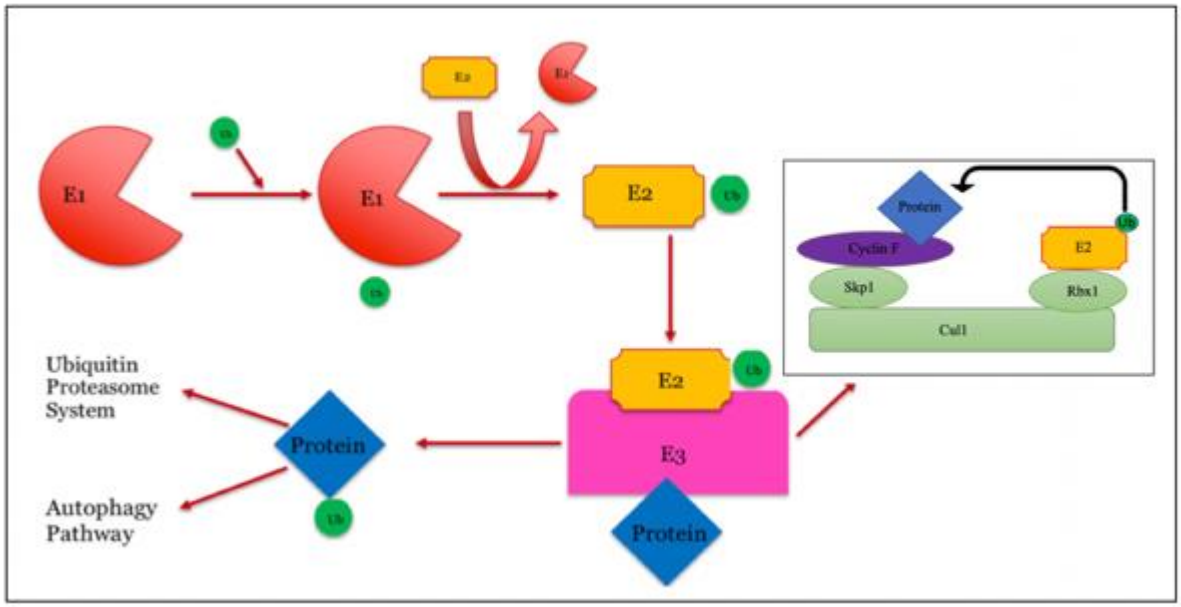

Figure 1-5. Schematic diagram of the protein ubiquitylation cascade.

E1 initiates the protein ubiquitylation cascade by attaching to a ubiquitin molecule. The E2 replaces the E1 in this cascade and carries the ubiquitin molecule to the E3 ligase complex. The E3 ligase complex, consisting of a cyclin F protein, assists with the binding of the ubiquitin molecule to a protein. The protein with the ubiquitin molecule then follows either the UPS or autophagy pathway for degradation. Adapted from (41).

1.6. The role of Cyclin F in ALS/FTD pathology

Recent studies have investigated the role of the cyclin F^{S621G} mutant, a familial candidate identified in a large Australian family cohort with ALS and FTD affecting four generations. In the 2016 study, *CCNF* variants were discovered, including the familial cyclin F^{S621G} mutant, using whole exome sequencing within 16 diverse cohorts (14). The novel variant amino acid substitutes within the *CCNF* gene were found to be highly conserved across various species. In addition, the familial ALS/FTD mutations displaying frequencies ranging from 0.6 to 3.3%, comparable to familial cohorts of the *TARDBP* and *FUS* mutants (68). Analysis within a replication cohort also identified rare protein-altering variants in sALS, validating that *CCNF* variants are found both in familial and sporadic ALS/FTD cases (14). As the cyclin F protein is a component of the SCF ubiquitin ligase complex, it was proposed that the presence of toxic cytoplasmic protein aggregates may be the result of UPS dysfunction, thus contributing towards the proteostasis impairment theory that leads to the neurotoxicity observed in ALS/FTD pathology (23). Using a green fluorescent degron reporter (GFPu) assay, researchers were able to determine that various novel familial and sporadic ALS/FTD mutants were associated with significant increases in UPS inhibition, independent of cyclin F expression levels. This

indicated that *CCNF* mutations leads to UPS dysfunction. Further examination using ubiquitin-independent proteasome activity assays, determined that UPS impairment did not arise as a result of altered proteasome activity but instead abnormal ubiquitylation or impairments to proteasome transport for the familial cyclin F^{S621G} mutant (14). Furthermore, the presence of high levels of ubiquitylated TDP-43 indicated that altered SCF cyclin F ligase machinery may be a contributing factor towards the proteostasis impairment theory (2, 14).

1.6.1. Aberrant ubiquitylation of aggregated proteins

Cyclin F plays an essential role in the ubiquitylation of proteins, therefore, any impairments to this multi-step quality control system can lead to proteostasis impairments, which in turn can cause neurotoxicity and ultimately neurodegeneration (43). To further understand the association of cyclin F and the presence of protein rich aggregates presented in ALS/FTD pathology, the familial cyclin F^{S621G} mutation was investigated. In a recent study, hyper-ubiquitylation activity of K48 polyubiquitin was demonstrated to be associated with autophagic machinery impairment with neuronal cells expressing cyclin F^{S621G} (54). This highlighted that variants in the cyclin F protein, a protein that is an essential component of quality control systems to maintain proteostasis, can lead to hyper-ubiquitylation of aggregated proteins in neuronal cells, a hallmark of ALS/FTD pathology.

1.6.2. Alteration of Cyclin F phosphorylation

The familial cyclin F^{S621G} mutation is located in one of seven phosphorylation sites on the cyclin F protein sequence. Interestingly, it is also one of five of the seven phosphorylation sites that lie within the PEST region (Figure 1-3) (61). The amino acid substitution made by this mutation, where the serine (S) residue is replaced by the glycine (G) residue inhibits phosphorylation at the Serine-621 (S621) site by casein kinase (CKII). This inhibition, elevates ubiquitylation activity of cyclin F and increases lysine48 (K48) ubiquitylated proteins (61). This disruption to phosphorylation at S621 caused by this *CCNF* mutation overall alters protein stability in regulating proteostasis, therefore it may generate toxic cytoplasmic environments within motor neurons.

1.6.3. The Cyclin F^{S621G} mutant leads to increased apoptosis

Further investigation by Hogan *et al.,* into the mechanisms of the familial cyclin F^{S621G} mutant was made with both *in vitro* and *in vivo* models. The *in vitro* cell culture model used a proteomic approach to determine the cellular pathways which are affected in cyclin F^{S621G} compared to

the cyclin F wild-type (WT). The *in vitro* proteomics data revealed increased caspase-3 activity, which was further validated within an *in vivo* zebrafish model (69). Overexpression of the familial ALS/FTD-linked cyclin F^{S621G} mutant in the zebrafish model elucidated motor neuron axonopathies as a result of up-regulated caspase-3 activity. This overexpression displayed decreased cell viability in the spinal cord, abnormal axonal outgrowth and an overall decrease in motor function.

1.7. Proteomic studies in ALS/FTD

Proteomic-based techniques are a powerful approach for in-depth analysis into understanding pathogenic mechanisms. Proteomics is a large-scale screening and protein profiling method that provides a biological perspective of the complex proteome system. Proteomics often uses mass spectrometry (MS) technology that combines liquid chromatography (LC) for peptide separation. The mass spectrometer measures the mass-to-charge ratio (*m/z*) of each ion that is derived from the peptide sample (70). This generates a swathe of mass spectra corresponding to the analysed peptides samples followed by processing and searching of the data with algorithmic programs that incorporate protein databases. Thus, identifying and profiling highly abundant proteins within the sample. With this information, combined with genomic data, this technique has enabled predictions of pathways that may be associated with neurodegenerative diseases, and potentially provide a targeted approach for an ALS/FTD biomarker or drug target. This is further discussed in Publication I: "Proteomics approach for biomarker and drug target discovery in ALS and FTD" (Appendix B).

Significant contributions have been made with proteomic-based techniques in identifying proteostasis dysfunction as an underlying mechanism of ALS and FTD, such as disruption to ubiquitylation and phosphorylation processes, observed in the familial cyclin F^{S621G} mutant (14, 54, 61, 69). Although this familial cyclin F mutant has provided pathological insight into ALS/FTD pathology, further investigation into the *CCNF* gene is essential to not only validate the pathogenesis but also determine whether sporadic mutations display a similar pathogenic pathway that causes proteostasis dysfunction. Therefore, the sporadic cyclin F^{E624K} mutant was investigated in this thesis using a combination of ELISA-based ubiquitylation activity assays, unbiased label free quantitative proteomics, immunoprecipitation techniques, and biochemical analysis.

1.8. Hypothesis and Aims

It is hypothesised that the sporadic cyclin F^{E624K} mutant causes perturbations to cellular pathways and protein networks similar to the well-characterised familial cyclin F^{S621G} mutant (18, 54, 61). This has been proposed as the sporadic cyclin F^{E624K} mutant is present within a CKII consensus motif for phosphorylation (^{618}DQESEGEKEG^{627}) in cyclin F. As the cyclin F^{E624K} mutant is within this phosphorylation motif and within the PEST region, a decrease in phosphorylation at the S621 site and an increase in K48 ubiquitylation was expected, as observed by the familial cyclin F^{S621G} mutant (54, 61). Thus, the sporadic cyclin F^{E624K} mutant, may indirectly affect ubiquitylation activity as the CKII loses its ability to phosphorylate at this specific S621 site.

There are four aims described to address the hypothesis proposed:

1. To generate the sporadic cyclin F^{E624K} mutant sequence with the addition of a FLAG epitope tag via site-directed mutagenesis.
2. To determine different or similar cellular pathway changes in HEK293 cells expressing the sporadic cyclin F^{E624K} mutant compared to cyclin F^{WT} and familial cyclin F^{S621G} mutant, using unbiased label-free global proteomics.
3. To identify PPIs in HEK293 cells expressing the sporadic cyclin F^{E624K} mutant and evaluate whether these protein interactors display novel or similar protein interactors to those bound to cyclin F^{WT} and the familial cyclin F^{S621G} mutant, using unbiased label-free quantitative proteomics combined with immunoprecipitation techniques.
4. To assess the ubiquitylation levels in HEK293 cells expressing the sporadic cyclin F^{E624K} mutant using the E3 ubiquitin ligase activity assay.

2. Methods

2.1. Plasmid preparation

The *CCNF* transgenes consisted of a fused FLAG epitope tag (1012Da). Details of each construct are presented in Table 2-1.

Table 2-1. Summary of constructs used.

Construct ID	Vector	Tag	Mutation Site	Antibiotic	Source
Empty Vector	pcDNA3.1	n/a	n/a	Ampicillin	Invitrogen Cat# V79020
CCNF ^{WT}-FLAG	pcDNA3.1	FLAG	n/a	Ampicillin	Custom generated from GenScript
CCNF^{S621G}-FLAG	pcDNA3.1	FLAG	S621G	Ampicillin	Custom generated from GenScript
CCNF^{E624K}-FLAG	pcDNA3.1	FLAG	E624K	Ampicillin	Q5 site-directed mutagenesis made during this thesis

2.2. Site-directed mutagenesis

All constructs except *CCNF*^{E624K}-FLAG were sourced from either Invitrogen or custom made from GenScript. The *CCNF*^{E624K}-FLAG construct was generated using the Q5 site-directed mutagenesis kit (New England Biolabs). The forward primer (5'ACAGCTCCCAGCGGCATC3') and reverse primer (5'GCCCTCACTCTCCTGGTC3') were designed and obtained from Sigma-Aldrich. The plasmid used for the site-directed mutagenesis protocol was the pcDNA3.1 vector with the *CCNF*^{WT} backbone that contained the FLAG epitope tag at the C terminus (Figure 1-1). For the polymerase chain reaction (PCR) step the PCR thermal master mix (Eppendorf) was used. Initial denaturation temperature was set at 98°C for 30 seconds. The annealing temperature was set to 68°C for 10-30 seconds. This consisted of 25 cycles. Elongation temperature was set at 72°C for 20-30 seconds. DpnI was used to cleave methylated recognition sites of DNA. Sequence verification was processed by Macrogen, Inc (Korea).

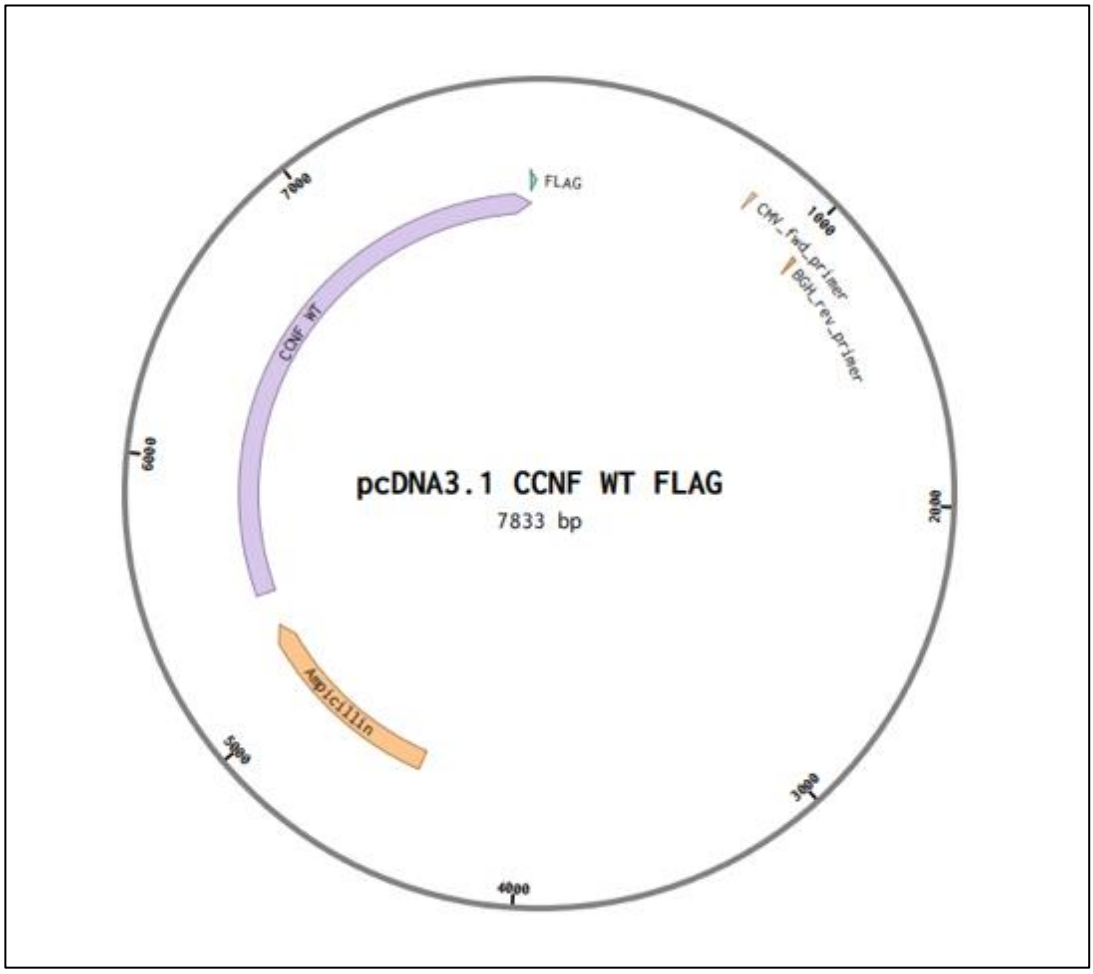

Figure 2-1. Plasmid map of *CCNF*^{WT}-FLAG construct in the pcDNA3.1 vector.

2.3. Transformation

Following the Q5 site-directed mutagenesis kit manual (New England Biolabs), approximately 25µl of Invitrogen One shot INVαF chemically competent *Escherichia coli* (*E. coli)* cells were mixed with 1µl of DNA and incubated on ice for 30 minutes. Cells were heat shocked for 30 seconds at 42°C and immediately placed on ice for 5 minutes. Approximately 950µl of SOC media was added and the mixture incubated for 1 hour at 37°C shaking at 300 revolutions per minute (rpm). Approximately 90µl of mixture was spread onto an ampicillin (100µg/ml) agar plate and incubated at 37°C overnight to select for colonies containing the plasmid DNA.

2.4. Plating constructs from glycerol stocks

The empty vector, *CCNF*^{WT}-FLAG, and *CCNF*^{S621G}-FLAG constructs were plated from their *E. coli* glycerol stocks. Approximately 5µl of the *E. coli* glycerol stock was incubated at 37°C for 7 hours in 5ml of Luria broth (LB) media. Approximately 90µl of the inoculated media was plated on ampicillin (100µg/ml) agar plates and incubated for ~12 hours at 37°C.

2.5. Preparation for midi-prep DNA purification

A single colony was selected from the agar plates containing the transformed *E. coli* cells. Incubation time consisted of 8 hours in LB media containing ampicillin. Dilutions of the starter culture (1:500) was made and was further incubated for 12-16 hours at 37°C. The *E.*coli cells were centrifuged at 3,700rpm at 4°C and the bacterial pellet was either stored at -80°C or proceeded immediately to midi-prep DNA purification step.

2.6. Midi-prep DNA purification and quantification of DNA concentration

Plasmid DNA purification was conducted with the QIAGEN Plasmid Midi Kit, following the manufacturer's instructions using the high yield protocol. The bacterial pellet lysed in Buffer P1 (lysis buffer) followed by buffer P2 (wash buffer) and buffer N3 (neutralisation buffer). The lysed cells were centrifuged at 13,000rpm for 10 minutes at room temperature. 800µl of supernatant was added to QIA prep 2.0 spin columns with buffer PB (binding buffer to allow DNA to bind to filter in spin columns) and centrifuged at 13,000rpm for <1 minute. Flow through was discarded and spin columns were washed with wash buffers and centrifuged at 13,000rpm for <1 minute. Buffer EB (10mM TrisCl, pH 8.5) was used to elute DNA for each sample. DNA concentration was calculated using the NanoDrop 2000 spectrophotometer (Thermo Scientific).

2.7. Mammalian cell culture

For this study, HEK293 cells were selected due to the ease in efficient transfection as these cells have a fast growth and long survival rate, beneficial for the limited time given for this research project (71). The HEK293 cells were obtained at a low passage from American Type Culture Collection (ATCC). The cells were maintained in T75 flasks (Thermo Scientific) with Dulbecco's modified eagle medium (DMEM; Thermo Scientific) supplemented with 10% foetal bovine serum (FBS; Sigma-Aldrich) without antibiotics. The flasks were kept in 37°C incubators with 5% CO_2 and 95% humidity. Passaging of cells occurred every 3-4 days or once cells reached 70-80% confluency. Cells were washed in pre-warmed PBS and detached with 2ml of pre-warmed trypsin prior to seeding.

2.7.1. Cell density calculations

Cell counting was required for seeding and transfection preparation. Cells that had reached 80-90% confluency were prepared for transfections. After cells were washed with pre-warmed PBS and detached with trypsin, a 1:1 dilution of cell suspension and trypan blue (Thermo Scientific) was made. Following the manufacturer's instructions, 10µl of cell suspension and trypan blue dilution was loaded onto a cell counting chamber slide and was inserted into the Countess™ automated cell counter (Thermo Scientific). The calculations for the required cell volume are as follows:

$$\textit{Required Cell Volume} = \frac{\textit{Desired Cell Density}}{\textit{Calculated Cell Density}} \times \textit{1000 (conversion to µl)}$$

Various desired cell density concentrations were used for the optimisation of obtaining the most suitable cell density in seeding cells for transfections into 10 cm Corning plastic culture dishes (Sigma-Aldrich). The most suitable cell density concentration was obtained at 1.6×10^6.

2.7.2. Transfections

Plates were seeded with 1.6×10^6 cells with DMEM + 10% FBS and incubated for 48 hours at 37°C and 5% CO_2. For transfections, an optimised protocol was used. Opti-MEM media (Thermo Scientific) and Lipofectamine 2000 (Thermo Scientific) were used with optimised concentrations for the HEK293 cells. For each sample, 325µl of Opti-MEM media was combined with 25µl of Lipofectamine 2000 for each plate. 10µg of prepared DNA combined with 305µl of Opti-MEM media was prepared and combined with the Opti-MEM/Lipofectamine media and was incubated for 20 minutes at room temperature. DMEM+ 10% FBS media was removed from cells and cells were washed with pre-warmed PBS. This was followed with adding prepared DNA with Opti-MEM/Lipofectamine media to each plate for transfection. Newly transfected cells were left for 37°C incubation for 4-5 hours in Opti-MEM media. After incubation the cells were washed with pre-warmed PBS and the Opti-MEM media was replaced with DMEM + 10% FBS. Three replicates were carried out for each sample.

2.8. Cell harvesting and cell lysis

The transfected HEK293 cells expressing empty vector and *CCNF*-FLAG transgenes were harvested at 80% confluency. Cells were scraped from the plates using ice cold PBS and collected with their respective supernatant. Cells and supernatants were centrifuged at 1,500

relative centrifugal force (rcf) to collect whole cells, supernatants were removed, and pellets were snap frozen on dry ice and stored at -80°C until required.

Frozen cell pellets were resuspended with Nonidet P-40 1% (NP40) lysis buffer, pH 7.4 (1.5mM NaCl, 50mM Tris-Cl) containing protease and phosphatase inhibitors (Roche) and left to thaw on ice. Cells were intermittently vortexed for 10 seconds every 10 minutes for 30 minutes. Sonication was performed using the Sonic Ruptor 250 (Omni-Inc) on setting 3 for 10-20 seconds. This was followed by centrifugation at 14,000rcf for 10 minutes at 4°C to collect cellular debris. Whole cell lysates were either stored at -80°C or quantified. Three replicates were collected for each sample.

2.9. Bicinchoninic acid (BCA) assay

Protein quantification was performed on samples using the Pierce bicinchoninic acid (BCA) protein assay kit (Thermo Scientific), following the manufacturer's instructions. Samples were prepared in triplicates of 1:3 dilutions in milliQ water. Bovine serum albumin (BSA) standard concentrations were prepared with NP40 lysis buffer to generate a standard curve for protein quantification measurements to be fitted on. Measurements were read at 562nm absorbance with the PHERAstar FS plate reader (BMG Labtech). This provided an accurate quantification of the protein content for each sample.

2.10. Sample preparation and immunoblotting

Immunoblotting preparation involved separating proteins for each sample using sodium dodecyl sulfate polyacrylamide gel electrophoresis (SDS-PAGE). Approximately 20µg of protein lysate was combined with 10x NuPAGE Dithiothreitol (DTT) reducing agent (Invitrogen), 4x NuPAGE lithium dodecyl sulfate (LDS) sample buffer (Invitrogen), and milliQ water to adjust for identical volumes across all samples. Samples were heated at 95°C for 5 minutes. The Invitrogen tanks (Thermo Scientific) were used for the SDS-PAGE with NuPAGE 4-12% Bis-Tris Midi protein 20-well gels. Approximately 20µl of samples and 3µl of Precision Plus Protein Dual Color Standards ladder (Bio-Rad) was loaded into wells. SDS-PAGE ran at 60 volts (V) for 10 minutes and was increased to 120V for ~1 hour. Gels were then rinsed in Transblot Turbo transfer buffer (Bio-Rad) and stacked against a nitrocellulose membrane and transfer stacks. Following the manufacturer's instruction, a semi-dry transfer (Bio-Rad) was performed for 10 minutes on high molecular weight (MW) setting (25 V, 2.5 A).

2.11. Protein visualisation

Following the protein transfer, the nitrocellulose membrane was rinsed in Tris-buffered saline (TBS) and blocked in the Odyssey Licor blocking buffer (1:1, with TBS) for 45 minutes, shaking at room temperature. Primary antibodies of different species were then added to membrane blots with either overnight incubation, shaking at 4°C or ~1-hour incubation, shaking at room temperature. Details of antibodies used are presented in Table 2-2.

The primary antibodies were removed, washed 3x with TBS containing 0.2% (v/v) tween 20 (TBS-T) and secondary Licor antibodies were added to membranes at 1:10,000 dilution, probing for anti-species of the primary antibodies at either 800nm or 680nm wave length. In between antibody incubations and after secondary antibody incubation, membranes were washed 3x for 5 minutes with TBS-T to remove any residual antibodies. Prior to imaging, membranes were washed in TBS and milliQ water and left to dry in the dark. Imaging was performed with the Licor Odyssey CLx scanner. For statistical analysis, a paired t-test was calculated using the GraphPad Prism 8 software.

Table 2-2. List of primary antibodies used for immunoblotting specific proteins.
Table consists of antibody type, the species the antibody was hosted in, dilution, and the company source.

Primary Antibody	Antibody type	Species Host	Dilution	Source
Anti-FLAG	Monoclonal	Mouse	1:1000	Sigma-Aldrich (USA)
Anti-lysine-48 (K48) Ubiquitin	Monoclonal	Rabbit	1:1000	Millipore Corp. (USA)
Anti-lysine-63 (K63) Ubiquitin	Monoclonal	Rabbit	1:500	Millipore Corp. (USA)
Anti-IgG	Monoclonal	Mouse		Cell Signalling (USA)
Anti-*beta*-actin	Monoclonal	Mouse	1:500	Sigma-Aldrich (USA)
Anti-*beta*-tubulin	Polyclonal	Rabbit	1:500	Abcam (UK)
Anti-phospho cyclin F S621	Polyclonal	Rabbit	1:500	Bethyl (USA) Custom designed
Anti-non-phospho cyclin F S621	Polyclonal	Rabbit	1:500	Bethyl (USA) Custom designed
Anti-Cyclin F	Polyclonal	Rabbit	1:500	Bethyl (USA)

2.12. Immunoprecipitation (IP)

For the IP assay, 500μg of protein lysate in NP40 lysis buffer and 1μg of anti-FLAG antibody was used. An anti-IgG pre-immune antibody with all combined samples was also used as a control. Prior to adding anti-FLAG antibody, 20μg of starting material (SM) was saved in separate microcentrifuge tubes. IP samples were then incubated overnight at 4°C, with rotating. This was followed by adding protein A/G magnetic beads (Pierce) to isolate the antibody: protein complex. For two hours the IP samples with magnetic beads underwent further incubation. After incubation, flow through (FT) was collected. To efficiently remove non-specific proteins, magnetic beads were washed with NP40 lysis buffer and washed twice with TBS. Approximately 20% of IP sample was saved for immunoblotting, whilst ~80% was prepared for MS.

2.13. Mass spectrometry (MS) preparation

MS preparation for whole lysate samples and IP samples were prepared via in-gel trypsin digestion and in-solution trypsin digestion, respectively. Whole lysate samples consisted of empty vector, cyclin F^{WT}-FLAG, cyclin F^{S621G}-FLAG, and cyclin F^{E624K}-FLAG. IP samples consisted of NP40 lysis buffer (negative control), IgG sample, empty vector, cyclin F^{WT}-FLAG, cyclin F^{S621G}-FLAG, and cyclin F^{E624K}-FLAG. Each sample consisted of three biological replicates.

2.13.1. In-gel trypsin digestion

Proteins were separated via SDS-PAGE, as described in section 2.10. After removing the gel from the cassette, the gel was fixed in fixing solution (50% (v/v) methanol, 10% (v/v) acetic acid) for 5-10 minutes. This solution was removed and incubated with the Coomassie blue G-250 (Bio-Rad) for 30 minutes. De-staining solution (25% (v/v) methanol) was then added for an overnight incubation to absorb any excess blue staining. This was followed by slicing each gel lane into three fractions and further slicing each fraction into 2-4mm gel pieces. Gel pieces were buffer exchanged in 50mM ammonium bicarbonate for 10 minutes, followed by dehydrating the gel pieces in 50mM ammonium bicarbonate, 50% (v/v) acetonitrile (ACN) for 10 minutes. This was then replaced with 100% (v/v) ACN for 30 seconds. The in-gel protein samples were then reduced and alkylated with 10mM DTT for 45 minutes at 37°C, and 20mM iodoacetamide (IAA) for 45 minutes in the dark, respectively. Samples were then digested with trypsin (1:50, trypsin: protein) for an overnight incubation at 37°C. Peptides were extracted

with 50% (v/v) ACN, 2% (v/v) formic acid (FA) for 15 minutes shaking, followed by 100% (v/v) ACN for 15 minutes shaking. The peptides were pooled and evaporated by vacuum centrifugation in an Eppendorf Concentrator 5301. Peptide samples were then stored at -80°C.

2.13.2. In-solution trypsin digestion

Following IP as described in section 2.12, the samples were washed in PBS. IP samples were then reduced and alkylated with 10mM DTT for 45 minutes at 37°C and 20mM IAA for 45 minutes in the dark, respectively. This was followed by digestion with trypsin (1:50, trypsin: protein) for an overnight incubation at 37°C.

2.13.3. Peptide clean-up

Prior to peptide de-salting, peptide samples were resuspended in 0.1% (v/v) FA. Using C_{18} zip tips (Agilent Technologies), that were pre-equilibrated, the peptide samples were pushed through the tips with 0.1% (v/v) FA. To elute peptides from the C_{18} column zip tips, 50% (v/v) ACN, 0.1% (v/v) FA was used. To elute peptides from the C_{18} column zip tips, 50% (v/v) ACN, 0.1% (v/v) FA was used. This eluate was evaporated by vacuum centrifugation using an Eppendorf Concentrator 5301. Peptide samples were then resuspended in 0.1% (v/v) FA solution for MS analysis.

2.14. Mass spectrometry (MS)

Quantitative proteomics was performed on whole cell lysates and IP samples of empty vector and *CCNF* transgenes.

2.14.1. Global proteomic parameters

The three fractions of each three biological replicates expressing the *CCNF* transgenes in the HEK293 cell line were analysed using C_{18} reverse phase nanoscale liquid chromatography tandem Q-Exactive mass spectrometer (Thermo Scientific). The peptide samples were injected into the 0.5mm C-18 reverse phase Orbitrap Velos (Thermo Scientific) and desalted at a low rate of 15µl/minute with buffer A (0.1% (v/v) FA) for 3.9 minutes. The desalted peptides were then separated on an Acclaim PepMap 100 C18 LC column (3µm particle size, 75µm x 150 mm length, Thermo Scientific) using buffer B (80% (v/v) ACN/0.1% (v/v) FA) for ~40 minutes at a 0-33% gradient. Between 40 to 50 minutes, the gradient increased to 63%, and between 50 to 57 minutes the gradient reached 95%. The flow rate is at 300nL/min.

The MS scan range was between 400 to 2,000 m/z at a resolution of 70,000 for precursor ions and a resolution of 17,500 for product ions. Acquisition was set to positive charge mode with a default charge state of 2, focusing on doubly charged ions. The automatic gain control (AGC) for precursor ions was set to $1x10^6$, and AGC for product ions was set to $2x10^4$. The mass spectrometer was calibrated to collect for 30 milliseconds in its precursor acquisition mode before selecting the top 10 peptides for fragmentation. These top 10 peptides in this mode underwent subsequent scanning in the product ion acquisition mode (MS/MS scan) for 50 milliseconds with an isolation window of 2 m/z. The normalised collision energy (NCE) was set at 27 and charge exclusion was set at 1, >6.

2.14.2. Immunoprecipitation (IP) proteomic parameters

Three biological replicates of the IP samples expressing the *CCNF* transgenes in the HEK293 cell line were analysed using C18 reverse phase nanoscale liquid chromatography tandem mass spectrometry. Peptide samples were fractionated using the same setup as described in section 2.14.1.

The MS scan range was between 400 to 2,000 m/z at a resolution of 70,000 for precursor ions and a resolution of 17,500 for product ions. Acquisition was set to positive charge mode with a default charge state of 2, focusing on doubly charged ions. The AGC for precursor ions was set to $5x10^5$, and AGC for product ions was set to $1x10^5$. The mass spectrometer was calibrated to collect for 50 ms in its precursor acquisition mode before selecting the top 10 peptides for fragmentation. These top 10 peptides in this mode underwent subsequent scanning in the product ion acquisition mode (MS/MS scan) for 110 ms with an isolation window of 1.5 m/z. Charge exclusion was set at 1.

2.15. Proteomic data analysis

The MS data obtained for whole cell lysates and cyclin F immunoprecipitants were analysed using the Sequest algorithm software coupled to a bioinformatics database searching software, Proteome Discoverer (PD) 2.3 (Thermo). Peptide samples were searched against the Homo sapiens protein SwissProt database (2017) that consisted of 42,253 sequence entries using the following parameters. The peptide identifications were determined using a 20-ppm precursor mass tolerance a 0.01 Da MS/MS fragment mass tolerance. For static modifications the carbamidomethylation modification of cysteines was used. Oxidation of methionine and acetylation of protein N-terminus was considered dynamic modifications with a maximum of

three equal modification per peptide, and a maximum of two missed cleavage sites with trypsin selected as the enzyme. PD and excel files of proteomic data can be accessed from: https://cloudstor.aarnet.edu.au/plus/s/ioX19GQvg1cs6P5.

Using the PD 2.3 incorporating Minora Feature detection node for label-free quantitation, three biological replicates from three transfection replicates were analysed. The default quantitation settings were applied to group the abundances for all identified peptides for each protein and the median peptide values was used to represent the relative protein abundance ratios as determined by the PD 2.3 software.

Using the PD 2.3 software, statistical analysis using a heat map was generated. Protein distance parameters were based on the Euclidean function using a complete linkage method. Samples were clustered using a hierarchical cluster analysis. This was based on the different abundant raw values from proteins to provide an overview on proteome similarities between the up- and down-regulated proteins quantified.

Using the PD 2.3 software, statistical analysis with volcano plots were generated to display comparisons between the *CCNF* mutants relative to cells expressing the cyclin F^{WT}. Proteins based on their abundance $\log_2$ ratio were plotted against the P-values in $\log_{10}$. The volcano plots were generated with R, based on the software default parameters. For global proteomic data, this indicated whether cells expressing the cyclin F mutant proteins were down- or up-regulated relative to cells expressing the cyclin F^{WT}. For IP proteomic data, this indicated whether cells expressing protein interactors displayed *loss-of*-binding or *enhanced*-binding to the cyclin F protein relative to cells expressing the cyclin F^{WT}. Proteins that displayed a $\log_2$ ratio value of -6.64 and 6.64 were significant proteins that were either not identified or identified, respectively relative to cells expressing the cyclin F^{WT}.

Gene ontology (GO) analysis was performed with the PANTHER GO classification system database (72). GO charts were exported for data analysis. The Ingenuity Pathway Analysis® (IPA) determined specific networks that were either activated or inhibited in HEK293 cells expressing cyclin F^{WT}, cyclin F^{S621G}, and cyclin F^{E624K}. This was based on the log abundance values for the proteins identified in both global proteomic and IP proteomics data sets. IPA networks and pathways were determined based on proteins that clustered towards a specific protein network and/or pathway.

2.16. E3 ubiquitin ligase activity assay

The ELISA-based ubiquitylation activity assay was performed with the E3LITE Customizable Ubiquitin Ligase Kit (EnzoLifeSensors), following manufacturer's instructions. The empty vector, cyclin F^{WT}-FLAG, cyclin F^{S621G}-FLAG, and cyclin F^{E624K}-FLAG, E3 ligase buffer negative control, and E1-E2-E3 positive control were prepared as IP samples (as described in section 2.12) for this E3 ubiquitin ligase activity assay. The ubiquitin E2 conjugating enzyme selected for this protocol was the UBE2D3. Magnetic beads were first washed in PBS, followed by assay buffer (100mM Tris-HCl, 10mM $MgCl_2$, 0.2mM DTT, pH 8.0). To each well of the microtiter plate, which was precoated with LifeSensor's proprietary polyubiquitin capture reagent, the enzyme cocktail (E1-E2-ubiquitin in assay buffer) was added. This was followed by the immunoprecipitated cyclin F samples and the positive control E1-E2-E3 solution. To initiate the enzymatic reaction, 0.4mM ATP was added and incubated at room temperature for 45 minutes. This was followed by an incubation with the detection solution for 1 hour, and further incubation with streptavidin-HRP for 1 hour. ECL reagent was added to each well and chemiluminescence was measured at a gain level of 1000 with the PHERAstar FS plate reader (BMG Labtech).

3. Results

3.1. Site-directed mutagenesis of *CCNF*^{E624K} -FLAG

Site-directed mutagenesis was performed to generate the ALS/FTD-causative gene mutation *CCNF*^{E624K}-FLAG. Together with PCR machinery and oligonucleotide primers designed, the controlled and precise point mutation (A1882G) within the PEST region (1746-2289) of the *CCNF*^{WT} DNA sequence was generated. To validate that this PCR product was sequenced successfully, a 2μg sample of the whole plasmid consisting of the site-directed mutation was sent to Macrogen Inc. (South Korea). The results confirmed the A1882G mutation in the DNA sequence within the *CCNF*^{E624K} -FLAG sequence, where the *CCNF*^{E624} WT codon GAG was modified to the *CCNF*^{E624K} codon AAG. This allowed the translation from glutamic acid (E) to the lysine (K) residue at the 624 position (E624K) of the cyclin F protein sequence, thus successfully generating a site-directed mutagenesis sequence of *CCNF*^{E624K} -FLAG (Figure 3-1).

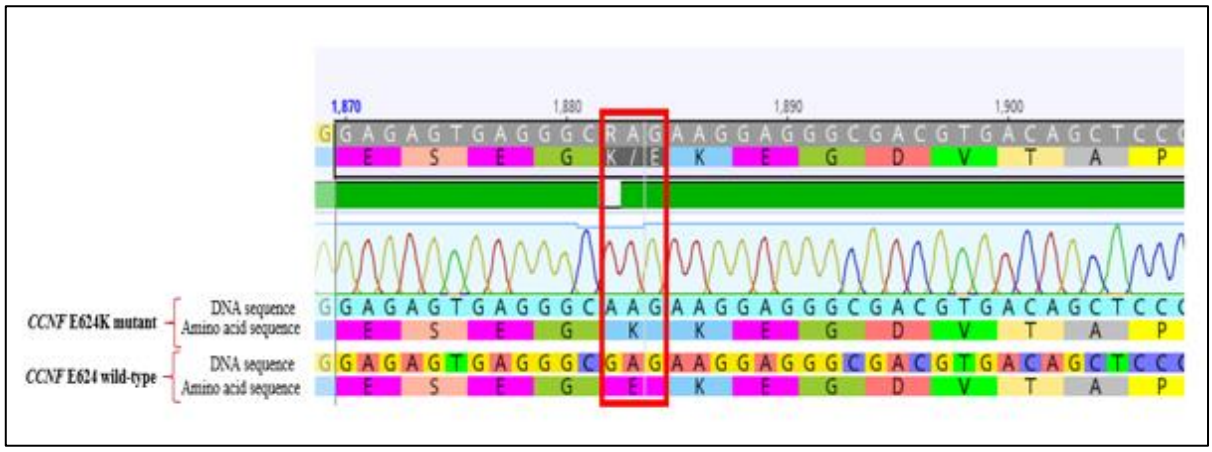

Figure 3-1. Sequence alignment of *CCNF*^{WT} and *CCNF*^{E624K} DNA sequences.
CCNF^{E624K} mutant and *CCNF*^{E624} WT sequence alignments that display the A1882G point mutation in the *CCNF-FLAG* DNA sequence, where the *CCNF*^{E624} WT codon GAG was modified to the *CCNF*^{E624K} codon AAG. This allowed the substitution of a glutamic acid (E) to a lysine (K) residue at the 624 position (E624K) of the cyclin F protein sequence.

3.2. Validating cyclin F-FLAG expression in HEK293 cells via immunoblotting

HEK293 cells were grown to ~80-90% confluence and transfected with pcDNA 3.1 empty vector, *CCNF*^{WT}-FLAG, *CCNF*^{S621G}-FLAG, and *CCNF*^{E624K}-FLAG constructs for ~18 hours. To validate transfection efficiency of the FLAG tagged *CCNF* constructs within the HEK293 cells, immunoblotting and statistical analysis for FLAG and cyclin F were performed (Figure 3-2). The molecular weight of cyclin F is ~87 kDa, and the FLAG tag epitope is 1012Da, therefore the expected molecular weight (MW) for FLAG tagged cyclin F is ~88 kDa.

Immunoblotting for FLAG revealed overexpression of FLAG tagged cyclin F in lanes corresponding to samples transfected with *CCNF*^{WT}, *CCNF*^{S621G} and *CCNF*^{E624K}, with no expression of FLAG observed in the empty vector control lane. Alternatively, immunoblotting for cyclin F also revealed overexpression of cyclin F as expected in samples transfected with *CCNF* transgenes, while low level of expression was observed in empty vector controls, which are indicative of endogenous cyclin F expression. The *beta*-actin loading control was used and displayed similar expression levels across all samples. (Figure 3-2.A).

Statistical analysis for FLAG and cyclin F fold changes were performed to determine transfection efficiencies of *CCNF* transgenes expressed in the HEK293 cells. The transfection of *CCNF*^{S621G}-FLAG (1.07-fold) and *CCNF*^{E624K}-FLAG (1.13-fold) were measured and normalised to *CCNF*^{WT}-FLAG (1-fold). The empty vector control revealed that no expression of cyclin F-FLAG was detected when probing, using the anti-FLAG antibody (Figure 3-2.B). Cyclin F overexpression for *CCNF*^{WT} (16.55-fold), *CCNF*^{S621G} (20.01-fold) and *CCNF*^{E624K} (17-fold) revealed similar overexpression levels of cyclin F compared to the empty vector control (1-fold) when probing, using the anti-cyclin F antibody (Figure 3-2.C).

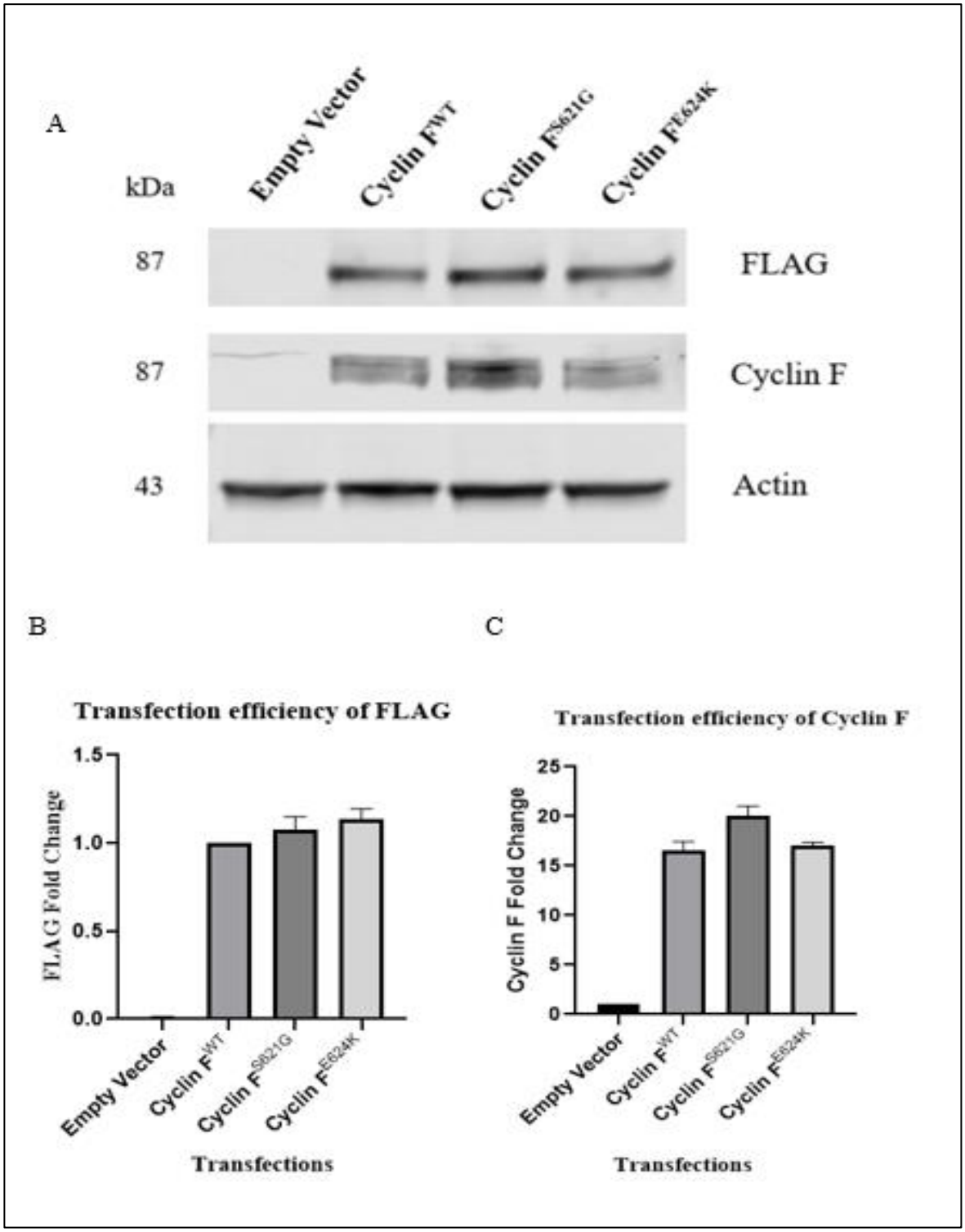

Figure 3-2. *CCNF*-FLAG expression levels of FLAG and Cyclin F are present in transfected cell lysates.

A) Immunoblot of FLAG and cyclin F expression levels are relatively consistent across lanes for cells expressing cyclin F^{WT}, cyclin F^{S621G} and cyclin F^{E624K}. In the empty vector control lane, there was no presence of FLAG and very low expression of cyclin F. The *beta*-actin loading control was used and displayed similar expression levels across all samples. **B)** Statistical analysis of transfected *CCNF*^{S621G}-FLAG (1.07-fold) and *CCNF*^{E624K}-FLAG (1.13-fold) were measured and normalised to *CCNF*^{WT}-FLAG (1-fold). The empty vector control revealed that no expression of cyclin F-FLAG was measured. **C)** Statistical analysis of Cyclin F overexpression for *CCNF*^{WT} (16.55-fold), *CCNF*^{S621G} (20.01-fold) and *CCNF*^{E624K} (17-fold) revealed similar overexpression levels of cyclin F compared to the empty vector control (1-fold). For all statistical analyses, n=3.

3.3. Characterisation of Cyclin F^{E624K} by unbiased proteomics analysis

Unbiased label-free global proteomic analysis was performed on cellular lysates of HEK293 cells expressing pcDNA 3.1 empty vector, cyclin F^{WT}, cyclin F^{S621G} and cyclin F^{E624K} to characterise differentially expressed proteins that may cluster to specific cellular pathways. Using this data, predictions and comparisons were made between the different signalling pathways that are affected in cells expressing the sporadic cyclin F^{E624K} mutant compared to cells expressing cyclin F^{WT} and the well-characterised familial cyclin F^{S621G} mutant. For the following global proteomic analysis, the cyclin F^{WT} was used as the baseline control relative to cyclin F^{S621G} and cyclin F^{E624K} to determine the abundance ratios of all quantifiable proteins.

Across all three biological samples, a total of 4,269 proteins were identified for all four samples. The empty vector control sample identified 49 *unique* proteins (1.1%), the cyclin F^{WT} sample identified 24 *unique* proteins (0.5%), the cyclin F^{S621G} identified 24 *unique* proteins (0.5%), and cyclin F^{E624K} identified 28 *unique* proteins (0.6%) (Figure 3-3). Although ~3% of unique proteins were identified between the empty vector and *CCNF* transgenes, this analysis revealed ~93% of the proteome coverage was *shared*. Thus, demonstrating the consistency between identified proteins with the cells transfected with empty vector and *CCNF* transgenes, and indicates that label-free quantitative proteomics would be beneficial to determine the differentially expressed proteins of the remaining ~ 7% of the proteome.

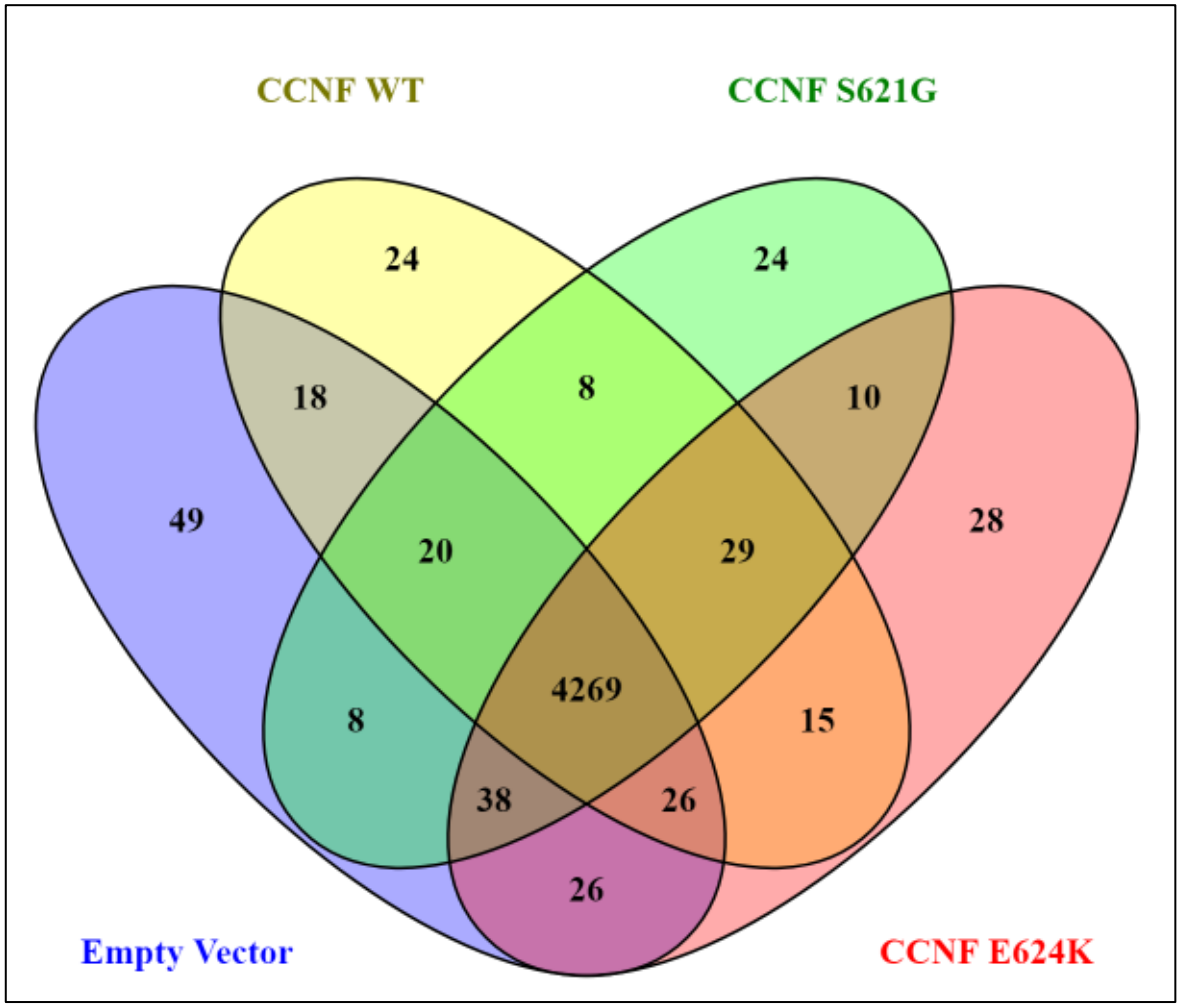

Figure 3-3. Quantified *shared* and *unique* global proteins identified from all four samples.
Venn diagram illustrating the quantified *shared* and *unique* proteins from whole cell lysates in HEK293 cells transfected with empty vector control, cyclin F^{WT}, cyclin F^{S621G}, and cyclin F^{E624K} (n= 3). Venn diagram generated with Venny 2.1. (73).

To gain a more consistent insight into the differences between the *CCNF* transgenes, the quantified proteins of HEK293 cells transfected with the empty vector from the analysis was removed (Figure 3-4). Thus, comparing quantified proteins from only cells expressing *CCNF* transgenes, a total of 4,298 proteins (94.6%) were identified across all three biological samples. Of these 4,298 proteins, 42 proteins (1.0%) were *unique* to cyclin F^{WT}, 32 proteins (0.7%) were *unique* to cyclin F^{S621G}, and 54 proteins (1.3%) were *unique* to cyclin F^{E624K}. Between each sample, cyclin F^{WT} *shared* 28 proteins (0.7%) with cyclin F^{S621G}, cyclin F^{S621G} *shared* 48 proteins (1.1%) with cyclin F^{E624K}, and cyclin F^{E624K} *shared* 41 proteins (1%) with cyclin F^{WT}. Here, ~3% of *unique* proteins were quantified in cells transfected with *CCNF* transgenes and ~2.5% of *shared* proteins between the *CCNF* transgenes. In total *shared* identifiable proteins covered ~94.5% of the proteome whereas ~5.5% of identified proteins were differentially expressed in the *CCNF* transgenes.

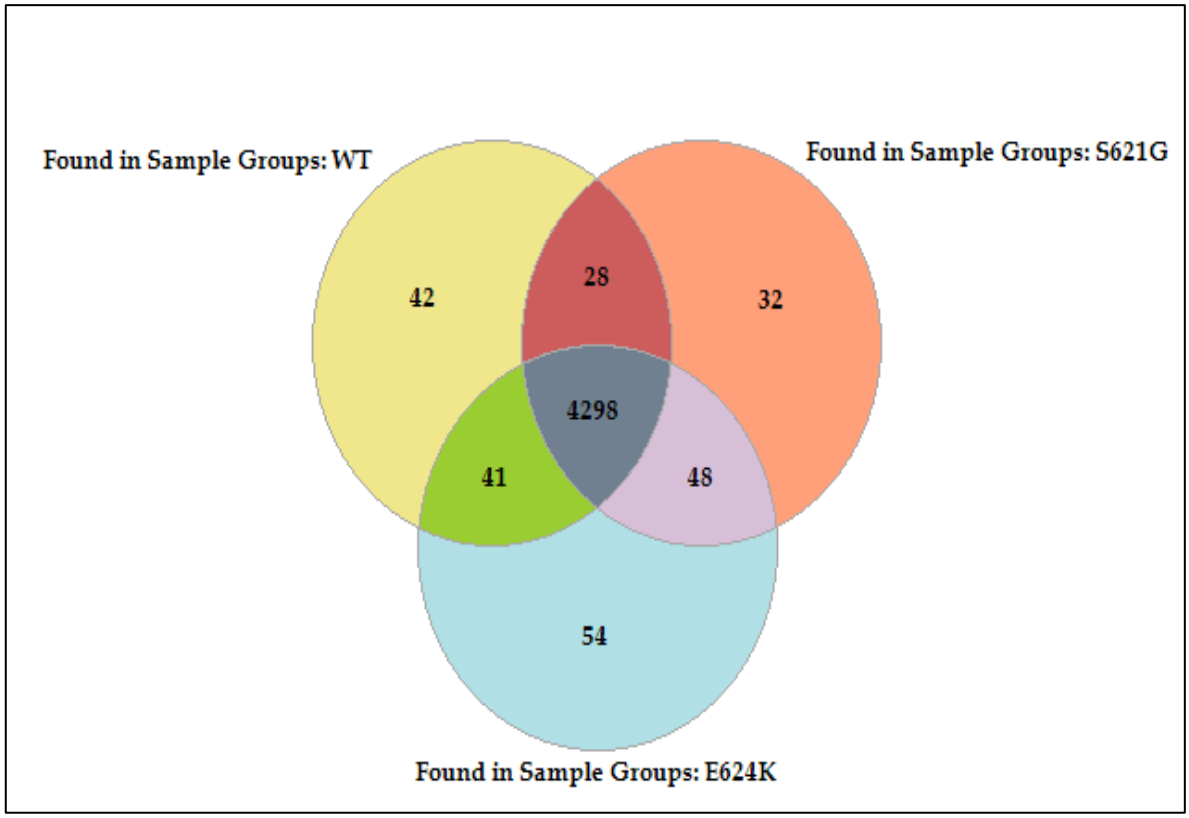

Figure 3-4. Quantified *shared* and *unique* global proteins identified in cells expressing *CCNF* transgenes.
Venn diagram illustrating the quantified *shared* and *unique* proteins identified in cells transfected with cyclin F^{WT}, cyclin F^{S621G}, and cyclin F^{E624K}. For all statistical analysis, n=3.Venn diagram generated with PD 2.3.

3.4. Gene ontology (GO) analysis of differentially expressed proteins in *CCNF* mutants

To determine the specific biological processes and pathways that are initiated in cells expressing differential proteins, GO analysis using PANTHER was employed. The PANTHER GO classification system clusters proteins into specific biological processes. Five different GO categories of biological processes and pathways were identified using data sets that consisted of *unique* and *shared* differentially expressed proteins from HEK293 cells expressing cyclin F^{WT}, cyclin F^{S621G} and cyclin F^{E624K} (Figure 3-5). In the GO categories "Response to stress" (e.g. NYFA, ANKZF1), "Huntington's disease" (SP1 and ACTA2), and "Ubiquitin ligase complex" (UBR2) displayed more abundant proteins expressed in the cyclin F^{E624K} mutant. Whereas differentially expressed cyclin F^{WT} displayed a higher abundance of proteins in the "Cell death" GO category (ADAM10 and ADAM9). In total nine proteins were identified in specific biological processes using the PANTHER GO analysis (Table 3-1).

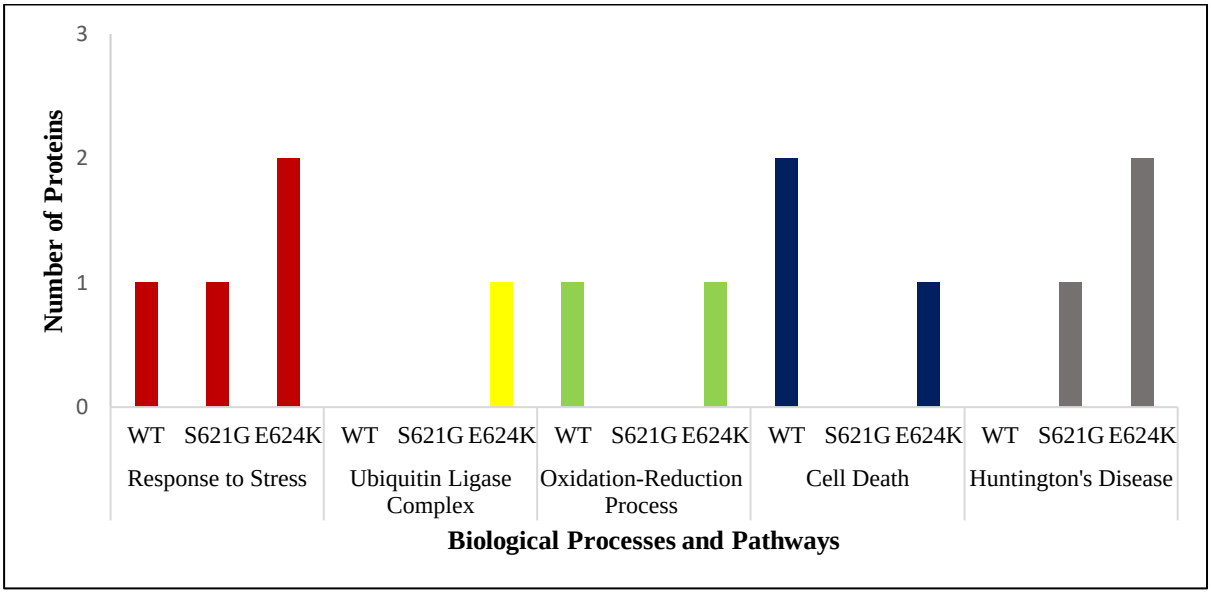

Figure 3-5. *Unique* and *shared* proteins identified *CCNF* transgenes categorised in GO biological processes.

Each biological process and pathway are categorised with a different colour. The column graphs measure the number of enriched differently expressed proteins identified in HEK293 cells expressing cyclin F^{WT}, cyclin F^{S621G}, and cyclin F^{E624K}.

Table 3-1. *Unique* and *shared* proteins identified *CCNF* transgenes categorised in GO biological processes.

UniProt ID	Protein Name	GO Biological Process	Found in Cyclin F^{WT}	Found in Cyclin F^{S621G}	Found in Cyclin F^{E624K}
P23511	**NFYA -** Nuclear transcription factor Y subunit alpha	Response to stress	No	No	Yes
Q9H8Y5	**ANKZF1 -** Ankyrin repeat and zinc finger domain-containing protein 1	Response to stress	No	No	Yes
O14672	**ADAM10 -** Disintegrin and metalloproteinase domain-containing protein 10	Cell death	Yes	No	Yes
Q13443	**ADAM9 -** Disintegrin and metalloproteinase domain-containing protein 9	Cell death	Yes	No	No
P07864	**LDHC -** L-lactate dehydrogenase C chain	Oxidation-reduction process	Yes	No	Yes
P08047	**SP1 -** Transcription factor Sp1	Huntington’s disease	No	Yes	Yes
P62736	**ACTA2 -** Actin, aortic smooth muscle	Huntington's disease	No	No	Yes
Q8IWV8	**UBR2 -** E3 ubiquitin-protein ligase UBR2	Ubiquitin ligase complex	No	No	Yes

3.5. Unbiased proteomics reveal differentially expressed proteins

To gain insight into the level of up- and down-regulated proteins across the four transfected samples a heat map was generated with hierarchical clustering to determine comparable samples, using the PD 2.3. The heat map displayed down-regulated proteins (red) measured with a z-score range between -1.5 and 0.0 and displayed up-regulated proteins (blue) measured with a z-score range between 0.0 and 1.5 (Figure 3-6). This demonstrates that there were differences across all four transfected samples, with the two cyclin F mutants clustered together closely indicating their proteome similarities compared to the proteome similarities between empty vector and cyclin F^{WT}.

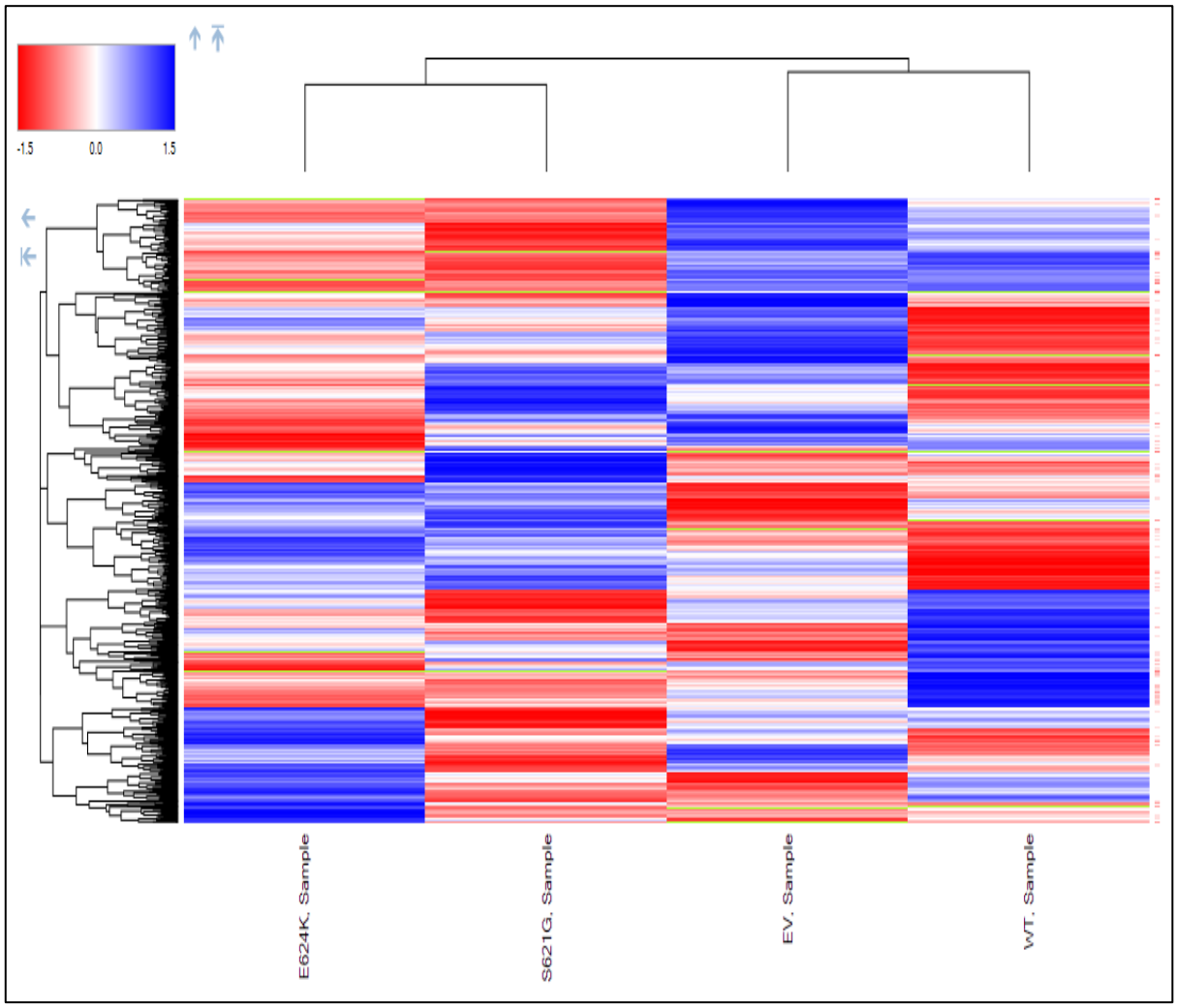

Figure 3-6. Heat map displaying up- and down-regulated global proteins.
The heat map displayed down-regulated proteins (red) measured with a z-score range between -1.5 and 0.0 and displayed up-regulated proteins (blue) measured with a z-score range between 0.0 and 1.5. HEK293 cells expressing empty vector (EV. Sample) and cyclin F^{WT} (WT. Sample) clustered together, and cells expressing cyclin F^{S621G} (S621G. Sample) and cyclin F^{E624K} (E624K. Sample) clustered together. Heat map generated using PD 2.3.

In order to identify specific up- and down-regulated enriched proteins in cells expressing the familial cyclin F^{S621G} and sporadic cyclin F^{E624K} mutants, volcano plots were generated using the log_2 ratio of every quantitated protein (Figure 3-7). The volcano plots display the relationship between the p-value ($\leq$0.05) and log_2 abundance ratios $\geq$1-fold (actual abundance ratio of $\geq$2-fold) for each cyclin F mutant. The cyclin F^{E624K} vs cyclin F^{WT} volcano plot displayed a total of 254 enriched regulated proteins (Figure 3-7.A). A total of 111 up-regulated proteins had a log_2 ratio $\geq$1-fold (actual abundance ratio of $\geq$2-fold) with a statistical significance of $p\leq0.05$, and a total of 143 down-regulated proteins had a log_2 abundance ratio of $\leq$ -1-fold (actual abundance ratio of $\leq$0.5-fold) with a statistical significance of $p\leq0.05$. The cyclin F^{S621G} vs cyclin F^{WT} volcano plot displayed a total of 331 enriched regulated proteins. A total of 105 up-regulated proteins had a log_2 abundance ratio $\geq$1-fold (actual abundance ratio of $\geq$2-fold) with a statistical significance of $p\leq0.05$, and a total of 226 down-regulated proteins had a log_2 abundance ratio $\leq$ -1-fold (actual abundance ratio of $\leq$0.5-fold) with a statistical significance of $p<0.05$ (Figure 3-7.B). Overall, the cells expressing cyclin F^{S621G} displayed a greater abundance of enriched proteins that were either up- or down- regulated compared to the enriched proteins in cells expressing cyclin F^{E624K}.

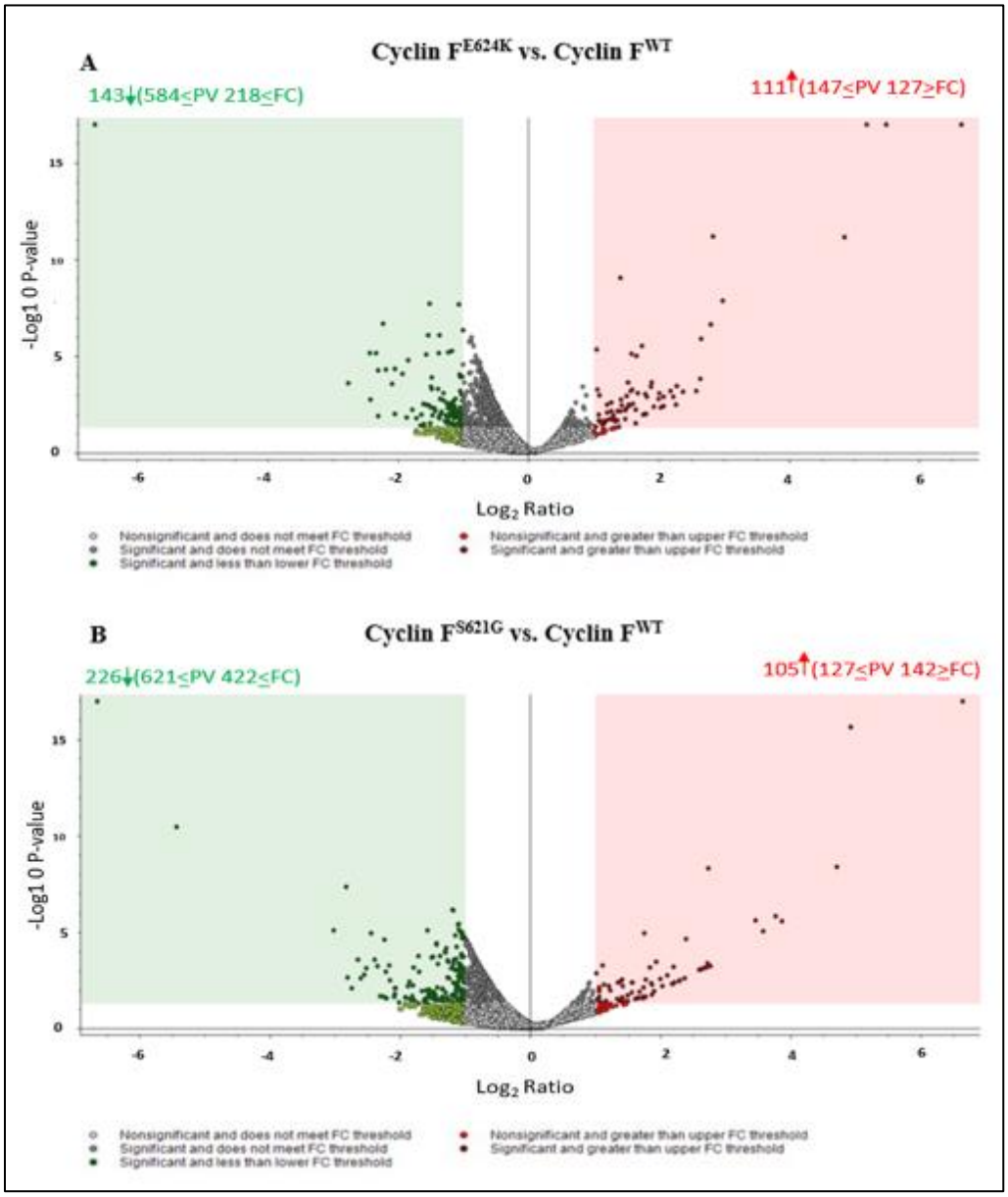

Figure 3-7. Volcano plots of differentially expressed proteins in cells expressing Cyclin F mutants.

A) The cyclin F^{E624K} vs cyclin F^{WT} volcano plot displayed the number of down- and up-regulated proteins that had a $\log_2$ abundance ratios of $\leq$ -1 and $\geq$ 1 respectively that were statistically significant (p-value $\leq$0.05). **B**) The cyclin F^{S621G} vs cyclin F^{WT} volcano plot displayed the number down- and up-regulated proteins that had a $\log_2$ abundance ratios of $\leq$ -1 and $\geq$ 1 respectively that were statistically significant (p-value $\leq$0.05).

3.6. Gene ontology (GO) analysis of up-regulated protein expressed in *CCNF* mutants

To determine whether specific biological processes are initiated in cells with up-regulated proteins expressed in the *CCNF* mutants, GO analysis using PANTHER was employed. A total of eight differentially expressed up-regulated proteins that were categorised into four different biological processes were identified amongst the up-regulated proteins identified in cyclin F^{E624K} and cyclin F^{S621G} (Figure 3-8). In the "Response to stress" GO category, the cyclin F^{E624K} identified four up-regulated proteins (ANKZF1, TMX4, EPPK1, and LIMD1) whilst cyclin F^{S621G} identified three proteins (IGHA1, TMX4, and EPPK1). Two up-regulated proteins each were identified in the "Apoptosis signalling pathway" (BAG4 and MAP4K5) and "Cell death" (TMX4 and BAG4) GO categories. Interestingly the cyclin F^{E624K} identified one up-regulated protein (e.g. SDHD) in the "Oxidation-reduction process" whilst cyclin F^{S621G} identified none. Overall, a high abundance of up-regulated proteins expressed in the cyclin F^{E624K} mutant and the cyclin F^{S621G} mutant compared to the cyclin F^{WT}, was clustered into the "Response to stress", "Apoptosis signalling pathway", "Cell death" and "Oxidative-reduction biological process" GO categories. This demonstrates that cells expressing both the sporadic and familial mutant may be inducing various stress signalling pathways including cell death.

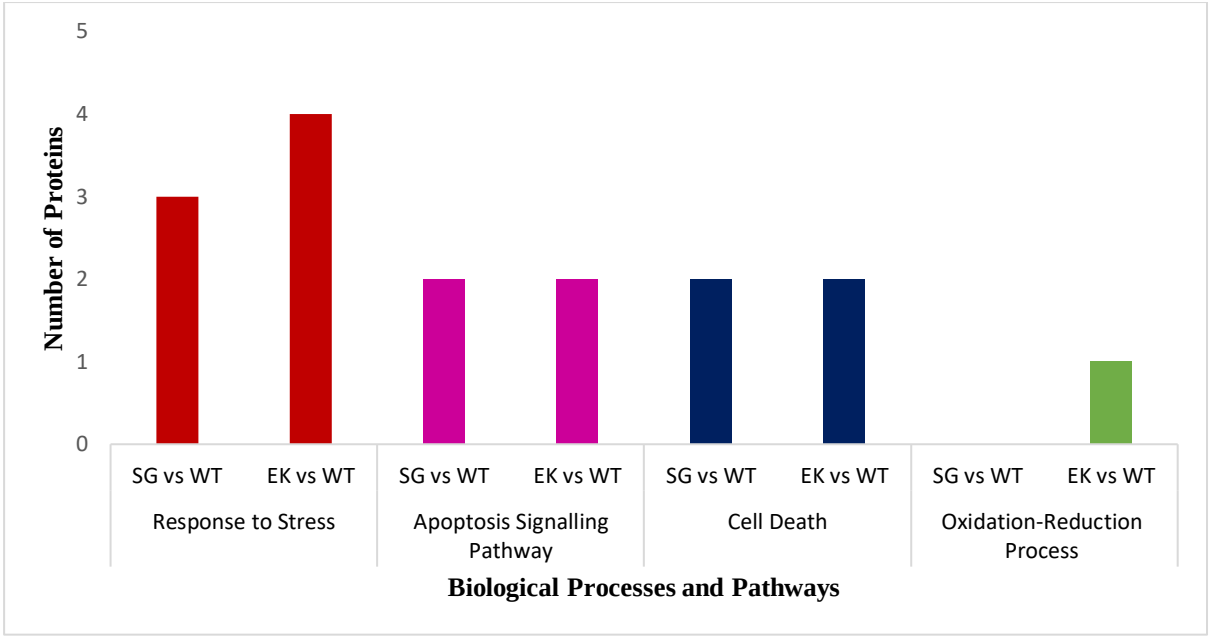

Figure 3-8. GO analysis of up-regulated differentially expressed proteins from global proteomic analysis.
Each biological process and pathway are categorised with a different colour. The column graphs measure the number of proteins identified as up-regulated in HEK293 cells expressing cyclin F^{S621G} and cyclin F^{E624K} relative to cyclin F^{WT}.

Table 3-2. GO analysis of up-regulated differentially expressed proteins from global proteomic analysis.

UniProt ID	Protein Name	Gene Ontology Biological Process	Found in cyclin F^{S621G}	Found in cyclin F^{E624K}
Q9H1E5	**TMX4** -Thioredoxin-related transmembrane protein 4	Response to stress Cell death	Yes Yes	Yes Yes
P58107	**EPPK1** - Epiplakin	Response to stress	Yes	Yes
Q9UGP4	**LIMD1** - LIM domain-containing protein 1	Response to stress	No	Yes
Q9H8Y5	**ANKZF1** - Ankyrin repeat and zinc finger domain-containing protein 1	Response to stress	No	Yes
O95429	**BAG4** - BAG family molecular chaperone regulator 4	Cell death Apoptosis signaling pathway	Yes Yes	Yes Yes
O14521	**SDHD** - Succinate dehydrogenase [ubiquinone] cytochrome b small subunit, mitochondrial	Oxidation-reduction process	No	Yes
Q9Y4K4	**MAP4K5 -** Mitogen-activated protein kinase kinase kinase kinase 5	Apoptosis signaling pathway	Yes	Yes

3.7. Ingenuity pathway analysis (IPA) of label-free quantitative proteomics data

IPA predictions and comparisons for canonical pathways and disease/function mechanisms were made for cells expressing the sporadic cyclin F^{E624K} mutant compared to the familial cyclin F^{S621G} mutant and cyclin F^{WT}.

3.7.1. Canonical pathway analysis of Cyclin F^{E624K} proteins

For the canonical pathways, the Fischer's Exact test scoring method with statistical significance ($p<0.05$) was applied to predict over-represented pathways using the IPA protein database. To determine whether these pathways are predicted to be inhibited or activated, z-scores were applied. The z-score measures the match between expected relationship direction and observed protein expression. Z-score values above 1 predicts the pathway to be activated (orange) and a z-score value below -1 is predicted to be inhibited (blue).

The HEK293 cells expressing cyclin F^{E624K} predicted 20 canonical pathways being either activated or inhibited (Figure 3-9), whilst cells expressing cyclin F^{S621G} predicted six canonical pathways being inhibited (Figure 3-10). Within these pathways, proteins that were identified in cells expressing the cyclin F mutants were measured based on the IPA $\log_2$ fold change. Proteins measured with $\log_2$ 6.64-fold or -6.64-fold were identified as proteins present or not present, respectively, in cells expressing either cyclin F mutant relative to cyclin F^{WT} control.

The second most statistically significant canonical pathway predicted in cells expressing cyclin F^{E624K} was the PTEN signalling, a pathway involved in apoptosis and cell migration (74). It was the only predicted active (z-score=1.633, $p=4.63x10^{-04}$) pathway based on the eight identified proteins, where seven proteins (e.g. NFKB2, PTK2) displayed up-regulation and one protein (RPS6KB1) displayed down regulation (Table 3-3). The remaining 19 canonical pathways were predicted to be inhibited, with Rac signalling (z-score=-2.53, $p=1.27x10^{-05}$) being the most statistically significant pathway inhibited based on the 10 proteins identified (Table 3-4). The down-regulated (NFKB2) and loss-of-binding proteins (PIK3C2A, PTK2, PIP51A) were clustered around Rac and predicted to affect actin cytoskeleton regulation and cell viability (Figure 3-11). In addition, the actin signalling pathway (z-score=-2.714, $p=1.64x10^{-04}$) was also predicted to be inhibited, with 12 down-regulated proteins identified (Table 3-5).

Like the cyclin F^{E624K}, the actin cytoskeleton signalling pathway was also predicted to be inhibited (z-score = -2.5, $p=4.08x10^{-07}$) in cells expressing the familial cyclin F^{S621G} mutant. Although similar down-regulated proteins (e.g. CYFIP1, ROCK2, VCL) were identified between the two cyclin F mutants, the PIP5K1A protein was up-regulated in cells expressing cyclin F^{S621G} (log_2 2.21-fold, p=0.0368), whereas it was not identified in cells expressing cyclin F^{E624K} (log_2 -6.64-fold, $p=3.5x10^{-16}$).

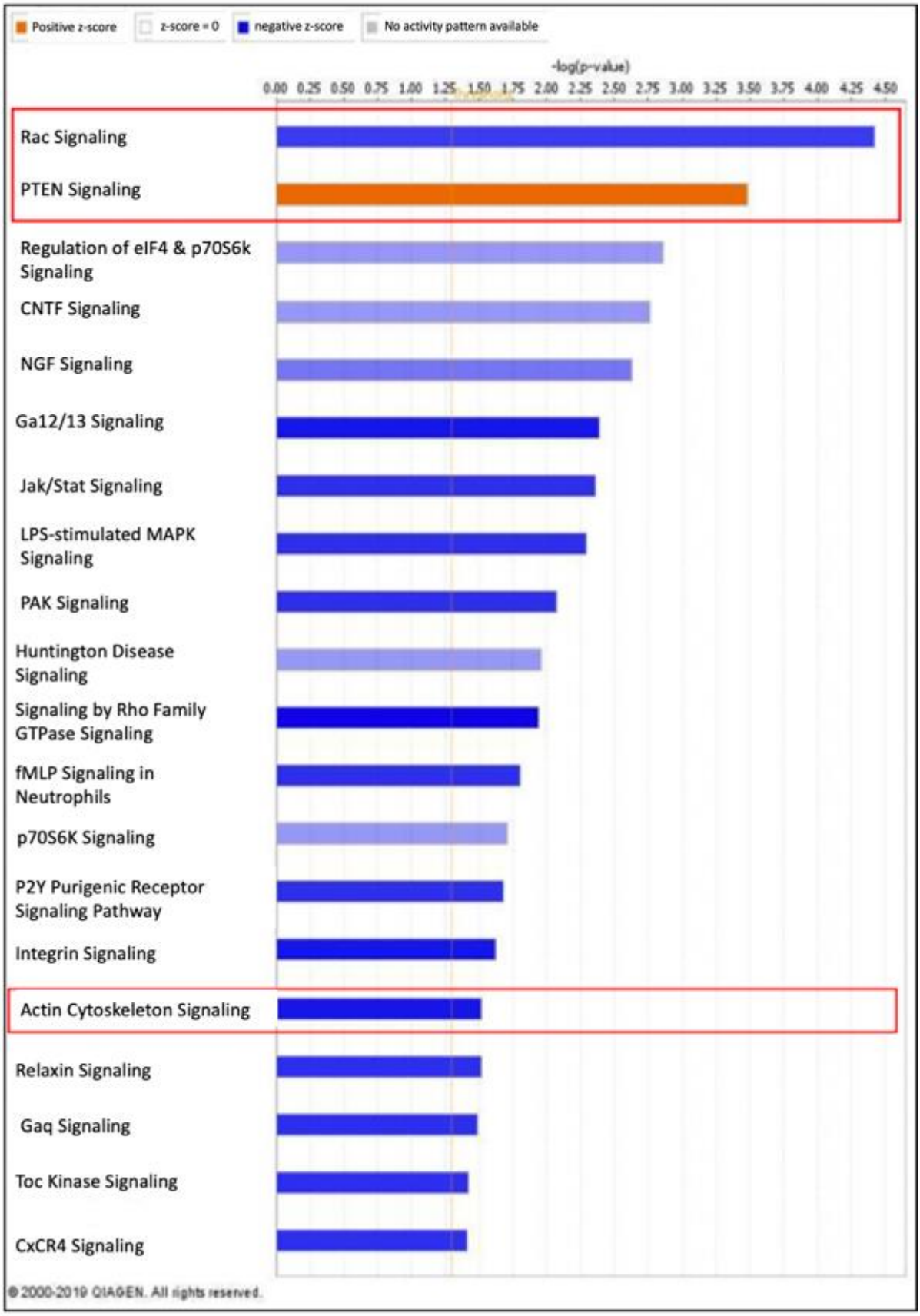

Figure 3-9. Top canonical pathways identified for cells expressing Cyclin F^{E624K}.
Figure generated with IPA.

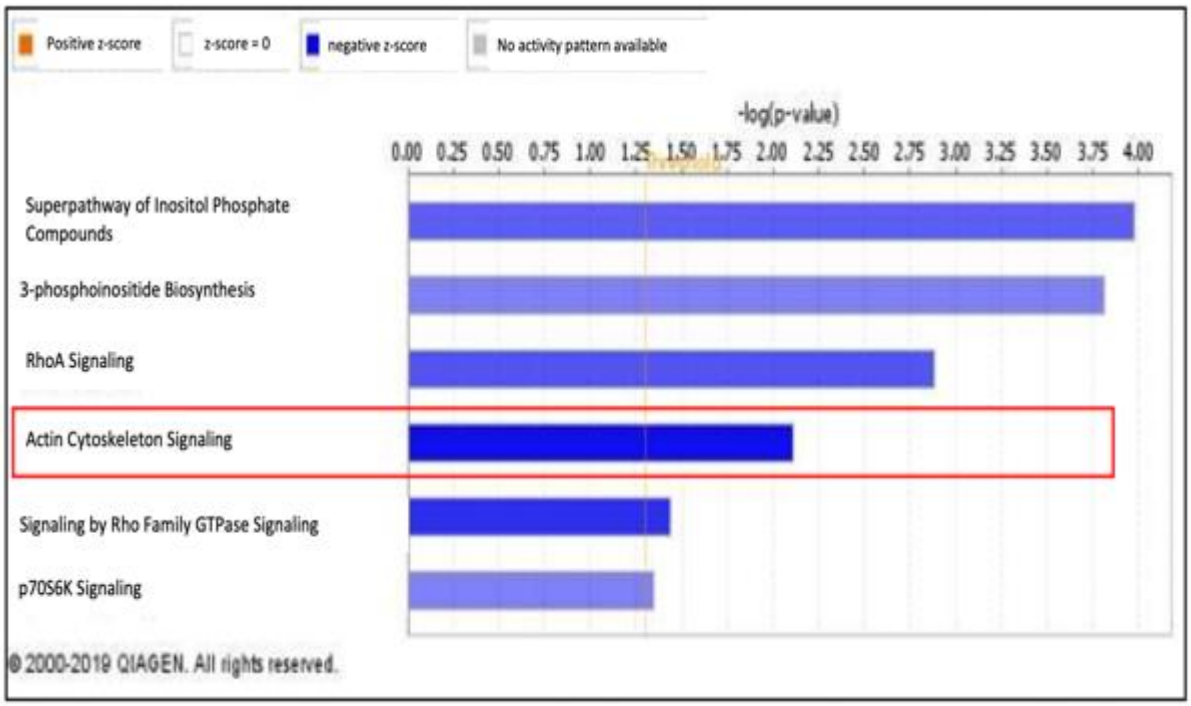

Figure 3-10. Top canonical pathways identified for cells expressing Cyclin F^{S621G}.
Figure generated with IPA.

Table 3-3. PTEN signalling proteins identified in cells expressing Cyclin F^{E624K}.
Up-regulated (red) and down-regulated (green) proteins based on IPA log_2 fold change. Normalised to cyclin F^{WT}.

UniProt ID	Protein Name	Log_2 Fold Change (EK/WT)	p-value (EK/WT)
P08069	**IGF1R** - insulin like growth factor 1 receptor	-6.64	$3.5x10^{-16}$
P11717	**IGF2R** - insulin like growth factor 2 receptor	-1.623	0.0314
P05556-1	**ITGB1** - integrin subunit beta 1	-1.65	0.00339
Q5TCQ9-1	**MAGI3** - membrane associated guanylate kinase, WW and PDZ domain containing 3	-6.64	$3.5 x10^{-16}$
Q02750	**MAP2K1** - mitogen-activated protein kinase kinase 1	-2.257	0.0291
Q00653-1	**NFkB2** - nuclear factor kappa B subunit 2	-2.358	0.0435
Q05397-5	**PTK2** - protein tyrosine kinase 2	-6.64	$3.5 x10^{-16}$
P23443-1	**RPS6KB1** - ribosomal protein S6 kinase B1	2.279	0.00627

Table 3-4. Rac signalling proteins identified in cells expressing Cyclin F^{E624K}.
Up-regulated (red) and down-regulated (green) proteins based on IPA log_2 fold change. Normalised to cyclin F^{WT}.

UniProt ID	Protein Name	Log_2 Fold Change (EK/WT)	p-value (EK/WT)
Q7L576-1	**CYFIP1** - cytoplasmic FMR1 interacting protein 1	-1.792	$8.77x10^{-05}$
Q9Y4H2	**IRS2** - insulin receptor substrate 2	-4.95	0.00128
P05556-1	**ITGB1** - integrin subunit beta 1	-1.65	0.00339
Q02750	**MAP2K1** - mitogen-activated protein kinase kinase 1	-2.257	0.0291
Q00653-1	**NFkB2**- nuclear factor kappa B subunit 2	-2.358	0.0435
P42356	**PI4KA** -phosphatidylinositol 4-kinase alpha	-1.757	0.0213
O00443	**PIK3C2A** - phosphatidylinositol-4-phosphate 3-kinase catalytic subunit type 2 alpha	-6.64	$3.5x10^{-16}$
Q99755	**PIP5K1A** - phosphatidylinositol-4-phosphate 5-kinase type 1 alpha	-6.64	$3.5x10^{-16}$
Q05397-5	**PTK2** - protein tyrosine kinase 2	-6.64	$3.5x10^{-16}$
P23443-1	**RPS6KB1** - ribosomal protein S6 kinase B1	2.279	0.00627

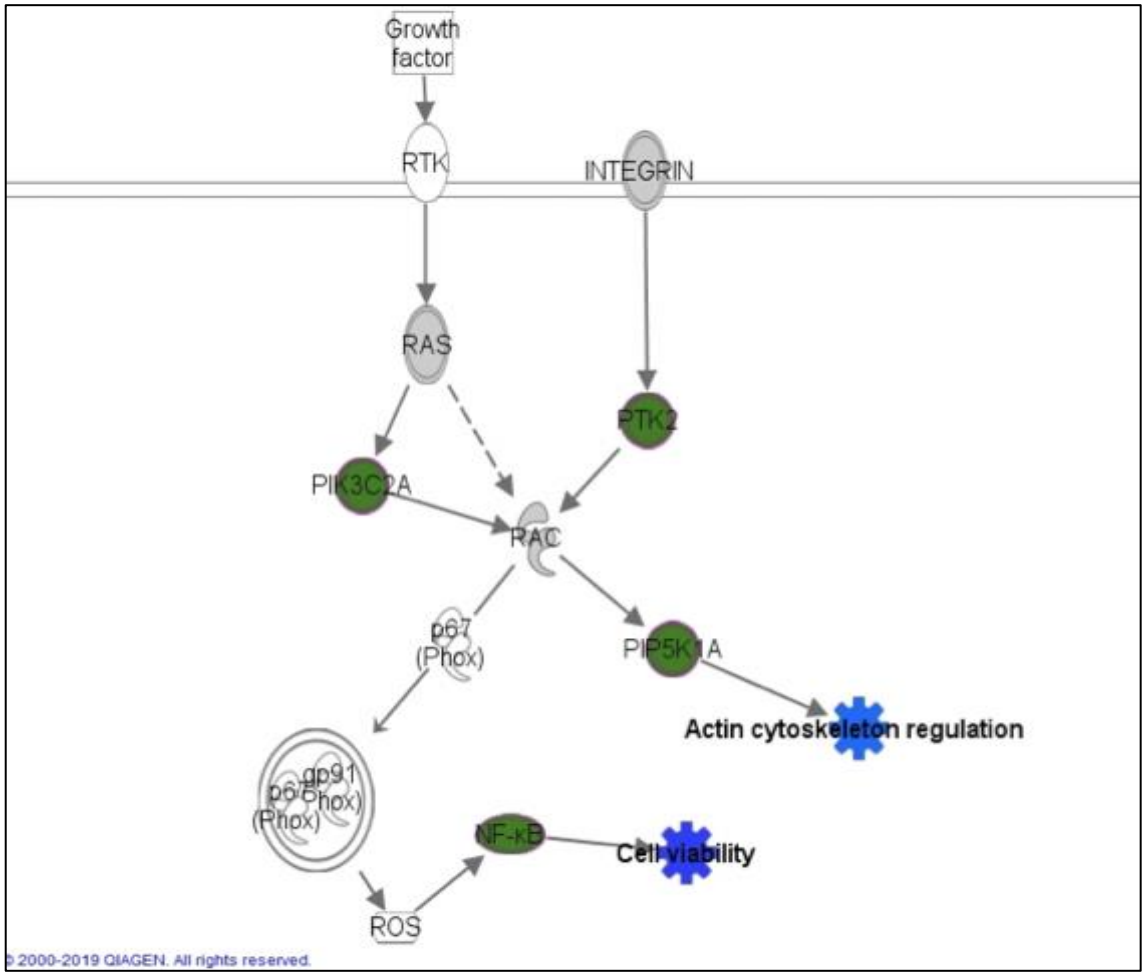

Figure 3-11. Rac signalling pathway

Down-regulated and non-identified proteins (green) in cells expressing cyclin F^{E624K}. Proteins identified in cells expressing cyclin F^{WT}, cyclin F^{S621G}, and cyclin F^{E624K} (grey) and predicted proteins/complexes in signalling pathway (white). Predicted inhibition (blue) for actin cytoskeleton regulation and cell viability mechanisms. Pathway generated using IPA.

Table 3-5. Actin cytoskeleton signalling proteins identified in cells expressing Cyclin F^{E624K} and Cyclin F^{S621G}.

Up-regulated (red) and down-regulated (green) proteins based on IPA log_2 fold change. Normalised to cyclin F^{WT}.

UniProt ID	Protein Name	Log_2 Fold Change (EK/WT)	p-value (EK/WT)	Log_2 Fold Change (SG/WT)	p-value (SG/WT)
Q7L576-1	**CYFIP1** - cytoplasmic FMR1 interacting protein 1	-1.792	$8.77x10^{-05}$	-1.898	0.00184
Q9Y4H2	**IRS2** - insulin receptor substrate 2	-4.95	0.00128		
P05556-1	**ITGB1** - integrin subunit beta 1	-1.65	0.00339	-1.715	0.0117
Q02750	**MAP2K1** - mitogen-activated protein kinase kinase 1	-2.257	0.0291		
Q7Z406-2	**MYH14** - myosin heavy chain 14	-1.577	0.00752		
O00443	**PIK3C2A** - phosphatidylinositol-4-phosphate 3-kinase catalytic subunit type 2 alpha	-6.64	3.5	-6.64	$3.07 x10^{-16}$
Q99755	**PIP5K1A** - phosphatidylinositol-4-phosphate 5-kinase type 1 alpha	-6.64	$3.5x10^{-16}$	2.21	0.0368
O14974	**PPP1R12A** - protein phosphatase 1 regulatory subunit 12A	-1.558	0.00361		
Q05397-5	**PTK2** - protein tyrosine kinase 2	-6.64	$3.5 x10^{-16}$		
O75116	**ROCK2** - Rho associated coiled-coil containing protein kinase 2	-1.739	0.00611	-2.075	0.0034
Q9Y490	**TLN1** - talin 1	-1.502	0.0116	-1.901	0.00139
P18206	**VCL** - vinculin	-1.55	0.00608	-1.555	0.0313
P12814-1	**ACTN1** - actinin alpha 1			-1.689	0.0102
O43707	**ACTN4** - actinin alpha 4			-1.667	0.0122
P25054-1	**APC** - Adenomatous polyposis coli protein			-3.257	0.0143
O60610-1	**DIAPH1 – protein** diaphanous related formin 1			-2.045	0.000479
P21333	**FLNA** - filamin A			-1.838	0.00247
P35580	**MYH10** - myosin heavy chain 10			-1.916	0.00118
Q7Z406-2	**MYH14** - myosin heavy chain 14			-2.066	0.000455
P35579-1	**MYH9** - myosin heavy chain 9			-1.912	0.00121
Q9Y2A7-2	**NCKAP1** - NCK associated protein 1			-1.835	0.00865
Q99570	**PIK3R4** - phosphoinositide-3-kinase regulatory subunit 4			-2.037	0.0372
O14974	**PPP1R12A** - protein phosphatase 1 regulatory subunit 12A			-1.689	0.0117

3.7.2. Disease/Function analysis of cells expressing Cyclin F^{E624K} proteins

Using IPA, comparative analysis for disease/function mechanisms were predicted with quantitative proteomic data from HEK293 cells expressing empty vector, cyclin F^{S621G}, and cyclin F^{E624K}, that were normalised to the cyclin F^{WT} control. Using the z-score measurement (>1-fold), various disease/function mechanisms were predicted to be inhibited (blue) or activated (orange). Three disease/function processes were selected for this comparative analysis. These processes included cell viability, cell death, and apoptosis (Figure 3-12). Interestingly, expression of cyclin F^{E624K} and cyclin F^{S621G} predicted the activation of apoptosis (z-score=1.29, $p=4.29x10^{-05}$ [E624K]; z -score=1.905, $p=3.6x10^{-08}$ [S621G]) and cell death (z-score=1.726, $p=1.2x10^{-06}$ [E624K]; z-score=2.725, $p=3.85x10^{-09}$ [S621G]) and predicted the inhibition of cell viability (z-score=-4.024, $p=3.51x10^{-05}$ [E624K]; z-score=-4.414, $p=3.51x10^{-10}$). Notably, no activation or inhibition of disease/function processes were predicted when comparing the empty vector to cyclin F^{WT}.

To gain further insight into which differentially expressed cyclin F^{E624K} proteins were involved and to determine whether these proteins were up- or down-regulated, clustered protein networks were generated. A total of 54 proteins contributed to the inhibition of cell viability; six proteins were selected and displayed in a protein network (Figure 3-13.A). Up-regulation was identified in BIRC2 (log_2 4.852-fold, $p=2.43x10^{-10}$), and KEAP1 (log_2 6.64-fold, $p=3.5x10^{-16}$) that act as activators for cell viability. Down-regulation was identified in HIP1 (log_2 -2.037-fold, p=0.0435), HSPA6 (log_2 -6.64-fold, $p=3.5x10^{-16}$), NFKB2 (log_2 -2.358-fol, p=0.0435), and USP10 (log_2 -1.678-fold, p=0.00686) that act as activators for cell viability.

A total of 114 proteins contributed to the activation of cell death activity, of which eight proteins were selected and displayed in a protein network (Figure 3-13.B). Up-regulation was identified in BAG4 (log_2 2.37-fold, p=0.0104), BIRC2 (log_2 4.852-fold, $p=2.43x10^{-10}$), KEAP1 (log_2 6.64-fold, $p=3.5x10^{-16}$), UACA (log_2 2.005-fold, p=0.0122), and UBR2 (log_2 6.64-fold, $p=3.\ 5x10^{-16}$) that acted as activators for cell death. Down-regulation was identified in HIP1 (log_2 -2.037-fold, p=0.0138), NFKB2 (log_2 -2.358-fold, p=0.0435), and USP10 (log_2-1.678-fold, p-value=0.00686) that acted as activators for cell death.

A total of 88 proteins contributed to the activation of apoptosis activity. Of the 88 proteins, five proteins were selected and displayed in a protein network (Figure 3-13.C). Up-regulation was identified in BAG4 (log_2=2.371, p=0.0104), BIRC2 ($log_2$4.852-fold, $p=2.43x10^{-10}$), KEAP1 ($log_2$6.64-fold, $p=3.5x10^{-16}$), and UBR2 ($log_2$6.64-fold, $p=3.5x10^{-16}$) acting as activators for

apoptosis. Down regulation was identified in NFKB2 (log_2 -2.358-fold, p=0.0435) acting as an activator for apoptosis.

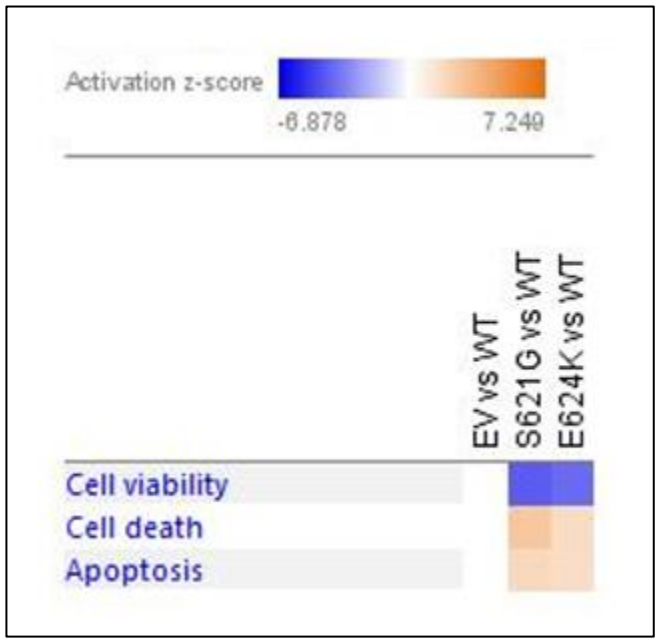

Figure 3-12. Disease/Function comparative analysis of cells expressing empty vector and Cyclin F mutants.
Heat map generated with IPA to predict the activation inhibition of biological processes in the cellular lysates of cells expressing empty vector control (EV), cyclin F^{S621G} (S621G) and cyclin F^{E624K} (E624K), normalised to cyclin F^{WT} (WT) control. Inhibition of cell viability was predicted in cyclin F^{S621G} and cyclin F^{E624K}. Activation of cell death and apoptosis was predicted in cyclin F^{S621G} and cyclin F^{E624K}. No prediction was made for empty vector control in all biological processes.

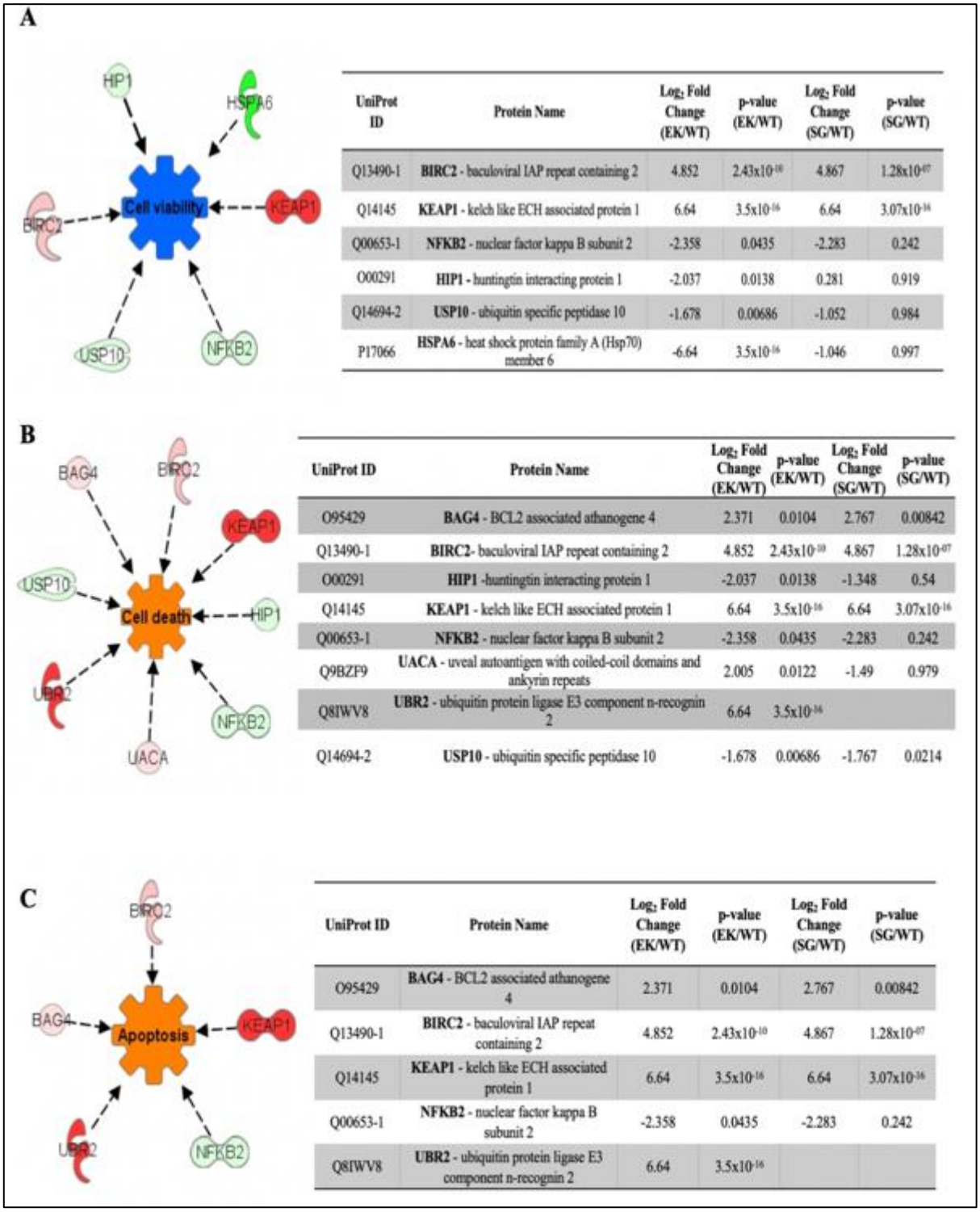

UniProt ID	Protein Name	Log_2 Fold Change (EK/WT)	p-value (EK/WT)	Log_2 Fold Change (SG/WT)	p-value (SG/WT)
Q13490-1	**BIRC2** - baculoviral IAP repeat containing 2	4.852	$2.43x10^{-10}$	4.867	$1.28x10^{-07}$
Q14145	**KEAP1** - kelch like ECH associated protein 1	6.64	$3.5x10^{-16}$	6.64	$3.07x10^{-16}$
Q00653-1	**NFKB2** - nuclear factor kappa B subunit 2	-2.358	0.0435	-2.283	0.242
O00291	**HIP1** - huntingtin interacting protein 1	-2.037	0.0138	0.281	0.919
Q14694-2	**USP10** - ubiquitin specific peptidase 10	-1.678	0.00686	-1.052	0.984
P17066	**HSPA6** - heat shock protein family A (Hsp70) member 6	-6.64	$3.5x10^{-16}$	-1.046	0.997

UniProt ID	Protein Name	Log_2 Fold Change (EK/WT)	p-value (EK/WT)	Log_2 Fold Change (SG/WT)	p-value (SG/WT)
O95429	**BAG4** - BCL2 associated athanogene 4	2.371	0.0104	2.767	0.00842
Q13490-1	**BIRC2**- baculoviral IAP repeat containing 2	4.852	$2.43x10^{-10}$	4.867	$1.28x10^{-07}$
O00291	**HIP1** -huntingtin interacting protein 1	-2.037	0.0138	-1.348	0.54
Q14145	**KEAP1** - kelch like ECH associated protein 1	6.64	$3.5x10^{-16}$	6.64	$3.07x10^{-16}$
Q00653-1	**NFKB2** - nuclear factor kappa B subunit 2	-2.358	0.0435	-2.283	0.242
Q9BZF9	**UACA** - uveal autoantigen with coiled-coil domains and ankyrin repeats	2.005	0.0122	-1.49	0.979
Q8IWV8	**UBR2** - ubiquitin protein ligase E3 component n-recognin 2	6.64	$3.5x10^{-16}$		
Q14694-2	**USP10** - ubiquitin specific peptidase 10	-1.678	0.00686	-1.767	0.0214

UniProt ID	Protein Name	Log_2 Fold Change (EK/WT)	p-value (EK/WT)	Log_2 Fold Change (SG/WT)	p-value (SG/WT)
O95429	**BAG4** - BCL2 associated athanogene 4	2.371	0.0104	2.767	0.00842
Q13490-1	**BIRC2** - baculoviral IAP repeat containing 2	4.852	$2.43x10^{-10}$	4.867	$1.28x10^{-07}$
Q14145	**KEAP1** - kelch like ECH associated protein 1	6.64	$3.5x10^{-16}$	6.64	$3.07x10^{-16}$
Q00653-1	**NFKB2** - nuclear factor kappa B subunit 2	-2.358	0.0435	-2.283	0.242
Q8IWV8	**UBR2** - ubiquitin protein ligase E3 component n-recognin 2	6.64	$3.5x10^{-16}$		

Figure 3-13. Cyclin F^{E624K} differentially expressed proteins predicted in cell viability inhibition, cell death activation and apoptosis activation.

The log_2 fold change and p-values are listed for cells expressing the sporadic cyclin F^{E624K} mutant and familial cyclin F^{S621G} mutant for each of the corresponding disease/function mechanisms. **A)** Clustered protein network for the cyclin F^{E624K} differentially expressed proteins identified in cell viability inhibition, displaying up-regulation (red) and down-regulation (green). **B)** Clustered protein network for the cyclin F^{E624K} differentially expressed proteins identified in cell death activation, displaying up-regulation and down-regulation. **C)** Clustered protein network for the cyclin F^{E624K} differentially expressed proteins identified in apoptosis activation, displaying up-regulation and down-regulation. Figure generated with IPA.

3.8. Validation of Cyclin F immunoprecipitations to characterise the interactome

Immunoprecipitations of cyclin F followed by MS was used to reveal whether the sporadic cyclin F^{E624K} mutation promoted a gain- or loss- of interaction with its putative protein partners and potentially new protein interactors. Prior to MS analysis, immunoprecipitation for cyclin-FLAG was carried out for HEK293 cells transfected with pcDNA3.1 empty vector, cyclin F^{WT}, cyclin F^{S621G}, and cyclin F^{E624K}. Two additional negative controls were added to the immunoprecipitation procedure, a negative control that consisted of NP40 lysis buffer and an IgG negative control that consisted of all transfected samples to identify non-specific proteins. To validate that immunoprecipitation of cyclin F-FLAG was successful, immunoblotting and verifying known cyclin F protein interactors were performed.

Immunoblotting for FLAG revealed overexpression of the FLAG tagged cyclin F in lanes corresponding to immunoprecipitant samples (IP) which consisted of the anti-FLAG antibody attached to cyclin F-FLAG protein and its interactors. The protein levels in the starting material (SM) and flow through (FT) lanes display decreased levels compared to the IP lane indicating a high amount of enrichment from the IP. The SM samples demonstrate that cyclin F-FLAG is present in original cell lysates, and the FT demonstrates that almost all cyclin F-FLAG was immunoprecipitated and consisted of mainly non-specific proteins. Cyclin F-FLAG proteins in the FT lanes is expected as the cells were transfected with overexpressed cyclin F-FLAG. Immunoblotting for negative control (lysis buffer) and empty vector control lanes revealed no expression and immunoblotting of IgG control expressed non-specific binding proteins. Immunoblotting for *beta*-tubulin was used as a loading control (Figure 3-14.A) The immunoprecipitation efficiency of cyclin F-FLAG in cyclin F^{WT} (42.7-fold), cyclin F^{S621G} (34.3-fold) and cyclin F^{E624K} (32.3-fold) revealed overexpression of immunoprecipitated cyclin F-FLAG compared to the empty vector controls (Figure 3-14.B). For all statistical analyses, n=3.

According to the STRING biological database, a prediction site for PPIs, there are ten known cyclin F protein interactors. Of the ten cyclin F protein interactors, four protein interactors (FBXW11, CUL1, UBE2S, and SKP1) in the HEK293 cells expressing *CCNF*^{WT} using label-free immunoprecipitation proteomic analysis were identified (Table 3-6). Proteins measured with 6.64-fold were identified as proteins present in cells expressing the cyclin F^{WT} and was not identified in the negative control consisting of NP40 lysis buffer. Thus, the

immunoprecipitation of cyclin F data is confirmed with its validated and published protein interactors.

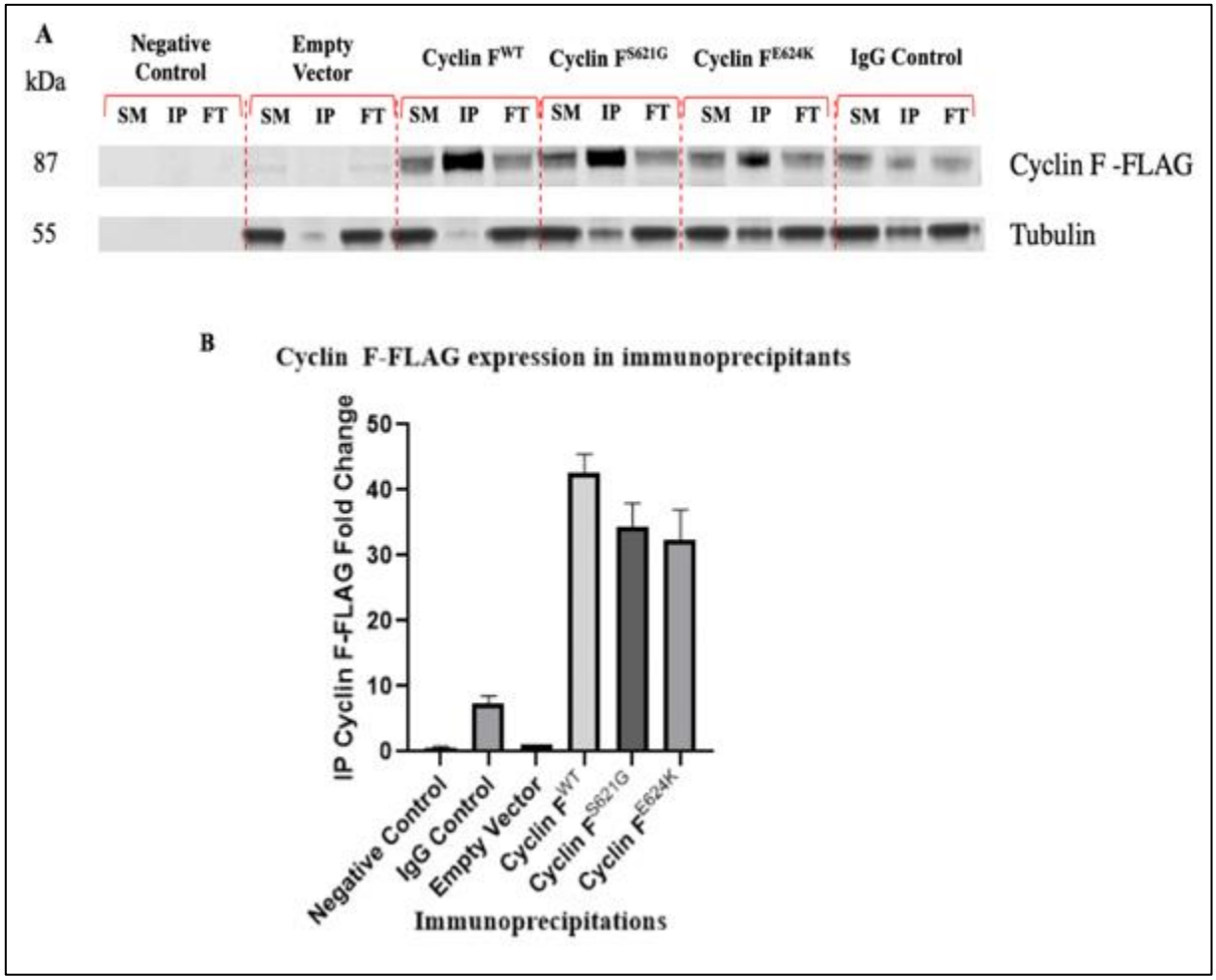

Figure 3-14. Cyclin F-FLAG expression levels present in Cyclin F immunoprecipitants.
A) Immunoblot of cyclin F-FLAG expression levels are relatively consistent across lanes *CCNF* transgenes. In the negative control (lysis buffer) and empty vector control lane, there was no presence of cyclin F-FLAG. In the IgG control lane displayed expression of non-specific proteins. The *beta*-tubulin loading control was used and displayed similar expression levels across all samples. **B)** Statistical analysis of the cyclin F-FLAG expression levels for all samples normalised to empty vector control. For all statistical analyses, n=3.

Table 3-6. Published Cyclin F protein interactors.
Cyclin F protein interactors that were present in label-free proteomic analysis of immunoprecipitated protein lysates. The fold change of cyclin F^{WT} normalised to negative control (lysis buffer).

UniProt ID	Protein Name	Log_2 Fold Change (WT/Neg. Ctrl)
Q9UKB1-1	**FBXW11** - F-box/WD repeat-containing protein 11	6.64
Q13616	**CUL1** - Cullin-1	6.64
Q16763	**UBE2S** - Ubiquitin-conjugating enzyme E2 S	6.64
P63208	**SKP1** - S-phase kinase-associated protein 1	6.64

3.9. Characterisation of enriched Cyclin F protein interactors from immunoprecipitated samples

Unbiased label-free proteomic analysis was performed on immunoprecipitated cyclin F from the HEK293 cells expressing pcDNA3.1 empty vector, cyclin F^{WT}, cyclin F^{S621G}, and cyclin F^{E624K} to characterise cyclin F protein interactors. Using this data, predictions and comparisons can be made between the differentially expressed cyclin F protein interactors that may be altering cyclin F's interactome. Thus, ultimately affecting various signalling pathways and disrupting the proteostasis of cells. For the following immunoprecipitation proteomic analysis, the cyclin F^{WT} was used as the baseline for comparisons to cyclin F^{S621G} and cyclin F^{E624K} to determine the abundance ratios of all quantifiable proteins that are indicative of *enhanced* (actual abundance $\geq$ 2-fold) or reduced (actual abundance $\leq$ 0.5-fold) protein-protein interactions. For proteomic analysis of the three biological immunoprecipitated replicates from three transfection replicates, equivalent default quantitation settings using the PD 2.3 were applied, as described in section 2.15.

Across all three biological samples, a total of 2,317 proteins were identified in IPs from cells expressing empty vector, cyclin F^{WT}, cyclin F^{S621G}, and cyclin F^{E624K}. Between all four samples, the empty vector sample identified 116 *unique* proteins (5%), the cyclin F^{WT} sample identified 49 *unique* proteins (2.1%), the cyclin F^{S621G} identified 83 *unique* proteins (3.6%), and cyclin F^{E624K} identified 26 *unique* proteins (1.1%) (Figure 3-15).

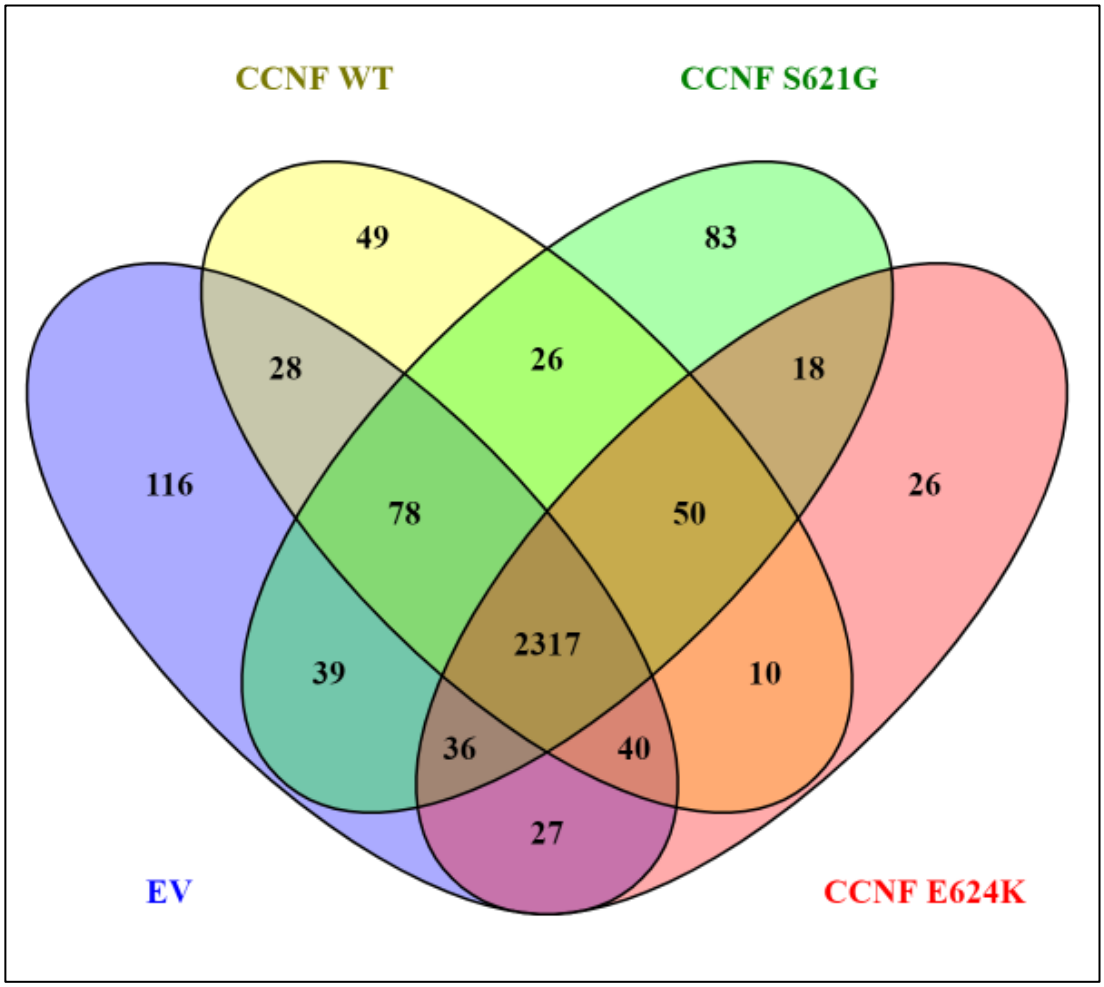

Figure 3-15. Quantified *shared* and *unique* Cyclin F immunoprecipitant proteins identified in all four samples.
Venn diagram illustrating the quantified *shared* and *unique* proteins identified in cyclin F immunoprecipitants from the HEK293 cells transfected with empty vector control, cyclin F^{WT}, cyclin F^{S621G}, and cyclin F^{E624K}. For all statistical analyses, n=3. Venn diagram generated with Venny 2.1 (73)

To gain a more consistent insight into the differences in IPs between the *CCNF* transgenes and to compare the mutants to a single control, cyclin F^{WT}, the protein identifications from transfected with the empty vector was removed (Figure 3-16). Comparing protein identifications of the IPs from only cells expressing *CCNF* transgenes, a total of 2,367 proteins were identified across all three biological samples. Of these 2,367 proteins, 77 were *unique* cyclin F^{WT} proteins (3.3%), 122 were *unique* cyclin F^{S621G} proteins (5.2%), and 53 were *unique* cyclin F^{E624K} proteins (2.2%). Between each sample, the cyclin F^{WT} *shared* 104 proteins with cyclin F^{S621G} (4.4%), the cyclin F^{S621G} *shared* 54 proteins with cyclin F^{E624K} (2.3%), and the cyclin F^{E624K} *shared* 50 proteins with the cyclin F^{WT} (2.1%).

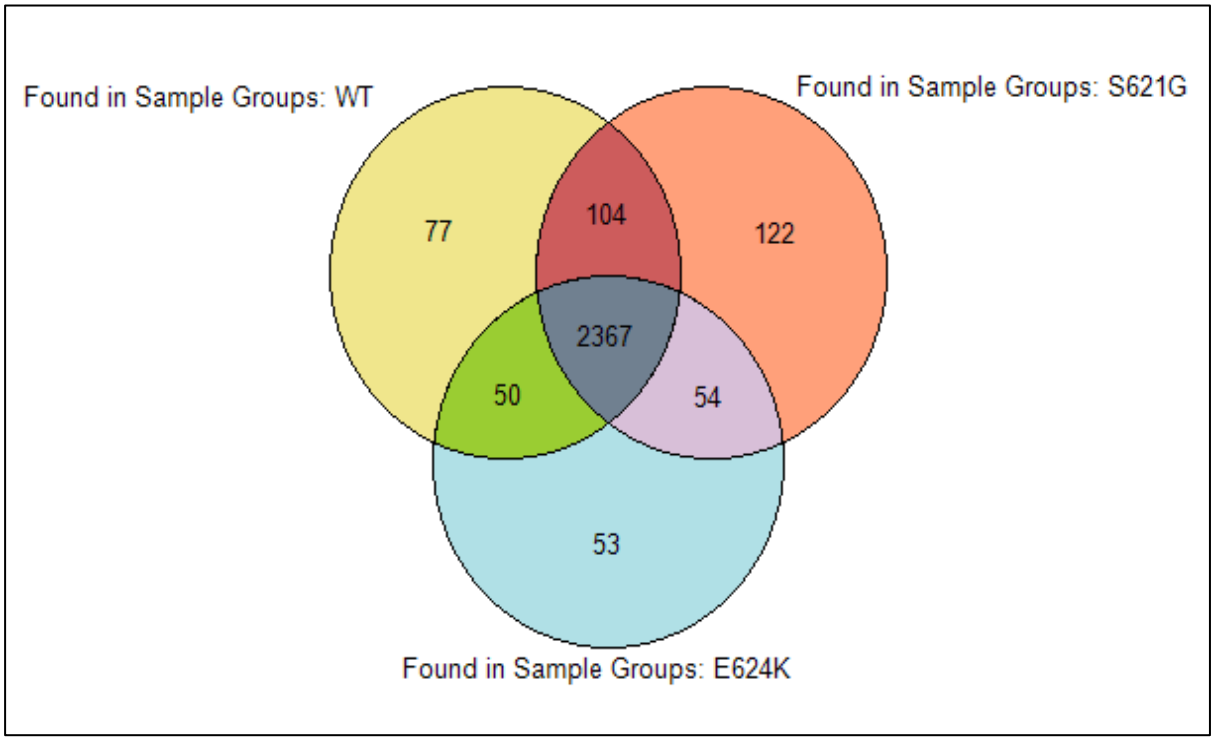

Figure 3-16. Quantified s*hared* and *unique* proteins identified in Cyclin F immunoprecipitants in cells expressing *CCNF* transgenes.
Venn diagram illustrating the number of *shared* and *unique* proteins identified from cyclin F immunoprecipitants of cells expressing cyclin F^{WT}, cyclin F^{S621G}, and cyclin F^{E624K}. For all statistical analysis, n=3. Venn diagram generated using PD 2.3.

3.10. Unbiased immunoprecipitation of Cyclin F proteomics reveal differential binding activity between *CCNF* mutants

In order to identify specific *enhanced*-binding and *reduced*-binding cyclin F protein interactors enriched in HEK293 cells expressing the familial cyclin F^{S621G} mutant and the sporadic cyclin F^{E624K} mutant, volcano plots were generated using a $\log_2$ ratio of every quantitated IP protein (Figure 3-17). The volcano plots display the relationship between the p-value ($\leq$0.05) and $\log_2$ abundance ratios $\geq$1-fold (actual abundance ratio of $\geq$2-fold) for each cyclin F mutant. The cyclin F^{E624K} vs cyclin F^{WT} volcano plot displayed a total of 322 enriched proteins. A total of 155 proteins displayed *enhanced* binding activity between cyclin F and its interactors with $\log_2$ ratio $\geq$1-fold (actual abundance ratio of $\geq$2-fold) with a statistical significance of $p\leq0.05$, and a total of 167 proteins displayed *reduced* binding activity between cyclin F and its interactors with a $\log_2$ abundance ratio of $\leq$ -1-fold (actual abundance ratio of $\leq$0.5-fold) with a statistical significance of $p\leq0.05$. (Figure 3-17.A). The cyclin F^{S621G} vs cyclin F^{WT} volcano plot displayed a total of 313 enriched proteins. A total of 190 proteins displayed *enhanced* binding activity between cyclin F and its interactors with a $\log_2$ abundance ratio $\geq$1-fold (actual abundance ratio of $\geq$2-fold) with a statistical significance of $p\leq0.05$, and a total of 123 proteins displayed

reduced binding activity between cyclin F and its interactors with a $\log_2$ abundance ratio $\geq$1-fold (actual abundance ratio of $\geq$2-fold) with a statistical significance of $p \leq 0.05$ (Figure 3-17.B Overall the sporadic cyclin F^{E624K} mutant displayed differences in the cyclin F interactome compared with the familial cyclin F^{S621G} and cyclin F^{WT} IPs. This suggests that different pathways may be initiated or altered with the expression of the sporadic cyclin F^{E624K} mutant.

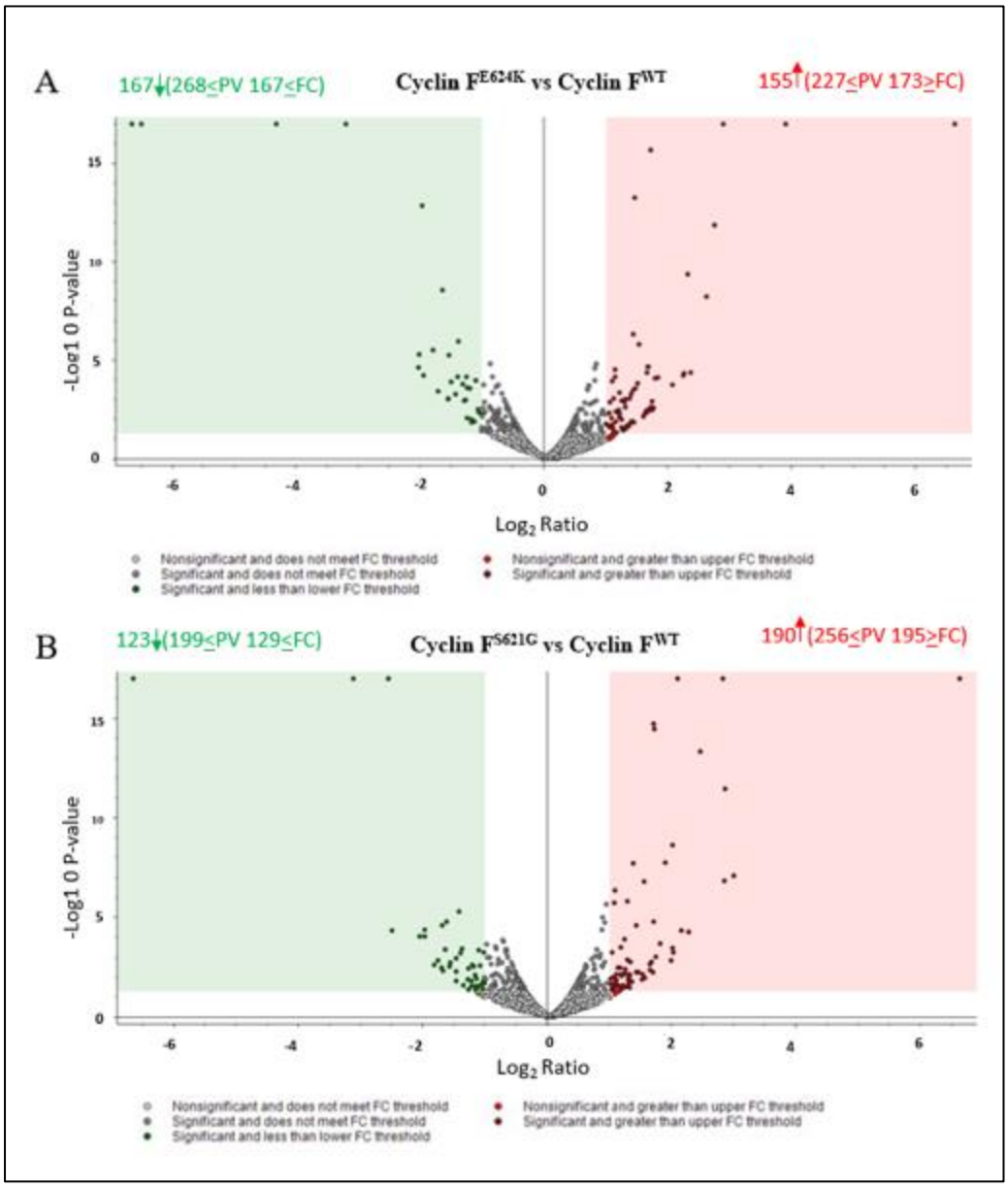

Figure 3-17. Volcano plots displaying *enhanced*-binding and *reduced*-binding Cyclin F protein interactors.
A) The cyclin F^{E624K} vs cyclin F^{WT} volcano plot displayed the number *enhanced*-binding and *reduced-binding* proteins that had a $\log_2$ abundance ratios of $\leq$ -1 and $\geq$ 1 respectively that were statistically significant (p-value $\leq$0.05). **B**) The cyclin F^{S621G} vs cyclin F^{WT} volcano plot displayed number *enhanced*-binding and *reduced-binding* proteins that had a $\log_2$ abundance ratios of $\leq$ -1 and $\geq$ 1 respectively that were statistically significant (p-value $\leq$0.05).

3.11. Gene ontology (GO) analysis of Cyclin F protein interactors

To determine the specific biological processes and pathways that are initiated with the immunoprecipitated cyclin F protein interactors in cells expressing cyclin F^{WT}, cyclin F^{S621G} and cyclin F^{E624K}, GO analysis using PANTHER was employed on two differentially expressed data sets. The first GO analysis was made with the *unique* and *shared* proteins between *CCNF* transgenes. The second GO analysis was on the *enhanced*-binding cyclin F protein interactors between cyclin F^{S621G} and cyclin F^{E624K} mutants.

Seven different biological processes and pathways were identified for the enriched *unique* and *shared* cyclin F protein interactors, based on protein abundance in each category (Figure 3-18). Across the different biological processes and pathways, one or more *unique* and/or *shared* proteins were identified in each category for the cyclin F^{E624K} mutant. For cells expressing the cyclin F^{E624K} mutant, the most abundant cyclin F protein interactors were clustered to the "Parkinson's disease" GO category. This included four proteins (HSPA14, PSMB3, STX12, and MAPK1) suggesting that it contributes to the interactome of this neurodegenerative disease. Whereas, the cyclin F^{E624K} mutant displayed a low abundance of one cyclin F protein interactor (HSPA14) in "Protein folding", one cyclin F protein interactor (VAT1) in "Huntington's disease", and one cyclin F protein interactor (PSMD7) in the "Ubiquitin proteasome pathway".

The GO categories of interest included "Response to stress", "Cell death", "Apoptosis signalling" and "Parkinson's disease". Depending on which GO category, cells expressing the cyclin F^{E624K} mutant shared an equal abundance of cyclin F protein interactors with cyclin F^{WT} or the familial cyclin F^{S621G} mutant. In the GO category "Response to stress", three different cyclin F protein interactors (SOD1, HMGB1, and HSPA14) were identified in the cyclin F^{E624K} mutant and the cyclin F^{WT} (HSPA6, PRDX4, and PIK3CB). In the "Cell death" GO category, two cyclin F protein interactors were identified in the cyclin F^{E624K} mutant (STAT3, and ADAM9), the cyclin F^{S621G} mutant (STAT3, and ADAM9), and the cyclin F^{WT} (FIS1, and TXNDC12). In the GO category "Apoptosis signalling pathway", two cyclin F protein interactors were identified in the cyclin F^{E624K} mutant (MAPK1, and HSPA14) and the cyclin F^{WT} (HSPA6, and HSPA14). In total 23 cyclin F protein interactors of the *CCNF* transgenes were identified in specific biological processes using PANTHER GO (Table 3-7).

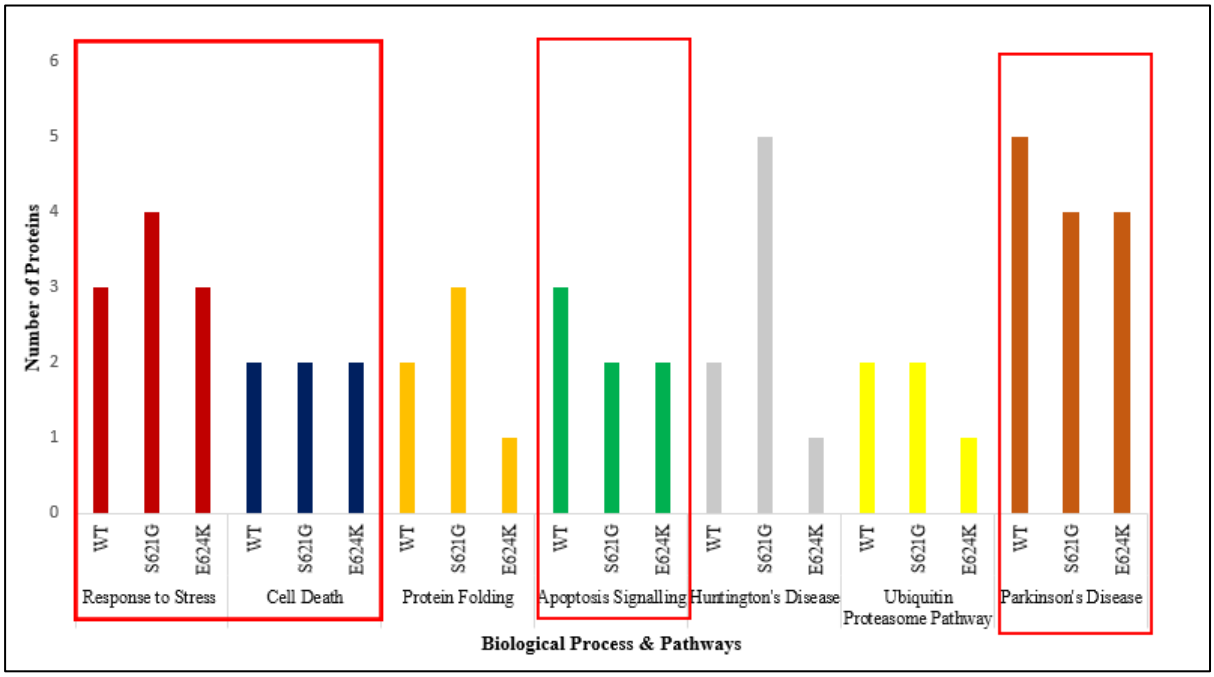

Figure 3-18. GO analysis of enriched unique and shared Cyclin F interactors.
The *unique* and *shared* quantified cyclin F interactors identified in the *CCNF* transgenes are categorised into biological processes and/or pathways. Biological processes and pathways of interest boxed in red.

Table 3-7. Enriched *unique* and *shared* Cyclin F protein interactors in *CCNF* transgenes.

UniProt ID	Protein Name	Gene Ontology Biological Process	Found in Cyclin F^{WT}	Found in Cyclin F^{S621G}	Found in Cyclin F^{E624K}
P17066	**HSPA6 -** Heat shock 70 kDa protein 6	Response to stress	Yes	Yes	No
		Protein folding	Yes	Yes	No
		Apoptosis signalling	Yes	Yes	No
		Parkinson's disease	Yes	Yes	No
Q13162	**PRDX4 -** Peroxiredoxin-4	Response to stress	Yes	Yes	No
P42338	**PIK3CB -** Phosphatidylinositol 4,5-bisphosphate 3-kinase catalytic subunit beta isoform	Response to stress	Yes	No	No
		Apoptosis signalling	Yes	No	No
P00441	**SOD1 -** Superoxide dismutase [Cu-Zn]	Response to stress	No	Yes	Yes
Q0VDF9	**HSPA14 -** Heat shock 70 kDa protein 14	Response to stress	No	Yes	Yes
		Parkinson's disease	No	Yes	Yes
P09429	**HMGB1 -** High mobility group protein B1	Response to stress	No	No	Yes
Q9Y3D6	**FIS1 -** Mitochondrial fission 1 protein	Cell Death	Yes	No	No
O95881	**TXNDC12 -** Thioredoxin domain-containing protein 12	Cell Death	Yes	No	No
P40763	**STAT3 -** Signal transducer and activator of transcription 3	Cell Death	No	Yes	Yes

Q13443	**ADAM9 -** Disintegrin and metalloproteinase domain-containing protein 9	Cell Death	No	Yes	Yes
P62942	**FKBP1A -** Peptidyl-prolyl cis-trans isomerase FKBP1A	Protein Folding	Yes	Yes	No
P28482	**MAPK1 -** Mitogen-activated protein kinase 1	Apoptosis Signalling	Yes	No	Yes
		Parkinson’s disease	Yes	No	Yes
P84095	**RHOG -** Rho-related GTP-binding protein RhoG	Huntington's Disease	Yes	Yes	No
P62330	**ARF6 -** ADP-ribosylation factor 6	Huntington's Disease	Yes	Yes	No
Q99536	**VAT1 -** Synaptic vesicle membrane protein VAT-1 homolog	Huntington's Disease	No	Yes	Yes
		Parkinson’s disease	No	Yes	Yes
P61006	**RAB8A -** Ras-related protein Rab-8A	Huntington's Disease	No	Yes	No
O15143	**ARPC1B -** Actin-related protein 2/3 complex subunit 1B	Huntington's Disease	No	Yes	No
Q9NPD8	**UBE2T -** Ubiquitin-conjugating enzyme E2 T	Ubiquitin Proteasome Pathway	Yes	No	No
P61086	**UBE2K -** Ubiquitin-conjugating enzyme E2 K	Ubiquitin Proteasome Pathway	Yes	Yes	No
P51665	**PSMD7 -** 26S proteasome non-ATPase regulatory subunit 7	Ubiquitin Proteasome Pathway	No	Yes	Yes
P60900	**PSMA6 -** Proteasome subunit alpha type-6	Parkinson’s Disease	Yes	Yes	No

P49720	**PSMB3 -** Proteasome subunit beta type-3	Parkinson's Disease	Yes	No	Yes
Q86Y82	**STX12 -** Syntaxin-12	Parkinson's Disease	No	No	Yes

3.12. Enhanced Cyclin F mutant protein interactors cluster in neurodegenerative diseases

To determine whether *enhanced* cyclin F protein interactors are involved in neurodegenerative disease, a comparative analysis was generated using PANTHER GO (Figure 3-19). The comparative analysis measured the abundance of *enhanced* cyclin F protein interactors between the familial cyclin F^{S621G} mutant and the sporadic cyclin F^{E624K} mutant normalised to the cyclin F^{WT} control. Proteins measured with a $\log_2$ 6.64-fold were identified as proteins co-immunoprecipitated with cyclin F in cells expressing the transgene mutant but not bound to cyclin F in cells expressing the cyclin F^{WT} control. A high abundance of enhanced cyclin F protein interactors in the cyclin F^{E624K} mutant were identified in "Parkinson's disease" (STX12, HSPA14, and PSMA2) and "Alzheimer's disease" (MAPK1 and KLC2). Whereas, a high abundance of *enhanced* cyclin F protein interactors in the cyclin F^{S621G} mutant were identified in the "Huntington's disease" GO category (ARL1 and CAPNS1). In total 9 *enhanced* cyclin F protein interactors of the sporadic cyclin F^{E624K} mutant were identified in neurodegenerative diseases category using PANTHER GO (Table 3-8).

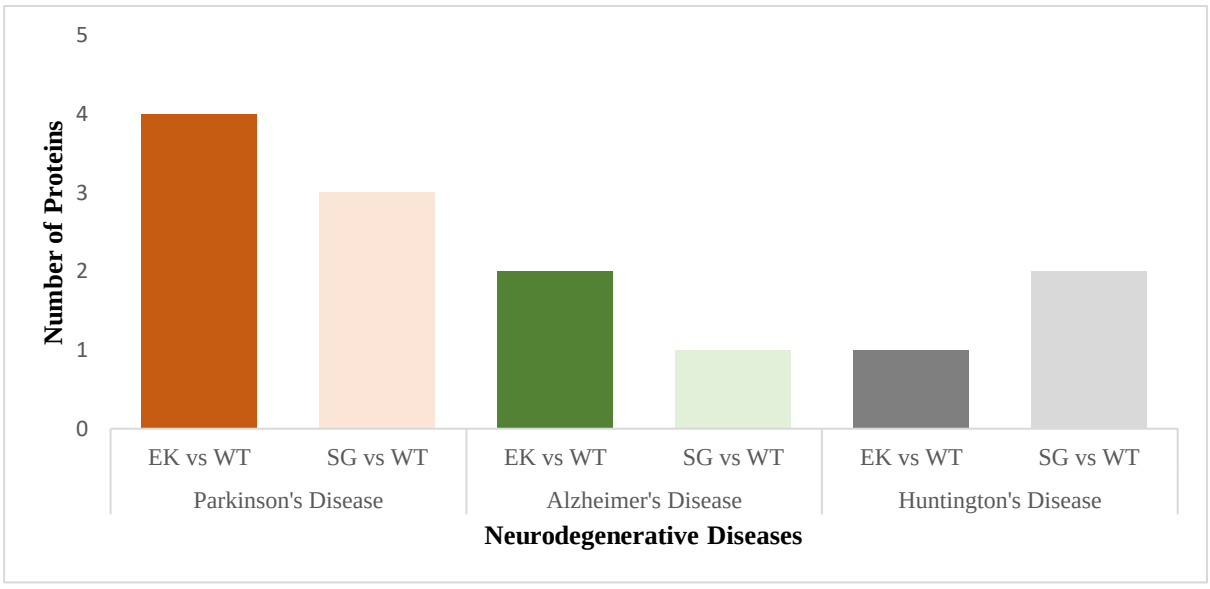

Figure 3-19. Comparative analysis of enhanced Cyclin F interactors associated with neurodegenerative diseases in Cyclin F mutants.
The cyclin F mutants are normalised to cyclin F^{WT} and proteins expressed in sporadic cyclin F^{E624K} are compared to proteins expressed in familial cyclin F^{S621G} for each GO category.

Table 3-8. Enhanced Cyclin F protein interactors associated with neurodegenerative diseases in sporadic Cyclin F^{E624K} mutant.

UniProt ID	Protein Name	Log_2 Fold Change (EK/WT)	Log_2 Fold Change (SG/WT)	Neurodegenerative Disease	Reference
P40616	**ARL1** - ADP-ribosylation factor-like protein 1	1.22	1.56	Huntington's disease	(75)
Q86Y82	**STX12 -** Syntaxin-12	6.64		Parkinson's disease	(76)
P28482	**MAPK1** - Mitogen-activated protein kinase 1	6.64		Parkinson's disease Alzheimer's disease	(77) (78)
Q0VDF9	**HSPA14** - Heat shock 70 kDa protein 14	6.64	6.64	Parkinson's disease	(79)
P25787	**PSMA2 -** Proteasome subunit alpha type-2	1.134	0.415	Parkinson's disease	(80)
Q9H0B6	**KLC2 -** Kinesin light chain 2	6.64	6.64	Alzheimer's disease	(81)

3.13. Ingenuity pathway analysis (IPA) of label-free quantitative immunoprecipitated proteomics data

IPA software was used to predict the disease/function mechanisms that were either inhibited or activated and what protein networks were identified in the sporadic cyclin F^{E624K} mutant. This provides insight into what signalling pathways the cyclin F protein interactors may be altering in response to cells expressing the cyclin F^{E624K} mutant in comparison to cells expressing cyclin F^{S621G} mutant. The relative abundance ratios (fold-change) for both cyclin F^{S621G} and cyclin F^{E624K} mutants were compared to the cyclin F^{WT} control.

3.13.1. Cyclin F interactors activate motor dysfunction in cells expressing Cyclin F^{E624K}

Using IPA, a disease/function comparative analysis was made with the quantitative data obtained from label-free proteomics of HEK293 cells expressing empty vector, cyclin F^{S621G}, and cyclin F^{E624K}, that were normalised to the cyclin F^{WT} control. The same parameters were used as in section 3.7.2. The expression of cyclin F^{E624K} predicted the activation of motor dysfunction (z-score=2.387, $p=4.1x10^{03}$) (Figure 3-20). Notably, no activation or inhibition of motor dysfunction pathways were predicted for cyclin F protein interactors identified from empty vector control and cyclin F^{S621G} samples (Figure 3-20.A). A total of 33 cyclin F protein interactors were identified, in which IPA has predicted the activation of motor dysfunction (Table 3-9). Of these 33 proteins, six were selected based on the literature that reveals their association with neurodegenerative diseases. This was displayed in Figure 3-20.B. Proteins with *reduced*-binding in regulating motor function were identified with BAX (log_2 -6.64-fold, $p=1.04x10^{-16}$), UQCRB (log_2 -6.64-fold, $p=1.04x10^{-16}$) and CTSD (log_2-6.64-fold, $p=1.04x10^{-16}$) that act as inhibitors for motor dysfunction. *Enhanced*-binding protein interactors that regulate motor function were identified: SOD1 (log_2 6.64-fold, $p=1.04x10^{-16}$), SGTA (log_2 1.68-fold, $p=2.58x10^{-02}$) and HSPB1 (log_2 1.75-fold, p=0.025).

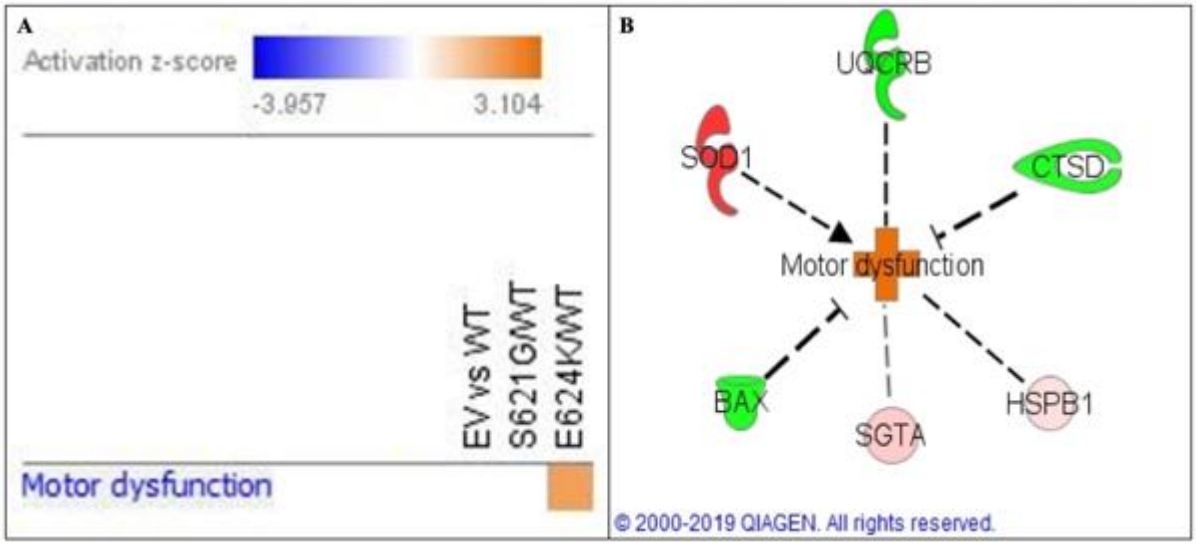

Figure 3-20. Disease/function analysis of Cyclin F protein interactors expressed in Cyclin F^{E624K} mutant.

A) Heat map displays activation and inhibition of motor dysfunction. Activation is identified in HEK293 cells expressing cyclin F^{E624K} (E624K) and no activity determined for empty vector control (EV) and cyclin F^{S621G} (S621G). All samples are normalised to cyclin F^{WT} control (WT). **B)** Motor dysfunction disease protein network that displays cyclin F protein interactors, *reduced*-binding (green) and *enhanced-reduced*-binding (red). Figures generated using IPA.

Table 3-9.Cyclin F protein interactors activating motor dysfunction expressed in the Cyclin F^{E624K} mutant.

The log_2 fold change and p-value determined for cells expressing cyclin F^{E624K} (EK). *Reduced*-binding cyclin F protein interactors highlighted in green and *enhanced*-binding highlighted in red. Normalised to cyclin F^{WT} control (WT).

UniProt ID	Protein Name	Log_2 Fold Change (EK/WT)	p-value (EK/WT)
Q07812	**BAX** - BCL2 associated X, apoptosis regulator	-6.64	$1.04x10^{-16}$
P07339	**CTSD** - Cathepsin D	-6.64	$1.04x10^{-16}$
P14927	**UQCRB** -Cytochrome b-c1 complex subunit 7	-6.64	$1.04x10^{-16}$
P04792	**HSPB1** - Heat shock protein family B (small) member 1	1.75	0.025
O43765	**SGTA** - Small glutamine rich tetratricopeptide repeat containing alpha	1.68	0.026
P00441	**SOD1** - Superoxide dismutase 1	6.64	$1.04x10^{-16}$

3.13.2. Protein networks detected in cells expressing Cyclin F^{E624K}

Further analysis was made using IPA to determine whether any of the cyclin F protein interactors involved in the activation of motor dysfunction were predicted to cluster into specific protein networks. Protein networks were predicted based on the *enhanced*- (red) or *reduced*-binding (green) with the sporadic cyclin F^{E624K} mutant and were normalised to the cyclin F^{WT} control.

Interestingly, one protein network identified four cyclin F protein interactors (BAX, CTSD, HSB1, and UQCRB) that were also identified in motor dysfunction activation (Figure 3-21). Within this protein network, various cytochrome b-c1 and cytochrome-c oxidase complexes were identified that made direct (solid line) and indirect (dashed line) interactions with other complexes and cyclin F protein interactors. The BAX, CTSD, CYCS, and UQCRB displayed *reduced*-binding (green), whereas the HSPB1 cyclin F protein interactor displayed *enhanced*-binding (red) within the clustered protein network. The PDCD6, PARP and COX6B1 protein interactors were identified in cells expressing cyclin F mutants and the empty vector control, with no differential binding activity between them. Overall, this protein network identified in the sporadic cyclin F^{E624K} mutant show that various cyclin F protein interactors, including the three protein interactors (BAX, CTSD, and HSB1) involved in activating motor dysfunction, have both direct and indirect interactions with the Akt signalling pathway and the family of NFkB proteins.

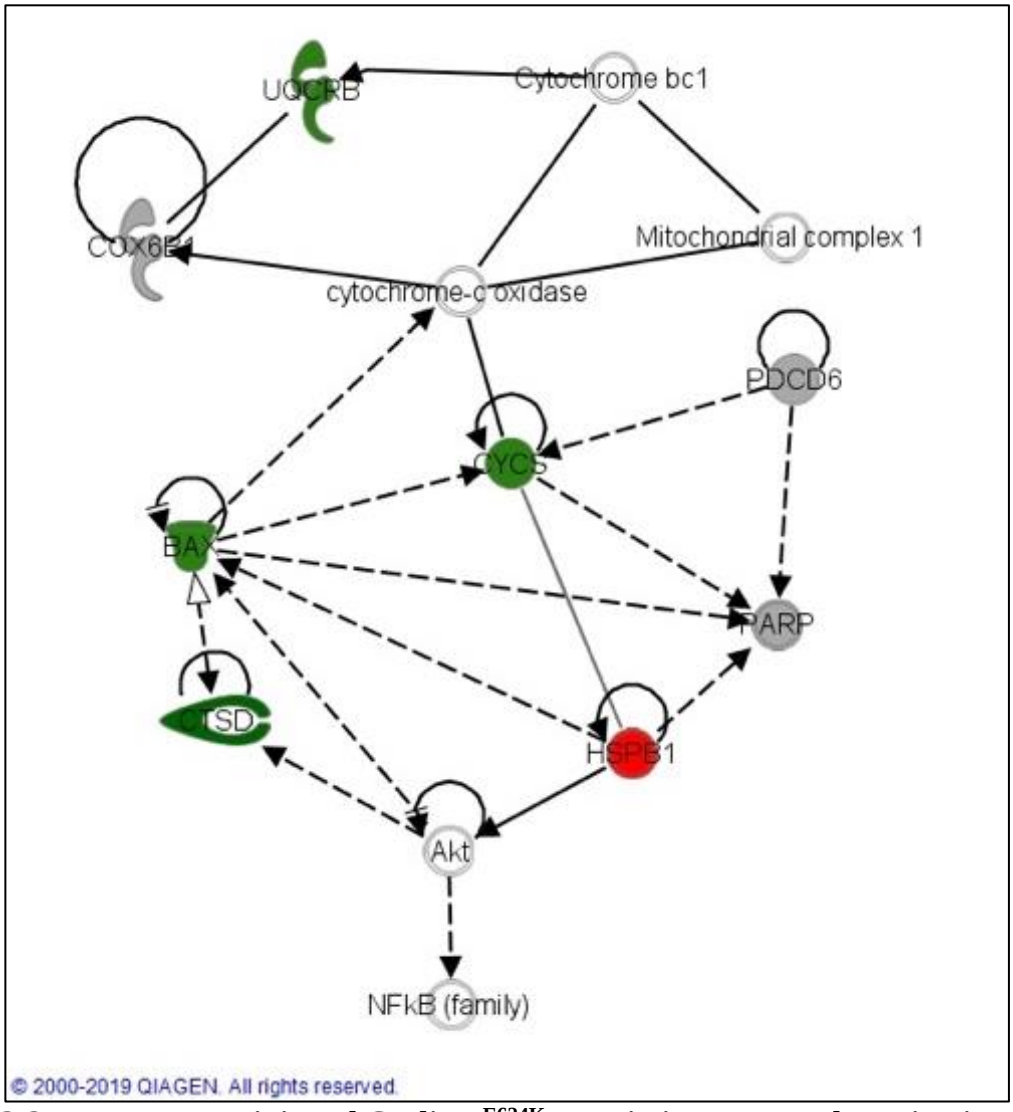

Figure 3-21. Immunoprecipitated Cyclin F^{E624K} protein interactors clustering in a cytochrome c oxidase protein network.

Immunoprecipitated cyclin F protein interactor displaying *reduced*-binding (green) and *enhanced*-binding (red) in HEK293 cells expressing the sporadic cyclin F^{E624K} mutant. Immunoprecipitated cyclin F protein interactors were identified in cells expressing empty vector, cyclin F^{S621G} mutant, and cyclin F^{E624K} mutant (grey), and protein/complexes were predicted by IPA (white). Direct (solid) and indirect (dashed) interactions were also predicted. Figure generated using IPA.

In another protein network, the SGTA cyclin F^{E624K} protein interactor that was identified in activating motor dysfunction, was clustered within a protein network that consisted of ubiquitin- and proteasome-associated proteins (Figure 3-22). Within the ubiquitin-associated protein network, the Ubiquitin molecule and UBE2 groups were identified and created both direct and indirect interactions between various cyclin F^{E624K} protein interactors. The FAF1, PJA2, UBE2K and UBE2T are the ubiquitin-associated proteins that displayed *reduced* binding, whereas, the EI24 and UBE2D1 displayed *enhanced*-binding with the cyclin F^{E624K} mutant. Within the proteasome-associated protein network, the 26S Proteasome complex was identified and created direct interactions between various cyclin F^{E624K} protein interactors. The

PSMA6, PSMB7, PSME2, and PSMA are proteasome subunits that were identified with *reduced*-binding. The SGTA was the only cyclin F protein interactor that displayed high binding activity with direct interaction to the 26S proteasome. Overall, sporadic cyclin F^{E624K} protein interactors were identified in a ubiquitin and proteasome protein network that displayed mainly *reduced*-binding and clustered around the NFkB complex.

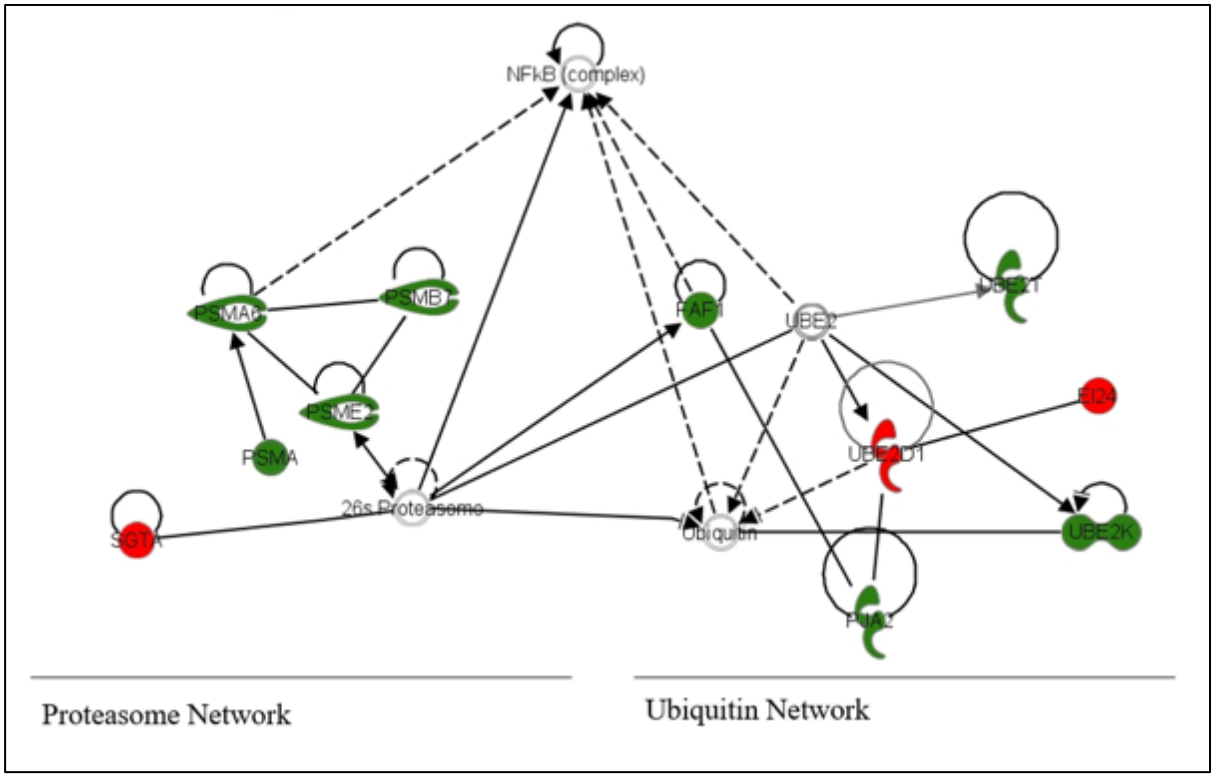

Figure 3-22. Immunoprecipitated Cyclin F^{E624K} protein interactors clustering in proteasome and ubiquitin protein network.
Immunoprecipitated cyclin F protein interactor displaying *reduced*-binding (green) and *enhanced*-binding (red) in HEK293 cells expressing the sporadic cyclin F^{E624K} mutant. Immunoprecipitated cyclin F protein interactors were identified in cells expressing empty vector, cyclin F^{S621G} mutant, and cyclin F^{E624K} mutant (grey), and protein/complexes were predicted by IPA (white). Direct (solid) and indirect (dashed) interactions were also predicted. Figure generated using IPA.

3.14. Decreased protein fold stability for sporadic Cyclin F^{E624K} mutant

To determine whether cyclin F protein fold stability is affected by the sporadic missense mutation, the STRUM protein fold stability online predictor tool was used (82). Predictions were measured using free energy differences (ΔΔG). The cyclin F^{E624K} mutation revealed a -0.7 ΔΔG for the missense mutation that changed the wild-type glutamic acid (E) amino acid residue to the mutant lysine (K) amino acid residue. The cyclin F^{S621G} mutation revealed a -0.57 ΔΔG for the point mutation that changed the wild-type serine (S) amino acid residue to the mutant glycine (G) amino acid residue.

3.15. Decreased phosphorylation at Serine 621 predicted in cells expressing Cyclin F^{E624K}

To determine whether phosphorylation of cyclin F at Serine 621 is affected by the sporadic cyclin F^{E624K} mutation (and potentially subsequent E3 ubiquitin ligase activity), predictions were made using the phosphorylation predictor site NetPhospho 3.1 (83) (Figure 3-23). Based on protein phosphorylation prediction algorithm, significant phosphorylation sites were determined with a prediction score of $\geq$0.5 (threshold). The scores revealed that predicted phosphorylation occupancy decreased with the presence of the cyclin F^{E624K} mutant (0.619) compared to the cyclin F^{WT} (0.983) at the serine 621 site (S621) with unspecified kinase phosphorylating this site. Based on casein kinase 2 (CKII) phosphorylation at the S621 site, phosphorylation decreased in cells expressing cyclin F^{E624K} (0.695) compared to cells expressing cyclin F^{WT} (0.532) (Table 3-10).

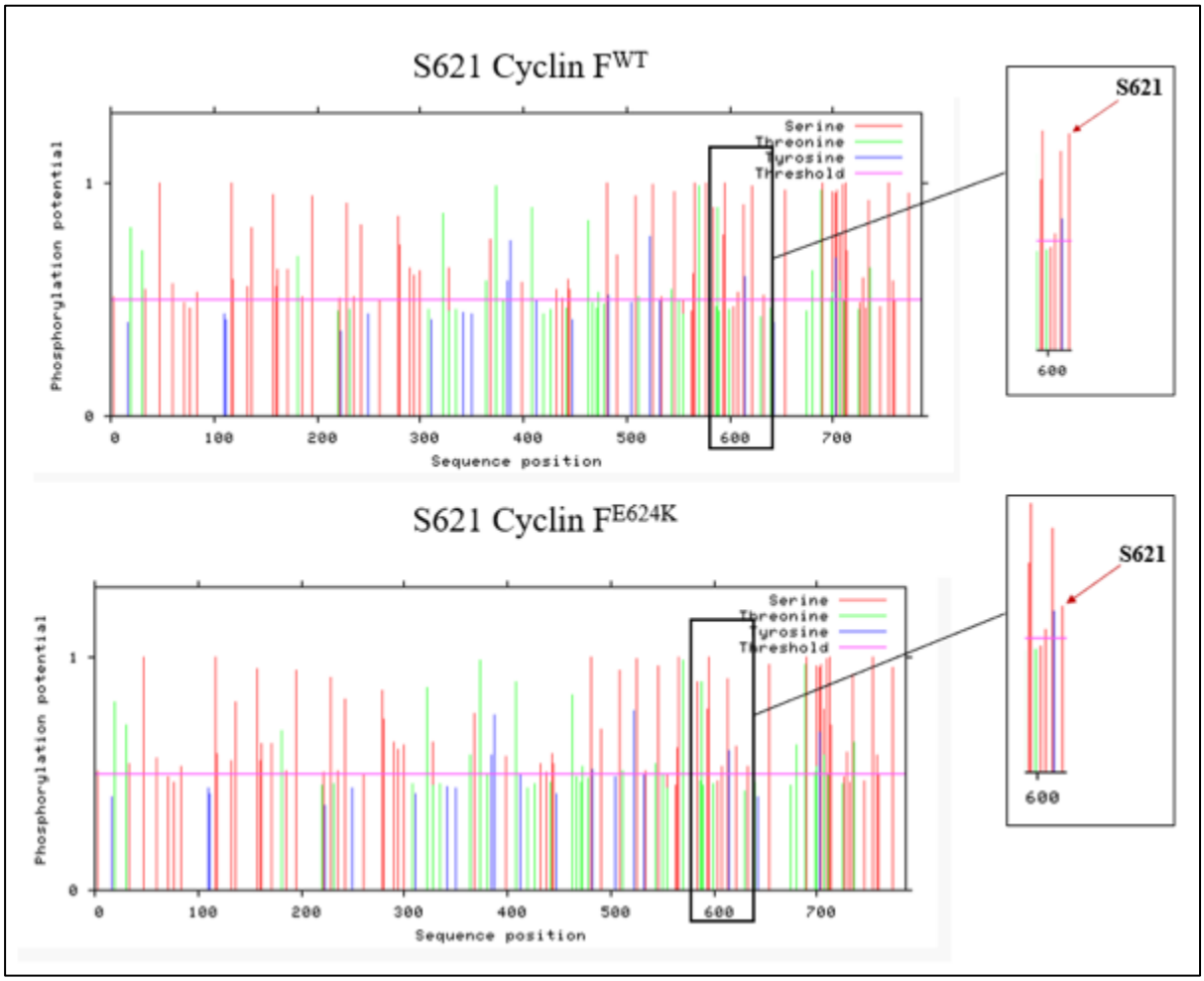

Figure 3-23. Predicted phosphorylation sites for Cyclin F.
Potential phosphorylation sites are predicted above the threshold (pink line) with unspecified kinases. Decrease phosphorylation is predicted in cells expressing cyclin F^{E624K} (0.619) compared to cyclin F^{WT} (0.983). Figures generated using NetPhospho3.1.

Table 3-10. Phosphorylation predictions scores for phosphorylation site S621 in Cyclin F^{E624K} and Cyclin F^{WT} based on CKII binding.

Sequence	Kinase	Prediction score
Cyclin F^{WT}	CKII	0.695
Cyclin F^{E624K}	CKII	0.532

3.16. Validating decreased phosphorylation in the sporadic Cyclin F^{E624K} mutant

To validate whether phosphorylation at S621 had decreased in the cyclin F^{E624K} mutant compared to the cyclin F^{WT}, immunoblotting and statistical analysis was performed using anti-FLAG, anti-phosphorylation S621 (custom rabbit antibody raised against ^{618}DQES(PO_4)EGEKEG^{627}), and anti-non-phosphorylation S621 antibodies (custom rabbit antibody raised against ^{618}DQESEGEKEG^{627}) (Table 2-2). Immunoblotting for FLAG revealed expression of FLAG tagged cyclin F proteins in the cyclin F^{WT}, cyclin F^{S621G} and cyclin F^{E624K} lanes (Figure 3-24.A). For cyclin F^{E624K}, immunoblotting of the phosphorylated S621 revealed a 0.096-fold ($p<0.0001$) decrease compared to the cyclin F^{WT} (Figure 3-24.B), and non-phosphorylated S621 revealed a 0.025-fold ($p<0.0001$) decrease compared to the cyclin F^{WT} (Figure 3-24.C). For cyclin F^{S621G}, immunoblots of phosphorylated S621 revealed a 0.740-fold ($p=0.0117$) decrease compared to the cyclin F^{WT}, and non-phosphorylation at the S621 site revealed a 0.621-fold ($p=0.0006$) decrease compared to the cyclin F^{WT}.

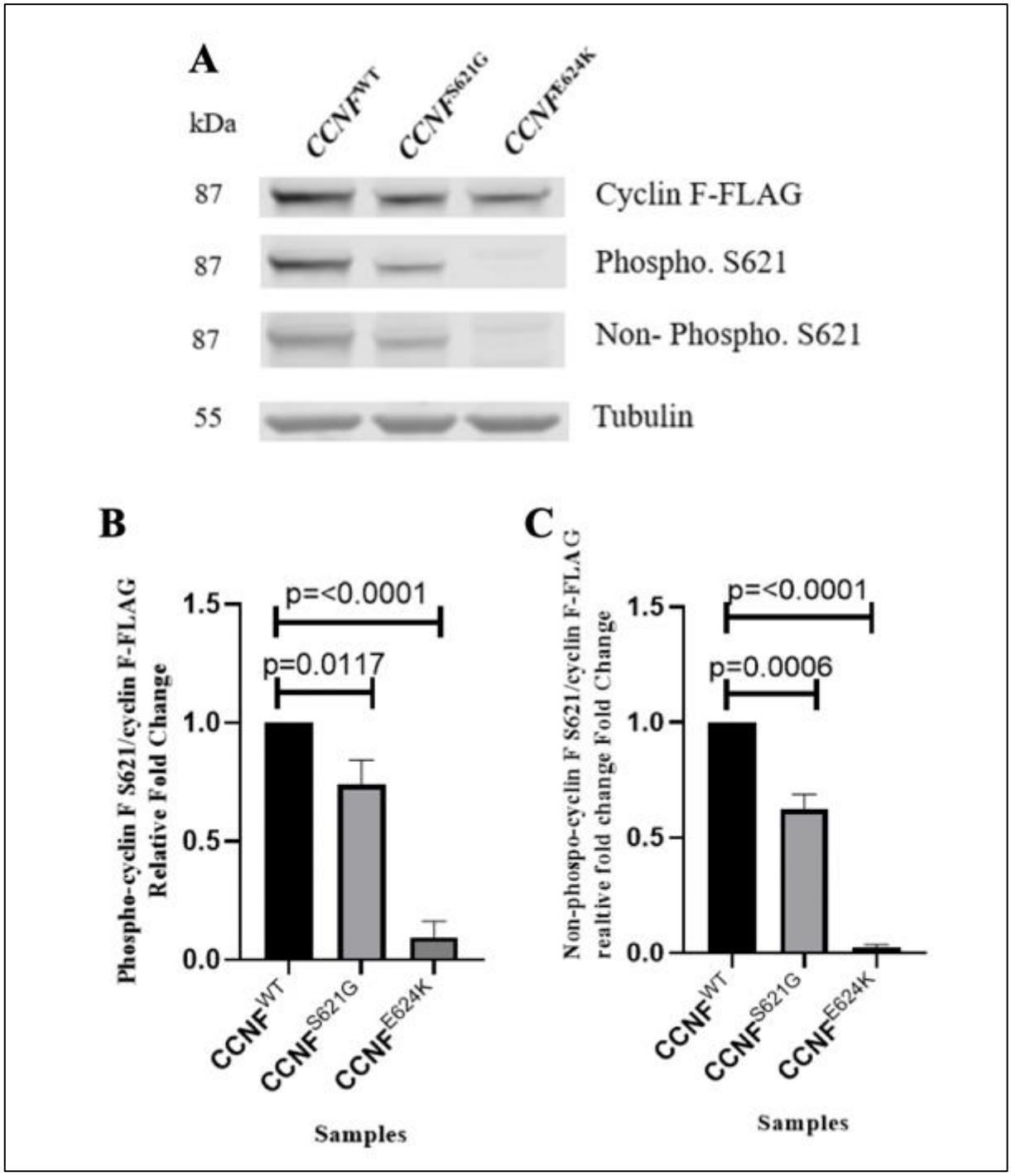

Figure 3-24. Cyclin F^{E624K} affects the phosphorylation of S621.

A) Immunoblots of cyclin F-FLAG expression in *CCNF* transgenes reveals phosphorylated cyclin F S621 expression in cyclin F^{WT}, decreased expression in cyclin F^{S621G} and no expression in cyclin F^{E624K}. Non-phosphorylated cyclin F S621 expression decreased in cyclin F^{WT} and cyclin F^{S621G} and no observable detection was apparent cells transfected with cyclin F^{E624K}. The *beta*-tubulin loading control was used and displayed similar expression levels across all samples. **B)** Relative fold change of phosphorylated-cyclin F S621 to cyclin F-FLAG for cyclin F^{E624K} decreased to 0.096-fold ($p<0.0001$) and cyclin F^{S621G} decreased to 0.74-fold ($p<0.0117$). **C)** Relative fold change of non-phosphorylated-cyclin F S621 to cyclin F-FLAG for cyclin F^{E624K} decreased to 0.025-fold ($p<0.0001$) and cyclin F^{S621G} decreased to 0.621-fold ($p<0.0006$). For all statistical analysis, n=3.

3.17. Ubiquitylation specificity in cells expressing Cyclin F^{E624K}

To determine the differential ubiquitylation levels in the HEK293 cells expressing empty vector control, cyclin F^{WT}, cyclin F^{S621G}, and cyclin F^{E624K}, immunoblotting for whole cell lysates was used to determine differences in specific ubiquitin linkages in K48 and K63 ubiquitylation. Immunoblotting for global K63-specific ubiquitin revealed decreased ubiquitylation for cyclin F^{E624K} (0.65-fold; p=0.0003) and cyclin F^{S621G} (0.809-fold; p=0.0083) compared to cyclin F^{WT} (1-fold) (Figure 3-25). Immunoblotting for global K48-specific ubiquitin revealed increased ubiquitylation for cyclin F^{E624K} (1.297-fold; p=0.0003) and cyclin F^{S621G} (1.211-fold; p=0.0135) compared to cyclin F^{WT} (1-fold) (Figure 3-26).

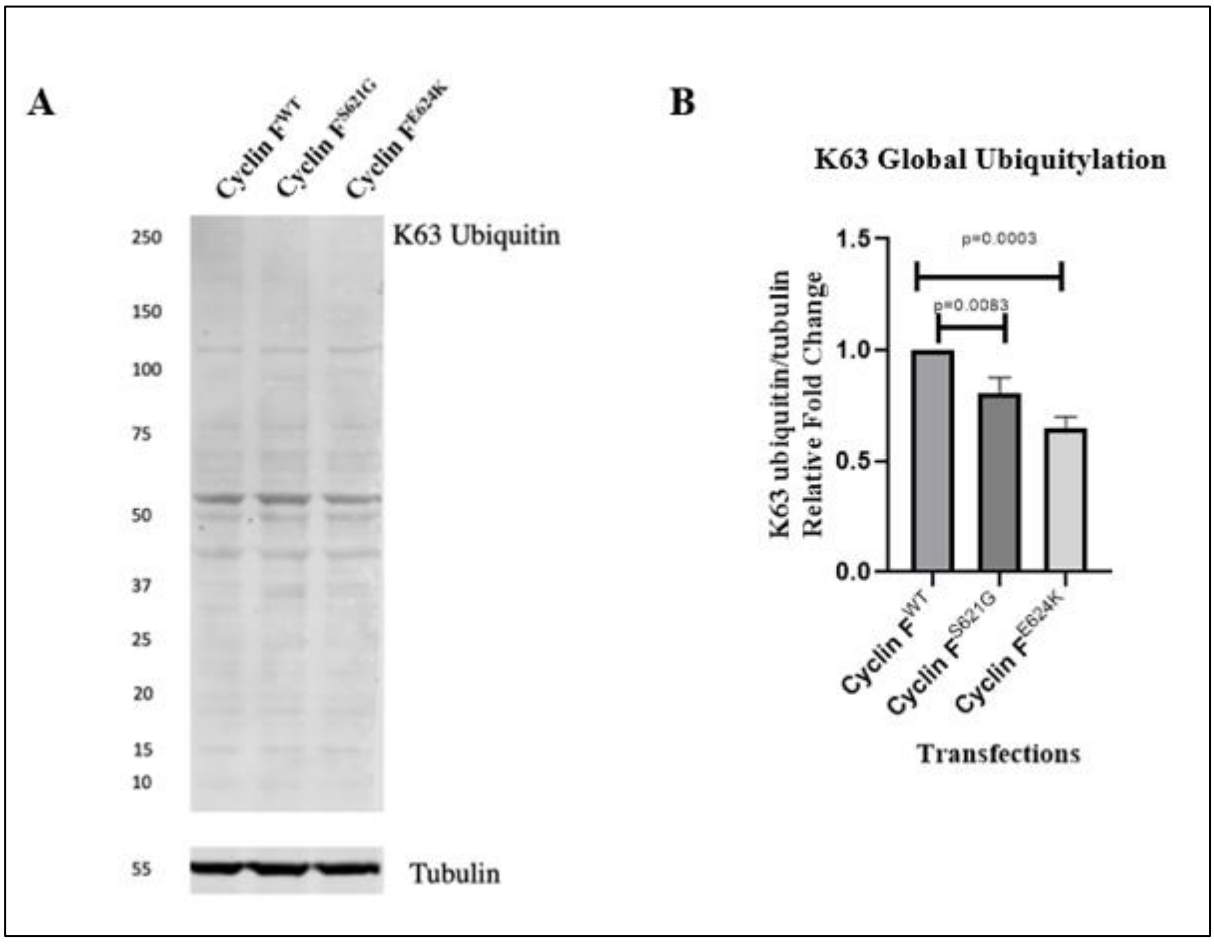

Figure 3-25. Decreased global K63 ubiquitylation in cells expressing Cyclin F^{E624K} and Cyclin F^{S621G}.

A) Immunoblots for global K63 ubiquitylation revealed relatively low expression in HEK293 cells expressing *CCNF* transgenes. The *beta*-tubulin loading control was used and displayed similar expression levels across all samples. **B)** Relative fold change of K63 ubiquitin normalised to *beta*-tubulin revealed decreased ubiquitylation by 0.65-fold for cyclin F^{E624K} compared to cyclin F^{WT}, and decreased ubiquitylation by 0.809-fold for cyclin F^{S621G} compared to cyclin F^{WT}. For all statistical analysis, n=3.

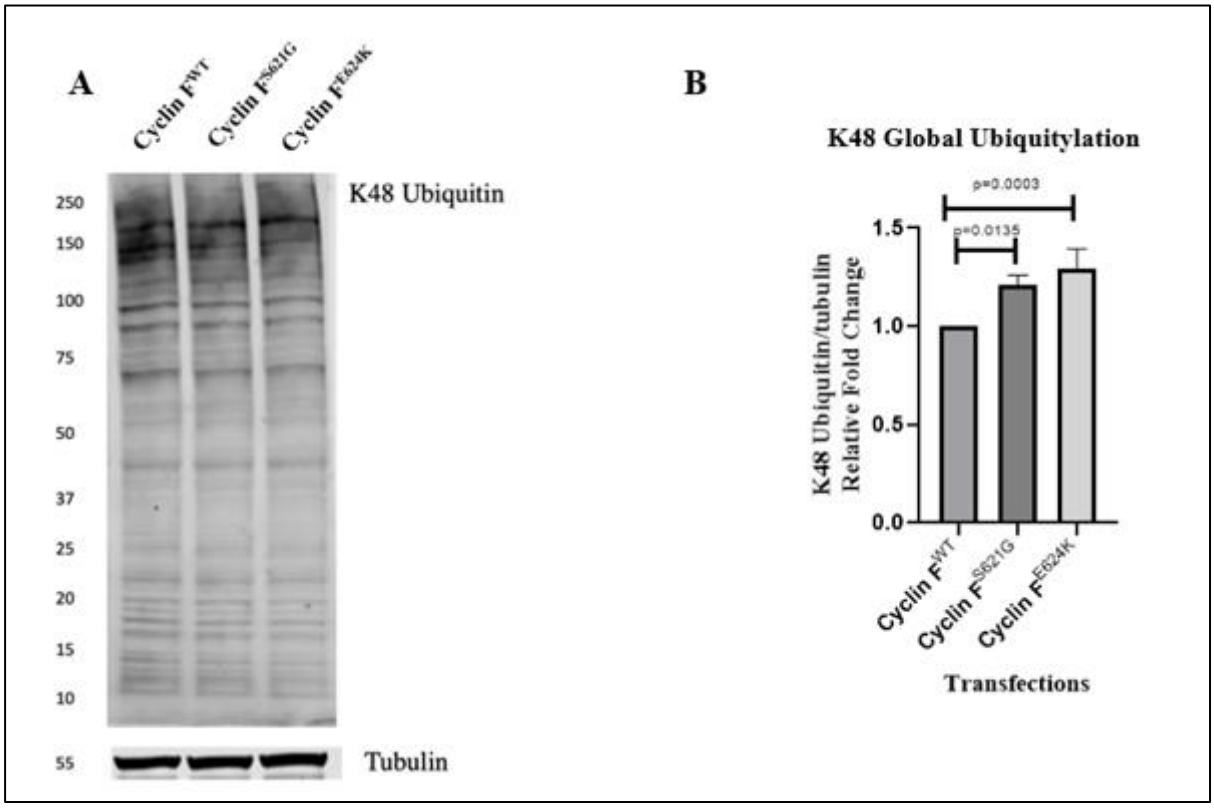

Figure 3-26. Increased global K48 ubiquitylation in cells expressing Cyclin F^{E624K} and Cyclin F^{S621G}.

A) Immunoblots for global K48 ubiquitylation revealed relatively high expression in HEK293 cells expressing *CCNF* transgenes. The *beta*-tubulin loading control was used and displayed similar expression levels across all samples. **B)** Relative fold change of K48 ubiquitin normalised to *beta*-tubulin revealed increased ubiquitylation by 1.297-fold for cyclin F^{E624K} compared to cyclin F^{WT}, and increased ubiquitylation by 1.211-fold for cyclin F^{S621G} compared to cyclin F^{WT}. For all statistical analysis, n=3.

3.18. No significant change in K48 ubiquitylation in the Cyclin F^{E624K} mutant using E3 ubiquitin ligase assay

To determine whether the E3 ubiquitin ligase activity in the HEK293 cells expressing the cyclin F^{E624K} protein interactors increases or decreases K48-specific ubiquitylation, the ELISA-based ubiquitylation activity assay was used. The ubiquitylation levels were measured based on luminescence expression (A.U) and the cyclin F mutants were normalised to cyclin F^{WT} to determine the relative fold change (Figure 3-27)**.** K48 ubiquitylation decreased (0.98-fold; 591,026 A.U) with no significant difference for cells expressing cyclin F^{E624K} compared to cyclin F^{WT} (1-fold; 608,458 A.U) was observed. K48 ubiquitylation increased (1.119-fold; 678,012 A.U) with no significant difference for cells expressing cyclin F^{S621G} compared to cyclin F^{WT} (1-fold; 608,458 A.U) was observed. The empty vector control (0.183-fold; 111,459 A.U), and negative control containing E3 ligase buffer (0.193-fold; 116,023 A.U) displayed relatively low expression of K48 ubiquitylation compared to cyclin F^{WT} (1-fold; 608,458 A.U).

The positive control containing E1-E2-E3 displayed a relatively low expression (0.682-fold; 410,140 A.U.) of K48 ubiquitylation compared to cyclin F^{WT} (1-fold; 608,458 A.U).

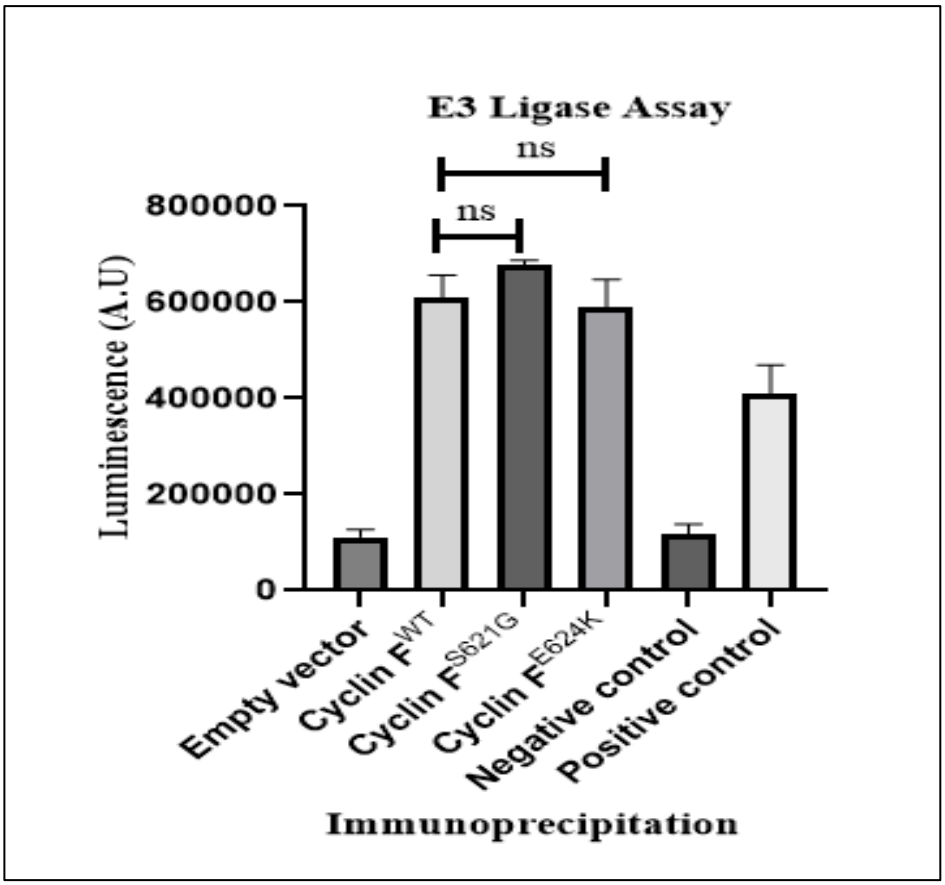

Figure 3-27. E3 ubiquitin ligase activity of K48 ubiquitylation of immunoprecipitant Cyclin F protein interactors in cells expressing empty vector and *CCNF* transgenes.
Decreased ubiquitylation (0.98-fold; 59,1026 A.U) is determined for cyclin F^{E624K} compared cyclin F^{WT} (1-fold; 60,8458 A.U). Increased ubiquitylation of (1.119-fold; 67,8012 A.U) is determined for cyclin F^{S621G} compared to cyclin F^{WT} (1-fold; 60,8458 A.U). For statistical analysis, n=3.

4. Discussion

The objective of this study was to investigate functional perturbations of the cellular pathways and protein networks caused by the sporadic cyclin F^{E624K} mutant, a causative missense mutation of ALS/FTD (14). The data obtained from this thesis provided the first characterisation and comparative analysis between the novel sporadic cyclin F^{E624K} mutant and the previously well-characterised familial cyclin F^{S621G} mutant, as well as the cyclin F^{WT}. Together with MS and biochemical analysis, the data generated determined different and similarly affected pathways, demonstrated a significant decrease in phosphorylation at the S621 phosphorylation site, assessed ubiquitylation activity, and identified both putative and novel PPIs. These findings demonstrate that proteostasis dysfunction arises in cells expressing sporadic cyclin F^{E624K} mutant, however revealed differences in perturbed mechanisms that ultimately contribute to ALS/FTD neurodegeneration.

In ALS/FTD research, familial mutations have been mainly focused on to generate and employ *in vitro* and *in vivo* models to expose novel pathogenic cellular mechanisms that allow the rapid progression of the highly fatal disease (84-86). The use of familial mutations to generate ALS/FTD models are based on the premise that familial mutations recapitulate clinical features that are representative of symptoms displayed in both familial and sporadic patients, as the clinical features of familial and sporadic ALS and/or FTD are indistinguishable (87). However, the study described in this thesis, which compares a familial cyclin F^{S621G} to a sporadic cyclin F^{E624K} in HEK293 cells demonstrates that whilst these mutations both cause ALS and/or FTD, the cellular pathways and protein interactions differ and potentially trigger different biological processes. For example, this is demonstrated where the PTEN signalling pathway was predicted to be activated in cyclin F^{E624K} compared to cyclin F^{S621G}, and the cyclin F^{E624K} protein interactome displayed a *reduced*-binding with oxidation-phosphorylation processes.

4.1. Site-directed mutagenesis of the *CCNF*^{E624K} provides the experimental foundation for this study

The first aim was to generate the sporadic *CCNF*^{E624K} mutant with the FLAG epitope tag attached to the C-terminus using the Q5 site-directed mutagenesis (New England BioLabs). For this study, site-directed mutagenesis involved the substitution of a single nucleotide (A1882G) within the *CCNF*^{WT} -FLAG DNA sequence for the generation of the sporadic *CCNF*^{E624K} mutant. Using this methodology, the highly evolutionary conserved target site in the cyclin F

PEST region was altered to generate the sporadic cyclin F^{E624K} mutation (14). Therefore, the site-directed mutagenesis experiment provided the basis for experimental study in replicating and investigating the altered cellular mechanisms of the sporadic ALS/FTD causative cyclin F^{E624K} mutant.

4.2. Global proteomics

For a general overview on whether cellular pathways were affected with the expression of cyclin F^{E624K} in whole cell lysates, unbiased label-free global proteomic analysis was performed. Based on this data, IPA predictions and comparisons were made between different canonical pathways that were affected in cells expressing the sporadic cyclin F^{E624K} mutant compared to the familial cyclin F^{S621G} mutant, that were normalised to the cyclin F^{WT}. The following global proteomic analysis revealed that the majority of significant canonical pathways were inhibited and disease/function predictions for apoptosis and cell death were activated whilst cell viability was inhibited in cells expressing cyclin F^{E624K} and cyclin F^{S621G}.

4.2.1. Activation of PTEN signalling in cells expressing Cyclin F^{E624K}

IPA revealed that most canonical pathways are inhibited, however the phosphate tensin homolog (PTEN) signalling was the only activated and second most statistically significant canonical pathway in cells expressing the sporadic cyclin F^{E624K} mutant (Figure 3-9). PTEN is a tumour repressor that interacts with various signalling pathways that regulates cellular development, apoptosis and cell migration (74). PTEN is mainly known for down-regulating PI3K/Akt phosphorylation activity, specifically on the phosphatidylinositol 3,4,5-trisphosphate (PIP3) (88, 89). Some studies have demonstrated neuroprotective roles in PTEN inhibition and regulation of PI3K/Akt pathways. In an Alzheimer's disease cell culture model, PTEN inhibitors were shown to reduce the tau hyperphosphorylation, an underlying mechanism for tauopathy-related neurodegenerative disorders (90). Furthermore, in a spinal muscular atrophy mouse model, the loss of PTEN function was shown to rescue the survival rates of mice with this neurodegenerative disorder via PI3K/Akt signalling (91). Therefore, the activation of the PTEN signalling pathway suggests attenuation of neuroprotective roles associated with the PI3K/Akt signalling. Notably the NFkB2 protein was also identified in this canonical pathway, providing rationale that apoptosis is potentially induced as a result of this activation. Although these studies provide evidence of the linkage between PTEN signalling and neurodegeneration, further investigation is required to determine

cyclin F's role in this canonical pathway, which may be investigated with IP proteomics to determine whether cyclin F enriches proteins that interact with this pathway.

4.2.2. Inhibition of cell survival response via Rac signalling

The Rac signalling pathway was the most statistically significant canonical pathway identified in cells expressing cyclin F^{E624K}. In this pathway, down-regulated proteins were enriched as well as significant proteins that were not identified (log_2 -6.64-fold) in the pathway (Table 3-4). The proteins of interest displayed connections to the Rac (RAC1) protein, a protein that is part of the Rho family of GTPases (Figure 3-11). This family of proteins involved in Rac signalling are known for controlling numerous downstream signalling pathways including cell viability and cytoskeleton regulation (92). One of the ten proteins displayed in the Rac signalling pathway is the nuclear factor-kappa-B p100 subunit 2 (NFkB2) protein. NFkB2 is a component of the transcription factor complex (NFkB) known to express various genes in response to oxidative stress (93). It mediates both pro-apoptotic and anti-apoptotic responses that drives many biological processes including cell survival (94). Further investigation by Matos and Jordan, identified that Rac1-associated proteins are located upstream of the NFkB complex, and with Rac1 repression it led to an apoptotic response (95). Therefore, the down-regulation of the NFkB protein may promote apoptosis activation and inhibit cell viability via the Rac signalling pathway, as it regulates anti-and pro-apoptotic responses. Although apoptosis is an activated signalling network in neurodegenerative diseases, further investigation is still required to determine the linkages between cyclin F's functional role in the Rac signalling pathway, which may be investigated with IP proteomics to determine whether cyclin F enriches proteins that interact with this pathway.

4.2.3. Inhibition of actin cytoskeleton regulation via Rac signalling and actin cytoskeleton signalling

Both Rac signalling and actin cytoskeleton signalling canonical pathways involved in actin cytoskeleton reorganisation, were predicted to be inhibited in cells expressing cyclin F^{E624K} (96). Notably within these canonical pathways, three significant kinases (PIK3C2A, PIP5K1A, and PTK2) were not identified (log_2-6.64-fold) in the cells expressing cyclin F^{E624K}, in which they are found in cells expressing cyclin F^{WT} (Table 3-4;Table 3-5). The phosphatidylinositol 4-phosphate 3-kinase C2 domain-containing subunit alpha (PIK3C2A) along with RAC1 proteins have previously been identified as regulators for cell growth and cell proliferation, cellular processors that are involved in actin cytoskeleton regulation (97). Therefore, this

suggests that the cyclin F^{E624K} protein's altered interactome may be influencing actin cytoskeleton regulation. The phosphatidylinositol-3-kinase (PI3K) family is composed of serine/threonine kinases including the phosphatidylinositol kinases (98). The phosphatidylinositol 4-phosphate 5-kinase type-1 alpha (PIP5K1A) is an essential class 1A kinase composed of p85 and p110 regulatory subunits that mediate the regulation of various pathways including actin cytoskeleton reorganisation through Rac protein activity (99).

Finally, the focal adhesion kinase 1 (PTK2) acts as a substrate for the neuron-specific Rac effector cyclin-dependent kinase 5 (CDK5), an important kinase for actin reorganisation (100, 101). Further investigation by Xie *et al,* demonstrated that PTK2 is a phosphorylated substrate for CDK5, an important regulator for actin reorganisation in neuronal cells and human cancer cells (101, 102). As the three kinases were not identified in the signalling networks for both canonical pathways this suggest that actin cytoskeleton regulation is impaired, thus predicting inhibition for both pathways in cells expressing the sporadic cyclin F^{E624K} mutant. However, further investigation is needed to identify the role of cyclin F^{E624K} in regard to the non-identified kinases, which may be investigated with IP proteomics to determine whether cyclin F enriches proteins that interact with these kinases.

Similarly, inhibition was predicted for the actin cytoskeleton signalling canonical pathway in cells expressing cyclin F^{S621G}. However, it differed to cells expressing cyclin F^{E624K} as the PIK3C2A and PIP5K1A were the only kinases listed in this canonical pathway (Table 3-5). The PIP5K1A kinase displayed up-regulation (log_2 2.21-fold; p=0.0369) suggesting that cells expressing the familial cyclin F^{S621G} mutant was not affected, and the PIK3C2A (log_2 -6.64-fold; p=3.07 $x10^{-16}$) was not identified in cells expressing the familial cyclin F^{S621G} mutant. Thus, there are differences in the underlying mechanisms that dysregulate actin cytoskeleton signalling between the familial cyclin F^{S621G} mutant and the sporadic cyclin F^{E624K} mutant.

4.2.4. Activated apoptosis and cell death and inhibited cell viability represented in cells expressing Cyclin F^{E624K}

Activation and inhibition predictions were made for specific disease/function mechanisms, providing insight into the overall health of the cell that may predict the outcomes of dysregulated actin cytoskeleton signalling. HEK293 cells expressing the sporadic cyclin F^{E624K} mutant, predicted activation of apoptosis and cell death as well as cell viability inhibition (Figure 3-12).

Baculoviral inhibitor of apoptosis (IAP) repeat-containing protein 2 (BIRC2), was identified in all three disease/function predicted mechanisms. This multifunctional protein, originally thought to only regulate caspase-dependent apoptosis, can act as an E3 ubiquitin ligase that activates the NFkB complex. As discussed previously, NFkB mediates both pro-apoptotic and anti-apoptotic responses that drives many cellular processes including cell survival (94). The NFkB2 protein subunit was also identified in all three disease/function predicted mechanisms. The ubiquitin-associated domain with the BIRC2 protein allows it to acts as an E3 ubiquitin ligase for the regulation of caspases-associated and NFkB-associated proteins (103, 104). Therefore, any disturbances that may affect BIRC2 or NFkB functions may change proteostasis impairment with prolonged dysfunction leading to apoptosis, and ultimately compromise cell viability.

The E3 ubiquitin-protein ligase UBR2 was identified in apoptosis and cell death activation for cells expressing cyclin F^{E624K}. UBR2 is a key component for protein quality control mechanisms in maintaining proteostasis in neuronal cells as it ubiquitylates crucial transcription factors (e.g. RPN4) that are involved in expressing proteasome subunit genes (105, 106). Interestingly, UBR2 was also expressed in peripheral blood lymphocyte samples of sALS patients (107). This could suggest that dysregulation of the E3 ubiquitin protein ligase may be exclusive to sALS pathology, therefore an E3 ubiquitin ligase activity assay using the UBR2 E3 ubiquitin ligase may assist in determining whether ubiquitylation is unique to sporadic ALS pathology compared to familial ALS.

Kelch-like ECH-associated protein 1 (KEAP1) was also significantly identified in all three disease/function predicted mechanism in cells expressing cyclin F^{E624k} and cyclin F^{S621G}. It acts as a substrate adaptor for an E3 ubiquitin ligase that maintains NRF2 levels, a key transcription factor known to respond to oxidative stresses and protect against ROS damage (108, 109). The up-regulation of KEAP1 may elucidate that oxidative damage is present in cells expressing the sporadic cyclin F^{E624K} mutant. Furthermore, a study by Fan *et al*, identified KEAP1 and SQSTM1/p62 protein interactions (110). The SQSTM1/p62 protein is known for its autophagy-assisted clearance of misfolded and aggregated proteins, and KEAP1 has been shown to enhance this process in neurodegenerative conditions (110, 111). This is further supported by analysis of post-mortem brain samples of patients presenting with neurodegenerative diseases, where KEAP1 was localised in aggregated protein inclusions (112). Overall, dysfunction to KEAP1 may preclude SQSTM1/p62-mediated autophagy in neurotoxic conditions, thus resulting in proteostasis impairment, a known underlying mechanism that inhibits cell viability

and activate apoptosis and cell death signalling pathways. The up-regulation of KEAP1 in cells expressing the sporadic cyclin F^{E624K} mutant may suggest that it is rescuing SQSTM1/p62 ubiquitylated substrates from residing in the cytoplasm to form aggregated protein inclusions. To determine whether KEAP1 is acting as a protective molecule and aggregated protein inclusions are forming without KEAP1 assisting SQSTM1/p62-mediated autophagy, a small interference RNA (siRNA) knockdown of KEAP1 expression in cells expressing cyclin F^{E624K} is suggested for future investigation.

The heat shock 70kDa protein 6 (HSPA6) stress-induced molecular chaperone was not identified (log_2-6.64-fold; $p=3.5x10^{-16}$) in the predicted inhibition of cell viability for cells expressing cyclin F^{E624K}, whereas it was identified in cells expressing cyclin F^{S621G} relative to cyclin F^{WT}(log_2-1.046-fold; p=0.997). The HSPA6 is part of the well-known HSP70 chaperone family of heat-shock proteins that shares high homology with one of the major stress-inducible HSP70 family member, HSPA1 (113). The HSPA6 have been localised in high neurotoxic areas during neuronal differentiation for human neuroblastoma cells (114). This suggests the loss of this molecular chaperone in cells expressing the cyclin F^{E624K} may prevent protein degradation and potentially contribute to neurotoxicity within cells. This may be investigated with co-localised studies to determine whether HSPA6 is present in aggregate protein inclusions for cells expressing the sporadic cyclin F^{E624K} mutant.

Although inhibition of various significant canonical pathways and disease/function predictions provides a general insight into what cellular processes are perturbed in cells expressing cyclin F^{E624K} compared to cells expressing cyclin F^{S621G}, the understanding of cyclin F's role in these pathways are limited. Therefore, to further elucidate cyclin F role in the predicted dysregulated pathways/mechanisms, analysis of the structural integrity of cyclin F^{E624K} was investigated to determine whether changes in cyclin F's protein fold stability affects its functional role in ubiquitylation of protein substrates and/or its protein interactome.

4.3. Protein fold stability is affected in the Cyclin F^{E624K} mutant

The cyclin F protein, as mentioned in section 1.5, is an essential substrate adaptor in the $SCF^{cyclin\ F}$ E3 ubiquitin ligase complex for ubiquitylating protein substrates that are directed to protein degradation clearance systems (e.g. UPS and/or autophagy-lysosomal pathway) (43). Hence, cyclin F is essential in protein quality control systems to maintain cellular proteostasis networks to prevent neurotoxic conditions in motor neurons (14). Compromising protein fold stability that may arise due to a missense mutation within the cyclin F DNA sequence could

therefore have detrimental effects on the protein's function. Cyclin F^{E624K} protein's fold stability predictions were made using the STRUM predictor tool. This revealed decreased fold stability for the sporadic cyclin F^{E624K} mutant when compared to the cyclin F^{WT}. Interestingly, it also predicted a higher protein fold instability when compared to the familial cyclin F^{S621G} mutant. For further insight into whether this protein fold instability in the cyclin F^{E624K} mutant led to a loss- or gain-of-function effects on the proteome, the phosphorylation at the nearby S621 phosphorylation site was investigated.

4.4. Decreased phosphorylation at S621 site due to protein fold instability in the sporadic Cyclin F^{E624K} mutant

As previously mentioned in section 1.5.2, the PEST region is a structural element located at the C-terminus of the cyclin F protein, a heavily phosphorylated region due to the abundance of serine and threonine amino acid residues (65). The S621 site is one of the seven phosphorylated sites that were identified, which displayed relatively low phosphorylation in the familial cyclin F^{S621G} mutant (61). As the cyclin F^{E624K} mutation lies within the phosphorylated S621 motif (^{618}DQE**S**EGKKEG^{627}) it predicted decreased phosphorylation at the S621 site (Figure 3-23;Table 3-10). NetPhos 3.1 predicted that the serine/threonine-selective kinase known as casein kinase 2 (CKII) phosphorylates at the S621 site and in the presence of the cyclin F^{E624K} mutant, the likelihood for phosphorylation to occur is decreased (Table 3-10). This was confirmed with immunoblots that probed for both the phosphorylated S621 motif (^{618}DQES(PO$_4$)EGEKEG^{627}) and non-phosphorylated S621 motif (^{618}DQESEGEKEG^{627}) in the cyclin F protein using custom made rabbit antibodies (Figure 3-24). The immunoblot data validates this prediction as a significant decrease was observed in the cyclin F^{E624K} mutant compared to the cyclin F^{WT} (Figure 3-24). This suggests that the mutational change from the negatively charged glutamic acid (E) to the positively charged lysine (K) loses its ability to bind to the phosphorylated and non-phosphorylated motifs in the antibodies, an essential requirement for CKII binding and phosphorylation which may also confer changes to the protein's function (115).

4.5. Insight into the K48 ubiquitylation activity in cells expressing the Cyclin F^{E624K} mutant

Previous literature, has shown that phosphorylation at the S621 site regulates the ubiquitylation activity of the E3 $SCF^{cyclin\ F}$ ubiquitin ligase complex (61). As a result of the significantly decreased phosphorylation at the S621 site in HEK293 cells expressing the cyclin F^{E624K}

mutant, global ubiquitylation was investigated using immunoblots. This determined whether alterations in substrate ubiquitylation was present with the sporadic cyclin F^{E624K} mutant, as cyclin F is an essential component of the E3 $SCF^{cyclin\ F}$ ubiquitin ligase complex in the ubiquitylation pathway (43). Overall, increased global K48-ubiquitylation levels were observed for the cyclin F^{E624K} mutant compared to the cyclin F^{WT}, and similarly were observed in the cyclin F^{S621G} mutant. This provided rationale to measure the K48 ubiquitylation activity of immunoprecipitated cyclin F and its protein interactors using an E3 ubiquitin ligase activity assay. However, these results revealed no significant difference in cells expressing cyclin F^{E624K} when compared to the K48 ubiquitylation activity for cyclin F^{WT} (Figure 3-27). To rule out whether this was the result of an experimental error, triplicates of the immunoprecipitated cyclin F was measured and the increase in K48 ubiquitylation for the cyclin F^{S621G} mutant in this study reflected previous research that also revealed increases in K48 ubiquitylation for the familial mutant (54). Therefore, the disparity observed for the immunoblotting (shown to increase in global K48-ubiquitylation) and E3 ubiquitin ligase activity assay (no difference in K48-specific ubiquitylation activity) of the cyclin F^{E624K} mutant, suggests that the structural change affecting phosphorylation at the S621 site could instead cause changes to the cyclin F protein interactome.

4.6. The protein interactome differs in cells expressing the Cyclin F^{E624K} mutant

Unbiased label-free proteomic analysis for immunoprecipitants provided insight into what putative and/or novel PPIs were made with sporadic cyclin F^{E624K} mutant. Here we evaluate whether these PPIs are involved in specific pathways altering the cellular interactome that may influence proteostasis in cells and ultimately lead to neurodegeneration.

4.6.1. Cyclin F^{E624K} protein interactors involved in neurodegenerative diseases

The IP proteomic analysis identified a total of 322 cyclin F protein interactors in HEK293 cells expressing the sporadic cyclin F^{E624K} mutant that displayed both *enhanced* and *non-enhanced* binding activity compared to cells expressing cyclin F^{WT} (Figure 3-17.A). Upon further investigation using PANTHER GO, it was revealed that the *enhanced* protein interactors clustered towards pathways involved in neurodegenerative diseases (Figure 3-19). The neurodegenerative diseases identified included “Parkinson’s disease”, “Alzheimer’s disease”, and “Huntington’s disease”. Interestingly, *enhanced*-binding cyclin F protein interactors

included PSMA2, a protein that displayed greater *enhanced*-binding to cyclin F^{E624K} ($log_2$1.134-fold) compared to the cyclin F^{S621G} ($log_2$0.415-fold), and HSPA14 that was identified in both cyclin F mutants ($log_2$6.64-fold) (Table 3-8).

The PSMA2 protein is proteasome α-subunit (type 2) that regulates the catalytic core of the 20S proteasome, a regulatory component for the ubiquitin-dependent 26S proteasome (116, 117). Previous literature has revealed that a loss of proteasome α-subunits in dopaminergic neurons located in the substantia nigra pars compacta is linked to proteostasis impairments, a common hallmark of Parkinson's disease (80, 118, 119). Although *beta*-subunits are the catalytic sites for proteasome machinery, the loss of *alpha*-subunits of the proteasome can consequently impair the proteasome functional activity, as they take part in regulating proteasome assembly (120). In this data, the PSMA2 was identified as an *enhanced* cyclin F^{E624K} protein interactor compared to the cyclin F^{S621G}. This could indicate that *enhanced* binding to the sporadic mutant could potentially be interfering with proteasome assembly by sequestering the subunit, a difference between the cyclin F mutants. Impairments or losses to the proteasome can therefore preclude degradation of unwanted and misfolded proteins, thus forming aggregated protein inclusions, a hallmark for not only Parkinson's disease but other neurodegenerative disease such as ALS and FTD (121, 122).

The heat shock 70kDa protein 14 (HSPA14) is a component of the Hsp70s chaperone family, essential in early protein folding and with additional co-chaperones, such as the c-terminal HSP70-interacting protein (CHIP), can direct misfolded proteins for protein degradation (123, 124). Specifically, the HSPA14 is a component of the mammalian ribosome-associated complex (RAC) with its main functional role in folding and maintaining the folded state for nascent polypeptides (125). Investigation by Roodveldt *et al*, revealed that decreased HSP70 activity may directly result in aggregated amyloid inclusions that consist of the toxic α-synuclein, a significant constitute of Lewy bodies in Parkinson's disease and TDP-43-associated neurodegenerative diseases (79, 126). In the data, the HSPA14 was identified exclusively in the cyclin F mutants, suggesting that binding of mutant cyclin F to this HSP70 chaperone may interrupt the protein folding activity and/or protein degradation signalling associated with CHIP. As CHIP also associates with ubiquitin ligases, interference in HSP70 activity could potentially lead to poor protein quality control and therefore proteostasis imbalance (124, 127).

Based on the cyclin F^{E624K} protein identified in neurodegenerative diseases, the data obtained demonstrates that mutations in cyclin F may be associated with dysregulation of the molecular chaperones and the UPS, specifically the structural assembly of the proteasome. This suggests that instead of affecting the ubiquitylation of proteins the cyclin F^{E624K} mutant may be binding to chaperones and proteasome subunits and therefore alter the function(s) of these components that are essential for cellular homeostasis.

4.6.2. Ubiquitin and proteasome protein-protein interactions (PPIs) identified in cells expressing Cyclin F^{E624K}

Regulation of the cellular proteostasis network is heavily influenced by the ubiquitin-conjugating E2 enzymes (that make up the ubiquitin cascade) and the proteasome, which together consists of the UPS (128). Therefore, further investigation into the cyclin F PPIs involved in the UPS-associated proteins enriched in cells expressing cyclin F^{E624K} was of great of interest. An E3 ubiquitin ligase enzyme (PJA2), a proteasome subunit (PSMA6) and co-chaperone (SGTA) that were enriched as cyclin F^{E624K} protein interactors and clustered together in the ubiquitin- and proteasome-associated protein network were investigated further (Figure 3-22).

The E3 ubiquitin-protein ligase Praja-2 (PJA2) is expressed in neuronal synapses in the brain (129). Although there is limited research on PJA2, it is an E2-dependent E3 ligase enzyme related to the family of RING finger proteins, a well-characterised domain that is found in most E3 ubiquitin ligases (130, 131). In the data obtained, the PJA2 displayed *reduced*-binding to the cyclin F^{E624K} protein relative to cells expressing cyclin F^{WT}. This suggests that due to altered structural state as a result of the mutation, the decreased interaction between PJA2 and the cyclin F^{E624K} protein may affect protein ubiquitylation and potentially lead to poor protein quality control, promoting proteostasis imbalance.

The proteasome subunits identified (PSMA6, PSME2, and PSMB7) displayed *reduced*-binding with the cyclin F^{E624K} mutant relative to cells expressing cyclin F^{WT}. This suggests that possibly transport of ubiquitylated substrates of cyclin F^{E624K} to the proteasome may be perturbed and/or that the proteasome subunits may be defective. As previously discussed, recent studies have shown proteasome dysfunction as a result of impaired proteasome subunits, which can also dysregulate proteostasis and exhibit neurodegenerative characteristics (80, 118). For example, the PSMC1 proteasome subunit of the 26S proteasome was conditionally knocked out in mice to demonstrate proteasome dysfunction in neurons, thus resembling aggregation of protein

inclusions as seen in many neurodegenerative diseases (50). Although loss-of-binding interactions is not as substantial as total depletion of proteasome subunits, it may provide insight into the association between cyclin F and UPS dysfunction.

The proteasome subunit alpha type-6 (PSMA6) was also discovered to have PPIs with proteins that are included in the core component of the SCF E3 ligase complex, CUL1 (132). Co-immunoprecipitated CUL1 identified PSMA6 as one of the three proteasome subunits in the study Bloom *et al* (133). Thus, demonstrating that the association between the proteasome and E3 SCF ligase complexes, such as $SCF^{cyclin\ F}$, are targeting ubiquitylated substrates for degradation. The result in this protein network, could indicate that *reduced*-binding of cyclin F^{E624K} with PSMA6 may preclude the transport of ubiquitylated proteins for degradation by the proteasome, as the cyclin F protein may act as an upstream regulator for PSMA6 in protein degradation. This may be investigated with a ubiquitin-independent 26S proteasome activity assay could be used to determine proteasome dysfunction.

Notably the small glutamine-rich tetratricopeptide repeat-containing protein alpha (SGTA) was enriched in this proteasome network, where it displayed *enhanced*-binding with cyclin F^{E624K} and made a direct interaction to the 26S Proteasome complex (Figure 3-22). It was also predicted as an activator for motor dysfunction activation (Figure 3-20). The SGTA acts as a co-chaperone for cytoplasmic hydrophobic misfolded proteins where they are delivered and processed to the ER, via the tail-anchored (TA) pathway (134). Together with another TA protein (BAG6), this SGTA-BAG6 complex sorts the ubiquitylated substrates to the proteasome for degradation, when delivery to the ER fails (e.g. ER stress) (135). Furthermore, SGTA association with the activation in motor dysfunction was revealed in a study by Chen *et al* (136). In this study co-localisation of SGTA and CASP3 in a spinal cord injury mouse model was presented, indicating SGTA may be interacting with neuronal apoptosis-induced motor dysfunction. Taken together with the results obtained from this present study, this suggests that the *enhanced* binding of SGTA to the cyclin F^{E624K} mutant may interfere with ERAD and UPS delivery of misfolded proteins, thus generating a proteostasis imbalance in the cells.

Based on the ubiquitin- and proteasome-associated protein network that was immunoprecipitated in cell expressing cyclin F^{E624K}, a toxic *reduced*-binding for PJA2 and PSMA6 and toxic *enhanced*-binding for SGTA may consequently lead to proteasome dysfunction which may be an underlying causative mechanism for ALS/FTD pathogenesis in this sporadic mutation.

4.6.3. Oxidative stress related protein-protein interactions (PPIs) in cells expressing Cyclin F^{E624K}

Oxidative stress is one of the many molecular mechanisms associated with neurodegeneration, in which mitochondrial dysfunction results in an imbalance of overproduced reactive oxygen species (ROS) and the inability to remove or repair the damage caused by the ROS (137). This can also impair ATP production that is generated from the mitochondrial oxidative phosphorylation process (138). The proteomic analysis of immunoprecipitated cyclin F data revealed several proteins and protein networks that are associated with oxidative stress response and oxidative stress-induced apoptosis. In the PANTHER GO analysis for the enriched *unique* and *shared* cyclin F^{E624K} protein interactors, SOD1 and HMGB1 were two of three represented proteins in the *response to stress* category (Figure 3-18;Table 3-7).

SOD1 was identified as a cyclin F protein interactor in both the familial and sporadic mutants, whereas it did not bind to cyclin F^{WT} (Table 3-7). It was also identified as a motor dysfunction activator in the IPA predictions for disease/function analysis (Figure 3-20). The main function of SOD1 is to act as a defence mechanism to protect against oxidative damage that may be caused by ROS, a by-product of the oxidative phosphorylation process that occurs in the mitochondrial (139). Mutations in SOD1 account for ~20% of fALS and have revealed linkages between increased oxidative stress and neurodegeneration (140). Mutations in SOD1 expressed in transgenic mouse models for ALS have shown a toxic gain-of-function, however the pathophysiological mechanisms that leads to neurodegeneration remains unclear (141-143). Although ALS-associated SOD1 research is focused on mutants causing a toxic gain-of-function, there is evidence to suggest linkages between a toxic loss-of-function in SOD1 activity and neurodegeneration (144). An *in vitro* study, demonstrated that mutant SOD1 aggregations with amyloid-*beta* plaques decreases the SOD activity in human neuroglioma cell culture (145). Furthermore, an overexpressed $SOD1^{WT}$ transgenic mouse study by Graffmo *et al*, displayed SOD1 protein aggregations in brain and spinal cord tissues with no changes in superoxide dismutase activity (146). Although no reduction in SOD1 activity was identified, the formation of aggregates can alter the structural-functional properties and perturb other proteins it aggregates with. Furthermore, studies have shown that SOD1 aggregations were prominent in sporadic ALS cases, highlighting that this may be a common underling mechanism in the pathogenesis of sALS (147, 148). Therefore, it would be interesting to distinguish whether SOD1 aggregates with the sporadic cyclin F^{E624K} and the familial cyclin F^{S621G} mutants are formed and disrupting SOD1's function in oxidative stress conditions. This

could provide rationale for the oxidative stress response that is occurring in cells and display an *enhanced*-binding toxicity in cells expressing the sporadic cyclin F^{E624K} mutant.

The high mobility group protein B1 (HMGB1) is a multifunctional protein that mainly acts as a DNA chaperone in the nucleus (reduced-state) and an extracellular signalling molecule in the cytoplasm (oxidised-state) (149, 150). The accumulation of oxidised HMGB1 in the cytoplasm can initiate an oxidative stress response if the capacity of this oxidised protein overcompensates thioredoxin availability to maintain HMGB1 in its reduced state (151). HMGB1 was identified as a cyclin F^{E624K} protein interactor, which suggests when oxidised HMGB1 is over-expressed it may lead to an oxidative stress response. A protein carbonyl assay using immunoblotting techniques may assist to determine whether oxidised HMGB1 are present in cells expressing the sporadic cyclin F^{E624K} mutant, as well as immunohistochemistry analysis to determine whether the oxidised HMGB1 is localised in the cytoplasm.

4.6.4. Oxidative stress-induced apoptosis in cells expressing Cyclin F^{E624K}

The IPA data revealed an immunoprecipitated protein network that consisted mainly of loss-of-binding proteins associated with cytochrome c oxidase proteins in cells expressing the cyclin F^{E624K} (Figure 3-21). The cytochrome c oxidase complex is a crucial component of the electron transport chain which takes part in oxidative-phosphorylation processing along the mitochondrial membrane (152). The protein network identified consists of several complexes and subunits that are essential for mitochondria function, including cellular ATP production and maintaining ROS levels (153, 154). The cyclin F^{E624K} protein interactors that were of interest included the UQCRB and CYCS. Loss-of-binding between both cyclin F^{E624K} and UQCRB and cyclin F^{E624K} and CYCS was observed. The cytochrome b-c1 complex subunit 7 (UQCRB) is an essential subunit for the cytochrome b-c1 complex (or complex III in the oxidative-phosphorylation system), with its role in redox-linked proton pumping in the electron transport chain (155). Deficiencies in the cytochrome b-c1 complex have been linked to neurodegeneration, where patients with neuromuscular disorders were screened for dysfunction in the cytochrome b complex (156). Consistent with the IPA results, the UQCRB was also identified in the activation of motor dysfunction for cyclin F^{E624K} immunoprecipitants (Figure 3-20).

The cytochrome c protein (CYCS) acts as an electron carrier to the cytochrome c complex (or complex IV) in the electron transport chain (157). When released from the mitochondria into the cytoplasm, CYCS can promote apoptotic cell death (158). The upstream regulators (CTSD

and BAX) of CYCS were also identified in this protein network, which are known to respond to oxidate stress (e.g. increase production of ROS) and induce apoptosis in neuronal cells (159). In addition, upstream from these proteins is the NFkB complex, a transcription factor complex known to express various genes in response to oxidative stress (108). The identification of this complex indicates that oxidative stress is evident in cells expressing the sporadic cyclin F^{E624K} mutant, suggesting that it may be a key pathogenic mechanism in sporadic ALS/FTD patients.

4.6.5. Motor dysfunction is activated in protein-protein interactions (PPIs) for cells expressing Cyclin F^{E624K}

As mentioned in previous sections of this discussion, IPA data has identified linkages between motor dysfunction and some cyclin F^{E624K} proteins interactors. A total of 33 cyclin F protein interactors were identified and six proteins of interest were selected: SOD1, BAX, CTSD, SGTA, HSPB1, and UQCRB (Figure 3-20).

The apoptosis regulator BAX has been shown to promote apoptosis in the presence of mitochondrial dysfunction, as it acts a pro-apoptotic protein upstream of cytochrome c-induced apoptosis in response to oxidative stress (160). In a Parkinson's disease mouse model, the removal of BAX was shown to attenuate neurodegeneration of dopaminergic neurons in the substantia nigra pars compacta of the brain (161). Although it does not cause motor dysfunction, high levels of BAX were also supported by the analysis of brain samples of patients with Alzheimer's disease, strengthening the link between dysregulation of BAX levels and neurodegeneration (162).

The cathepsin D (CTSD) acid protease is an upstream regulator, along with BAX, that promotes oxidative stress-induced apoptosis by releasing cytochrome c from the mitochondria (159). Deficiencies in CTSD that are BAX-independent for apoptosis, can induce an autophagic stress response that can lead to proteostasis dysfunction. This was demonstrated in a mouse model where phenotypic characteristics including motor dysfunction were presented as a result of depleted CTSD (163). Also CTSD deficiencies were found in human neurodegenerative disorders where protein degradation processes were defected (164).

The molecular chaperone (HSPB1) mainly functions to maintain proteostasis with its protective role in heat shock and oxidative stress conditions (165). However, recent studies have shown linkages between mutations of HSPB1 and axonopathy (166, 167). This additional role in mediating myelination of axons, provides insight into the molecular mechanisms that this

chaperone plays in neurodegeneration. The immunoprecipitated proteins identified demonstrate that cyclin F^{E624K} protein interactors can induce apoptosis and exhibit disastrous effects in motor neurons and ultimately lead to motor dysfunction, a well-known characteristic for many neurodegenerative diseases including ALS.

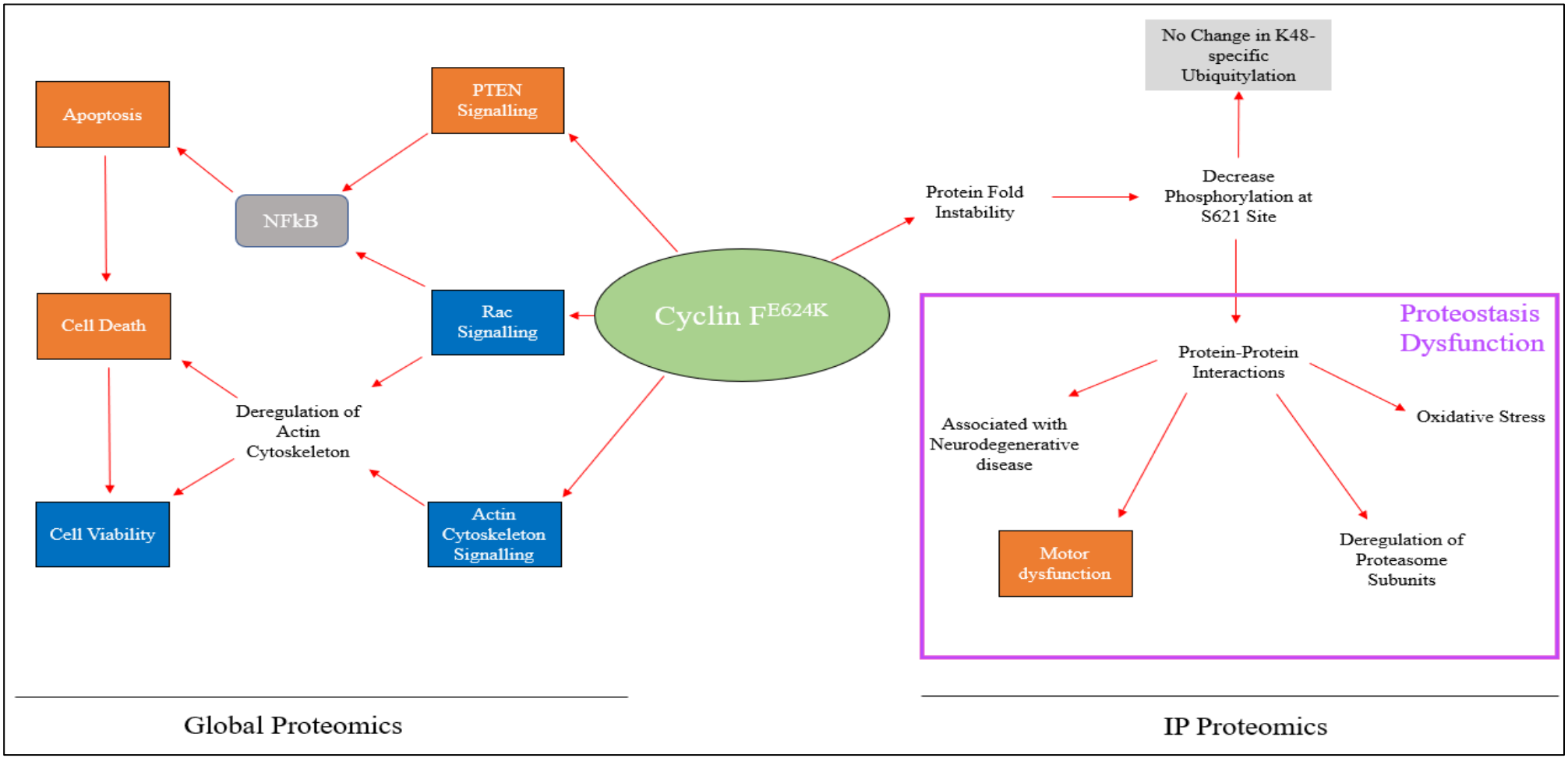

Figure 4-1. Summary of findings.

Global proteomic data displayed HEK293 cells expressing cyclin F^{E624K} activating PTEN signalling (orange) and inhibiting Rac and actin cytoskeleton signalling (blue). PTEN and Rac signalling share the down-regulated NFkB complex in their signalling networks, a protein complex involved in regulating apoptosis which was activated. Activation of apoptosis leads to activation of cell death and inhibition of cell viability. Inhibition of Rac and actin cytoskeleton signalling led to dysregulation of actin cytoskeleton organisation, which can potentially exhibit activated cell death and inhibit cell viability. Protein fold instability was predicted, and further investigation discovered decreased phosphorylation at the S621 site of the cyclin F protein. No change in K48-specific ubiquitylation was determined despite the significant decrease in phosphorylation, this suggested that the structural change affecting phosphorylation at the S621 site

could instead affect the differences in the cyclin F protein interactome, which was further investigated with IP proteomics. The investigation of PPIs revealed protein interactors associated with neurodegenerative diseases, activation of motor dysfunction, deregulation of proteasome subunits, and oxidative stress. The findings from the IP proteomic data supports the underlying causative mechanisms of proteostasis dysfunction in ALS/FTD pathology.

4.7. Limitations & future directions

A main limitation of this study was the transfection of the *CCNF* transgenes in HEK293 cells. HEK293 cells were selected due to the ease in efficient transfection as the cells have a fast growth and long survival rate, beneficial for the limited time given for this research project (71). However, the cell line does not fully recapitulate the dynamics of a neuron in how it expresses gene mutations in a manner that is similar to motor neurons of ALS/FTD patients. Instead human neuroblastoma cells such as SH-SY5Y cells or primary neurons may be an appropriate *in vitro* model to study the perturb cellular pathways and unique PPIs that were demonstrated in the sporadic cyclin F^{E624K} mutant and should be considered for future investigations.

Another limitation was the excessive number of immunoprecipitated proteins that were identified in the MS analysis. Over 2,000 protein were quantified, which may be because the *CCNF* gene is part of an E3 ligase complex where it binds and aggregates to many proteins or gives indication that many non-specific proteins were identified. The overexpression of the *CCNF* transgenes may also contribute to the excessive number identified. To prevent this in future studies, the generation of stable cell lines using a cell-based system such as Flp-In T-Rex system which incorporates only one gene to control the *CCNF* expression levels (168).

The other reason is due to non-specific proteins identified, as the mass spectrometer analyses the most abundant proteins, the non-specific proteins may have overshadowed other cyclin F specific protein interactions that may have a key role in the underlying pathogenic mechanisms of ALS/FTD pathology. Suggestions to overcome this limitation includes longer washing steps in the immunoprecipitation methodology, as well as alternative proximity-ligation approaches such as the biotin ligase proximity protein labelling technique (BioID) and ascorbate peroxidase proximity protein labelling technique (APEX) could be used to alleviate the potentially high amount of non-specific interactions (169). However, non-specific proteins may be beneficial as it may indicate proteome reproducibility in cells that can serve as a quality control. This coupled to an intensity profile analysis may assist in identifying weaker interactions, a proteomic approach that can be used in future studies (170).

The E3 ubiquitin ligase activity assay demonstrated non-significant changes in E3 ligase activity for cyclin F^{E624K} and cyclin F^{S621G} mutants compared to cyclin F^{WT}. Although three replicates were performed, it may be beneficial for future studies to increase the number of

replicates and include longer incubation times in the methodology, to determine whether a significant difference in K48 ubiquitylation is observed between cyclin F mutants and cyclin F^{WT}.

From this research project, several hypotheses can be considered for future directions with the investigation into the sporadic cyclin F^{E624K} mutation in ALS/FTD pathology. The first hypothesis is that the sporadic cyclin F^{E624K} mutation affects the fold stability of the protein and limits the K48-specific ubiquitylation. As the CKII does not bind to the phosphorylated S621 site, this may be due to alteration in the biochemistry of the cyclin F protein, where the negatively charged glutamic acid (E) residue is mutated to the positively charge (K) lysine residue, and therefore may limit ubiquitylation. X-ray crystallography provides structural determination of a protein as it generates a three-dimensional molecular structure in crystal form, therefore comparative analysis using this technique can determine the structural integrity of the sporadic cyclin F^{E624K} mutant compared to cyclin F^{WT} (171).

The second hypothesis is that the sporadic cyclin F^{E624K} mutant interacts and alters proteasome machinery via the PPIs that were identified with this data. The protein interactions made with cyclin F^{E624K} may perturb the functional properties of the proteasome subunits identified and lead to proteostasis impairment in motor neurons. It would be worth investigating as this may explain that the fold instability is not affecting the ubiquitylation role of $SCF^{cyclin\ F}$ complex, but instead losing protein interactions that are regulating the proteasome for efficient degradation of ubiquitylated proteins. A ubiquitin-independent 26S proteasome activity assay could be used to measure hydrolysis of a fluorophore substrate that is released during proteolytic activity (172).

The third hypothesis is that oxidative stress-induced apoptosis is an underlying pathogenic mechanism in sporadic ALS/FTD patients with the *CCNF* mutations. The numerous oxidative stress-related protein interactors identified in cells expressing the sporadic cyclin F^{E624K} mutant provides rationale that a toxic *enhanced*-binding of oxidised proteins and toxic loss-of-function for SOD1 is elucidated in sporadic ALS/FTD pathology. To strengthen this hypothesis, a protein carbonyl assay using immunoblotting techniques may assist in determining oxidised cyclin F^{E624K} protein interactors, and an siRNA knockdown of SOD1 in cells expressing cyclin F^{E624K} may determine whether SOD1 interactions with cyclin F^{E624K} are limiting its function in regulating oxidative-phosphorylation processes when compared to siRNA knockdown of SOD1 cells expressing the cyclin F^{WT}.

5. Concluding Statements

This study has investigated for the first time the similarities and differences in both cellular pathways and protein-protein interactive networks in the sporadic cyclin F^{E624K} mutant. Comparative analysis with cyclin F^{WT} and the recently-characterised familial cyclin F^{S621G} mutant assisted in determining novel and similar perturbed cellular pathways to elucidate differences in pathogenic mechanisms between familial and sporadic ALS/FTD. The proteomic data obtained has suggested that proteostasis imbalances in cells expressing the sporadic cyclin F^{E624K} are the result of perturbed protein stability, oxidative stress, and dysregulation of the proteasome machinery. In addition, the use of proteomic-based techniques described in this thesis can elucidate and discriminates on a biological level the differences between familial and sporadic ALS/FTD pathogenic mechanisms. Together with this data and the future directions listed, this study shows promising evidence that may contribute to a better understanding in the underlying cellular mechanisms that distinguish familial with sporadic ALS/FTD pathology and may ultimately assist in the development of sporadic-based ALS/FTD therapeutics.

6. References:

1. Arai T, Hasegawa M, Akiyama H, Ikeda K, Nonaka T, Mori H, Mann D, Tsuchiya K, Yoshida M, Hashizume Y. TDP-43 is a component of ubiquitin-positive tau-negative inclusions in frontotemporal lobar degeneration and amyotrophic lateral sclerosis. Biochemical and biophysical research communications. 2006;351(3):602-11.

2. Neumann M, Sampathu DM, Kwong LK, Truax AC, Micsenyi MC, Chou TT, Bruce J, Schuck T, Grossman M, Clark CM. Ubiquitinated TDP-43 in frontotemporal lobar degeneration and amyotrophic lateral sclerosis. Science. 2006;314(5796):130-3.

3. Cleveland DW, Rothstein JD. From Charcot to Lou Gehrig: deciphering selective motor neuron death in ALS. Nature reviews neuroscience. 2001;2(11):806.

4. Goetz CG. Amyotrophic lateral sclerosis: early contributions of Jean-Martin Charcot. Muscle & Nerve: Official Journal of the American Association of Electrodiagnostic Medicine. 2000;23(3):336-43.

5. Kumar DR, Aslinia F, Yale SH, Mazza JJ. Jean-Martin Charcot: the father of neurology. Clinical medicine & research. 2011;9(1):46-9.

6. Rowland LP, Shneider NA. Amyotrophic lateral sclerosis. New England Journal of Medicine. 2001;344(22):1688-700.

7. DA E. Economic analysis of motor neurone disease in Australia, report for Motor Neurone Disease Australia Canberra: Deloitte Access Economics; 2015 [22/11/18].

8. Mandrioli J, Faglioni P, Nichelli P, Sola P. Amyotrophic lateral sclerosis: prognostic indicators of survival. Amyotrophic lateral sclerosis. 2006;7(4):217-26.

9. Van Langenhove T, van der Zee J, Van Broeckhoven C. The molecular basis of the frontotemporal lobar degeneration–amyotrophic lateral sclerosis spectrum. Annals of medicine. 2012;44(8):817-28.

10. Pick A. Über einen weiteren Symptomenkomplex im Rahmen der Dementia senilis, bedingt durch umschriebene stärkere Hirnatrophie (gemischte Apraxie). European Neurology. 1906;19(2):97-108.

11. Alzheimer A. Uner eignearte Krankenheitsfalle des spatern Alters. Zeitschr Ges Neur Psych. 1911;4:356-85.

12. Seelaar H, Rohrer JD, Pijnenburg YA, Fox NC, Van Swieten JC. Clinical, genetic and pathological heterogeneity of frontotemporal dementia: a review. Journal of Neurology, Neurosurgery & Psychiatry. 2011;82(5):476-86.

13. Rabinovici GD, Miller BL. Frontotemporal lobar degeneration. CNS drugs. 2010;24(5):375-98.

14. Williams K, Topp S, Yang S, Smith B, Fifita J, Warraich S, Zhang K, Farrawell N, Vance C, Hu X, Chesi A, Leblond C, Lee A, Rayner S, Sundaramoorthy V, Dobson-Stone C,

Molloy M, Van Blitterswijk M, Dickson D, Petersen R, Graff-Radford N, Boeve B, Murray M, Pottier C, Don E, Winnick C, McCann E, Hogan A, Daoud H, Levert A, Dion P, Mitsui J, Ishiura H, Takahashi Y, Goto J, Kost J, Gellera C, Gkazi A, Miller J, Stockton J, Brooks W, Boundy K, Polak M, Muñoz-Blanco J, Esteban-Pérez J, Rábano A, Hardiman O, Morrison K, Ticozzi N, Silani V, De Belleroche J, Glass J, Kwok JB, Guillemin G, Chung R, Tsuji S, Brown R, García-Redondo A, Rademakers R, Landers J, Gitler A, Rouleau G, Cole N, Yerbury J, Atkin J, Shaw C, Nicholson G, Blair I. CCNF mutations in amyotrophic lateral sclerosis and frontotemporal dementia. Nature Communications. 2016;7:11253.

15. Rosen DR, Siddique T, Patterson D, Figlewicz DA, Sapp P, Hentati A, Donaldson D, Goto J, O'Regan JP, Deng H-X. Mutations in Cu/Zn superoxide dismutase gene are associated with familial amyotrophic lateral sclerosis. Nature. 1993;362(6415):59.

16. Forsberg K, Andersen PM, Marklund SL, Brännström T. Glial nuclear aggregates of superoxide dismutase-1 are regularly present in patients with amyotrophic lateral sclerosis. Acta neuropathologica. 2011;121(5):623-34.

17. Carrì MT, Valle C, Bozzo F, Cozzolino M. Oxidative stress and mitochondrial damage: importance in non-SOD1 ALS. Frontiers in cellular neuroscience. 2015;9:41.

18. De Vos KJ, Chapman AL, Tennant ME, Manser C, Tudor EL, Lau K-F, Brownlees J, Ackerley S, Shaw PJ, McLoughlin DM. Familial amyotrophic lateral sclerosis-linked SOD1 mutants perturb fast axonal transport to reduce axonal mitochondria content. Human molecular genetics. 2007;16(22):2720-8.

19. Liu J, Lillo C, Jonsson PA, Velde CV, Ward CM, Miller TM, Subramaniam JR, Rothstein JD, Marklund S, Andersen PM. Toxicity of familial ALS-linked SOD1 mutants from selective recruitment to spinal mitochondria. Neuron. 2004;43(1):5-17.

20. Gurney ME, Pu H, Chiu AY, Dal Canto MC, Polchow CY, Alexander DD, Caliendo J, Hentati A, Kwon YW, Deng H-X. Motor neuron degeneration in mice that express a human Cu, Zn superoxide dismutase mutation. Science. 1994;264(5166):1772-5.

21. Kwiatkowski TJ, Bosco D, Leclerc A, Tamrazian E, Vanderburg C, Russ C, Davis A, Gilchrist J, Kasarskis E, Munsat T. Mutations in the FUS/TLS gene on chromosome 16 cause familial amyotrophic lateral sclerosis. Science. 2009;323(5918):1205-8.

22. Sreedharan J, Blair IP, Tripathi VB, Hu X, Vance C, Rogelj B, Ackerley S, Durnall JC, Williams KL, Buratti E. TDP-43 mutations in familial and sporadic amyotrophic lateral sclerosis. Science. 2008;319(5870):1668-72.

23. Ling S-C, Polymenidou M, Cleveland DW. Converging mechanisms in ALS and FTD: disrupted RNA and protein homeostasis. Neuron. 2013;79(3):416-38.

24. Wang IF, Wu LS, Shen CK. TDP-43: an emerging new player in neurodegenerative diseases. Trends Mol Med. 2008;14(11):479-85.

25. Kabashi E, Valdmanis PN, Dion P, Spiegelman D, McConkey BJ, Velde CV, Bouchard J-P, Lacomblez L, Pochigaeva K, Salachas F. TARDBP mutations in individuals with sporadic and familial amyotrophic lateral sclerosis. Nature genetics. 2008;40(5):572.

26. Hartl FU, Bracher A, Hayer-Hartl M. Molecular chaperones in protein folding and proteostasis. Nature. 2011;475(7356):324.

27. Morimoto RI. Proteotoxic stress and inducible chaperone networks in neurodegenerative disease and aging. Genes & development. 2008;22(11):1427-38.

28. Hipp MS, Park S-H, Hartl FU. Proteostasis impairment in protein-misfolding and-aggregation diseases. Trends in cell biology. 2014;24(9):506-14.

29. Balch WE, Morimoto RI, Dillin A, Kelly JW. Adapting proteostasis for disease intervention. science. 2008;319(5865):916-9.

30. Tanaka K, Matsuda N. Proteostasis and neurodegeneration: the roles of proteasomal degradation and autophagy. Biochimica et Biophysica Acta (BBA)-Molecular Cell Research. 2014;1843(1):197-204.

31. Ruegsegger C, Saxena S. Proteostasis impairment in ALS. Brain research. 2016;1648:571-9.

32. Schubert U, Anton LC, Gibbs J, Norbury CC, Yewdell JW, Bennink JR. Rapid degradation of a large fraction of newly synthesized proteins by proteasomes. Nature. 2000;404(6779):770.

33. Aisen PS, Davis KL. Inflammatory mechanisms in Alzheimer's disease: implications for therapy. The American journal of psychiatry. 1994;151(8):1105-13.

34. Perutz M. Glutamine repeats and inherited neurodegenerative diseases: molecular aspects. Current opinion in structural biology. 1996;6(6):848-58.

35. Polymeropoulos MH, Lavedan C, Leroy E, Ide SE, Dehejia A, Dutra A, Pike B, Root H, Rubenstein J, Boyer R. Mutation in the α-synuclein gene identified in families with Parkinson's disease. science. 1997;276(5321):2045-7.

36. Anelli T, Sitia R. Protein quality control in the early secretory pathway. The EMBO journal. 2008;27(2):315-27.

37. Braakman I, Bulleid NJ. Protein folding and modification in the mammalian endoplasmic reticulum. Annual review of biochemistry. 2011;80:71-99.

38. Hetz C, Mollereau B. Disturbance of endoplasmic reticulum proteostasis in neurodegenerative diseases. Nature Reviews Neuroscience. 2014;15(4):233.

39. Walter P, Ron D. The unfolded protein response: from stress pathway to homeostatic regulation. Science. 2011;334(6059):1081-6.

40. Hetz C. The unfolded protein response: controlling cell fate decisions under ER stress and beyond. Nature reviews Molecular cell biology. 2012;13(2):89.

41. Ciechanover A. The ubiquitin–proteasome pathway: on protein death and cell life. The EMBO journal. 1998;17(24):7151-60.

42. Ravid T, Hochstrasser M. Degradation signal diversity in the ubiquitin-proteasome system. Nature reviews Molecular cell biology. 2008;9(9):679.

43. Galper J, Rayner SL, Hogan AL, Fifita JA, Lee A, Chung RS, Blair IP, Yang S. Cyclin F: A component of an E3 ubiquitin ligase complex with roles in neurodegeneration and cancer. The international journal of biochemistry & cell biology. 2017;89:216-20.

44. Ikeda F, Dikic I. Atypical ubiquitin chains: new molecular signals. EMBO reports. 2008;9(6):536-42.

45. Matsumoto G, Wada K, Okuno M, Kurosawa M, Nukina N. Serine 403 phosphorylation of p62/SQSTM1 regulates selective autophagic clearance of ubiquitinated proteins. Molecular cell. 2011;44(2):279-89.

46. Lippai M, Lőw P. The role of the selective adaptor p62 and ubiquitin-like proteins in autophagy. BioMed research international. 2014;2014.

47. Long J, Gallagher TR, Cavey JR, Sheppard PW, Ralston SH, Layfield R, Searle MS. Ubiquitin recognition by the ubiquitin-associated domain of p62 involves a novel conformational switch. Journal of Biological Chemistry. 2008;283(9):5427-40.

48. Coux O, Tanaka K, Goldberg AL. Structure and functions of the 20S and 26S proteasomes. Annual review of biochemistry. 1996;65(1):801-47.

49. Finley D. Recognition and processing of ubiquitin-protein conjugates by the proteasome. Annual review of biochemistry. 2009;78:477-513.

50. Bedford L, Hay D, Devoy A, Paine S, Powe DG, Seth R, Gray T, Topham I, Fone K, Rezvani N. Depletion of 26S proteasomes in mouse brain neurons causes neurodegeneration and Lewy-like inclusions resembling human pale bodies. Journal of Neuroscience. 2008;28(33):8189-98.

51. Tashiro Y, Urushitani M, Inoue H, Koike M, Uchiyama Y, Komatsu M, Tanaka K, Yamazaki M, Abe M, Misawa H. Motor neuron-specific disruption of proteasomes, but not autophagy, replicates amyotrophic lateral sclerosis. Journal of Biological Chemistry. 2012:jbc. M112. 417600.

52. Komatsu M, Ueno T, Waguri S, Uchiyama Y, Kominami E, Tanaka K. Constitutive autophagy: vital role in clearance of unfavorable proteins in neurons. Cell death and differentiation. 2007;14(5):887.

53. Yang Z, Klionsky DJ. Mammalian autophagy: core molecular machinery and signaling regulation. Current opinion in cell biology. 2010;22(2):124-31.

54. Lee A, Rayner SL, Gwee SS, De Luca A, Shahheydari H, Sundaramoorthy V, Ragagnin A, Morsch M, Radford R, Galper J. Pathogenic mutation in the ALS/FTD gene, CCNF, causes elevated Lys48-linked ubiquitylation and defective autophagy. Cellular and Molecular Life Sciences. 2017:1-20.

55. Lattante S, de Calbiac H, Le Ber I, Brice A, Ciura S, Kabashi E. Sqstm1 knock-down causes a locomotor phenotype ameliorated by rapamycin in a zebrafish model of ALS/FTLD. Human molecular genetics. 2014;24(6):1682-90.

56. Parzych KR, Klionsky DJ. An Overview of Autophagy: Morphology, Mechanism, and Regulation. Antioxidants & Redox Signaling. 2014;20(3):46-473.

57. Bai C, Richman R, Elledge SJ. Human cyclin F. The EMBO journal. 1994;13(24):6087.

58. Johnson D, Walker C. Cyclins and cell cycle checkpoints. Annual review of pharmacology and toxicology. 1999;39.

59. Minshull J, Pines J, Golsteyn R, Standart N, Mackie S, Colman A, Blow J, Ruderman Jv, Wu M, Hunt T. The role of cyclin synthesis, modification and destruction in the control of cell division. J Cell Sci. 1989;1989(Supplement 12):77-97.

60. D'Angiolella V, Donato V, Vijayakumar S, Saraf A, Florens L, Washburn MP, Dynlacht B, Pagano M. SCF Cyclin F controls centrosome homeostasis and mitotic fidelity through CP110 degradation. Nature. 2010;466(7302):138.

61. Lee A, Rayner SL, De Luca A, Gwee SSL, Morsch M, Sundaramoorthy V, Shahheydari H, Ragagnin A, Shi B, Yang S, Williams KL, Don EK, Walker AK, Zhang KY, Yerbury JJ, Cole NJ, Atkin JD, Blair IP, Molloy MP, Chung RS. Casein kinase II phosphorylation of cyclin F at serine 621 regulates the Lys48-ubiquitylation E3 ligase activity of the SCF(cyclin F) complex. Open Biology. 2017;7(10).

62. Fung TK, Siu WY, Yam CH, Lau A, Poon RYC. Cyclin F Is Degraded during G 2 -M by Mechanisms Fundamentally Different from Other Cyclins. Journal of Biological Chemistry. 2002;277(38):35140-9.

63. Rogers S, Wells R, Rechsteiner M. Amino acid sequences common to rapidly degraded proteins: the PEST hypothesis. Science. 1986;234(4774):364-8.

64. Carillo S, Pariat M, Steff A-M, Jariel-Encontre I, Poulat F, Berta P, Piechaczyk M. PEST motifs are not required for rapid calpain-mediated proteolysis of c-fos protein. Biochemical Journal. 1996;313(1):245-51.

65. García-Alai MM, Gallo M, Salame M, Wetzler DE, McBride AA, Paci M, Cicero DO, de Prat-Gay G. Molecular basis for phosphorylation-dependent, PEST-mediated protein turnover. Structure. 2006;14(2):309-19.

66. Cardozo T, Pagano M. The SCF ubiquitin ligase: insights into a molecular machine. Nature reviews Molecular cell biology. 2004;5(9):739.

67. Weissman AM. Ubiquitin and proteasomes: themes and variations on ubiquitylation. Nature reviews Molecular cell biology. 2001;2(3):169.

68. Robberecht W, Philips T. The changing scene of amyotrophic lateral sclerosis. Nature Reviews Neuroscience. 2013;14(4):248.

69. Hogan AL, Don EK, Rayner SL, Lee A, Laird AS, Watchon M, Winnick C, Tarr IS, Morsch M, Fifita JA. Expression of ALS/FTD-linked mutant CCNF in zebrafish leads to increased cell death in the spinal cord and an aberrant motor phenotype. Human Molecular Genetics. 2017:ddx136.

70. Aebersold R, Mann M. Mass spectrometry-based proteomics. Nature. 2003;422(6928):198.

71. Thomas P, Smart TG. HEK293 cell line: a vehicle for the expression of recombinant proteins. Journal of pharmacological and toxicological methods. 2005;51(3):187-200.

72. Thomas PD, Kejariwal A, Guo N, Mi H, Campbell MJ, Muruganujan A, Lazareva-Ulitsky B. Applications for protein sequence–function evolution data: mRNA/protein expression analysis and coding SNP scoring tools. Nucleic acids research. 2006;34(suppl_2):W645-W50.

73. Oliveros JC. VENNY. An interactive tool for comparing lists with Venn Diagrams. 2007. 2007.

74. Stiles B, Groszer M, Wang S, Jiao J, Wu H. PTENless means more. Developmental biology. 2004;273(2):175-84.

75. Harjes P, Wanker EE. The hunt for huntingtin function: interaction partners tell many different stories. Trends in biochemical sciences. 2003;28(8):425-33.

76. Jung J-J, Inamdar SM, Tiwari A, Choudhury A. Regulation of intracellular membrane trafficking and cell dynamics by syntaxin-6. Bioscience reports. 2012;32(4):383-91.

77. Bravo-San Pedro JM, Gómez-Sánchez R, Niso-Santano M, Pizarro-Estrella E, Aiastui-Pujana A, Gorostidi A, Climent V, Lopez de Maturana R, Sanchez-Pernaute R, Lopez de Munain A. The MAPK1/3 pathway is essential for the deregulation of autophagy observed in G2019S LRRK2 mutant fibroblasts. Autophagy. 2012;8(10):1537-9.

78. Ekinci FJ, Malik KU, Shea TB. Activation of the L Voltage-sensitive Calcium Channel by Mitogen-activated Protein (MAP) Kinase following Exposure of Neuronal Cells to β-Amyloid Map Kinase Mediates B-Amyloid-Induced Neurodegeneration. Journal of Biological Chemistry. 1999;274(42):30322-7.

79. Roodveldt C, Bertoncini CW, Andersson A, Van Der Goot AT, Hsu ST, Fernández-Montesinos R, de Jong J, van Ham TJ, Nollen EA, Pozo D. Chaperone proteostasis in Parkinson's disease: stabilization of the Hsp70/α-synuclein complex by Hip. The EMBO journal. 2009;28(23):3758-70.

80. Mandel S, Grunblatt E, Riederer P, Amariglio N, Hirsch JJ, Rechavi G, Youdim MB. Gene expression profiling of sporadic Parkinson's disease substantia nigra pars compacta reveals impairment of ubiquitin-proteasome subunits, SKP1A, aldehyde dehydrogenase, and chaperone HSC-70. Annals of the New York Academy of Sciences. 2005;1053(1):356-75.

81. Kamal A, Almenar-Queralt A, LeBlanc JF, Roberts EA, Goldstein LS. Kinesin-mediated axonal transport of a membrane compartment containing β-secretase and presenilin-1 requires APP. Nature. 2001;414(6864):643.

82. Quan L, Lv Q, Zhang Y. STRUM: Structure-based stability change prediction upon single-point mutation. Bioinformatics. 2016;32:2911-9.

83. Blom N, Sicheritz-Pontén T, Gupta R, Gammeltoft S, Brunak S. Prediction of post-translational glycosylation and phosphorylation of proteins from the amino acid sequence. Proteomics. 2004;4(6):1633-49.

84. Lutz C. Mouse models of ALS: Past, present and future. Brain research. 2018;1693:1-10.

85. Di Giorgio FP, Carrasco MA, Siao MC, Maniatis T, Eggan K. Non–cell autonomous effect of glia on motor neurons in an embryonic stem cell–based ALS model. Nature neuroscience. 2007;10(5):608.

86. Walker AK, Spiller KJ, Ge G, Zheng A, Xu Y, Zhou M, Tripathy K, Kwong LK, Trojanowski JQ, Lee VM-Y. Functional recovery in new mouse models of ALS/FTLD after clearance of pathological cytoplasmic TDP-43. Acta neuropathologica. 2015;130(5):643-60.

87. Turner MR, Al-Chalabi A, Chio A, Hardiman O, Kiernan MC, Rohrer JD, Rowe J, Seeley W, Talbot K. Genetic screening in sporadic ALS and FTD. BMJ Publishing Group Ltd; 2017.

88. Maehama T, Dixon JE. The tumor suppressor, PTEN/MMAC1, dephosphorylates the lipid second messenger, phosphatidylinositol 3, 4, 5-trisphosphate. Journal of Biological Chemistry. 1998;273(22):13375-8.

89. Sun H, Lesche R, Li D-M, Liliental J, Zhang H, Gao J, Gavrilova N, Mueller B, Liu X, Wu H. PTEN modulates cell cycle progression and cell survival by regulating phosphatidylinositol 3, 4, 5,-trisphosphate and Akt/protein kinase B signaling pathway. Proceedings of the National Academy of Sciences. 1999;96(11):6199-204.

90. Chen Z, Chen B, Xu W-F, Liu R-F, Yang J, Yu C-X. Effects of PTEN inhibition on regulation of tau phosphorylation in an okadaic acid-induced neurodegeneration model. International Journal of Developmental Neuroscience. 2012;30(6):411-9.

91. Godena VK, Ning K. Phosphatase and tensin homologue: a therapeutic target for SMA. Signal Transduction and Targeted Therapy. 2017;2:17038.

92. Malliri A, Collard JG. Role of Rho-family proteins in cell adhesion and cancer. Current opinion in cell biology. 2003;15(5):583-9.

93. Van den Berg R, Haenen G, Van den Berg H, Bast A. Transcription factor NF-κB as a potential biomarker for oxidative stress. British Journal of Nutrition. 2001;86(S1):S121-S7.

94. Gyrd-Hansen M, Darding M, Miasari M, Santoro MM, Zender L, Xue W, Tenev T, Da Fonseca PC, Zvelebil M, Bujnicki JM. IAPs contain an evolutionarily conserved ubiquitin-binding domain that regulates NF-κB as well as cell survival and oncogenesis. Nature cell biology. 2008;10(11):1309.

95. Matos P, Jordan P. Expression of Rac1b stimulates NF-κB-mediated cell survival and G1/S progression. Experimental cell research. 2005;305(2):292-9.

96. Fan Z, Li C, Qin C, Xie L, Wang X, Gao Z, Wang T, Yu L, Liu H. Role of the PI3K/AKT pathway in modulating cytoskeleton rearrangements and phenotype switching in rat pulmonary arterial vascular smooth muscle cells. DNA and cell biology. 2014;33(1):12-9.

97. Yoon S, Han E, Choi Y-C, Kee H, Jeong Y, Yoon J, Baek K. Inhibition of cell proliferation and migration by miR-509-3p that targets CDK2, Rac1, and PIK3C2A. Molecules and cells. 2014;37(4):314.

98. Hiles ID, Otsu M, Volinia S, Fry MJ, Gout I, Dhand R, Panayotou G, Ruiz-Larrea F, Thompson A, Totty NF. Phosphatidylinositol 3-kinase: structure and expression of the 110 kd catalytic subunit. Cell. 1992;70(3):419-29.

99. Hennessy BT, Smith DL, Ram PT, Lu Y, Mills GB. Exploiting the PI3K/AKT pathway for cancer drug discovery. Nature reviews Drug discovery. 2005;4(12):988.

100. Nikolic M, Chou MM, Lu W, Mayer BJ, Tsai L-H. The p35/Cdk5 kinase is a neuron-specific Rac effector that inhibits Pak1 activity. Nature. 1998;395(6698):194.

101. Kallergi G, Agelaki S, Markomanolaki H, Georgoulias V, Stournaras C. Activation of FAK/PI3K/Rac1 signaling controls actin reorganization and inhibits cell motility in human cancer cells. Cellular Physiology and Biochemistry. 2007;20(6):977-86.

102. Xie Z, Sanada K, Samuels BA, Shih H, Tsai L-H. Serine 732 phosphorylation of FAK by Cdk5 is important for microtubule organization, nuclear movement, and neuronal migration. Cell. 2003;114(4):469-82.

103. Blankenship JW, Varfolomeev E, Goncharov T, Fedorova AV, Kirkpatrick DS, Izrael-Tomasevic A, Phu L, Arnott D, Aghajan M, Zobel K. Ubiquitin binding modulates IAP antagonist-stimulated proteasomal degradation of c-IAP1 and c-IAP2 1. Biochemical Journal. 2009;417(1):149-65.

104. Choi YE, Butterworth M, Malladi S, Duckett CS, Cohen GM, Bratton SB. The E3 ubiquitin ligase cIAP1 binds and ubiquitinates caspase-3 and-7 via unique mechanisms at distinct steps in their processing. Journal of Biological Chemistry. 2009;284(19):12772-82.

105. Nillegoda NB, Theodoraki MA, Mandal AK, Mayo KJ, Ren HY, Sultana R, Wu K, Johnson J, Cyr DM, Caplan AJ. Ubr1 and Ubr2 function in a quality control pathway for degradation of unfolded cytosolic proteins. Molecular biology of the cell. 2010;21(13):2102-16.

106. Wang L, Mao X, Ju D, Xie Y. Rpn4 is a physiological substrate of the Ubr2 ubiquitin ligase. Journal of Biological Chemistry. 2004;279(53):55218-23.

107. Mougeot J-LC, Li Z, Price AE, Wright FA, Brooks BR. Microarray analysis of peripheral blood lymphocytes from ALS patients and the SAFE detection of the KEGG ALS pathway. BMC medical genomics. 2011;4(1):74.

108. Itoh K, Wakabayashi N, Katoh Y, Ishii T, Igarashi K, Engel JD, Yamamoto M. Keap1 represses nuclear activation of antioxidant responsive elements by Nrf2 through binding to the amino-terminal Neh2 domain. Genes & development. 1999;13(1):76-86.

109. Rushmore TH, Morton MR, Pickett CB. The antioxidant responsive element. Activation by oxidative stress and identification of the DNA consensus sequence required for functional activity. Journal of Biological Chemistry. 1991;266(18):11632-9.

110. Fan W, Tang Z, Chen D, Moughon D, Ding X, Chen S, Zhu M, Zhong Q. Keap1 facilitates p62-mediated ubiquitin aggregate clearance via autophagy. Autophagy. 2010;6(5):614-21.

111. Wooten MW, Hu X, Babu JR, Seibenhener ML, Geetha T, Paine MG, Wooten MC. Signaling, polyubiquitination, trafficking, and inclusions: sequestosome 1/p62's role in neurodegenerative disease. BioMed Research International. 2006;2006.

112. Tanji K, Maruyama A, Odagiri S, Mori F, Itoh K, Kakita A, Takahashi H, Wakabayashi K. Keap1 is localized in neuronal and glial cytoplasmic inclusions in various neurodegenerative diseases. Journal of Neuropathology & Experimental Neurology. 2013;72(1):18-28.

113. Leung T, Rajendran M, Monfries C, Hall C, Lim L. The human heat-shock protein family. Expression of a novel heat-inducible HSP70 (HSP70B′) and isolation of its cDNA and genomic DNA. Biochemical Journal. 1990;267(1):125-32.

114. Khalouei S, Chow AM, Brown IR. Stress-induced localization of HSPA6 (HSP70B′) and HSPA1A (HSP70-1) proteins to centrioles in human neuronal cells. Cell Stress and Chaperones. 2014;19(3):321-7.

115. Meggio F, Marin O, Pinna L. Substrate specificity of protein kinase CK2. Cellular & molecular biology research. 1994;40(5-6):401-9.

116. Tamura T, Lee DH, Osaka F, Fujiwara T, Shin S, Chung CH, Tanaka K, Ichihara A. Molecular cloning and sequence analysis of cDNAs for five major subunits of human proteasomes (multi-catalytic proteinase complexes). Biochimica et Biophysica Acta (BBA)-Gene Structure and Expression. 1991;1089(1):95-102.

117. Voges D, Zwickl P, Baumeister W. The 26S proteasome: a molecular machine designed for controlled proteolysis. Annual review of biochemistry. 1999;68(1):1015-68.

118. McNaught KSP, Belizaire R, Jenner P, Olanow CW, Isacson O. Selective loss of 20S proteasome α-subunits in the substantia nigra pars compacta in Parkinson's disease. Neuroscience letters. 2002;326(3):155-8.

119. McNaught KSP, Belizaire R, Isacson O, Jenner P, Olanow CW. Altered proteasomal function in sporadic Parkinson's disease. Experimental neurology. 2003;179(1):38-46.

120. Myeku N, Metcalfe MJ, Huang Q, Figueiredo-Pereira M. Assessment of proteasome impairment and accumulation/aggregation of ubiquitinated proteins in neuronal cultures. Neurodegeneration: Springer; 2011. p. 273-96.

121. Bendotti C, Marino M, Cheroni C, Fontana E, Crippa V, Poletti A, De Biasi S. Dysfunction of constitutive and inducible ubiquitin-proteasome system in amyotrophic lateral sclerosis: implication for protein aggregation and immune response. Progress in neurobiology. 2012;97(2):101-26.

122. Ross CA, Poirier MA. Protein aggregation and neurodegenerative disease. Nature medicine. 2004;10(7):S10.

123. Frydman J, Nimmesgern E, Ohtsuka K, Hartl FU. Folding of nascent polypeptide chains in a high molecular mass assembly with molecular chaperones. Nature. 1994;370(6485):111.

124. Ballinger CA, Connell P, Wu Y, Hu Z, Thompson LJ, Yin L-Y, Patterson C. Identification of CHIP, a novel tetratricopeptide repeat-containing protein that interacts with heat shock proteins and negatively regulates chaperone functions. Molecular and cellular biology. 1999;19(6):4535-45.

125. Otto H, Conz C, Maier P, Wölfle T, Suzuki CK, Jenö P, Rücknagel P, Stahl J, Rospert S. The chaperones MPP11 and Hsp70L1 form the mammalian ribosome-associated complex. Proceedings of the National Academy of Sciences. 2005;102(29):10064-9.

126. Nakashima-Yasuda H, Uryu K, Robinson J, Xie SX, Hurtig H, Duda JE, Arnold SE, Siderowf A, Grossman M, Leverenz JB. Co-morbidity of TDP-43 proteinopathy in Lewy body related diseases. Acta neuropathologica. 2007;114(3):221-9.

127. Cyr DM, Höhfeld J, Patterson C. Protein quality control: U-box-containing E3 ubiquitin ligases join the fold. Trends in biochemical sciences. 2002;27(7):368-75.

128. McKinnon C, Tabrizi SJ. The ubiquitin-proteasome system in neurodegeneration. Antioxidants & redox signaling. 2014;21(17):2302-21.

129. Yu P, Chen Y, Tagle DA, Cai T. PJA1, encoding a RING-H2 finger ubiquitin ligase, is a novel human X chromosome gene abundantly expressed in brain. Genomics. 2002;79(6):869-74.

130. Joazeiro CA, Weissman AM. RING finger proteins: mediators of ubiquitin ligase activity. Cell. 2000;102(5):549-52.

131. Ardley HC, Robinson PA. The role of ubiquitin-protein ligases in neurodegenerative disease. Neurodegenerative Diseases. 2004;1(2-3):71-87.

132. Zhang W, Wei Q. Calcineurin stimulates the expression of inflammatory factors in RAW 264.7 cells by interacting with proteasome subunit alpha type 6. Biochemical and biophysical research communications. 2011;407(4):668-73.

133. Bloom J, Peschiaroli A, DeMartino G, Pagano M. Modification of Cul1 regulates its association with proteasomal subunits. Cell Division. 2006;1(1):5.

134. Leznicki P, Warwicker J, High S. A biochemical analysis of the constraints of tail-anchored protein biogenesis. Biochemical Journal. 2011;436(3):719-27.

135. Shao S, Rodrigo-Brenni MC, Kivlen MH, Hegde RS. Mechanistic basis for a molecular triage reaction. Science. 2017;355(6322):298-302.

136. Chen M, Xia X, Zhu X, Cao J, Xu D, Ni Y, Liu Y, Yan S, Cheng X, Liu Y. Expression of SGTA correlates with neuronal apoptosis and reactive gliosis after spinal cord injury. Cell and tissue research. 2014;358(2):277-88.

137. Betteridge DJ. What is oxidative stress? Metabolism. 2000;49(2):3-8.

138. Lemasters JJ, Qian T, Bradham CA, Brenner DA, Cascio WE, Trost LC, Nishimura Y, Nieminen A-L, Herman B. Mitochondrial dysfunction in the pathogenesis of necrotic and apoptotic cell death. Journal of bioenergetics and biomembranes. 1999;31(4):305-19.

139. Crapo JD, Oury T, Rabouille C, Slot JW, Chang L-Y. Copper, zinc superoxide dismutase is primarily a cytosolic protein in human cells. Proceedings of the National Academy of Sciences. 1992;89(21):10405-9.

140. Kiernan MC, Vucic S, Cheah BC, Turner MR, Eisen A, Hardiman O, Burrell JR, Zoing MC. Amyotrophic lateral sclerosis. The lancet. 2011;377(9769):942-55.

141. Dal Canto MC, Gurney ME. Neuropathological changes in two lines of mice carrying a transgene for mutant human Cu, Zn SOD, and in mice overexpressing wild type human SOD: a model of familial amyotrophic lateral sclerosis (FALS). Brain research. 1995;676(1):25-40.

142. Mattiazzi M, D'Aurelio M, Gajewski CD, Martushova K, Kiaei M, Beal MF, Manfredi G. Mutated human SOD1 causes dysfunction of oxidative phosphorylation in mitochondria of transgenic mice. Journal of biological chemistry. 2002;277(33):29626-33.

143. Kaur SJ, McKeown SR, Rashid S. Mutant SOD1 mediated pathogenesis of amyotrophic lateral sclerosis. Gene. 2016;577(2):109-18.

144. Saccon RA, Bunton-Stasyshyn RK, Fisher EM, Fratta P. Is SOD1 loss of function involved in amyotrophic lateral sclerosis? Brain. 2013;136(8):2342-58.

145. Yoon EJ, Park H-J, Kim G-Y, Cho H, Choi J-H, Park H-Y, Jang J-Y, Rhim H, Kang S. Intracellular amyloid beta interacts with SOD1 and impairs the enzymatic activity of SOD1: implications for the pathogenesis of amyotrophic lateral sclerosis. Experimental & molecular medicine. 2009;41(9):611.

146. Graffmo KS, Forsberg K, Bergh J, Birve A, Zetterström P, Andersen PM, Marklund SL, Brännström T. Expression of wild-type human superoxide dismutase-1 in mice causes amyotrophic lateral sclerosis. Human molecular genetics. 2012;22(1):51-60.

147. Forsberg K, Jonsson PA, Andersen PM, Bergemalm D, Graffmo KS, Hultdin M, Jacobsson J, Rosquist R, Marklund SL, Brännström T. Novel antibodies reveal inclusions containing non-native SOD1 in sporadic ALS patients. PloS one. 2010;5(7):e11552.

148. Bosco DA, Morfini G, Karabacak NM, Song Y, Gros-Louis F, Pasinelli P, Goolsby H, Fontaine BA, Lemay N, McKenna-Yasek D. Wild-type and mutant SOD1 share an aberrant conformation and a common pathogenic pathway in ALS. Nature neuroscience. 2010;13(11):1396.

149. Bonaldi T, Längst G, Strohner R, Becker PB, Bianchi ME. The DNA chaperone HMGB1 facilitates ACF/CHRAC-dependent nucleosome sliding. The EMBO journal. 2002;21(24):6865-73.

150. Müller S, Scaffidi P, Degryse B, Bonaldi T, Ronfani L, Agresti A, Beltrame M, Bianchi ME. The double life of HMGB1 chromatin protein: architectural factor and extracellular signal. The EMBO journal. 2001;20(16):4337-40.

151. Sahu D, Debnath P, Takayama Y, Iwahara J. Redox properties of the A-domain of the HMGB1 protein. FEBS letters. 2008;582(29):3973-8.

152. Srinivasan S, Avadhani NG. Cytochrome c oxidase dysfunction in oxidative stress. Free Radical Biology and Medicine. 2012;53(6):1252-63.

153. Galati D, Srinivasan S, Raza H, Prabu SK, Hardy M, Chandran K, Lopez M, Kalyanaraman B, Avadhani NG. Role of nuclear-encoded subunit Vb in the assembly and stability of cytochrome c oxidase complex: implications in mitochondrial dysfunction and ROS production. Biochemical Journal. 2009;420(3):439-49.

154. Fornuskova D, Stiburek L, Wenchich L, Vinsova K, Hansikova H, Zeman J. Novel insights into the assembly and function of human nuclear-encoded cytochrome c oxidase subunits 4, 5a, 6a, 7a and 7b. Biochemical Journal. 2010;428(3):363-74.

155. Mitchell P. Possible molecular mechanisms of the protonmotive function of cytochrome systems. Journal of theoretical biology. 1976;62(2):327-67.

156. Bénit P, Lebon S, Rustin P. Respiratory-chain diseases related to complex III deficiency. Biochimica et Biophysica Acta (BBA)-Molecular Cell Research. 2009;1793(1):181-5.

157. Capaldi RA. Structure and function of cytochrome c oxidase. Annual review of biochemistry. 1990;59(1):569-96.

158. Roberg K, Johansson U, Öllinger K. Lysosomal release of cathepsin D precedes relocation of cytochrome c and loss of mitochondrial transmembrane potential during apoptosis induced by oxidative stress. Free Radical Biology and Medicine. 1999;27(11-12):1228-37.

159. Castino R, Bellio N, Nicotra G, Follo C, Trincheri NF, Isidoro C. Cathepsin D–Bax death pathway in oxidative stressed neuroblastoma cells. Free Radical Biology and Medicine. 2007;42(9):1305-16.

160. Korsmeyer SJ, Shutter JR, Veis DJ, Merry DE, Oltvai ZN, editors. Bcl-2/Bax: a rheostat that regulates an anti-oxidant pathway and cell death. Seminars in cancer biology; 1993.

161. Vila M, Jackson-Lewis V, Vukosavic S, Djaldetti R, Liberatore G, Offen D, Korsmeyer SJ, Przedborski S. Bax ablation prevents dopaminergic neurodegeneration in the 1-methyl-4-phenyl-1, 2, 3, 6-tetrahydropyridine mouse model of Parkinson's disease. Proceedings of the National Academy of Sciences. 2001;98(5):2837-42.

162. Lu G, Kwong W, Li Q, Wang X, Feng Z, Yew DT. bcl2, bax and nestin in the brains of patients with neurodegeneration and those of normal aging. Journal of molecular neuroscience. 2005;27(2):167-74.

163. Shacka JJ, Klocke BJ, Young C, Shibata M, Olney JW, Uchiyama Y, Saftig P, Roth KA. Cathepsin D deficiency induces persistent neurodegeneration in the absence of Bax-dependent apoptosis. Journal of Neuroscience. 2007;27(8):2081-90.

164. Steinfeld R, Reinhardt K, Schreiber K, Hillebrand M, Kraetzner R, Brück W, Saftig P, Gärtner J. Cathepsin D deficiency is associated with a human neurodegenerative disorder. The American Journal of Human Genetics. 2006;78(6):988-98.

165. Rogalla T, Ehrnsperger M, Preville X, Kotlyarov A, Lutsch G, Ducasse C, Paul C, Wieske M, Arrigo A-P, Buchner J. Regulation of Hsp27 oligomerization, chaperone function, and protective activity against oxidative stress/tumor necrosis factor α by phosphorylation. Journal of Biological Chemistry. 1999;274(27):18947-56.

166. Srivastava AK, Renusch SR, Naiman NE, Gu S, Sneh A, Arnold WD, Sahenk Z, Kolb SJ. Mutant HSPB1 overexpression in neurons is sufficient to cause age-related motor neuronopathy in mice. Neurobiology of disease. 2012;47(2):163-73.

167. Maeda K, Idehara R, Hashiguchi A, Takashima H. A family with distal hereditary motor neuropathy and a K141Q mutation of small heat shock protein HSPB1. Internal Medicine. 2014;53(15):1655-8.

168. Ward RJ, Alvarez-Curto E, Milligan G. Using the Flp-In™ T-Rex™ system to regulate GPCR expression. Receptor Signal Transduction Protocols: Springer; 2011. p. 21-37.

169. Che Y, Khavari PA. Research Techniques Made Simple: Emerging Methods to Elucidate Protein Interactions through Spatial Proximity. Journal of Investigative Dermatology. 2017;137(12):e197-e203.

170. Keilhauer EC, Hein MY, Mann M. Accurate protein complex retrieval by affinity enrichment mass spectrometry (AE-MS) rather than affinity purification mass spectrometry (AP-MS). Molecular & Cellular Proteomics. 2015;14(1):120-35.

171. Klug HP, Alexander LE. X-ray diffraction procedures: for polycrystalline and amorphous materials. X-Ray Diffraction Procedures: For Polycrystalline and Amorphous Materials, 2nd Edition, by Harold P Klug, Leroy E Alexander, pp 992 ISBN 0-471-49369-4 Wiley-VCH, May 1974. 1974:992.

172. Kisselev AF, Goldberg AL. Monitoring activity and inhibition of 26S proteasomes with fluorogenic peptide substrates. Methods in enzymology. 2005;398:364-78.

Appendix A of this thesis has been removed as it may contain sensitive/confidential content

Appendix B. Publication I. Proteomics approaches for understanding the pathogenesis of ALS/FTD

frontiers

Proteomics approaches for understanding the pathogenesis of ALS/FTD

Thomas J. Hedl[1], Rebecca San Gil[1], Flora Cheng[2], Stephanie L. Rayner[2], Jennilee Davidson[2], Alana De Luca[2], Maria D. Villalva[2], Heath Ecroyd[3, 4], Adam K. Walker[1*], Albert Lee[2*]

[1]Queensland Brain Institute, University of Queensland, Australia, [2]Centre for Motor Neuron Disease Research, Department of Biomedical Sciences, Faculty of Medicine & Health Sciences, Macquarie University, Australia, [3]School of Biological Sciences, Faculty of Science, Medicine and Health, University of Wollongong, Australia, [4]Illawarra Health and Medical Research Institute, University of Wollongong, Australia

Submitted to Journal:
Frontiers in Neuroscience

Specialty Section:
Neurodegeneration

Article type:
Review Article

Manuscript ID:
459952

Received on:
14 Mar 2019

Frontiers website link:
www.frontiersin.org

Conflict of interest statement

The authors declare that the research was conducted in the absence of any commercial or financial relationships that could be construed as a potential conflict of interest

Author contribution statement

TH, RS, FC, SR, JD, AD, and MV were responsible for drafting, writing and editing the manuscript. HE, AW and AL conceived the overall layout of the manuscript and were responsible for the final editing and proof-reading of the manuscript. All authors read and approved the final manuscript.

Keywords

Proteomics, ALS (Amyotrophic lateral sclerosis), Frontotemporal dementia (FTD), Proteostasis Cell Stress and Aging, Post-translational modification (PTM), Mass Spectrometry, Flow Cytometry, protein aggregation, Protein Clearance, Supersaturation, neurodegeneration, Label-free Proteomics, TMT (tandem mass tags), SILAC, Protein interactome, BioID proximity labeling, APEX proximity labeling, Ubiquitylation (Ubiquitination), Phosphorylation, Bioinformatics (genome and proteome) databases, TDP43 proteinopathies, Tau & phospho-Tau protein

Abstract

Word count: 326

Neurodegenerative disorders such as amyotrophic lateral sclerosis (ALS) and frontotemporal dementia (FTD) are increasing in prevalence but lack targeted therapeutics. Although the pathological mechanisms behind these diseases remain unclear, both ALS and FTD are characterized pathologically by aberrant protein aggregation and inclusion formation within neurons, which correlates with neurodegeneration. Notably, aggregation of several key proteins, including TAR DNA binding protein of 43 kDa (TDP-43), superoxide dismutase 1 (SOD1), and tau, have been implicated in these diseases. Proteomics methods are being increasingly applied to better understand disease-related mechanisms and to identify biomarkers of disease, using model systems as well as human samples. Proteomics-based approaches offer unbiased, high-throughput, and quantitative results with numerous applications for investigating proteins of interest. Here, we review recent advances in the understanding of ALS and FTD pathophysiology obtained using proteomics approaches, and we assess technical and experimental limitations. We compare findings from various mass spectrometry approaches including quantitative proteomics methods such as stable isotope labelling by amino acids in cell culture (SILAC) and tandem mass tagging (TMT) to approaches such as label-free quantitation (LFQ) and sequential windowed acquisition of all theoretical fragment ion mass spectra (SWATH-MS) in studies of ALS and FTD. Similarly, we describe disease-related protein-protein interaction (PPI) studies using approaches including immunoprecipitation mass spectrometry (IP-MS) and proximity dependent biotin identification (BioID), and discuss future application of new techniques including proximity-dependent ascorbic acid peroxidase labelling (APEX) and biotinylation by antibody recognition (BAR). Futhermore, we explore the use of mass spectrometry to detect post-translational modifications, such as ubiquitination and phosphorylation, of disease-relevant proteins in ALS and FTD. We also discuss upstream technologies that enable enrichment of proteins of interest, highlighting the contributions of new techniques to isolate disease-relevant protein inclusions including flow cytometric analysis of inclusions and trafficking (FloIT). These recently developed approaches, as well as related advances yet to be applied to studies of these neurodegenerative diseases, offer numerous opportunities for discovery of potential therapeutic targets and biomarkers for ALS and FTD.

Contribution to the field

Dear A/Prof Belbin, We appreciate your consideration for granting us an extension to submit our manuscript to Frontiers in Neuroscience. It is our great pleasure to submit this review manuscript entitled "Proteomics approaches for understanding the pathogenesis of ALS/FTD" for consideration in Frontiers in Neuroscience. I confirm that this manuscript has been submitted in accordance with the journal's editorial policies, and that we have no conflicts of interest to declare in relation to the research and perspectives reported in this manuscript. Background rationale for this review: One of the main caveats that precludes the development of potential therapies as well as biomarkers for ALS and FTD, is a clear understanding of the pathological mechanisms behind these diseases. Both ALS and FTD are characterized pathologically by aberrant protein aggregation and inclusion formation within neurons, which correlates strongly with neurodegeneration. Perturbations to protein clearance mechanisms and decreased protein solubility are likely to contribute to the early triggers of disease. We are now beginning to see an influx of research employing alternative -omics strategies to understand this disease. Therefore, this review is a timely opportunity to explore the proteomics methods that are being increasingly applied to address these biological questions to better understand disease-related mechanisms of ALS, using model systems as well as human brain and spinal cord samples. Depending on the biological questions, proteomics-based approaches offer unbiased, high-throughput and quantitative results with numerous applications for screening

proteins of interest. Here, we review recent advances in the understanding of pathophysiology in ALS and FTD obtained using new and established proteomics approaches and evaluate the limitations to detection, resolution and quantitation of results. While we acknowledge there is a wealth of review articles focused on the biology of ALS pathogenesis as well as reviews on the technical aspects of quantitative proteomics approaches; to our knowledge, there has not been a recent review (<2 years) that discusses the combination of both ALS biology and how proteomic methods can facilitate and enhance research in this area. The main aspects of what makes our submitted review unique is a major focus on the methodological approaches that are specific and fit-for-purpose to answer a biological question, such as 'What are the cellular pathways affected from ALS mutations? What are the protein interaction partners of my ALS protein of interest? How can we use proteomics to discover a panel of biomarkers that may have clinical use? The implementation of these techniques is expected to facilitate the rapid expansion of research in the ALS and FTD fields, and highlights potential future strategies that may be of use to study neurodegenerative diseases. Key points reported in this review: • Novel proteomic-based methods have emerged facilitating the unbiased identification and quantification of proteins providing a snapshot of the cellular pathway changes in disease models. • Highlighted main features of ALS biology that can be triggered by dysfunctional proteostasis, supersaturation and protein aggregation. • Preparative and quantitative proteomic approaches that are fit-for-purpose and the considerations and limitations for the methods chosen. • These novel proteomic strategies, alongside the use of bioinformatics programs can be used to quickly identify high confidence snapshots of the biology from large proteomic data-sets that enable further hypotheses to be developed. • Overall, this review is aimed to help guide a researcher who is new to either ALS biology or proteomics of the newest techniques that are routinely employed. Statement of significance of findings to the field, and relevance to readership of Frontiers in Neuroscience In the context of neurodegenerative diseases, this review is expected to enhance the research in this field that will assist readers on the current proteomic techniques that can be employed to study ALS/FTD. The review evaluates the triggers that set of a chain of events that are caused by dysfunctional proteostasis leading to protein aggregation and subsequently motor neuron cell death. We explore the well-established and newer proteomic strategies that have been used in a small number but highly impactful ALS/FTD studies and the contribution of these findings to our growing understanding of the disease. We propose that this review will be of broad interest to the general readership of Frontiers in Neuroscience. Thank you for considering our manuscript for publication. I would be happy to provide any further information you require in regards to this submission.

Funding statement

This work and related studies was supported by the Australian Government Department of Education and Training RTP, QBI Research Higher Degree Top Up Scholarship, the MND Research Institute of Australia (GIA1628, 1715 and 1727), the Australian National Health and Medical Research Council (Project Grant 1124005, 1095215 and 1107644 and RD Wright Career Development Fellowship 1140386), the Ross Maclean Fellowship, and the Brazil Family Program for Neurology.

Data availability statement

Generated Statement: No datasets were generated or analyzed for this study.

Proteomics approaches for biomarker and drug target discovery in ALS and FTD

Thomas J. Hedl[1], Rebecca San Gil[1], Flora Cheng[2], Stephanie L Rayner[2], Jennilee Davidson[2], Alana De Luca[2], Maria Villalva[2], Heath Ecroyd[3,4], Adam K. Walker[1,2*], Albert Lee[2*]

[1] Neurodegeneration Pathobiology Laboratory, Queensland Brain Institute, The University of Queensland, St Lucia, QLD 4072, Australia
[2] Centre for Motor Neuron Disease Research, Department of Biomedical Sciences, Faculty of Medicine and Health Sciences, Macquarie University, North Ryde, NSW 2109, Australia
[3] School of Chemistry and Molecular Bioscience, University of Wollongong, Wollongong, NSW 2522, Australia
[4] Illawarra Health and Medical Research Institute, Wollongong, NSW 2522, Australia

*** Correspondence:**
Albert Lee; Adam Walker
albert.lee@mq.edu.au; adam.walker@uq.edu.au

Keywords: amyotrophic lateral sclerosis, frontotemporal dementia, proteomics, mass spectrometry, protein aggregation

Figures: 1, Tables: 6, Words: 8788

ABSTRACT

Neurodegenerative disorders such as amyotrophic lateral sclerosis (ALS) and frontotemporal dementia (FTD) are increasing in prevalence but lack targeted therapeutics. Although the pathological mechanisms behind these diseases remain unclear, both ALS and FTD are characterized pathologically by aberrant protein aggregation and inclusion formation within neurons, which correlates with neurodegeneration. Notably, aggregation of several key proteins, including TAR DNA binding protein of 43 kDa (TDP-43), superoxide dismutase 1 (SOD1), and tau, have been implicated in these diseases. Proteomics methods are being increasingly applied to better understand disease-related mechanisms and to identify biomarkers of disease, using model systems as well as human samples. Proteomics-based approaches offer unbiased, high-throughput, and quantitative results with numerous applications for investigating proteins of interest. Here, we review recent advances in the understanding of ALS and FTD pathophysiology obtained using proteomics approaches, and we assess technical and experimental limitations. We compare findings from various mass spectrometry approaches including quantitative proteomics methods such as stable isotope labelling by amino acids in cell culture (SILAC) and tandem mass tagging (TMT) to approaches such as label-free quantitation (LFQ) and sequential windowed acquisition of all theoretical fragment ion mass spectra (SWATH-MS) in studies of ALS and FTD. Similarly, we describe disease-related protein-protein interaction (PPI) studies using approaches including immunoprecipitation mass spectrometry (IP-MS) and proximity dependent biotin identification (BioID), and discuss future application of new techniques including proximity-dependent ascorbic acid peroxidase labelling (APEX) and biotinylation by antibody recognition (BAR). Futhermore, we explore the use of mass spectrometry to detect post-translational modifications, such as ubiquitination and

phosphorylation, of disease-relevant proteins in ALS and FTD. We also discuss upstream technologies that enable enrichment of proteins of interest, highlighting the contributions of new techniques to isolate disease-relevant protein inclusions including flow cytometric analysis of inclusions and trafficking (FloIT). These recently developed approaches, as well as related advances yet to be applied to studies of these neurodegenerative diseases, offer numerous opportunities for discovery of potential therapeutic targets and biomarkers for ALS and FTD.

1 Introduction

Neurodegenerative diseases, including amyotrophic lateral sclerosis (ALS) and frontotemporal dementia (FTD), demonstrate dysfunctional protein clearance and accumulation of protein-rich inclusions in neuronal cells. Resolving whether these inclusions are a cause of cellular degeneration or a symptom of homeostatic dysfunction has proven difficult, and the pathological mechanisms underlying their formation are still largely unknown. However, through attempting to answer these questions, the fundamental roles of protein aggregation and protein clearance in the pathology of these diseases have been established. Recent advances in proteomics technologies have advanced our understanding of both the primary pathological proteins as well as other associated proteins that may play downstream roles in disease mechanisms. The purpose of this review is to evaluate the current proteomic tools and techniques being used to understand these diseases, to summarise the state of knowledge gained from proteomic studies on ALS and FTD, and to discuss development of more effective disease-modifying treatments and biomarkers for clinical assessment driven by new advances in proteomic technologies.

1.1 Pathology and disease mechanisms of ALS and FTD

ALS and FTD are both debilitating neurodegenerative diseases caused by selective loss of subsets of neurons. In ALS, disease pathology primarily affects the motor neurons of the primary motor cortex and spinal cord (Foster & Salajegheh, 2019), and in FTD, neurons of the frontal and temporal lobe are the primary targets of degeneration (Olney et al., 2017). Characteristic of these neurodegenerative diseases is the accumulation of protein inclusions in the cytoplasm of neurons (Ling et al., 2013). These pathological proteins, which may be affected by inherited mutations in familial disease or undergo unclear pathological changes in sporadic cases of disease, include but are not limited to TAR DNA binding protein of 43kDa (TDP-43), superoxide dismutase 1 (SOD1) and microtubule-associated protein tau (Ling et al., 2013). Numerous mutations in these and other proteins have been shown to individually cause either ALS or FTD, or indeed both diseases in the same patient or within the same family; however the vast majority of ALS cases and approximately half of all FTD cases have no known underlying dominant mechanism of inheritance (Ling et al., 2013; Nguyen et al., 2018)

Prominent amongst these pathological proteins is TDP-43, which is a highly conserved predominantly nuclear protein with functional roles in RNA metabolism (Ayala et al., 2008; Weskamp & Barmada, 2018). TDP-43 has been reproducibly identified as one of the components of cytosolic protein inclusions, a pathological hallmark in almost all ALS and some FTD cases (known pathologically as frontotemporal lobar degeneration with TDP-43 pathology, FTLD-TDP), irrespective of genetic inheritance or mutation (Neumann et al., 2007; Neumann et al., 2006; Wang et al., 2008). Aberrant cytoplasmic TDP-43 has been reported in neurons and glial cells of the central nervous system in patients with either ALS or FTD (Arai et al., 2006; Neumann et al., 2006), and TDP-43 is therefore a primary target for

studies of mechanisms of these diseases. Indeed, mutations in numerous other ALS-linked genes, including C9ORF72, are also characterised by the presence of TDP-43 pathology (Chew et al., 2015).

Although TDP-43 is the main pathological protein in almost all ALS cases, the first known causative mutations linked to ALS were identified in the protein SOD1 (Rosen et al., 1993), and these account for approximately 20% of all familial ALS cases (Pasinelli & Brown, 2006). SOD1 is a cytosolic protein responsible for catalyzing the breakdown of harmful superoxide radicals (Field et al., 2003; Sea et al., 2015). However, disease-causative mutations in the SOD1 protein variably affect protein function, and knockout of SOD1 in animals does not result in an ALS-like disease, such that the primary mechanism of toxicity of mutant SOD1 is considered to be a gain-of-function even if alterations in SOD1 function may modify disease presentation (Saccon et al., 2013; Valentine et al., 2005). Mutant SOD1 forms large intraneuronal inclusions in people with ALS-linked SOD1 mutations as well as in cellular and animal model systems (Ayers et al., 2017; Bruijn et al., 1998; Kato et al., 2000).

Unlike SOD1, tau is a primarily neuronal axoplasmic protein that stabilises microtubules (Kadavath et al., 2015). Numerous other roles for tau have been also been described, such as inhibition of HDAC6, a protein involved in tubulin acetylation (Perez et al., 2009), and in intraneuronal transport (Bodea et al., 2016). Importantly, phosphorylation of tau has been shown to correlate with the formation of tau inclusions that are present in tissue from people with FTD (Vega et al., 2005), and mutations within the *MAPT* gene encoding tau are a prominent cause of non-TDP-43-associated cases of FTD (Rademakers et al., 2004). Indeed, aggregation of tau and alterations in tau function are prominent in FTLD-tau as well as other neurodegenerative diseases, including Alzheimer's disease (Frost et al., 2015).

Overall, numerous mechanisms have been implicated in the pathogenesis of these diseases, related to mutations and/or dysfunctions which impact on neuronal viability via changes in numerous pathways including intracellular transport, cellular stress responses, RNA metabolism and protein clearance machinery (Atkin et al., 2008; Ling et al., 2013; Tank et al., 2018; Zhang et al., 2015). However, despite the diversity of possible upstream causes of disease, the prominence of changes in protein aggregation suggest that this plays a key role in the determining neurodegeneration in ALS and FTD.

1.2 Proteostasis and protein aggregation in ALS and FTD

Proteins are the functional components that drive the majority of cellular processes. Protein homeostasis or "proteostasis" describes a network of constitutively expressed housekeeping and cellular stress-inducible molecular pathways that maintain proteins in a biologically active conformation, or degrade them, to ensure that cell viability is not compromised (Balch et al., 2008; Hipp et al., 2014). The proteostasis network can be clustered into several pathways including the heat shock response, unfolded protein response, ubiquitin-proteasome system (UPS), and autophagy machinery (Webster et al., 2017). Under physiological conditions, the mechanisms of proteostasis function sufficiently to maintain cell viability. However, if proteostasis deteriorates or becomes overwhelmed, for example in the context of ALS and FTD, aberrant protein accumulation and aggregation can occur, and cell viability may be threatened.

Under normal cellular conditions, proteins exist in their native conformation, consisting of external hydrophilic surfaces and an

internal hydrophobic core. Apart from the folding that occurs for nascent polypeptides as they are synthesised on the ribosome, protein folding and unfolding occurs at other important times during the lifespan of many proteins. For example, proteins unfold and are refolded during trafficking across intracellular membranes, cellular secretion, and during times of cellular stress (Gregersen & Bross, 2010; Kincaid & Cooper, 2007). When proteins are subjected to cellular stresses, such as oxidative stress or increased burden to mitochondria or the endoplasmic reticulum, they may unfold and form partially folded protein intermediates that expose the hydrophobic regions of the polypeptide to the cytosol, which are otherwise buried within the protein (Hipp et al., 2014). Exposed hydrophobic regions are attracted to similar hydrophobic regions on adjacent partially folded proteins intermediates, which may aggregate together and enter thermodynamically favourable pathways that lead to the formation of higher-order oligomers (Stefani, 2008). These oligomers may be toxic and also form the building blocks of larger aggregates and protein inclusions in neurodegenerative diseases (Ait-Bouziad et al., 2017; Blair et al., 2013; Lasagna-Reeves et al., 2012; Shafiei et al., 2017).

The maintenance of functional proteostasis to ameliorate protein aggregation is particularly important in post-mitotic cells such as neurons, since disrupted proteostasis cannot be simply counteracted by apoptosis and replacement with new healthy neurons unlike most other cell types (Morimoto, 2008). A recent review has discussed evidence that cellular stress in the spinal cord of the $SOD1^{G93A}$ mouse, the most widely used model of ALS, does not result in the induction of the anti-aggregation heat shock response, which may suggest that this pathway is impaired in disease (San Gil et al., 2017). Impairment of proteasomal degradation likely also contributes to the accumulation of ubiquitinated proteins, including SOD1 and TDP-43 (Cheroni et al., 2009; Cheroni et al., 2005; Scotter et al., 2014). Numerous factors, such as activation of cellular stress responses and dysfunctions in proteasome activity and autophagy, may contribute to varying degrees to the accumulation of proteins in disease, although the underlying mechanisms of inclusion formation and associated pathophysiology remain unclear (Tanaka & Matsuda, 2014). However, since protein aggregation and inclusion formation are hallmarks of these diseases, understanding these processes, and how protein aggregation perturbs neuronal function, is likely to reveal new ways to delay or prevent neurodegeneration.

Proteins that are supersaturated, meaning that their concentration in the cell is greater than their predicted solubility, also have a higher propensity to aggregate (Ciryam et al., 2017). In ALS and FTD, proteins such as TDP-43 have been shown to be supersaturated due to an increase in concentration (Ciryam et al., 2017). Phase transitions may result in proteins precipitating out in the cytoplasm, a liquid-liquid separation, and proteins with low complexity domains such as TDP-43 may be more prone to this transition (Li et al., 2018). Indeed, recently RNA has been proposed as a regulator of protein phase separation, suggesting that dysregulation of RNA:protein interactions may contribute to the formation of protein aggregates (Maharana et al., 2018; Zacco et al., 2019).

By analysing how disease-related proteins aggregate, identification of the interaction partners of native and aggregated pathological proteins, and determination of the consequences of protein aggregation within neurons will elucidate the patho-mechanisms involved in of ALS and FTD. The remainder of this review will focus on the methods and outcomes of previous and potential future studies using proteomics technologies to address these fundamental issues. By developing an understanding of the numerous tools available for these experiments and devising the most relevant biological questions, these studies offer the

potential to elucidate the mechanisms of pathogenesis of ALS/FTD, and also to identify biomarkers for these diseases. Together, this information may allow the future development of better treatments for people living with ALS and FTD.

2 Proteomic approaches to study ALS and FTD

Proteomic-based platforms are becoming increasingly powerful to identify both potential disease mechanisms as well as disease biomarkers. Proteomics involves using highly complex protein screening technology for biological understanding on a wide-scale level. This information can then be used in combination with genomic data to provide an understanding of the fundamental biological mechanisms underlying neurodegenerative diseases. The emergence of newer sophisticated mass spectrometry (MS) technology in the past decade, with higher resolution and faster scan rates, has enabled smoother and quicker identification of highly complex proteomes with shorter analysis periods (Chapman et al., 2014). The typical sample preparation procedures for proteomics analysis involves digesting proteins into peptides using a protease (e.g. trypsin and/or Lys-C) followed by reverse phase C_{18} liquid chromatographic separation and analysis by mass spectrometry (LC-MS/MS) (Kiraly et al., 2016). The peptides that are eluted from the C_{18} column are directly ionised into the mass spectrometer for analysis, where they can be fragmented (MS/MS) further for peptide identification. The data generated by MS can be searched using algorithms that incorporate protein databases to generate lists of identified proteins. The two major streams for quantitative proteomics that are widely used are label-free and labelled quantitation (Figure 1). Both methods are used for the identification and quantitation of protein components between altered physiological states such as those in ALS and FTD, to differentiate their cellular and molecular mechanisms.

2.1 Label-free quantitation proteomics studies of ALS and FTD

Label-free quantitation (LFQ) can use either data-dependent or data-independent acquisition analyses. Data-dependent acquisition quantitation can be performed on either spectral counts or spectrometric signal intensity of product ions from selected precursors generated by the mass spectrometer (Yu et al., 2016). Recently, label-free quantitation has been more frequently adopted for biomarker discovery studies since it is less expensive than labelled methods and allows comparative analysis of large groups of samples. For a comprehensive review of the technical aspects of label-free quantitative proteomic approaches see (Neilson et al., 2011). LFQ proteomics can also be used as an unbiased approach to characterize changes to a human proteome at a pathway level. As an example, amongst the identification of hundreds of proteins, overlapping mitochondrial and metabolic pathway alterations have been identified from samples of both human ALS and FTD brain and spinal cord samples, highlighting the dysfunctional similarities between these diseases (Iridoy et al., 2018). Similar analysis of brain tissues has provided insight into the various subtypes of ALS and FTD, distinguishing between them by highlighting differences in levels of numerous proteins as well as differences in protein aggregate assembly, distribution and morphology (Laferriere et al., 2019; Umoh et al., 2018). A sequential biochemical extraction technique to purify detergent-insoluble aggregated protein resulted in enrichment of phosphorylated TDP-43 and identification of associated low-solubility proteins associated with TDP-43 pathology (Laferriere et al., 2019). Subsequent MS of these enriched proteins determined distinct patterns of enrichment amongst ALS (23 proteins) and subtypes of FTLD (FTLD-A: 8

proteins; FTLD-C: 10 proteins), providing insights into potential causes of disease heterogeneity (Laferriere et al., 2019). A summary of studies to investigate the mechanisms of ALS and FTD that have used human samples for LFQ are presented in **Table 1**.

[Table 1 Here]

LFQ proteomics has also been applied to animal models, identifying interactors of misfolded SOD1 in the spinal cord of $SOD1^{G93A}$ mice over three presymptomatic time points in disease (Ruegsegger et al., 2016). Only 5 proteins were found shared across these groups with high confidence, including HSPA8. The bulk of proteins found to interact with misfolded SOD1 were identified at the latest time point and selected hits were validated via immunoblotting (Ruegsegger et al., 2016). Of all mutant SOD1 interactors, the activity of Na^+/K^+ATPase-α3 was decreased and exhibited higher levels of protein expression in high-vulnerability motor neurons (Ruegsegger et al., 2016).

Mutations in cyclin F (*CCNF*^{S621G}), which cause rare familial cases of ALS/FTD, have been studied by overexpression in neuronal cell lines and zebrafish to investigate the effects and mechanisms of ALS/FTD (Lee et al., 2018a; Williams et al., 2016). Hundreds of proteins were increased or decreased upon expression of disease-linked mutant cyclin F protein (Lee et al., 2018a). The differentially expressed proteins clustered to cell pathways involved with cellular survival and toxicity, and predicted activation of caspase-3 mediated cell death (Hogan et al., 2017). Studies such as these that combine analysis of different models, such as cells and *in vivo* systems, using both proteomics and complementary validation approaches offer the best approach to identify biologically-relevant changes. The selection of proteins for validation is often based on the statistically significant findings from the proteomic analysis as well as previously published work in the literature, however pathway-level approaches for analysis of large datasets are often more informative than extensive analysis of individual proteins. A summary of ALS and FTD studies that have used animal models for LFQ are presented in **Table 2.**

[Table 2 Here]

The majority of the previous investigative studies have used heterogeneous samples, which poses a limitation. Rather than representing proteomes from only a specific cell type of interest, they largely consist of populations of homogenized and variable cell types. To account for this, reemergence of laser-capture microdissection of tissues has been used to isolate distinct cell-types, and with recent advances in MS technologies this can now be successfully applied to proteomics studies of neurons from brain samples (Aring et al., 2018). Newer technology that is highly sensitive and specific can thus generate a greater number of protein hits from small amounts of extracted sample, and this offers opportunities for future studies of both model systems and human ALS and FTD samples.

In addition to studies of tissue samples, much proteomics research has been applied to understanding ALS and FTD pathogenesis using cell culture models. This approach, which usually makes use of homogenous populations of cells such as immortalised cell lines, removes the confound of studying mixed samples that is often inherent using tissue samples and biofluids. Expression of disease-associated proteins, including mutant SOD1, TDP-43 and tau, recapitulate some features of disease in cell models, such as protein aggregation, inclusion formation and cellular toxicity (Celona et al., 2017; Cohen et al., 2015; Gauthier-Kemper et al., 2011; Monahan et al., 2017; Wang et al., 2017). Proteomics studies of these models has been used to identify proteins that co-aggregate or interact with the known pathological proteins, which may provide insight into

disease pathogenesis. Identification of proteins associated with disease pathology may also help reveal proteins of potential therapeutic use if, for example, those proteins are able to modulate protein aggregation or toxicity (Celona et al., 2017; Mallik et al., 2018). A summary of ALS and FTD studies that have used cell models for LFQ are presented in **Table 3**.

[Table 3 Here]

The main limitations of LFQ using data-dependent acquisition is the generally low proteome coverage and low sensitivity, since many low intensity ions (often from low abundance proteins or poorly ionized peptides) are missed in precursor ion selection. In order to improve this coverage, additional sample prefractionation steps (such as strong cation exchange or basic reverse phase chromatography) can be used to reduce the complexity of the sample to be analysed by MS. A recent LFQ approach that is being more widely adopted relies on data independent quantitation with methods such as Sequential Window Acquisition of all Theoretical Mass Spectra (SWATH) that attempt to circumvent some of these issues associated with analyzing complex samples by data-dependent acquisition.

SWATH, or data-independent acquisition (DIA), acquires data by cycling through predefined sequential windows of a chromatographic elution range generating a larger number of identified proteins from a complex mixture (Gillet et al., 2012). Recently, SWATH has been used to identify differences in blood samples between 42 ALS patients and 18 healthy controls, which revealed a panel of novel potential biomarkers for diagnosis and use in clinical trials (Xu et al., 2018). This study found significant differences in the expression of 30 proteins that varied in ALS patients with or without cognitive impairments. This study highlights the potential of data-independent acquisition methodologies, such as SWATH, to discover markers in biofluids that may have further utility for clinical use that offers promise to provide further advances in ALS and FTD studies. A comprehensive review of the technical aspects of SWATH is discussed elsewhere (Ludwig et al., 2018).

Matrix-assisted laser desorption ionisation (MALDI) is an alternative method to introduce a sample into a MS. This differs from electro-spray ionisation (ESI) through focusing laser energy at a matrix-embedded sample for low fragmentation and reduced multi-charged ion states (Nadler et al., 2017a). Typically ESI dominates the literature as the intermediate in LC-MS, used in all the studies presented in **Tables 1**, **2** and **3**. There are limitations to each technique, which are discussed elsewhere (Nadler et al., 2017b), and the choice of technique generally depends on the biological question. In ALS and FTD studies, MALDI has been used successfully applied to identify increased levels of ubiquitin carboxy-terminal hydrolase L1 (UCHL1) in FTLD-tau cortex (Schweitzer et al., 2006) as well as increased carbonylation of UCHL1 in the spinal cord of SOD1 mice (Poon et al., 2005). Together these findings have highlighted the roles of the oxidative stress response and ubiquitin-mediated degradation in ALS and FTD. MALDI-MS has also been used to identify increased levels of proprotein convertase 1 inhibitor (ProSAAS) in FTD CSF (Davidsson et al., 2002) and potentially pathologically involved ProSAAS N-terminal fragments in the temporal lobe of FTD samples (Kikuchi et al., 2003). More recently, MALDI has been used to identify interactions between Staufen1 and dynein, mediated via protein phosphatase 1-beta, implicating a role of Staufen1 in regulating mRNA localisation (Gershoni-Emek et al., 2016). This has been reinforced through a described link between Staufen1 RNA stress granules and autophagy through interaction with ataxin-2 (Paul et al., 2018). A summary of ALS and FTD studies that have used MALDI-MS is presented in **Table 4**.

[Table 4 here]

2.2 Quantitation via labelling proteomics approaches for ALS and FTD

Labelled-based approaches have considerably higher quantitation accuracy in exchange for lower proteome coverage compared to label-free quantitation (Megger et al., 2014). The labelling techniques involve the introduction of stable isotope labels on the proteins or peptides, which allow the mass spectrometer to distinguish between identical peptides from different samples within a mixture. Quantitative labelling methods can also be used for protein-protein interactions and post-translational modifications (PTM) analyses which are discussed below (Russell et al., 2017; Sullivan et al., 2016). For a comprehensive review of the technical aspects of labelled-based proteomic approaches refer to (Lindemann et al., 2017).

2.2.1 Stable isotope labelling by amino acids in cell culture (SILAC)

Stable Isotope Labelling by Amino acids in Cell culture (SILAC) labeling of cells is achieved by growing cells in culture with growth medium containing different isotopically-labelled amino acids that are incorporated during protein synthesis (Ong et al., 2002). The protein lysates from different isotope-labelled cell culture are pooled together in equal amounts and prepared as one grouped sample to decrease sample preparation variability. High resolution mass spectrometers can analyse and resolve the different precursor (peptide) ions within an experiment and detect the signal intensities of the labelled peptides. The intensities of the precursor ions are used as a measure of the relative abundance of the protein within each sample. One limitation of SILAC, however, is the relatively small number of labelled amino acid combinations (maximum reported to date is 6-plex (Wang et al., 2013)) that can be used in one experiment, which limits the number of comparisons.

The versatility of SILAC can extend to the generation of an internal standard in a cell-line to quantify low abundance proteins in tissue (known as "Super SILAC"). This was applied to investigate the accumulated proteins in detergent-insoluble brain lysates from four control and four FTLD brain samples, with comparison to a HEK293 standard (Seyfried et al., 2012). A summary of ALS and FTD studies that have used SILAC is presented with other labelled methods in **Table 5.**

2.2.2 Tandem mass tags (TMT)

Unlike SILAC, which incorporates isotopically labelled amino acids at the protein level, the Tandem Mass Tag (TMT) system is used to label peptides following proteolytic digestions (Thompson et al., 2003). TMT tags are covalently coupled to both N-terminal α-amino groups and ε-amino groups of lysine residues (Thompson et al., 2003). Once labelled, peptide samples are pooled (up to 10-plex), and subsequently fractionated and analysed by a high-resolution mass spectrometer. The secondary detection of reporter ions (MS2) allow the peptides to be quantitated based on the signal intensities, which can be extended to a third round (MS3) to decrease ratio distortion (Ting et al., 2011).

TMT-based quantitative proteomics is being increasingly applied in neuroscience, including in several investigations of proteome-wide nucleocytoplasmic changes in cell-based models of ALS. In mouse motor neuron-like NSC-34 cells overexpressing mutant hSOD1^{G93A}, TMT-labeling of peptides combined with the results of RNA-Seq demonstrated impairments to nuclear and cytoplasmic transport (Kim et al., 2017). Specifically, proteins enriched in the nuclear fraction of mutant SOD1-expressing cells were related to RNA transport/processing and known Huntington's

disease/Alzheimer's disease pathways, whilst proteins enriched in cytoplasmic fractions were involved in protein folding, aminoacyl-tRNA biosynthesis, Wnt signaling, synaptic vesicle cycle and Hippo signaling pathways (Kim et al., 2017). In another study, TMT 10-plex was used to analyse ALS patient fibroblast-derived iPSC cells to validate genome-wide RNA instability in ALS and FTD patients (Tank et al., 2018). Bromouridine tagging of RNA transcripts identified profound destabilization of ribosomal and mitochondrial transcripts, which was verified by TMT-quantitative proteomics and revealed corresponding decreases in mitochondrial components and compensatory increases in protein synthesis (Tank et al., 2018). Using this proteogenomic approach, the observations from this study suggest that TDP-43 deposition leads to targeted RNA instability in ALS and FTD, and may ultimately cause cell death by disrupting energy production and protein synthesis pathways (Tank et al., 2018). A summary of studies that have used various labelling-based MS techniques such as TMT for investigation of ALS and FTD is presented in **Table 5**.

[Table 5 here]

2.3 Protein-protein interactions

Interrogating protein-protein interactions in cultured cells, animal models of disease and from human tissue can provide valuable insight into mechanisms that underlie neurodegeneration. Characterising the interactome of proteins of interest in both healthy and disease states not only reveals normal protein function but also sheds light on pathogenic changes. Characterising protein-protein interactions also has therapeutic value since specific interactions may be amenable to therapeutic modulation.

MS-based methods enable high-throughput identification of protein-protein interactions and have been extensively used to characterise the interactomes of many proteins implicated in neurodegeneration (Hosp et al., 2015). Standard methods used to identify PPIs are based on immunoprecipitation followed by MS (IP-MS); however, in recent years, proximity-ligation methods have emerged which complement standard IPs and provide additional insight into protein interactomes. These methods include proximity-dependent biotin identification (BioID) and ascorbate peroxidase (APEX)-based proximity tagging (Chu et al., 2017; Roux et al., 2013; Roux et al., 2012). BioID, APEX and related techniques can also be used to study interaction partners of insoluble proteins, a feature which makes these methods particularly useful in neurodegenerative diseases characterised by protein aggregation(Roux et al., 2013).

2.3.1 Immunoprecipitation and MS (IP-MS)

A standard method that is used to identify PPIs relies on maintaining the physical interaction between the interaction partners. Prior to immunoprecipitation (IP), cells are lysed in non-denaturing buffers which can maintain stable but not transient interactions. A typical process for IP-MS studies is based on antibody recognition of a protein of interest within a lysate, followed by specific isolation of the antibody (and associated proteins) using protein A or G conjugated to beads (Markham et al., 2007). Of note, this method requires that PPIs remain stable after cell lysis and that the protein complex of interest remains soluble in the chosen lysis buffers. In ALS and FTD studies, IP-MS has been used to identify interacting partners of TDP-43, revealing many proteins involved in RNA metabolism (Freibaum et al., 2010). Recently, interactors of RNA-binding protein 45 (RBM45), a protein that colocalises with ALS and FTD inclusions, were identified as hnRNP and EIF proteins involved in RNA metabolism, suggesting distubrance of these processes upon pathology formation in

disease (Li et al., 2016). As IP-MS studies generally incorporate label-free MS they have been included amongst studies previously discussed **Tables 1, 2 and 3**.

2.3.2 Proximity-ligation methods

BioID and APEX are proximity-ligation methods which facilitate the covalent attachment of biotin onto proteins in close proximity to a protein of interest. The application of these methods for interrogating PPIs of proteins is based on the strong interaction between biotin and streptavidin (K_d of 4×10^{-14} M) (Green, 1990) and the stability of streptavidin in a large range of conditions. This includes stability in denaturing buffers containing ionic detergents such as sodium dodecylsulfate (SDS) (Sano et al., 1998) and chaotrophic reagents such as urea (Kurzban et al., 1991), such that these approaches are applicable to studies of both detergent-soluble and -insoluble proteins from cells and tissues.

2.3.2.1 Proximity-dependent biotin identification (BioID)

Proximity-dependent biotin identification or BioID is based on the use of an engineered biotin ligase which carries an R118G mutation within its active site, effectively nullifying self-association and DNA binding (Roux et al., 2012). Normally, biotin ligase (BirA) works by converting biotin to a highly reactive biotinoyl-AMP intermediate in an ATP-dependent manner. This intermediate is then deposited onto lysine residues within the natural substrate of BirA, Biotin Carboxyl Carrier Protein (BCCP) (Cronan, 1990). Engineered biotin ligase (BirA*) is also able to convert biotin to a highly reactive intermediate however, due to this R118G mutation, the intermediate is prematurely released from the active site of BirA* and diffuses away leading to biotinylation of nearby lysine residues (Kwon et al., 2000). In this way BirA* can biotinylate lysine residues of proteins in close proximity to the protein of interest. In a typical BioID workflow, a construct encoding BirA* in frame with a protein of interest is first generated and expressed in live cells. Exogenous biotin is then added to cell culture media such that biotin can be processed by BirA* and deposited onto proteins within proximity to the fusion protein. Here, labelling typically occurs over 12-24 hours to generate enough material for analysis. In addition, the half-life of the biotin intermediate is in the minutes range which results in a large labelling radius (Rhee et al., 2013). Cells can then be lysed before streptavidin-conjugated beads are used to isolate biotinylated proteins from the complex mixture. These isolated biotinylated proteins can then be identified using standard MS-based workflows. BioID approaches have only recently begun to be applied to studies to understand mechanisms of ALS and FTD. Most notably, a BioID approach was used to characterise the interactome of TDP-43 and the pathological C-terminal fragment which revealed a correlation between C-terminal fragments and nuclear pore defects (Chou et al., 2018).

In recent years, a smaller, more efficient form of the biotin ligase, termed BioID2, has been established (Kim et al., 2016). BirA* has also been modified using directed evolution which has improved the labeling kinetics of biotin ligase such that labeling can be completed in 10 minutes. This variant of BirA*, termed "TurboID" has been implemented in live organisms including *Caenorhabditis elegans* and *Drosophila melanogaster* (Branon et al., 2018), demonstrating the versatility of this method to interrogate the interactome of proteins in both live cells and organisms. These improvements make this system a key new technology for future application to the understanding of protein interactions in neurodegeneration, using both cultured cells and animal models of disease.

2.3.2.2 APEX

APEX is a 28 kDa engineered peroxidase that is derived from dimeric pea or soybean ascorbate peroxidases (Martell et al., 2012; Rhee et al., 2013). APEX can be used in a similar manner to BioID for the biotinylation of proteins in the vicinity of a protein of interest. Like BioID, constructs are first generated to encode engineered soybean peroxidase in frame with a protein of interest before the fusion protein is expressed in live cells. Notably, APEX can be used for temporally resolved proteomics as well as high-resolution microscopy, making this a flexible technique for studies of protein interactions.

Once the APEX fusion protein is expressed in live cells, exogenous biotin is added to cell culture media. For labelling of proximal proteins, hydrogen peroxide (H_2O_2) and biotin phenol is added to media such that APEX can catalyse a one-electron oxidisation of biotin phenol to a biotinphenoxyl radical which subsequently biotinylates proteins in proximity (Lam et al., 2015). Notably, labeling kinetics of APEX is fast. The produced biotin-phenoxyl radical lasts for <1 ms which enables labelling times of 1 minute and limits the labeling radius to 20 nm (Chu et al., 2017). After 1 minute, the reaction is stopped with quenching buffer to prevent further biotinylation post-lysis. Cells may then be lysed before biotinylated proteins are isolated by streptavidin conjugated to beads and identified using MS-based workflows. An advantage of the short labeling timeframe is that APEX can be used to capture dynamic changes in protein-protein interactions. This may become advantageous for time course studies where protein interactions may dynamically change in response to various stimuli such as cell stress or drug treatments.

APEX can also be applied to analysis by electron microscopy (EM) (Lam et al., 2015; Martell et al., 2012), thereby enabling the interrogation of protein localisation at high resolution. Here, fusion proteins are expressed in cells before cells are fixed and treated with diaminobenzidine (DAB) and H_2O_2 (Lam et al., 2015). APEX catalyses the polymerisation and local deposition of DAB in the vicinity of the fusion protein, enabling subsequent recruitment of electron dense osmium for EM applications (Lam et al., 2015). Recently, the APEX technique has been applied to profile the components of stress granules, which are enriched in RNA-binding proteins including the ALS/FTD-linked proteins TDP-43 and FUS (Markmiller et al., 2018). Notably, these studies revealed previously unrecognised SG proteins that also displayed alterations in induced pluripotent stem cell-derived motor neurons from ALS patients and for which modulation of expression was protective in Drosophila ALS models, suggesting disturbances in SGs may be related to disease pathogenesis (Markmiller et al., 2018).

By applying APEX for both proteomics and EM workflows, APEX can be used to characterise dynamic changes in the protein interactome of live cells whilst also accurately defining protein localisation at high resolution. In recent years, variations of APEX have emerged. This includes APEX2 (Lam et al., 2015) which has improved catalytic efficiency and split APEX (sAPEX) which enables the interrogation of two known protein interaction partners or proteins known to be in close proximity (Han et al., 2018). Recently, the APEX technique has been applied to profile the components of stress granules, which are enriched in RNA-binding proteins including the ALS/FTD-linked proteins TDP-43 and FUS (Markmiller et al., 2018). Notably, these studies revealed previously unrecognised SG proteins that also displayed alterations in induced pluripotent stem cell-derived motor neurons from ALS patients and for which modulation of expression was protective in Drosophila ALS models, suggesting disturbances in SGs may be related to disease pathogenesis (Markmiller et al., 2018).

2.3 Future applications of proximity labelling techniques

Biotinylation by Antibody Recognition (BAR) is another proximity-labelling technique which has recently been established for investigating PPIs in fixed samples (Bar et al., 2018). Here, cultured cells or tissue are fixed and permeabilised before a primary antibody is used to target a protein of interest. A secondary antibody conjugated to horseradish peroxidase (HRP) is then used to recognise the primary antibody, and labelling of proximal proteins is achieved by HRP in the presence of H_2O_2 and biotin phenol. The conjugation of biotin enables the isolation of these proximal proteins. Although this method has not yet been applied for the study of neurodegenerative diseases, it is a promising technique for future analysis of proteins involved in ALS and FTD and may be particularly useful for analysis of detergent-insoluble protein aggregates and inclusions.

2.4 Analysis of protein post-translational modifications in ALS and FTD

Post-translational modifications (PTMs) provide the basis of biological diversity in the proteome by enabling the same protein to carry out diverse functions through characteristic variations of modifications and their temporal regulation. PTMs are small, covalent, amino acid modifications added onto a protein; they are highly dynamic and play key roles in selectively regulating protein function in cells, tissue, and biofluids, such as CSF (Guldbrandsen et al., 2014). PTMs regulate most aspects of intracellular function involving but not limited to, DNA repair, proliferation, subcellular localization, transport, and proteolytic cleavage of functional units or protein degradation. On a larger scale PTMs also modulate intercellular functions like cell signaling and adhesion (Minguez et al., 2012; Olsen & Mann, 2013; Theillet et al., 2012). Various types of PTMs exist (Prabakaran et al., 2012), with arguably the most studied in proteostasis and neurodegenerative diseases being: ubiquitination, phosphorylation, nitration, acetylation, oxidation, glycosylation, methylation, sumoylation (Minguez et al., 2012).

Pathological phosphorylation of proteins such as tau, TDP-43, α-synuclein or FUS contribute to the formation of protein inclusions in neurodegenerative disease (Cykowski et al., 2018; Hasegawa et al., 2008a; Lee et al., 2017a; Monahan et al., 2017; Wang et al., 2017). While the underlying mechanisms of misfolded protein aggregation and neurotoxicity in neurodegeneration is not yet understood, PTMs such as ubiquitination are of interest given their regulatory role in protein degradation. For example, the temporal regulation of phosphorylation and ubiquitination in protein signaling cascades, and hyperubiquitination by mutant cyclin F cause defects to protein degradation pathways that are associated with ALS/FTD (Lee et al., 2017a). Furthermore, other examples of aberrant PTMs including acetylation of glial fibrillary acidic protein in ALS (Liu et al., 2013), phosphorylated TDP-43 in ALS and FTLD (Hasegawa et al., 2008b) and phosphorylated tau in diseases containing tauopathies, such as FTD and AD (Ferrer et al., 2002)

2.4.1 Detecting PTMs by mass spectrometry

Many PTMs can be mapped by tandem MS (MS/MS) (Dephoure et al., 2013), which offers an unbiased approach that can be verified by alternative biochemical methods such as immunoblotting and immunofluorescence microscopy. To date, the presence of PTMs such as ubiquitination, phosphorylation, acetylation and nitration, and their stoichiometric analysis have been

enabled by qualitative and quantitative proteomics, respectively, on a global proteomic scale in ALS-linked proteins (Lee et al., 2017a; Liu et al., 2013; Sacksteder et al., 2006; Shi et al., 2013a; Wang et al., 2017). Despite the capabilities of MS to identify PTMs, they are often difficult to detect as they vary in physiochemical properties, can exist as transient modifications, be present in sub-stoichiometric concentrations and are sensitive to sample preparative steps that include high and low pH buffers, trypsinization and de-salting steps (Olsen & Mann, 2013; Wei & Li, 2008).

To circumvent many of the issues associated with analyzing PTMs such as ubiquitination and phosphorylation (reviewed in (Arrington et al., 2017), which are the most commonly studied PTMs in neurodegenerative disease research, enrichment strategies to isolate peptides containing these modifications together with quantitative proteomic approaches can provide a more in-depth analysis of the sub-proteome. For example, a popular enrichment strategy for identifying ubiquitination sites on peptides called diglycine (diGLY) enrichment exploits the cleavage sites (K-ε-GG) of ubiquitinated proteins following trypsin digestion. The covalent attachment of ubiquitin on lysine residues on proteins allows trypsin to cleave both the C-terminus of ubiquitin and the C-terminus of the lysine amino acid on the ubiquitinated protein exposing two glycine residues. Ubiquitin remnant motif (K-ε-GG) antibodies are used to enrich peptides containing the di-GlyGly motif, followed by elution and analysis by LC-MS/MS in which the presence of the GlyGly residue on lysine (+ m/z 114.04) in the MS spectra is an indication of a ubiquitinated peptide (Fulzele & Bennett, 2018; Peng et al., 2003; Xu et al., 2010). However, ubiquitin-like proteins also exist that may be identified using this method such as SUMO (sumoylation), NEDD8 (neddylation) and interferon-stimulated gene 15 (ISG15; isg15ylation) also known as ubiquitin cross-reactive protein (UCRP) (Kim et al., 2011). Quantitative assessment of the stoichiometry of site-specific ubiquitination can be achieved using the recently reported 'isotopically balanced quantification of ubiquitination' (IBAQ-Ub) method which employs an amine-reactive chemical tag (AcGG-NHS) that is structurally homologous to a tryptically cleaved ubiquitinated peptide containing a GG remnant of ubiquitin on the modified lysine residue. These AcGG-NHS tagged peptides allows the generation of structurally identical peptides from ubiquitinated and unmodified lysine residues that can be further labelled using a secondary stable isotope (Li et al., 2019). Other areas which are generating interest are investigating the specific poly-ubiquitin linkages, in which isotope-labelling of the lysine residues in ubiquitin can be used, such as the 'UB-AQUA' and detected by high resolution MS via narrow window extracted ion chromatogram or by selected reaction monitoring (SRM-MS) using a triple quadrupole MS (Phu et al., 2011). Overall, these various methods enable stoichiometric analysis of the poly-ubiquitin modifications on target proteins, which could provide insights into the ubiquitin code underlying altered protein degradation in neurodegeneration.

2.5 Bioinformatics

Tandem mass spectra generated by MS are analysed using specialised software and algorithms to identify and quantitate peptides and proteins using two main approaches: database search and de novo search. Database searching follows the "Exact Pattern-Matching rule", which consists of only selecting spectra masses that exactly match a sequence in a multi-species- or species-specific database. The most frequently used programs with a database search implemented are SEQUEST (Eng et al., 1994), Mascot (Perkins et al., 1999), and X!Tandem (Craig & Beavis, 2004). These programs not only extract candidate proteins using a combination of the open access

database and their own in-built database but also score them using algorithms based on the ion signals observed in the spectra. Some limitations of the database search method include that a large portion of acquired spectra will be rejected because of the "Exact Pattern-Matching rule" and not all organisms have a complete protein sequence reference.

De novo peptide sequencing generates a list of all the highest scored peptides from the MS/MS spectra and the mass values given without the need of a reference database. With high resolution mass spectrometers producing quality data, the performance of *de novo* sequencing has remarkably improved. However, a significant caveat pertains to resolving amino acids with or without modifications, due to either identical mass or near-identical masses. In addition, there is an inverse relationship between the accuracy of this method and peptide length (Muth & Renard, 2018). New strategies are being created in this space to overcome these limitations, such as *post novo*, which post-processes *de novo* sequence filter prediction (Miller et al., 2018).

Commonly used bioinformatics programs such as STRING, BioGrid, Ingenuity Pathway Analysis (IPA), and DAVID are frequently used to interrogate the data obtained from large scale quantitative proteomic experiments to get a snapshot of the expressional changes that occur within a sub-proteome. Notably, depending on the biological question, these informatic tools can assist in quickly identifying networks, pathways and functions to facilitate further experiments and generate new hypotheses. For example, proteomics data generated from IP of TDP-43 from HEK293 lysates were analysed by STRING, which demonstrated clear nuclear and cytoplasmic interaction networks (Freibaum et al., 2010). Assigning protein functions using bioinformatic software therefore provides a higher-level overview into changes and perturbations occurring during disease, for example allowing the identification of disease relevant biochemical pathways. A more detailed review of the bioinformatics tools used for proteomics is discussed elsewhere (Martens & Vizcaino, 2017; Schmidt et al., 2014).

2.6 Flow cytometric purification of inclusion bodies associated with ALS and FTD

Determination of the composition of insoluble inclusions formed in many neurodegenerative diseases is key to understanding the pathogenesis of these disease. The use of proteomics will allow greater understanding of the global protein composition of these inclusions and allow us to identify proteins and cellular pathways that are either involved in the assembly or attempted disassembly of the inclusion and distinguish these from proteins that were "accidentally" sequestered. Comparing the protein composition of inclusions formed from a variety of pathogenic proteins (e.g. TDP-43- or SOD1-positive inclusions in ALS) could also help to establish common pathways involved in this process in across different types of neurodegenerative diseases.

Fluorescence activated cell sorting (FACS) is one technique that can be used to purify insoluble protein or inclusions from cell culture or tissues. Regarding cell-based models of neurodegenerative disease-associated protein aggregation, gentle plasma membrane permeabilisation in combination with FACS could be employed to purify inclusions for proteomic analyses. A method for this was recently described, whereby cells are permeabilised with 0.5% (v/v) TritonX-100 in PBS supplemented with protease/phosphatase inhibitors to quantify and characterise inclusions comprised of fluorescently-tagged proteins of interest by flow cytometry (Whiten et al., 2016). This work also demonstrated that fluorescent aggregates and nuclei can be sorted by FACS (Whiten et al., 2016). Alternatively, cells can

be treated with 0.03% (w/v) saponin to selectively-permeabilise the plasma membrane, allowing soluble proteins to diffuse out of the cytoplasm, while retaining the nucleus and inclusions intact (Farrawell et al., 2018; Pokrishevsky et al., 2018). These treated cells can be washed to remove the soluble proteins that have diffused out of the cells and subsequently purify cells with inclusions by FACS. It follows that inclusions comprised of fluorescently-tagged proteins, or fluorescent antibody-labelled inclusions can be purified by FACS from cells and tissues and subjected to proteomic analysis to determine their composition.

Purification of inclusions by FACS for proteomic analysis has previously been adopted to investigate the protein composition of Huntington's disease-associated polyglutamine inclusions (Mitsui et al., 2006; Mitsui et al., 2002). Using this strategy heat shock protein 84 and elongation factor 1α were identified as novel inclusion-interacting proteins and their over-expression in cell-based assays demonstrated cytoprotective activities (Mitsui et al., 2006; Mitsui et al., 2002). Future experiments could employ this strategy to purify insoluble protein and inclusions for proteomic analysis from ALS/FTD patient samples, rodent tissues, or cell-based models of ALS/FTLD.

3 Biomarker studies of ALS and FTD

As high-throughput technologies have advanced, many proteomic-based biomarker studies have presented an abundance of potential candidates; however it is often not feasible to properly validate each individual protein considering the heterogeneity amongst different patient cohorts, which can hinder the level of accuracy and reproducibility. Selection of which candidates to validate is not clearly defined, uniform, or standardised. This selection can be made based on a combination of statistics, current literature as well as assessed potential based on protein-protein interactions, both predicted and real.

One of the major issues that arises as a result of subjective validation is the variation of proteins identified across parallel studies, rarely reinforcing the previously presented data. For example, measurements of HeLa cells prepared identically and analysed across different laboratories using the same instrumentation revealed a high level of biological heterogeneity on both transcriptomic and proteomic levels (Liu et al., 2019). This occurs for a number of reasons, including the sample composition and sample cohorts, environmental conditions affecting instrument parameters, as well as technical variation due to extraction/digestion procedures (Piehowski et al., 2013). Alternatively, the same protein could be reported with differing results across samples, such as decreased levels of galectin-3 in the plasma of SOD1 mice (Zubiri et al., 2018) and increased levels in human CSF (Zhou et al., 2010). These results are not necessarily conflicting but highlight the importance of validation across multiple large cohorts for biological relevance.

In recent years, an increased number of small and large-scale biomarker studies have been performed on human ALS samples by LFQ, as recently reviewed (Barschke et al., 2017). CSF from ALS, primary lateral sclerosis (PLS), cross-sectional healthy and disease controls (Parkinsons' disease and ALS mimic disorders) were analysed via LFQ for novel biomarker discovery (Thompson et al., 2018). Elevation in levels of chitotriosidase, chitinase-3-like protein 1 and chitinase-3-like protein 2 in a cohort of 43 patients with ALS has been revealed, indicating neuroinflammation due to increased microglial activation (Thompson et al., 2018). No direct validation was performed to confirm the proteomic data, although reference to previous ELISA studies of these chitinase proteins in ALS patient samples (likely including some from the same cohort), suggested a similar trend (Varghese et al., 2013).

Biofluid sample usage is prominent due to the need for a directly translatable and easily retrievable marker for rapid and accurate diagnosis. Alongside disease diagnosis, the ability to distinguish between subtypes of a disease would prove instrumental in developing personalized treatments. Whilst usefulness of biofluid MS for biomarker elucidation, identifying relevant disease-related proteins such as tau (Macron et al., 2018). In the context of biomarker discovery, newer labelled methods are being utilised to narrow down on protein hits of interest due to the greater quantitation accuracy compared to label-free methods (Megger et al., 2014). A summary of ALS and FTD biomarker elucidation studies in the last decade that have used both label-free and labelled methods is presented in **Table 6**. Ultimately, it is crucial to have a clear biological question to pursue for selection of sample, technique and subsequent validation research laterally, solidifying findings to progress with ensuing biological questions. Incorporation of parallel approaches such as transcriptomics using RNASeq alongside results from proteomics can reinforce potential hits of interest. Studies have successfully combined transcriptomic and proteomics findings to provide mechanistic insights, such as the finding of lysosomal changes in Grn-/- mice that are modulated by the FTD-risk protein TMEM106B (Klein et al., 2017). Additional recent advances in this area have included correlation of transcriptomic findings with underlying TDP-43 pathology burden in a study of ALS spinal cord laser-capture dissected motor neurons (Krach et al., 2018). This was one of the first studies that utilised overlapping distinct datasets to stratify patient cohorts to identify the more relevant and important proteins involved in disease. Previously, careful patient sub-type selection has led to the identification of genetic contributors to disease, such as the finding that TMEM106b genotype is a risk modifier of FTD by GWAS of a highly specific and well-defined subgroup of FTLD samples with confirmed TDP-43 histopathology (Van Deerlin et al., 2010). These findings suggest that planning sample selection to allow multiple comparisons of disease subtypes, alongside the combined use of new protein- and RNA-profiling technologies, will lead to further advances in the field of ALS and FTD research.

Focus should also be given to the comparison of findings from ALS and FTD proteomics datasets with those obtained from other neurodegenerative diseases, since there are likely to be overlap in mechanisms which may be broadly involved in neurodegeneration. This may also provide information on how disease-specific alterations arise and why certain cell populations or CNS regions are susceptible to different neurodegenerative disease processes. For example, recent studies have applied TMT to identify changes in various Alzheimer's disease mice, identifying hundreds of differentially expressed proteins (Kim et al., 2018). Previously, these comparisons have also been used for biomarker elucidation, attempting to highlight differences between similar many studies have identified altered proteins across cohorts of patients, others focus on teasing apart unclear differences such as those found in subtypes of FTD (Teunissen et al., 2016). Recently, a CSF-wide proteomic analysis was performed to highlight the approaches, although unbiased screening of potential disease-related biofluid alterations may help identify previously unrecognised research directions.

[Table 6 here]

4. Future directions and conclusion

The technologies presented in this review have demonstrated their utility when applied to neurodegenerative diseases such as ALS and FTD. However, there needs to be a focus on validating the

neurodegenerative diseases such as FTD and Alzheimer's disease (Teunissen et al., 2016).

Finally, it will also be informative to use these powerful techniques to more closely investigate biochemical changes longitudinally in disease, particularly in studies of model systems from which brain and spinal cord samples can be collected at pre-defined time points. Strategies such as this are most likely to illuminate the earliest pathogenic changes in disease, which may be most amenable to therapeutic intervention, but which may not be identified by studies at later disease time points or by using end-stage human tissue samples alone. The use of comparative studies and recent advances in new technologies and labelling techniques offers great hope for future understanding of ALS and FTD, and development of clinical tests and therapeutics based on these findings.

Author Contributions

TH, RS, FC, SR, JD, AD, and MV were responsible for drafting, writing and editing the manuscript. HE, AW and AL conceived the overall layout of the manuscript and were responsible for the final editing and proof-reading of the manuscript. All authors read and approved the final manuscript.

Acknowledgements

This work and related studies was supported by the Australian Government Department of Education and Training RTP, QBI Research Higher Degree Top Up Scholarship, the MND Research Institute of Australia (GIA1628, 1715 and 1727), the Australian National Health and Medical Research Council (Project Grant 1124005, 1095215 and 1107644 and RD Wright Career Development Fellowship 1140386), the Ross Maclean Fellowship, and the Brazil Family Program for Neurology. We thank Dr Nick Valmas for assistance with graphic design.

References

Acquadro, E., Caron, I., Tortarolo, M., Bucci, E. M., Bendotti, C., & Corpillo, D. (2014). Human SOD1-G93A specific distribution evidenced in murine brain of a transgenic model for amyotrophic lateral sclerosis by MALDI imaging mass spectrometry. *J Proteome Res, 13*(4), 1800-1809. doi:10.1021/pr400942n

Ait-Bouziad, N., Lv, G., Mahul-Mellier, A.-L., Xiao, S., Zorludemir, G., Eliezer, D., . . . Lashuel, H. A. (2017). Discovery and characterization of stable and toxic Tau/phospholipid oligomeric complexes. *Nature Communications,* 8(1), 1678. doi:10.1038/s41467-017-01575-4

Almeida, S., Zhou, L., & Gao, F.-B. (2011). Progranulin, a glycoprotein deficient in frontotemporal dementia, is a novel substrate of several protein disulfide isomerase family proteins. *PLoS One, 6*(10), e26454-e26454. doi:10.1371/journal.pone.0026454

Alonso, R., Pisa, D., Marina, A. I., Morato, E., Rabano, A., Rodal, I., & Carrasco, L. (2015). Evidence for fungal infection in cerebrospinal fluid and brain tissue from patients with amyotrophic lateral sclerosis. *Int J Biol Sci, 11*(5), 546-558. doi:10.7150/ijbs.11084

Arai, T., Hasegawa, M., Akiyama, H., Ikeda, K., Nonaka, T., Mori, H., . . . Hashizume, Y. (2006). TDP-43 is a component of ubiquitin-positive tau-negative inclusions in frontotemporal lobar degeneration and amyotrophic lateral sclerosis. *Biochemical and biophysical research communications, 351*(3), 602-611.

Aring, L., Steinbach, S., Marcus, K., & May, C. (2018). Isolation of Distinct Types of Neurons from Fresh Brain Tissue Using Laser Microdissection in Combination with High-Performance Liquid Chromatography-Mass Spectrometry. *Methods Mol Biol, 1723*, 247-260. doi:10.1007/978-1-4939-7558-7_14

Arrington, J. V., Hsu, C.-C., Elder, S. G., & Andy Tao, W. (2017). Recent advances in phosphoproteomics and application to neurological diseases. *Analyst, 142*(23), 4373-4387. doi:10.1039/C7AN00985B

Atkin, J. D., Farg, M. A., Walker, A. K., McLean, C., Tomas, D., & Horne, M. K. (2008). Endoplasmic reticulum stress and induction of the unfolded protein response in human sporadic amyotrophic lateral sclerosis. *Neurobiol Dis, 30*(3), 400-407. doi:10.1016/j.nbd.2008.02.009

Ayala, Y. M., Zago, P., D'Ambrogio, A., Xu, Y. F., Petrucelli, L., Buratti, E., & Baralle, F. E. (2008). Structural determinants of the cellular localization and shuttling of TDP-43. *J Cell Sci, 121*(Pt 22), 3778-3785. doi:10.1242/jcs.038950

Ayers, J. I., McMahon, B., Gill, S., Lelie, H. L., Fromholt, S., Brown, H., . . . Borchelt, D. R. (2017). Relationship between mutant Cu/Zn superoxide dismutase 1 maturation and inclusion formation in cell models. *J Neurochem, 140*(1), 140-150. doi:10.1111/jnc.13864

Balch, W. E., Morimoto, R. I., Dillin, A., & Kelly, J. W. (2008). Adapting proteostasis for disease intervention. *science, 319*(5865), 916-919.

Bar, D. Z., Atkatsh, K., Tavarez, U., Erdos, M. R., Gruenbaum, Y., & Collins, F. S. (2018). Biotinylation by antibody recognition-a method for proximity labeling. *Nat Methods, 15*(2), 127-133. doi:10.1038/nmeth.4533

Barschke, P., Oeckl, P., Steinacker, P., Ludolph, A., & Otto, M. (2017). Proteomic studies in the discovery of cerebrospinal fluid biomarkers for amyotrophic lateral sclerosis. *Expert Rev Proteomics, 14*(9), 769-777. doi:10.1080/14789450.2017.1365602

Basso, M., Samengo, G., Nardo, G., Massignan, T., D'Alessandro, G., Tartari, S., . . . Bonetto, V. (2009). Characterization of detergent-insoluble proteins in ALS indicates

a causal link between nitrative stress and aggregation in pathogenesis. *PLoS One, 4*(12), e8130. doi:10.1371/journal.pone.0008130

Bereman, M. S., Beri, J., Enders, J. R., & Nash, T. (2018). Machine Learning Reveals Protein Signatures in CSF and Plasma Fluids of Clinical Value for ALS. *Sci Rep, 8*(1), 16334. doi:10.1038/s41598-018-34642-x

Bergemalm, D., Forsberg, K., Jonsson, P. A., Graffmo, K. S., Brannstrom, T., Andersen, P. M., . . . Marklund, S. L. (2009). Changes in the spinal cord proteome of an amyotrophic lateral sclerosis murine model determined by differential in-gel electrophoresis. *Mol Cell Proteomics, 8*(6), 1306-1317. doi:10.1074/mcp.M900046-MCP200

Blair, L. J., Nordhues, B. A., Hill, S. E., Scaglione, K. M., O'Leary, J. C., 3rd, Fontaine, S. N., . . . Dickey, C. A. (2013). Accelerated neurodegeneration through chaperone-mediated oligomerization of tau. *The Journal of clinical investigation, 123*(10), 4158-4169. doi:10.1172/JCI69003

Blokhuis, A. M., Koppers, M., Groen, E. J., van den Heuvel, D. M., Dini Modigliani, S., Anink, J. J., . . . Pasterkamp, R. J. (2016). Comparative interactomics analysis of different ALS-associated proteins identifies converging molecular pathways. *Acta Neuropathol, 132*(2), 175-196. doi:10.1007/s00401-016-1575-8

Bodea, L. G., Eckert, A., Ittner, L. M., Piguet, O., & Gotz, J. (2016). Tau physiology and pathomechanisms in frontotemporal lobar degeneration. *J Neurochem, 138 Suppl 1*, 71-94. doi:10.1111/jnc.13600

Boeynaems, S., Bogaert, E., Kovacs, D., Konijnenberg, A., Timmerman, E., Volkov, A., . . . Van Den Bosch, L. (2017). Phase Separation of C9orf72 Dipeptide Repeats Perturbs Stress Granule Dynamics. *Mol Cell, 65*(6), 1044-1055.e1045. doi:10.1016/j.molcel.2017.02.013

Brancia, C., Noli, B., Boido, M., Boi, A., Puddu, R., Borghero, G., . . . Cocco, C. (2016). VGF Protein and Its C-Terminal Derived Peptides in Amyotrophic Lateral Sclerosis: Human and Animal Model Studies. *PLoS One, 11*(10), e0164689. doi:10.1371/journal.pone.0164689

Branon, T. C., Bosch, J. A., Sanchez, A. D., Udeshi, N. D., Svinkina, T., Carr, S. A., . . . Ting, A. Y. (2018). Efficient proximity labeling in living cells and organisms with TurboID. *Nat Biotechnol, 36*(9), 880-887. doi:10.1038/nbt.4201

Bruijn, L. I., Houseweart, M. K., Kato, S., Anderson, K. L., Anderson, S. D., Ohama, E., . . . Cleveland, D. W. (1998). Aggregation and Motor Neuron Toxicity of an ALS-Linked SOD1 Mutant Independent from Wild-Type SOD1. *Science, 281*(5384), 1851. doi:10.1126/science.281.5384.1851

Capitanio, D., Vasso, M., Ratti, A., Grignaschi, G., Volta, M., Moriggi, M., . . . Gelfi, C. (2012). Molecular signatures of amyotrophic lateral sclerosis disease progression in hind and forelimb muscles of an SOD1(G93A) mouse model. *Antioxid Redox Signal, 17*(10), 1333-1350. doi:10.1089/ars.2012.4524

Celona, B., Dollen, J. V., Vatsavayai, S. C., Kashima, R., Johnson, J. R., Tang, A. A., . . . Black, B. L. (2017). Suppression of C9orf72 RNA repeat-induced neurotoxicity by the ALS-associated RNA-binding protein Zfp106. *Elife, 6*. doi:10.7554/eLife.19032

Chan, P. K., Chattopadhyay, M., Sharma, S., Souda, P., Gralla, E. B., Borchelt, D. R., . . . Valentine, J. S. (2013). Structural similarity of wild-type and ALS-mutant superoxide dismutase-1 fibrils using limited proteolysis and atomic force microscopy. *Proc Natl Acad Sci U S A, 110*(27), 10934-10939. doi:10.1073/pnas.1309613110

Chapman, J. D., Goodlett, D. R., & Masselon, C. D. (2014). Multiplexed and data-independent tandem mass spectrometry for global proteome profiling. *Mass Spectrometry Reviews, 33*(6), 452-470. doi:doi:10.1002/mas.21400

Chassefeyre, R., Martínez-Hernández, J., Bertaso, F., Bouquier, N., Blot, B., Laporte, M., . . . Goldberg, Y. (2015). Regulation of postsynaptic function by the dementia-related ESCRT-III subunit CHMP2B. *J Neurosci, 35*(7), 3155-3173. doi:10.1523/JNEUROSCI.0586-14.2015

Chen, D., Wang, Y., & Chin, E. R. (2015). Activation of the endoplasmic reticulum stress response in skeletal muscle of G93A*SOD1 amyotrophic lateral sclerosis mice. *Front Cell Neurosci, 9*, 170. doi:10.3389/fncel.2015.00170

Chen, Y., Liu, X. H., Wu, J. J., Ren, H. M., Wang, J., Ding, Z. T., & Jiang, Y. P. (2016). Proteomic analysis of cerebrospinal fluid in amyotrophic lateral sclerosis. *Exp Ther Med, 11*(6), 2095-2106. doi:10.3892/etm.2016.3210

Cheroni, C., Marino, M., Tortarolo, M., Veglianese, P., De Biasi, S., Fontana, E., . . . Bendotti, C. (2009). Functional alterations of the ubiquitin-proteasome system in motor neurons of a mouse model of familial amyotrophic lateral sclerosis. *Hum Mol Genet, 18*(1), 82-96. doi:10.1093/hmg/ddn319

Cheroni, C., Peviani, M., Cascio, P., Debiasi, S., Monti, C., & Bendotti, C. (2005). Accumulation of human SOD1 and ubiquitinated deposits in the spinal cord of SOD1G93A mice during motor neuron disease progression correlates with a decrease of proteasome. *Neurobiol Dis, 18*(3), 509-522. doi:10.1016/j.nbd.2004.12.007

Chew, J., Gendron, T. F., Prudencio, M., Sasaguri, H., Zhang, Y.-J., Castanedes-Casey, M., . . . Petrucelli, L. (2015). C9ORF72 repeat expansions in mice cause TDP-43 pathology, neuronal loss, and behavioral deficits. *Science, 348*(6239), 1151. doi:10.1126/science.aaa9344

Chou, C. C., Zhang, Y., Umoh, M. E., Vaughan, S. W., Lorenzini, I., Liu, F., . . . Rossoll, W. (2018). TDP-43 pathology disrupts nuclear pore complexes and nucleocytoplasmic transport in ALS/FTD. *Nat Neurosci, 21*(2), 228-239. doi:10.1038/s41593-017-0047-3

Chu, Q., Rathore, A., Diedrich, J. K., Donaldson, C. J., Yates, J. R., 3rd, & Saghatelian, A. (2017). Identification of Microprotein-Protein Interactions via APEX Tagging. *Biochemistry, 56*(26), 3299-3306. doi:10.1021/acs.biochem.7b00265

Ciryam, P., Lambert-Smith, I. A., Bean, D. M., Freer, R., Cid, F., Tartaglia, G. G., . . . Yerbury, J. J. (2017). Spinal motor neuron protein supersaturation patterns are associated with inclusion body formation in ALS. *Proceedings of the National Academy of Sciences of the United States of America, 114*(20), E3935-E3943. doi:10.1073/pnas.1613854114

Cohen, T. J., Hwang, A. W., Restrepo, C. R., Yuan, C. X., Trojanowski, J. Q., & Lee, V. M. (2015). An acetylation switch controls TDP-43 function and aggregation propensity. *Nat Commun, 6*, 5845. doi:10.1038/ncomms6845

Collins, M. A., An, J., Hood, B. L., Conrads, T. P., & Bowser, R. P. (2015). Label-Free LC-MS/MS Proteomic Analysis of Cerebrospinal Fluid Identifies Protein/Pathway Alterations and Candidate Biomarkers for Amyotrophic Lateral Sclerosis. *J Proteome Res, 14*(11), 4486-4501. doi:10.1021/acs.jproteome.5b00804

Conraux, L., Pech, C., Guerraoui, H., Loyaux, D., Ferrara, P., Guillemot, J. C., . . . Lacomblez, L. (2013). Plasma peptide biomarker discovery for amyotrophic lateral sclerosis by MALDI-TOF mass spectrometry profiling. *PLoS One, 8*(11), e79733. doi:10.1371/journal.pone.0079733

Conti, A., Riva, N., Pesca, M., Iannaccone, S., Cannistraci, C. V., Corbo, M., . . . Alessio, M. (2014). Increased expression of Myosin binding protein H in the skeletal muscle of amyotrophic lateral sclerosis patients. *Biochim Biophys Acta, 1842*(1), 99-106. doi:10.1016/j.bbadis.2013.10.013

Craig, R., & Beavis, R. C. (2004). TANDEM: matching proteins with tandem mass spectra. *Bioinformatics, 20*(9), 1466-1467. doi:10.1093/bioinformatics/bth092

Cronan, J. E., Jr. (1990). Biotination of proteins in vivo. A post-translational modification to label, purify, and study proteins. *J Biol Chem, 265*(18), 10327-10333.

Cykowski, M. D., Powell, S. Z., Appel, J. W., Arumanayagam, A. S., Rivera, A. L., & Appel, S. H. (2018). Phosphorylated TDP-43 (pTDP-43) aggregates in the axial skeletal muscle of patients with sporadic and familial amyotrophic lateral sclerosis. *Acta Neuropathologica Communications, 6*(1), 28. doi:10.1186/s40478-018-0528-y

Dammer, E. B., Fallini, C., Gozal, Y. M., Duong, D. M., Rossoll, W., Xu, P., . . . Bassell, G. J. (2012). Coaggregation of RNA-binding proteins in a model of TDP-43 proteinopathy with selective RGG motif methylation and a role for RRM1 ubiquitination. *PLoS One, 7*(6), e38658.

David, D. C., Hauptmann, S., Scherping, I., Schuessel, K., Keil, U., Rizzu, P., . . . Gotz, J. (2005). Proteomic and functional analyses reveal a mitochondrial dysfunction in P301L tau transgenic mice. *J Biol Chem, 280*(25), 23802-23814. doi:10.1074/jbc.M500356200

Davidsson, P., Sjogren, M., Andreasen, N., Lindbjer, M., Nilsson, C. L., Westman-Brinkmalm, A., & Blennow, K. (2002). Studies of the pathophysiological mechanisms in frontotemporal dementia by proteome analysis of CSF proteins. *Brain Res Mol Brain Res, 109*(1-2), 128-133.

Davis, S. A., Itaman, S., Khalid-Janney, C. M., Sherard, J. A., Dowell, J. A., Cairns, N. J., & Gitcho, M. A. (2018). TDP-43 interacts with mitochondrial proteins critical for mitophagy and mitochondrial dynamics. *Neurosci Lett, 678*, 8-15. doi:10.1016/j.neulet.2018.04.053

De Benedetti, S., Gianazza, E., Banfi, C., Marocchi, A., Lunetta, C., Penco, S., . . . Iametti, S. (2017). Serum Proteome in a Sporadic Amyotrophic Lateral Sclerosis Geographical Cluster. *Proteomics Clin Appl, 11*(11-12). doi:10.1002/prca.201700043

Dephoure, N., Gould, K. L., Gygi, S. P., Kellogg, D. R., & Drubin, D. G. (2013). Mapping and analysis of phosphorylation sites: a quick guide for cell biologists. *Mol Biol Cell, 24*(5), 535-542. doi:10.1091/mbc.e12-09-0677

Duplan, L., Bernard, N., Casseron, W., Dudley, K., Thouvenot, E., Honnorat, J., . . . Pettmann, B. (2010). Collapsin response mediator protein 4a (CRMP4a) is upregulated in motoneurons of mutant SOD1 mice and can trigger motoneuron axonal degeneration and cell death. *J Neurosci, 30*(2), 785-796. doi:10.1523/jneurosci.5411-09.2010

Ekegren, T., Hanrieder, J., Aquilonius, S. M., & Bergquist, J. (2006). Focused proteomics in post-mortem human spinal cord. *J Proteome Res, 5*(9), 2364-2371. doi:10.1021/pr060237f

Elf, K., Shevchenko, G., Nygren, I., Larsson, L., Bergquist, J., Askmark, H., & Artemenko, K. (2014). Alterations in muscle proteome of patients diagnosed with amyotrophic lateral sclerosis. *J Proteomics, 108*, 55-64. doi:10.1016/j.jprot.2014.05.004

Eng, J. K., McCormack, A. L., & Yates, J. R. (1994). An approach to correlate tandem mass spectral data of peptides with amino acid sequences in a protein database. *J Am Soc Mass Spectrom, 5*(11), 976-989. doi:10.1016/1044-0305(94)80016-2

Engelen-Lee, J., Blokhuis, A. M., Spliet, W. G. M., Pasterkamp, R. J., Aronica, E., Demmers, J. A. A., . . . Van Den Berg, L. H. (2017). Proteomic profiling of the spinal cord in ALS: decreased ATP5D levels suggest synaptic dysfunction in ALS pathogenesis. *Amyotroph Lateral Scler Frontotemporal Degener, 18*(3-4), 210-220. doi:10.1080/21678421.2016.1245757

Farg, M. A., Sundaramoorthy, V., Sultana, J. M., Yang, S., Atkinson, R. A. K., Levina, V., . . . Atkin, J. D. (2014). C9ORF72, implicated in amytrophic lateral sclerosis and frontotemporal dementia, regulates endosomal trafficking. *Human Molecular Genetics, 23*(13), 3579-3595. doi:10.1093/hmg/ddu068

Farrawell, N. E., Yerbury, M. R., Plotkin, S. S., McAlary, L., & Yerbury, J. J. (2018). CuATSM protects against the in vitro cytotoxicity of wild type-like SOD1 mutants but not mutants that disrupt metal binding. *ACS Chem Neurosci*. doi:10.1021/acschemneuro.8b00527

Feneberg, E., Steinacker, P., Lehnert, S., Schneider, A., Walther, P., Thal, D. R., . . . Otto, M. (2014). Limited role of free TDP-43 as a diagnostic tool in neurodegenerative diseases. *Amyotroph Lateral Scler Frontotemporal Degener, 15*(5-6), 351-356. doi:10.3109/21678421.2014.905606

Ferrer, I., Barrachina, M., & Puig, B. (2002). Anti-tau phospho-specific Ser262 antibody recognizes a variety of abnormal hyper-phosphorylated tau deposits in tauopathies including Pick bodies and argyrophilic grains. *Acta Neuropathol, 104*(6), 658-664. doi:10.1007/s00401-002-0600-2

Field, L. S., Furukawa, Y., O'Halloran, T. V., & Culotta, V. C. (2003). Factors controlling the uptake of yeast copper/zinc superoxide dismutase into mitochondria. *J Biol Chem, 278*(30), 28052-28059. doi:10.1074/jbc.M304296200

Foster, L. A., & Salajegheh, M. K. (2019). Motor Neuron Disease: Pathophysiology, Diagnosis, and Management. *The American Journal of Medicine, 132*(1), 32-37. doi:https://doi.org/10.1016/j.amjmed.2018.07.012

Freibaum, B. D., Chitta, R. K., High, A. A., & Taylor, J. P. (2010). Global analysis of TDP-43 interacting proteins reveals strong association with RNA splicing and translation machinery. *J Proteome Res, 9*(2), 1104-1120. doi:10.1021/pr901076y

Frost, B., Gotz, J., & Feany, M. B. (2015). Connecting the dots between tau dysfunction and neurodegeneration. *Trends Cell Biol, 25*(1), 46-53. doi:10.1016/j.tcb.2014.07.005

Fukada, K., Zhang, F., Vien, A., Cashman, N. R., & Zhu, H. (2004). Mitochondrial proteomic analysis of a cell line model of familial amyotrophic lateral sclerosis. *Molecular & cellular proteomics : MCP, 3*(12), 1211-1223. doi:10.1074/mcp.M400094-MCP200

Fulzele, A., & Bennett, E. J. (2018). Ubiquitin diGLY Proteomics as an Approach to Identify and Quantify the Ubiquitin-Modified Proteome. *Methods Mol Biol, 1844*, 363-384. doi:10.1007/978-1-4939-8706-1_23

Gauthier-Kemper, A., Weissmann, C., Golovyashkina, N., Sebo-Lemke, Z., Drewes, G., Gerke, V., . . . Brandt, R. (2011). The frontotemporal dementia mutation R406W blocks tau's interaction with the membrane in an annexin A2-dependent manner. *J Cell Biol, 192*(4), 647-661. doi:10.1083/jcb.201007161

Gershoni-Emek, N., Mazza, A., Chein, M., Gradus-Pery, T., Xiang, X., Li, K. W., . . . Perlson, E. (2016). Proteomic Analysis of Dynein-Interacting Proteins in Amyotrophic Lateral Sclerosis Synaptosomes Reveals Alterations in the RNA-Binding Protein Staufen1. *Mol Cell Proteomics, 15*(2), 506-522. doi:10.1074/mcp.M115.049965

Gillet, L. C., Navarro, P., Tate, S., Rost, H., Selevsek, N., Reiter, L., . . . Aebersold, R. (2012). Targeted data extraction of the MS/MS spectra generated by data-independent acquisition: a new concept for consistent and accurate proteome analysis. *Mol Cell Proteomics, 11*(6), O111 016717. doi:10.1074/mcp.O111.016717

Gozal, Y. M., Dammer, E. B., Duong, D. M., Cheng, D., Gearing, M., Rees, H. D., . . . Levey, A. I. (2011a). Proteomic analysis of hippocampal dentate granule cells in frontotemporal lobar degeneration: application of laser capture technology. *Frontiers in neurology, 2*, 24-24. doi:10.3389/fneur.2011.00024

Gozal, Y. M., Seyfried, N. T., Gearing, M., Glass, J. D., Heilman, C. J., Wuu, J., . . . Lah, J. J. (2011b). Aberrant septin 11 is associated with sporadic frontotemporal lobar degeneration. *Mol Neurodegener, 6*, 82-82. doi:10.1186/1750-1326-6-82

Green, N. M. (1990). Avidin and streptavidin. *Methods Enzymol, 184*, 51-67.

Gregersen, N., & Bross, P. (2010). Protein misfolding and cellular stress: an overview. *Methods Mol Biol, 648*, 3-23. doi:10.1007/978-1-60761-756-3_1

Guldbrandsen, A., Vethe, H., Farag, Y., Oveland, E., Garberg, H., Berle, M., . . . Berven, F. S. (2014). In-depth characterization of the cerebrospinal fluid proteome displayed through the CSF Proteome Resource (CSF-PR). *Molecular & Cellular Proteomics*, mcp.M114.038554. doi:10.1074/mcp.M114.038554

Gunawardana, C. G., Mehrabian, M., Wang, X., Mueller, I., Lubambo, I. B., Jonkman, J. E. N., . . . Schmitt-Ulms, G. (2015). The Human Tau Interactome: Binding to the Ribonucleoproteome, and Impaired Binding of the Proline-to-Leucine Mutant at Position 301 (P301L) to Chaperones and the Proteasome. *Molecular & cellular proteomics : MCP, 14*(11), 3000-3014. doi:10.1074/mcp.M115.050724

Haines, D. S., Lee, J. E., Beauparlant, S. L., Kyle, D. B., den Besten, W., Sweredoski, M. J., . . . Deshaies, R. J. (2012). Protein interaction profiling of the p97 adaptor UBXD1 points to a role for the complex in modulating ERGIC-53 trafficking. *Mol Cell Proteomics, 11*(6), M111.016444. doi:10.1074/mcp.M111.016444

Han, Y., Martell, J., Branon, T., Boassa, D., Shechner, D., Ellisman, M., & Ting, A. (2018). Directed evolution of split APEX peroxidase. *bioRxiv, 452888*, in press. doi:10.1101/452888

Hans, F., Eckert, M., von Zweydorf, F., Gloeckner, C. J., & Kahle, P. J. (2018). Identification and characterization of ubiquitinylation sites in TAR DNA-binding protein of 43 kDa (TDP-43). *J Biol Chem, 293*(41), 16083-16099. doi:10.1074/jbc.RA118.003440

Hartmann, H., Hornburg, D., Czuppa, M., Bader, J., Michaelsen, M., Farny, D., . . . Edbauer, D. (2018). Proteomics and C9orf72 neuropathology identify ribosomes as poly-GR/PR interactors driving toxicity. *Life Sci Alliance, 1*(2), e201800070. doi:10.26508/lsa.201800070

Hasegawa, M., Arai, T., Nonaka, T., Kametani, F., Yoshida, M., Hashizume, Y., . . . Akiyama, H. (2008a). Phosphorylated TDP-43 in frontotemporal lobar degeneration and amyotrophic lateral sclerosis. *Ann Neurol, 64*(1), 60-70. doi:10.1002/ana.21425

Hasegawa, M., Arai, T., Nonaka, T., Kametani, F., Yoshida, M., Hashizume, Y., . . . Akiyama, H. (2008b). Phosphorylated TDP-43 in frontotemporal lobar degeneration and amyotrophic lateral sclerosis. *Annals of neurology, 64*(1), 60-70. doi:10.1002/ana.21425

Hipp, M. S., Park, S.-H., & Hartl, F. U. (2014). Proteostasis impairment in protein-misfolding and-aggregation diseases. *Trends in cell biology, 24*(9), 506-514.

Hogan, A. L., Don, E. K., Rayner, S. L., Lee, A., Laird, A. S., Watchon, M., . . . Cole, N. J. (2017). Expression of ALS/FTD-linked mutant CCNF in zebrafish leads to increased cell death in the spinal cord and an aberrant motor phenotype. *Hum Mol Genet, 26*(14), 2616-2626. doi:10.1093/hmg/ddx136

Hosp, F., Vossfeldt, H., Heinig, M., Vasiljevic, D., Arumughan, A., Wyler, E., . . . Selbach, M. (2015). Quantitative interaction proteomics of neurodegenerative disease proteins. *Cell Rep, 11*(7), 1134-1146. doi:10.1016/j.celrep.2015.04.030

Huang, Y. H., Shih, C. M., Huang, C. J., Lin, C. M., Chou, C. M., Tsai, M. L., . . . Chen, C. T. (2006). Effects of cadmium on structure and enzymatic activity of Cu,Zn-SOD and oxidative status in neural cells. *J Cell Biochem, 98*(3), 577-589. doi:10.1002/jcb.20772

Iridoy, O. M., Zubiri, I., Zelaya, V. M., Martinez, L., Ausin, K., Lachen-Montes, M., . . . Jericó, I. (2018). Neuroanatomical Quantitative Proteomics Reveals Common Pathogenic Biological Routes between Amyotrophic Lateral Sclerosis (ALS) and Frontotemporal Dementia (FTD). *International Journal of Molecular Sciences, 20*(1). doi:10.3390/ijms20010004

Kadavath, H., Hofele, R. V., Biernat, J., Kumar, S., Tepper, K., Urlaub, H., . . . Zweckstetter, M. (2015). Tau stabilizes microtubules by binding at the interface between tubulin heterodimers. *Proc Natl Acad Sci U S A, 112*(24), 7501-7506. doi:10.1073/pnas.1504081112

Kamelgarn, M., Chen, J., Kuang, L., Arenas, A., Zhai, J., Zhu, H., & Gal, J. (2016). Proteomic analysis of FUS interacting proteins provides insights into FUS function and its role in ALS. *Biochim Biophys Acta, 1862*(10), 2004-2014. doi:10.1016/j.bbadis.2016.07.015

Kametani, F., Obi, T., Shishido, T., Akatsu, H., Murayama, S., Saito, Y., . . . Hasegawa, M. (2016). Mass spectrometric analysis of accumulated TDP-43 in amyotrophic lateral sclerosis brains. *Scientific Reports, 6*, 23281. doi:10.1038/srep23281

Kanekura, K., Yagi, T., Cammack, A. J., Mahadevan, J., Kuroda, M., Harms, M. B., . . . Urano, F. (2016). Poly-dipeptides encoded by the C9ORF72 repeats block global protein translation. *Human Molecular Genetics, 25*(9), 1803-1813. doi:10.1093/hmg/ddw052

Kato, S., Horiuchi, S., Liu, J., Cleveland, D. W., Shibata, N., Nakashima, K., . . . Ohama, E. (2000). Advanced glycation endproduct-modified superoxide dismutase-1 (SOD1)-positive inclusions are common to familial amyotrophic lateral sclerosis patients with SOD1 gene mutations and transgenic mice expressing human SOD1 with a G85R mutation. *Acta Neuropathol, 100*(5), 490-505. doi:10.1007/s004010000226

Kikuchi, K., Arawaka, S., Koyama, S., Kimura, H., Ren, C. H., Wada, M., . . . Kato, T. (2003). An N-terminal fragment of ProSAAS (a granin-like neuroendocrine peptide precursor) is associated with tau inclusions in Pick's disease. *Biochem Biophys Res Commun, 305*(3), 646-654.

Kim, D. I., Jensen, S. C., Noble, K. A., Kc, B., Roux, K. H., Motamedchaboki, K., & Roux, K. J. (2016). An improved smaller biotin ligase for BioID proximity labeling. *Mol Biol Cell, 27*(8), 1188-1196. doi:10.1091/mbc.E15-12-0844

Kim, D. K., Park, J., Han, D., Yang, J., Kim, A., Woo, J., . . . Mook-Jung, I. (2018). Molecular and functional signatures in a novel Alzheimer's disease mouse model assessed by quantitative proteomics. *Mol Neurodegener, 13*(1), 2. doi:10.1186/s13024-017-0234-4

Kim, J. E., Hong, Y. H., Kim, J. Y., Jeon, G. S., Jung, J. H., Yoon, B. N., . . . Sung, J. J. (2017). Altered nucleocytoplasmic proteome and transcriptome distributions in an in vitro model of amyotrophic lateral sclerosis. *PLoS One, 12*(4), e0176462. doi:10.1371/journal.pone.0176462

Kim, W., Bennett, E. J., Huttlin, E. L., Guo, A., Li, J., Possemato, A., . . . Gygi, S. P. (2011). Systematic and quantitative assessment of the ubiquitin-modified proteome. *Mol Cell, 44*(2), 325-340. doi:10.1016/j.molcel.2011.08.025

Kincaid, M. M., & Cooper, A. A. (2007). Misfolded proteins traffic from the endoplasmic reticulum (ER) due to ER export signals. *Mol Biol Cell, 18*(2), 455-463. doi:10.1091/mbc.e06-08-0696

Kiraly, M., Dalmadine Kiss, B., Vekey, K., Antal, I., & Ludanyi, K. (2016). [Mass spectrometry: past and present]. *Acta Pharm Hung, 86*(1), 3-11.

Klein, Z. A., Takahashi, H., Ma, M., Stagi, M., Zhou, M., Lam, T. T., & Strittmatter, S. M. (2017). Loss of TMEM106B Ameliorates Lysosomal and Frontotemporal Dementia-

Related Phenotypes in Progranulin-Deficient Mice. *Neuron, 95*(2), 281-296.e286. doi:10.1016/j.neuron.2017.06.026

Krach, F., Batra, R., Wheeler, E. C., Vu, A. Q., Wang, R., Hutt, K., . . . Ravits, J. (2018). Transcriptome-pathology correlation identifies interplay between TDP-43 and the expression of its kinase CK1E in sporadic ALS. *Acta Neuropathol, 136*(3), 405-423. doi:10.1007/s00401-018-1870-7

Kurzban, G. P., Bayer, E. A., Wilchek, M., & Horowitz, P. M. (1991). The quaternary structure of streptavidin in urea. *J Biol Chem, 266*(22), 14470-14477.

Kwon, K., Streaker, E. D., Ruparelia, S., & Beckett, D. (2000). Multiple disordered loops function in corepressor-induced dimerization of the biotin repressor. *J Mol Biol, 304*(5), 821-833. doi:10.1006/jmbi.2000.4249

Laferriere, F., Maniecka, Z., Perez-Berlanga, M., Hruska-Plochan, M., Gilhespy, L., Hock, E. M., . . . Polymenidou, M. (2019). TDP-43 extracted from frontotemporal lobar degeneration subject brains displays distinct aggregate assemblies and neurotoxic effects reflecting disease progression rates. *Nat Neurosci, 22*(1), 65-77. doi:10.1038/s41593-018-0294-y

Lam, S. S., Martell, J. D., Kamer, K. J., Deerinck, T. J., Ellisman, M. H., Mootha, V. K., & Ting, A. Y. (2015). Directed evolution of APEX2 for electron microscopy and proximity labeling. *Nat Methods, 12*(1), 51-54. doi:10.1038/nmeth.3179

Lasagna-Reeves, C. A., Castillo-Carranza, D. L., Sengupta, U., Sarmiento, J., Troncoso, J., Jackson, G. R., & Kayed, R. (2012). Identification of oligomers at early stages of tau aggregation in Alzheimer's disease. *Faseb j, 26*(5), 1946-1959. doi:10.1096/fj.11-199851

Lee, A., Rayner, S. L., Gwee, S. S. L., De Luca, A., Shahheydari, H., Sundaramoorthy, V., . . . Chung, R. S. (2018a). Pathogenic mutation in the ALS/FTD gene, CCNF, causes elevated Lys48-linked ubiquitylation and defective autophagy. *Cell Mol Life Sci, 75*(2), 335-354. doi:10.1007/s00018-017-2632-8

Lee, A., Rayner Stephanie, L., De Luca, A., Gwee Serene, S. L., Morsch, M., Sundaramoorthy, V., . . . Chung Roger, S. (2017a). Casein kinase II phosphorylation of cyclin F at serine 621 regulates the Lys48-ubiquitylation E3 ligase activity of the SCF(cyclin F) complex. *Open Biology, 7*(10), 170058. doi:10.1098/rsob.170058

Lee, C. W., Stankowski, J. N., Chew, J., Cook, C. N., Lam, Y. W., Almeida, S., . . . Petrucelli, L. (2017b). The lysosomal protein cathepsin L is a progranulin protease. *Mol Neurodegener, 12*(1), 55. doi:10.1186/s13024-017-0196-6

Lee, K. H., Zhang, P., Kim, H. J., Mitrea, D. M., Sarkar, M., Freibaum, B. D., . . . Taylor, J. P. (2016). C9orf72 Dipeptide Repeats Impair the Assembly, Dynamics, and Function of Membrane-Less Organelles. *Cell, 167*(3), 774-788.e717. doi:10.1016/j.cell.2016.10.002

Lee, Y. C., Huang, W. C., Lin, J. H., Kao, T. J., Lin, H. C., Lee, K. H., . . . Huang, C. C. (2018b). Znf179 E3 ligase-mediated TDP-43 polyubiquitination is involved in TDP-43- ubiquitinated inclusions (UBI) (+)-related neurodegenerative pathology. *J Biomed Sci, 25*(1), 76. doi:10.1186/s12929-018-0479-4

Li, H.-R., Chiang, W.-C., Chou, P.-C., Wang, W.-J., & Huang, J.-r. (2018). TAR DNA-binding protein 43 (TDP-43) liquid-liquid phase separation is mediated by just a few aromatic residues. *Journal of Biological Chemistry*. doi:10.1074/jbc.AC117.001037

Li, Q., Vande Velde, C., Israelson, A., Xie, J., Bailey, A. O., Dong, M. Q., . . . Miller, T. M. (2010). ALS-linked mutant superoxide dismutase 1 (SOD1) alters mitochondrial protein composition and decreases protein import. *Proc Natl Acad Sci U S A, 107*(49), 21146-21151. doi:10.1073/pnas.1014862107

Li, Y., Collins, M., An, J., Geiser, R., Tegeler, T., Tsantilas, K., . . . Bowser, R. (2016). Immunoprecipitation and mass spectrometry defines an extensive RBM45 protein-protein interaction network. *Brain Res, 1647*, 79-93. doi:10.1016/j.brainres.2016.02.047

Li, Y., Evers, J., Luo, A., Erber, L., Postler, Z., & Chen, Y. (2019). A Quantitative Chemical Proteomics Approach for Site-specific Stoichiometry Analysis of Ubiquitination. *Angew Chem Int Ed Engl, 58*(2), 537-541. doi:10.1002/anie.201810569

Liebl, M. P., Kaya, A. M., Tenzer, S., Mittenzwei, R., Koziollek-Drechsler, I., Schild, H., . . . Clement, A. M. (2014). Dimerization of visinin-like protein 1 is regulated by oxidative stress and calcium and is a pathological hallmark of amyotrophic lateral sclerosis. *Free Radic Biol Med, 72*, 41-54. doi:10.1016/j.freeradbiomed.2014.04.008

Lin, P. Y., Simon, S. M., Koh, W. K., Folorunso, O., Umbaugh, C. S., & Pierce, A. (2013). Heat shock factor 1 over-expression protects against exposure of hydrophobic residues on mutant SOD1 and early mortality in a mouse model of amyotrophic lateral sclerosis. *Mol Neurodegener, 8*, 43. doi:10.1186/1750-1326-8-43

Lindemann, C., Thomanek, N., Hundt, F., Lerari, T., Meyer, H. E., Wolters, D., & Marcus, K. (2017). Strategies in relative and absolute quantitative mass spectrometry based proteomics. *Biol Chem, 398*(5-6), 687-699. doi:10.1515/hsz-2017-0104

Ling, S. C., Albuquerque, C. P., Han, J. S., Lagier-Tourenne, C., Tokunaga, S., Zhou, H., & Cleveland, D. W. (2010). ALS-associated mutations in TDP-43 increase its stability and promote TDP-43 complexes with FUS/TLS. *Proc Natl Acad Sci U S A, 107*(30), 13318-13323. doi:10.1073/pnas.1008227107

Ling, S. C., Polymenidou, M., & Cleveland, D. W. (2013). Converging mechanisms in ALS and FTD: disrupted RNA and protein homeostasis. *Neuron, 79*(3), 416-438. doi:10.1016/j.neuron.2013.07.033

Liu, C., Song, X., Nisbet, R., & Gotz, J. (2016). Co-immunoprecipitation with Tau Isoform-specific Antibodies Reveals Distinct Protein Interactions and Highlights a Putative Role for 2N Tau in Disease. *J Biol Chem, 291*(15), 8173-8188. doi:10.1074/jbc.M115.641902

Liu, D., Liu, C., Li, J., Azadzoi, K., Yang, Y., Fei, Z., . . . Yang, J.-H. (2013). Proteomic Analysis Reveals Differentially Regulated Protein Acetylation in Human Amyotrophic Lateral Sclerosis Spinal Cord. *PLoS One, 8*(12), e80779. doi:10.1371/journal.pone.0080779

Liu, J., Akhavan, A., Lu, M., Gruzman, A., Lingappa, V. R., An, J., & Bowser, R. (2010). Carbonic anhydrase I is recognized by an SOD1 antibody upon biotinylation of human spinal cord extracts. *Int J Mol Sci, 11*(10), 4051-4062. doi:10.3390/ijms11104051

Liu, Y., Mi, Y., Mueller, T., Kreibich, S., Williams, E. G., Van Drogen, A., . . . Aebersold, R. (2019). Multi-omic measurements of heterogeneity in HeLa cells across laboratories. *Nature Biotechnology, 37*(3), 314-322. doi:10.1038/s41587-019-0037-y

Ludwig, C., Gillet, L., Rosenberger, G., Amon, S., Collins, B. C., & Aebersold, R. (2018). Data-independent acquisition-based SWATH-MS for quantitative proteomics: a tutorial. *Mol Syst Biol, 14*(8), e8126. doi:10.15252/msb.20178126

Macron, C., Lane, L., Nunez Galindo, A., & Dayon, L. (2018). Deep Dive on the Proteome of Human Cerebrospinal Fluid: A Valuable Data Resource for Biomarker Discovery and Missing Protein Identification. *J Proteome Res*. doi:10.1021/acs.jproteome.8b00300

Maharana, S., Wang, J., Papadopoulos, D. K., Richter, D., Pozniakovsky, A., Poser, I., . . . Alberti, S. (2018). RNA buffers the phase separation behavior of prion-like RNA binding proteins. *Science, 360*(6391), 918. doi:10.1126/science.aar7366

Mallik, M., Catinozzi, M., Hug, C. B., Zhang, L., Wagner, M., Bussmann, J., . . . Storkebaum, E. (2018). Xrp1 genetically interacts with the ALS-associated FUS orthologue caz and mediates its toxicity. *J Cell Biol, 217*(11), 3947-3964. doi:10.1083/jcb.201802151

Markham, K., Bai, Y., & Schmitt-Ulms, G. (2007). Co-immunoprecipitations revisited: an update on experimental concepts and their implementation for sensitive interactome investigations of endogenous proteins. *Anal Bioanal Chem, 389*(2), 461-473. doi:10.1007/s00216-007-1385-x

Markmiller, S., Soltanieh, S., Server, K. L., Mak, R., Jin, W., Fang, M. Y., . . . Yeo, G. W. (2018). Context-Dependent and Disease-Specific Diversity in Protein Interactions within Stress Granules. *Cell, 172*(3), 590-604.e513. doi:10.1016/j.cell.2017.12.032

Martell, J. D., Deerinck, T. J., Sancak, Y., Poulos, T. L., Mootha, V. K., Sosinsky, G. E., . . . Ting, A. Y. (2012). Engineered ascorbate peroxidase as a genetically encoded reporter for electron microscopy. *Nat Biotechnol, 30*(11), 1143-1148. doi:10.1038/nbt.2375

Martens, L., & Vizcaino, J. A. (2017). A Golden Age for Working with Public Proteomics Data. *Trends Biochem Sci, 42*(5), 333-341. doi:10.1016/j.tibs.2017.01.001

Martins, D., & English, A. M. (2014). SOD1 oxidation and formation of soluble aggregates in yeast: relevance to sporadic ALS development. *Redox Biol, 2*, 632-639. doi:10.1016/j.redox.2014.03.005

Massignan, T., Casoni, F., Basso, M., Stefanazzi, P., Biasini, E., Tortarolo, M., . . . Bonetto, V. (2007). Proteomic analysis of spinal cord of presymptomatic amyotrophic lateral sclerosis G93A SOD1 mouse. *Biochem Biophys Res Commun, 353*(3), 719-725. doi:10.1016/j.bbrc.2006.12.075

May, S., Hornburg, D., Schludi, M. H., Arzberger, T., Rentzsch, K., Schwenk, B. M., . . . Edbauer, D. (2014). C9orf72 FTLD/ALS-associated Gly-Ala dipeptide repeat proteins cause neuronal toxicity and Unc119 sequestration. *Acta Neuropathol, 128*(4), 485-503. doi:10.1007/s00401-014-1329-4

Maziuk, B. F., Apicco, D. J., Cruz, A. L., Jiang, L., Ash, P. E. A., da Rocha, E. L., . . . Wolozin, B. (2018). RNA binding proteins co-localize with small tau inclusions in tauopathy. *Acta Neuropathologica Communications, 6*(1), 71-71. doi:10.1186/s40478-018-0574-5

McAlary, L., Aquilina, J. A., & Yerbury, J. J. (2016). Susceptibility of Mutant SOD1 to Form a Destabilized Monomer Predicts Cellular Aggregation and Toxicity but Not In vitro Aggregation Propensity. *Front Neurosci, 10*, 499. doi:10.3389/fnins.2016.00499

Megger, D. A., Pott, L. L., Ahrens, M., Padden, J., Bracht, T., Kuhlmann, K., . . . Sitek, B. (2014). Comparison of label-free and label-based strategies for proteome analysis of hepatoma cell lines. *Biochim Biophys Acta, 1844*(5), 967-976. doi:10.1016/j.bbapap.2013.07.017

Miller, S. E., Rizzo, A. I., & Waldbauer, J. R. (2018). Postnovo: Postprocessing Enables Accurate and FDR-Controlled de Novo Peptide Sequencing. *J Proteome Res, 17*(11), 3671-3680. doi:10.1021/acs.jproteome.8b00278

Min, S.-W., Cho, S.-H., Zhou, Y., Schroeder, S., Haroutunian, V., Seeley, W. W., . . . Gan, L. (2010). Acetylation of tau inhibits its degradation and contributes to tauopathy. *Neuron, 67*(6), 953-966. doi:10.1016/j.neuron.2010.08.044

Minguez, P., Parca, L., Diella, F., Mende, D. R., Kumar, R., Helmer-Citterich, M., . . . Bork, P. (2012). Deciphering a global network of functionally associated post-translational modifications. *Mol Syst Biol, 8*, 599. doi:10.1038/msb.2012.31

Mitsui, K., Doi, H., & Nukina, N. (2006). Proteomics of polyglutamine aggregates. In *Methods in Enzymology* (Vol. 412, pp. 63-76): Academic Press.

Mitsui, K., Nakayama, H., Akagi, T., Nekooki, M., Ohtawa, K., Takio, K., . . . Nukina, N. (2002). Purification of Polyglutamine Aggregates and Identification of Elongation Factor-1α and Heat Shock Protein 84 as Aggregate-Interacting Proteins. *The Journal of Neuroscience, 22*(21), 9267-9277. doi:10.1523/jneurosci.22-21-09267.2002

Moens, T. G., Niccoli, T., Wilson, K. M., Atilano, M. L., Birsa, N., Gittings, L. M., . . . Isaacs, A. M. (2019). C9orf72 arginine-rich dipeptide proteins interact with ribosomal proteins in vivo to induce a toxic translational arrest that is rescued by eIF1A. *Acta Neuropathol*. doi:10.1007/s00401-018-1946-4

Monahan, Z., Ryan, V. H., Janke, A. M., Burke, K. A., Rhoads, S. N., Zerze, G. H., . . . Fawzi, N. L. (2017). Phosphorylation of the FUS low-complexity domain disrupts phase separation, aggregation, and toxicity. *Embo j, 36*(20), 2951-2967. doi:10.15252/embj.201696394

Morimoto, R. I. (2008). Proteotoxic stress and inducible chaperone networks in neurodegenerative disease and aging. *Genes & development, 22*(11), 1427-1438.

Muntane, G., Dalfo, E., Martinez, A., Rey, M. J., Avila, J., Perez, M., . . . Ferrer, I. (2006). Glial fibrillary acidic protein is a major target of glycoxidative and lipoxidative damage in Pick's disease. *J Neurochem, 99*(1), 177-185. doi:10.1111/j.1471-4159.2006.04032.x

Muth, T., & Renard, B. Y. (2018). Evaluating de novo sequencing in proteomics: already an accurate alternative to database-driven peptide identification? *Brief Bioinform, 19*(5), 954-970. doi:10.1093/bib/bbx033

Nadler, W. M., Waidelich, D., Kerner, A., Hanke, S., Berg, R., Trumpp, A., & Rosli, C. (2017a). MALDI versus ESI: The Impact of the Ion Source on Peptide Identification. *J Proteome Res, 16*(3), 1207-1215. doi:10.1021/acs.jproteome.6b00805

Nadler, W. M., Waidelich, D., Kerner, A., Hanke, S., Berg, R., Trumpp, A., & Rösli, C. (2017b). MALDI versus ESI: The Impact of the Ion Source on Peptide Identification. *Journal of Proteome Research, 16*(3), 1207-1215. doi:10.1021/acs.jproteome.6b00805

Narayan, M., Seeley, K. W., & Jinwal, U. K. (2016). Identification of Apo B48 and other novel biomarkers in amyotrophic lateral sclerosis patient fibroblasts. *Biomark Med, 10*(5), 453-462. doi:10.2217/bmm-2016-0025

Nardo, G., Pozzi, S., Mantovani, S., Garbelli, S., Marinou, K., Basso, M., . . . Bonetto, V. (2009). Nitroproteomics of peripheral blood mononuclear cells from patients and a rat model of ALS. *Antioxid Redox Signal, 11*(7), 1559-1567. doi:10.1089/ars.2009.2548

Nardo, G., Pozzi, S., Pignataro, M., Lauranzano, E., Spano, G., Garbelli, S., . . . Bonetto, V. (2011). Amyotrophic lateral sclerosis multiprotein biomarkers in peripheral blood mononuclear cells. *PLoS One, 6*(10), e25545. doi:10.1371/journal.pone.0025545

Neilson, K. A., Ali, N. A., Muralidharan, S., Mirzaei, M., Mariani, M., Assadourian, G., . . . Haynes, P. A. (2011). Less label, more free: approaches in label-free quantitative mass spectrometry. *Proteomics, 11*(4), 535-553. doi:10.1002/pmic.201000553

Neumann, M., Kwong, L. K., Sampathu, D. M., Trojanowski, J. Q., & Lee, V. M.-Y. (2007). TDP-43 proteinopathy in frontotemporal lobar degeneration and amyotrophic lateral sclerosis: protein misfolding diseases without amyloidosis. *Archives of neurology, 64*(10), 1388-1394.

Neumann, M., Sampathu, D. M., Kwong, L. K., Truax, A. C., Micsenyi, M. C., Chou, T. T., . . . Clark, C. M. (2006). Ubiquitinated TDP-43 in frontotemporal lobar degeneration and amyotrophic lateral sclerosis. *science, 314*(5796), 130-133.

Nguyen, H. P., Van Broeckhoven, C., & van der Zee, J. (2018). ALS Genes in the Genomic Era and their Implications for FTD. *Trends Genet, 34*(6), 404-423. doi:10.1016/j.tig.2018.03.001

Olney, N. T., Spina, S., & Miller, B. L. (2017). Frontotemporal Dementia. *Neurologic clinics, 35*(2), 339-374. doi:10.1016/j.ncl.2017.01.008

Olsen, J. V., & Mann, M. (2013). Status of large-scale analysis of post-translational modifications by mass spectrometry. *Mol Cell Proteomics, 12*(12), 3444-3452. doi:10.1074/mcp.O113.034181

Ong, S. E., Blagoev, B., Kratchmarova, I., Kristensen, D. B., Steen, H., Pandey, A., & Mann, M. (2002). Stable isotope labeling by amino acids in cell culture, SILAC, as a simple and accurate approach to expression proteomics. *Mol Cell Proteomics, 1*(5), 376-386.

Palma, A. S., De Carvalho, M., Grammel, N., Pinto, S., Barata, N., Conradt, H. S., & Costa, J. (2008). Proteomic analysis of plasma from Portuguese patients with familial amyotrophic lateral sclerosis. *Amyotroph Lateral Scler, 9*(6), 339-349. doi:10.1080/17482960801934239

Pasinelli, P., & Brown, R. H. (2006). Molecular biology of amyotrophic lateral sclerosis: insights from genetics. *Nature Reviews Neuroscience, 7*, 710. doi:10.1038/nrn1971 https://www.nature.com/articles/nrn1971#supplementary-information

Patel, A., Lee, H. O., Jawerth, L., Maharana, S., Jahnel, M., Hein, M. Y., . . . Alberti, S. (2015). A Liquid-to-Solid Phase Transition of the ALS Protein FUS Accelerated by Disease Mutation. *Cell, 162*(5), 1066-1077. doi:10.1016/j.cell.2015.07.047

Paul, S., Dansithong, W., Figueroa, K. P., Scoles, D. R., & Pulst, S. M. (2018). Staufen1 links RNA stress granules and autophagy in a model of neurodegeneration. *Nature Communications, 9*(1), 3648. doi:10.1038/s41467-018-06041-3

Peggion, C., Massimino, M. L., Biancotto, G., Angeletti, R., Reggiani, C., Sorgato, M. C., . . . Stella, R. (2017). Absolute quantification of myosin heavy chain isoforms by selected reaction monitoring can underscore skeletal muscle changes in a mouse model of amyotrophic lateral sclerosis. *Anal Bioanal Chem, 409*(8), 2143-2153. doi:10.1007/s00216-016-0160-2

Peng, J., Schwartz, D., Elias, J. E., Thoreen, C. C., Cheng, D., Marsischky, G., . . . Gygi, S. P. (2003). A proteomics approach to understanding protein ubiquitination. *Nature Biotechnology, 21*, 921. doi:10.1038/nbt849

Perez, M., Santa-Maria, I., Gomez de Barreda, E., Zhu, X., Cuadros, R., Cabrero, J. R., . . . Avila, J. (2009). Tau--an inhibitor of deacetylase HDAC6 function. *J Neurochem, 109*(6), 1756-1766. doi:10.1111/j.1471-4159.2009.06102.x

Perkins, D. N., Pappin, D. J., Creasy, D. M., & Cottrell, J. S. (1999). Probability-based protein identification by searching sequence databases using mass spectrometry data. *Electrophoresis, 20*(18), 3551-3567. doi:10.1002/(SICI)1522-2683(19991201)20:18<3551::AID-ELPS3551>3.0.CO;2-2

Perluigi, M., Fai Poon, H., Hensley, K., Pierce, W. M., Klein, J. B., Calabrese, V., . . . Butterfield, D. A. (2005). Proteomic analysis of 4-hydroxy-2-nonenal-modified proteins in G93A-SOD1 transgenic mice-A model of familial amyotrophic lateral sclerosis. *Free Radical Biology and Medicine, 38*(7), 960-968. doi:https://doi.org/10.1016/j.freeradbiomed.2004.12.021

Phu, L., Izrael-Tomasevic, A., Matsumoto, M. L., Bustos, D., Dynek, J. N., Fedorova, A. V., . . . Kirkpatrick, D. S. (2011). Improved quantitative mass spectrometry methods for characterizing complex ubiquitin signals. *Mol Cell Proteomics, 10*(5), M110.003756. doi:10.1074/mcp.M110.003756

Piehowski, P. D., Petyuk, V. A., Orton, D. J., Xie, F., Moore, R. J., Ramirez-Restrepo, M., . . . Myers, A. J. (2013). Sources of technical variability in quantitative LC-MS proteomics: human brain tissue sample analysis. *Journal of Proteome Research, 12*(5), 2128-2137. doi:10.1021/pr301146m

Pokrishevsky, E., McAlary, L., Farrawell, N. E., Zhao, B., Sher, M., Yerbury, J. J., & Cashman, N. R. (2018). Tryptophan 32-mediated SOD1 aggregation is attenuated by pyrimidine-like compounds in living cells. *Scientific reports, 8*(1), 15590-15590. doi:10.1038/s41598-018-32835-y

Poon, H. F., Hensley, K., Thongboonkerd, V., Merchant, M. L., Lynn, B. C., Pierce, W. M., . . . Butterfield, D. A. (2005). Redox proteomics analysis of oxidatively modified proteins in G93A-SOD1 transgenic mice--a model of familial amyotrophic lateral sclerosis. *Free Radic Biol Med, 39*(4), 453-462. doi:10.1016/j.freeradbiomed.2005.03.030

Prabakaran, S., Lippens, G., Steen, H., & Gunawardena, J. (2012). Post-translational modification: nature's escape from genetic imprisonment and the basis for dynamic information encoding. *Wiley Interdiscip Rev Syst Biol Med, 4*(6), 565-583. doi:10.1002/wsbm.1185

Rademakers, R., Cruts, M., & van Broeckhoven, C. (2004). The role of tau (MAPT) in frontotemporal dementia and related tauopathies. *Hum Mutat, 24*(4), 277-295. doi:10.1002/humu.20086

Rhee, H. W., Zou, P., Udeshi, N. D., Martell, J. D., Mootha, V. K., Carr, S. A., & Ting, A. Y. (2013). Proteomic mapping of mitochondria in living cells via spatially restricted enzymatic tagging. *Science, 339*(6125), 1328-1331. doi:10.1126/science.1230593

Rhoads, S. N., Monahan, Z. T., Yee, D. S., Leung, A. Y., Newcombe, C. G., O'Meally, R. N., . . . Shewmaker, F. P. (2018). The prionlike domain of FUS is multiphosphorylated following DNA damage without altering nuclear localization. *Mol Biol Cell, 29*(15), 1786-1797. doi:10.1091/mbc.E17-12-0735

Rosen, D. R., Siddique, T., Patterson, D., Figlewicz, D. A., Sapp, P., Hentati, A., . . . et al. (1993). Mutations in Cu/Zn superoxide dismutase gene are associated with familial amyotrophic lateral sclerosis. *Nature, 362*(6415), 59-62. doi:10.1038/362059a0

Rotunno, M. S., Auclair, J. R., Maniatis, S., Shaffer, S. A., Agar, J., & Bosco, D. A. (2014). Identification of a misfolded region in superoxide dismutase 1 that is exposed in amyotrophic lateral sclerosis. *J Biol Chem, 289*(41), 28527-28538. doi:10.1074/jbc.M114.581801

Roux, K. J., Kim, D. I., & Burke, B. (2013). BioID: a screen for protein-protein interactions. *Curr Protoc Protein Sci, 74*, Unit 19.23. doi:10.1002/0471140864.ps1923s74

Roux, K. J., Kim, D. I., Raida, M., & Burke, B. (2012). A promiscuous biotin ligase fusion protein identifies proximal and interacting proteins in mammalian cells. *J Cell Biol, 196*(6), 801-810. doi:10.1083/jcb.201112098

Ruegsegger, C., Maharjan, N., Goswami, A., Filezac de L'Etang, A., Weis, J., Troost, D., . . . Saxena, S. (2016). Aberrant association of misfolded SOD1 with Na(+)/K(+)ATPase-alpha3 impairs its activity and contributes to motor neuron vulnerability in ALS. *Acta Neuropathol, 131*(3), 427-451. doi:10.1007/s00401-015-1510-4

Russell, C. L., Mitra, V., Hansson, K., Blennow, K., Gobom, J., Zetterberg, H., . . . Pike, I. (2017). Comprehensive Quantitative Profiling of Tau and Phosphorylated Tau Peptides in Cerebrospinal Fluid by Mass Spectrometry Provides New Biomarker Candidates. *J Alzheimers Dis, 55*(1), 303-313. doi:10.3233/JAD-160633

Saccon, R. A., Bunton-Stasyshyn, R. K., Fisher, E. M., & Fratta, P. (2013). Is SOD1 loss of function involved in amyotrophic lateral sclerosis? *Brain, 136*(Pt 8), 2342-2358. doi:10.1093/brain/awt097

Sacksteder, C. A., Qian, W.-J., Knyushko, T. V., Wang, H., Chin, M. H., Lacan, G., . . . Bigelow, D. J. (2006). Endogenously Nitrated Proteins in Mouse Brain: Links to Neurodegenerative Disease. *Biochemistry, 45*(26), 8009-8022. doi:10.1021/bi060474w

San Gil, R., Ooi, L., Yerbury, J. J., & Ecroyd, H. (2017). The heat shock response in neurons and astroglia and its role in neurodegenerative diseases. *Mol Neurodegener, 12*(1), 65. doi:10.1186/s13024-017-0208-6

Sano, T., Vajda, S., & Cantor, C. R. (1998). Genetic engineering of streptavidin, a versatile affinity tag. *J Chromatogr B Biomed Sci Appl, 715*(1), 85-91.

Schmidt, A., Forne, I., & Imhof, A. (2014). Bioinformatic analysis of proteomics data. *BMC Syst Biol, 8 Suppl 2*, S3. doi:10.1186/1752-0509-8-s2-s3

Schweitzer, K., Decker, E., Zhu, L., Miller, R. E., Mirra, S. S., Spina, S., . . . Murrell, J. (2006). Aberrantly regulated proteins in frontotemporal dementia. *Biochem Biophys Res Commun, 348*(2), 465-472. doi:10.1016/j.bbrc.2006.07.113

Scotter, E. L., Vance, C., Nishimura, A. L., Lee, Y. B., Chen, H. J., Urwin, H., . . . Shaw, C. E. (2014). Differential roles of the ubiquitin proteasome system and autophagy in the clearance of soluble and aggregated TDP-43 species. *J Cell Sci, 127*(Pt 6), 1263-1278. doi:10.1242/jcs.140087

Sea, K., Sohn, S. H., Durazo, A., Sheng, Y., Shaw, B. F., Cao, X., . . . Valentine, J. S. (2015). Insights into the role of the unusual disulfide bond in copper-zinc superoxide dismutase. *J Biol Chem, 290*(4), 2405-2418. doi:10.1074/jbc.M114.588798

Sengupta-Ghosh, A., Dominguez, S. L., Xie, L., Barck, K. H., Jiang, Z., Earr, T., . . . Easton, A. (2019). Muscle specific kinase (MuSK) activation preserves neuromuscular junctions in the diaphragm but is not sufficient to provide a functional benefit in the SOD1G93A mouse model of ALS. *Neurobiology of Disease, 124*, 340-352. doi:https://doi.org/10.1016/j.nbd.2018.12.002

Seyfried, N. T., Gozal, Y. M., Donovan, L. E., Herskowitz, J. H., Dammer, E. B., Xia, Q., . . . Peng, J. (2012). Quantitative analysis of the detergent-insoluble brain proteome in frontotemporal lobar degeneration using SILAC internal standards. *J Proteome Res, 11*(5), 2721-2738. doi:10.1021/pr2010814

Shafiei, S. S., Guerrero-Muñoz, M. J., & Castillo-Carranza, D. L. (2017). Tau Oligomers: Cytotoxicity, Propagation, and Mitochondrial Damage. *Frontiers in aging neuroscience, 9*, 83-83. doi:10.3389/fnagi.2017.00083

Sharma, A., Varghese, A. M., Vijaylakshmi, K., Sumitha, R., Prasanna, V. K., Shruthi, S., . . . Srinivas Bharath, M. M. (2016). Cerebrospinal Fluid from Sporadic Amyotrophic Lateral Sclerosis Patients Induces Mitochondrial and Lysosomal Dysfunction. *Neurochem Res, 41*(5), 965-984. doi:10.1007/s11064-015-1779-7

Shi, Y., Mowery, R. A., & Shaw, B. F. (2013a). Effect of metal loading and subcellular pH on net charge of superoxide dismutase-1. *J Mol Biol, 425*(22), 4388-4404. doi:10.1016/j.jmb.2013.07.018

Shi, Y., Rhodes, N. R., Abdolvahabi, A., Kohn, T., Cook, N. P., Marti, A. A., & Shaw, B. F. (2013b). Deamidation of asparagine to aspartate destabilizes Cu, Zn superoxide dismutase, accelerates fibrillization, and mirrors ALS-linked mutations. *J Am Chem Soc, 135*(42), 15897-15908. doi:10.1021/ja407801x

Silverman, J. M., Christy, D., Shyu, C. C., Moon, K.-M., Fernando, S., Gidden, Z., . . . Cashman, N. R. (2019). CNS-derived extracellular vesicles from superoxide dismutase 1 (SOD1)G93A ALS mice originate from astrocytes and neurons and carry misfolded SOD1. *Journal of Biological Chemistry*. doi:10.1074/jbc.RA118.004825

Skorupa, A., Urbach, S., Vigy, O., King, M. A., Chaumont-Dubel, S., Prehn, J. H., & Marin, P. (2013). Angiogenin induces modifications in the astrocyte secretome: relevance to amyotrophic lateral sclerosis. *J Proteomics, 91*, 274-285. doi:10.1016/j.jprot.2013.07.028

Song, Y., Nagy, M., Ni, W., Tyagi, N. K., Fenton, W. A., Lopez-Giraldez, F., . . . Brady, S. T. (2013). Molecular chaperone Hsp110 rescues a vesicle transport defect produced

by an ALS-associated mutant SOD1 protein in squid axoplasm. *Proc Natl Acad Sci U S A, 110*(14), 5428-5433. doi:10.1073/pnas.1303279110
Songsrirote, K., Li, Z., Ashford, D., Bateman, A., & Thomas-Oates, J. (2010). Development and application of mass spectrometric methods for the analysis of progranulin N-glycosylation. *J Proteomics, 73*(8), 1479-1490. doi:10.1016/j.jprot.2010.02.013
Stalekar, M., Yin, X., Rebolj, K., Darovic, S., Troakes, C., Mayr, M., . . . Rogelj, B. (2015). Proteomic analyses reveal that loss of TDP-43 affects RNA processing and intracellular transport. *Neuroscience, 293*, 157-170. doi:10.1016/j.neuroscience.2015.02.046
Stefani, M. (2008). Protein folding and misfolding on surfaces. *Int J Mol Sci, 9*(12), 2515-2542. doi:10.3390/ijms9122515
Sullivan, P. M., Zhou, X., Robins, A. M., Paushter, D. H., Kim, D., Smolka, M. B., & Hu, F. (2016). The ALS/FTLD associated protein C9orf72 associates with SMCR8 and WDR41 to regulate the autophagy-lysosome pathway. *Acta Neuropathol Commun, 4*(1), 51. doi:10.1186/s40478-016-0324-5
Sun, S., Ling, S. C., Qiu, J., Albuquerque, C. P., Zhou, Y., Tokunaga, S., . . . Cleveland, D. W. (2015). ALS-causative mutations in FUS/TLS confer gain and loss of function by altered association with SMN and U1-snRNP. *Nat Commun, 6*, 6171. doi:10.1038/ncomms7171
Tanaka, K., & Matsuda, N. (2014). Proteostasis and neurodegeneration: the roles of proteasomal degradation and autophagy. *Biochimica et Biophysica Acta (BBA)-Molecular Cell Research, 1843*(1), 197-204.
Taniguchi-Watanabe, S., Arai, T., Kametani, F., Nonaka, T., Masuda-Suzukake, M., Tarutani, A., . . . Hasegawa, M. (2016). Biochemical classification of tauopathies by immunoblot, protein sequence and mass spectrometric analyses of sarkosyl-insoluble and trypsin-resistant tau. *Acta Neuropathol, 131*(2), 267-280. doi:10.1007/s00401-015-1503-3
Tank, E. M., Figueroa-Romero, C., Hinder, L. M., Bedi, K., Archbold, H. C., Li, X., . . . Barmada, S. J. (2018). Abnormal RNA stability in amyotrophic lateral sclerosis. *Nat Commun, 9*(1), 2845. doi:10.1038/s41467-018-05049-z
Teunissen, C. E., Elias, N., Koel-Simmelink, M. J., Durieux-Lu, S., Malekzadeh, A., Pham, T. V., . . . Pijnenburg, Y. A. (2016). Novel diagnostic cerebrospinal fluid biomarkers for pathologic subtypes of frontotemporal dementia identified by proteomics. *Alzheimers Dement (Amst), 2*, 86-94. doi:10.1016/j.dadm.2015.12.004
Theillet, F. X., Smet-Nocca, C., Liokatis, S., Thongwichian, R., Kosten, J., Yoon, M. K., . . . Selenko, P. (2012). Cell signaling, post-translational protein modifications and NMR spectroscopy. *J Biomol NMR, 54*(3), 217-236. doi:10.1007/s10858-012-9674-x
Thompson, A., Schäfer, J., Kuhn, K., Kienle, S., Schwarz, J., Schmidt, G., . . . Hamon, C. (2003). Tandem Mass Tags: A Novel Quantification Strategy for Comparative Analysis of Complex Protein Mixtures by MS/MS. *Anal Chem, 75*(8), 1895-1904. doi:10.1021/ac0262560
Thompson, A. G., Gray, E., Thezenas, M. L., Charles, P. D., Evetts, S., Hu, M. T., . . . Turner, M. R. (2018). Cerebrospinal fluid macrophage biomarkers in amyotrophic lateral sclerosis. *Ann Neurol, 83*(2), 258-268. doi:10.1002/ana.25143
Ting, L., Rad, R., Gygi, S. P., & Haas, W. (2011). MS3 eliminates ratio distortion in isobaric multiplexed quantitative proteomics. *Nature methods, 8*(11), 937-940. doi:10.1038/nmeth.1714
Trippier, P. C., Zhao, K. T., Fox, S. G., Schiefer, I. T., Benmohamed, R., Moran, J., . . . Silverman, R. B. (2014). Proteasome activation is a mechanism for pyrazolone small

molecules displaying therapeutic potential in amyotrophic lateral sclerosis. *ACS Chem Neurosci, 5*(9), 823-829. doi:10.1021/cn500147v

Umoh, M. E., Dammer, E. B., Dai, J., Duong, D. M., Lah, J. J., Levey, A. I., . . . Seyfried, N. T. (2018). A proteomic network approach across the ALS-FTD disease spectrum resolves clinical phenotypes and genetic vulnerability in human brain. *EMBO Mol Med, 10*(1), 48-62. doi:10.15252/emmm.201708202

Valentine, J. S., Doucette, P. A., & Zittin Potter, S. (2005). Copper-zinc superoxide dismutase and amyotrophic lateral sclerosis. *Annu Rev Biochem, 74*, 563-593. doi:10.1146/annurev.biochem.72.121801.161647

Van Deerlin, V. M., Sleiman, P. M., Martinez-Lage, M., Chen-Plotkin, A., Wang, L. S., Graff-Radford, N. R., . . . Lee, V. M. (2010). Common variants at 7p21 are associated with frontotemporal lobar degeneration with TDP-43 inclusions. *Nat Genet, 42*(3), 234-239. doi:10.1038/ng.536

Varghese, A. M., Sharma, A., Mishra, P., Vijayalakshmi, K., Harsha, H. C., Sathyaprabha, T. N., . . . Raju, T. R. (2013). Chitotriosidase - a putative biomarker for sporadic amyotrophic lateral sclerosis. *Clinical proteomics, 10*(1), 19-19. doi:10.1186/1559-0275-10-19

Vega, I. E., Cui, L., Propst, J. A., Hutton, M. L., Lee, G., & Yen, S. H. (2005). Increase in tau tyrosine phosphorylation correlates with the formation of tau aggregates. *Brain Res Mol Brain Res, 138*(2), 135-144. doi:10.1016/j.molbrainres.2005.04.015

Viode, A., Fournier, C., Camuzat, A., Fenaille, F., Latouche, M., Elahi, F., . . . Becher, F. (2018). New Antibody-Free Mass Spectrometry-Based Quantification Reveals That C9ORF72 Long Protein Isoform Is Reduced in the Frontal Cortex of Hexanucleotide-Repeat Expansion Carriers. *Front Neurosci, 12*, 589. doi:10.3389/fnins.2018.00589

Wang, F., Cheng, K., Wei, X., Qin, H., Chen, R., Liu, J., & Zou, H. (2013). A six-plex proteome quantification strategy reveals the dynamics of protein turnover. *Scientific Reports, 3*, 1827-1827. doi:10.1038/srep01827

Wang, I. F., Wu, L. S., & Shen, C. K. (2008). TDP-43: an emerging new player in neurodegenerative diseases. *Trends Mol Med, 14*(11), 479-485. doi:10.1016/j.molmed.2008.09.001

Wang, P., Wander, C. M., Yuan, C.-X., Bereman, M. S., & Cohen, T. J. (2017). Acetylation-induced TDP-43 pathology is suppressed by an HSF1-dependent chaperone program. *Nature Communications, 8*(1), 82. doi:10.1038/s41467-017-00088-4

Wang, T., Jiang, X., Chen, G., & Xu, J. (2015). Interaction of amyotrophic lateral sclerosis/frontotemporal lobar degeneration–associated fused-in-sarcoma with proteins involved in metabolic and protein degradation pathways. *Neurobiology of Aging, 36*(1), 527-535. doi:https://doi.org/10.1016/j.neurobiolaging.2014.07.044

Webster, C. P., Smith, E. F., Shaw, P. J., & De Vos, K. J. (2017). Protein Homeostasis in Amyotrophic Lateral Sclerosis: Therapeutic Opportunities? *Front Mol Neurosci, 10*, 123-123. doi:10.3389/fnmol.2017.00123

Wei, X., & Li, L. (2008). Mass spectrometry-based proteomics and peptidomics for biomarker discovery in neurodegenerative diseases. *International journal of clinical and experimental pathology, 2*(2), 132-148.

Weskamp, K., & Barmada, S. J. (2018). TDP43 and RNA instability in amyotrophic lateral sclerosis. *Brain Res, 1693*(Pt A), 67-74. doi:10.1016/j.brainres.2018.01.015

Whiten, D. R., San Gil, R., McAlary, L., Yerbury, J. J., Ecroyd, H., & Wilson, M. R. (2016). Rapid flow cytometric measurement of protein inclusions and nuclear trafficking. *Sci Rep, 6*, 31138. doi:10.1038/srep31138

Williams, K. L., Topp, S., Yang, S., Smith, B., Fifita, J. A., Warraich, S. T., . . . Blair, I. P. (2016). CCNF mutations in amyotrophic lateral sclerosis and frontotemporal dementia. *Nature Communications, 7*, 11253. doi:10.1038/ncomms11253
https://www.nature.com/articles/ncomms11253#supplementary-information
Xu, G., Paige, J. S., & Jaffrey, S. R. (2010). Global analysis of lysine ubiquitination by ubiquitin remnant immunoaffinity profiling. *Nat Biotechnol, 28*(8), 868-873. doi:10.1038/nbt.1654
Xu, Z., Lee, A., Nouwens, A., Henderson, R. D., & McCombe, P. A. (2018). Mass spectrometry analysis of plasma from amyotrophic lateral sclerosis and control subjects. *Amyotroph Lateral Scler Frontotemporal Degener, 19*(5-6), 362-376. doi:10.1080/21678421.2018.1433689
Yin, S., Lopez-Gonzalez, R., Kunz, R. C., Gangopadhyay, J., Borufka, C., Gygi, S. P., . . . Reed, R. (2017). Evidence that C9ORF72 Dipeptide Repeat Proteins Associate with U2 snRNP to Cause Mis-splicing in ALS/FTD Patients. *Cell Rep, 19*(11), 2244-2256. doi:10.1016/j.celrep.2017.05.056
Yokoi, S., Udagawa, T., Fujioka, Y., Honda, D., Okado, H., Watanabe, H., . . . Sobue, G. (2017). 3'UTR Length-Dependent Control of SynGAP Isoform alpha2 mRNA by FUS and ELAV-like Proteins Promotes Dendritic Spine Maturation and Cognitive Function. *Cell Rep, 20*(13), 3071-3084. doi:10.1016/j.celrep.2017.08.100
Yu, F., Qiu, F., & Meza, J. (2016). 12 - Design and Statistical Analysis of Mass-Spectrometry-Based Quantitative Proteomics Data. In P. Ciborowski & J. Silberring (Eds.), *Proteomic Profiling and Analytical Chemistry (Second Edition)* (pp. 211-237). Boston: Elsevier.
Zacco, E., Graña-Montes, R., Martin, S. R., de Groot, N. S., Alfano, C., Tartaglia, G. G., & Pastore, A. (2019). RNA as a key factor in driving or preventing self-assembly of the TAR DNA-binding protein 43. *J Mol Biol*. doi:https://doi.org/10.1016/j.jmb.2019.01.028
Zetterstrom, P., Graffmo, K. S., Andersen, P. M., Brannstrom, T., & Marklund, S. L. (2011). Proteins that bind to misfolded mutant superoxide dismutase-1 in spinal cords from transgenic amyotrophic lateral sclerosis (ALS) model mice. *J Biol Chem, 286*(23), 20130-20136. doi:10.1074/jbc.M111.218842
Zhai, J., Strom, A. L., Kilty, R., Venkatakrishnan, P., White, J., Everson, W. V., . . . Zhu, H. (2009). Proteomic characterization of lipid raft proteins in amyotrophic lateral sclerosis mouse spinal cord. *Febs j, 276*(12), 3308-3323. doi:10.1111/j.1742-4658.2009.07057.x
Zhang, J., Huang, P., Wu, C., Liang, H., Li, Y., Zhu, L., . . . Xu, R. (2018a). Preliminary Observation about Alteration of Proteins and Their Potential Functions in Spinal Cord of SOD1 G93A Transgenic Mice. *Int J Biol Sci, 14*(10), 1306-1320. doi:10.7150/ijbs.26829
Zhang, K., Donnelly, C. J., Haeusler, A. R., Grima, J. C., Machamer, J. B., Steinwald, P., . . . Rothstein, J. D. (2015). The C9orf72 repeat expansion disrupts nucleocytoplasmic transport. *Nature, 525*(7567), 56-61. doi:10.1038/nature14973
Zhang, Y., Burberry, A., Wang, J. Y., Sandoe, J., Ghosh, S., Udeshi, N. D., . . . Eggan, K. (2018b). The C9orf72-interacting protein Smcr8 is a negative regulator of autoimmunity and lysosomal exocytosis. *Genes Dev, 32*(13-14), 929-943. doi:10.1101/gad.313932.118
Zhou, J. Y., Afjehi-Sadat, L., Asress, S., Duong, D. M., Cudkowicz, M., Glass, J. D., & Peng, J. (2010). Galectin-3 is a candidate biomarker for amyotrophic lateral sclerosis: discovery by a proteomics approach. *J Proteome Res, 9*(10), 5133-5141. doi:10.1021/pr100409r

Zhuang, X., Zhao, B., Liu, S., Song, F., Cui, F., Liu, Z., & Li, Y. (2016). Noncovalent Interactions between Superoxide Dismutase and Flavonoids Studied by Native Mass Spectrometry Combined with Molecular Simulations. *Anal Chem, 88*(23), 11720-11726. doi:10.1021/acs.analchem.6b03359

Zubiri, I., Lombardi, V., Bremang, M., Mitra, V., Nardo, G., Adiutori, R., . . . Malaspina, A. (2018). Tissue-enhanced plasma proteomic analysis for disease stratification in amyotrophic lateral sclerosis. *Mol Neurodegener, 13*(1), 60. doi:10.1186/s13024-018-0292-2

Tables and Table Legends

Table 1. Human tissue proteomics studies using label-free techniques for mechanistic insight into ALS and FTD.

Sample	Summary	Remarks	Reference
ALS (TDP-43+) and FTLD-TDP brain	Isolation of phosphorylated TDP-43 with numerous other insoluble proteins, which differentiate ALS and FTLD-TDP subtypes	TDP-43 proteinopathy variation may stem from alternate pathological TDP-43 conformations	(Laferriere et al., 2019)
ALS (TDP-43+) and FTLD-TDP spinal cord and frontal cortex	281 proteins ↑/↓ in ALS and 52 ↑/↓ in FTLD-TDP (33 proteins overlap)	ALS and FTD share molecular alterations including mitochondrial and metabolic impairment	(Irwin et al., 2018)
ALS and FTLD-TDP brain	Identified 15 modules of co-regulated proteins (8 significantly different across subtypes of ALS and FTLD-TDP)	Subtypes of FTLD-TDP and ALS differentiated by insoluble protein proteomic signature, possibly reflecting common/differing mechanisms	(Umoh et al., 2018)
ALS brain	Phosphorylation, deamidation and cleavage sites of TDP-43 almost all in the glycine-rich C-terminus	Modifications of TDP-43 may affect molecular pathways in disease	(Kametani et al., 2016)
ALS frontal cortex	Fungal antigens in human ALS brain within cytoplasmic structures	Fungal infection may contribute to pathogenesis of ALS	(Alonso et al., 2015)
ALS spinal cord	Altered detergent-insoluble protein acetylation, including GFAP, in ALS	Dysregulation of protein acetylation may be involved in ALS pathology	(Liu et al., 2013)
FTD frontal cortex	↓ C9ORF72 long protein isoform in disease	Novel method for quantifying C9ORF72 isoforms	(Viode et al., 2018)
FTLD-TDP brain	↑/↓ 50 proteins FTLD-TDP, including TDP-43 and septin 11	Identified and characterised enriched proteins in the detergent-insoluble fraction	(Gozal et al., 2011b)
FTLD-TDP hippocampus	↑ 54 proteins (including TDP-43) and ↓ 19 proteins in FTLD-TDP laser-captured dentate gyrus neurons	Potential pathology-associated proteins identified	(Gozal et al., 2011a)
PSP brain	C-terminus of tau is protease-resistant, cleavage pattern may differentiate subtypes of FTD and AD	Analysis of tau C-terminus in FTD potentially useful in classifying disease subtypes	(Taniguchi-Watanabe et al., 2016)
sALS spinal cord	21 proteins ↑/↓, ↑ mitochondrial metabolism proteins, ↓ ATP5D and calmodulin	Synaptic mitochondrial changes potentially involved in ALS	(Engelen-Lee et al., 2017)

↑ denotes increase; ↓ denotes decrease; ATP5D, mitochondrial membrane ATP synthase; FTD, frontotemporal dementia; FTLD, frontotemporal lobar degeneration; GFAP, glial fibrillary acidic protein; PSP, progressive supranuclear palsy; sALS, sporadic amyotrophic lateral sclerosis; TDP-43, TAR DNA binding protein of 43kDa

Table 2. Animal model proteomics studies using label-free techniques for mechanistic insight into ALS and FTD.

Sample	Summary	Remarks	Reference
Grn$^{-/-}$, *TMEM106B*$^{-/-}$ mouse brain	↑ 17 and ↓ 2 lysosomal proteins with Grn$^{-/-}$, phenotype normalized by Tmem106b$^{-/-}$	Alterations in lysosomal function may contribute to risk of FTD	(Klein et al., 2017)
Non-transgenic mouse cortex	IP-MS of TDP-43 suggests interactions with mitochondrial proteins, including PHB2	Normal function of TDP-43 may be related to mitochondria	(Davis et al., 2018)
rTg4510 mice (P301L 4R0N) brain	↑ nucleotide-binding proteins ↓ RNA binding and ribonucleoproteins in tauopathy	Identified proteins that co-localise with tau inclusions and changes in expression	(Mazinik et al., 2018)
SOD1^{G93A} mouse brain and spinal cord EVs	Only 1 protein ↑/↓ in SOD1^{G93A} EVs (↓ MOG)	EVs may originate from astrocytes and contain RBPs, but little change in disease	(Silverman et al., 2019)
SOD1^{G93A} mouse muscle tissue	ER stress response is activated in skeletal muscle of SOD1 mice ↑ CHOP, BiP and PERK	ER stress leads to reduced protein translation, involvement in muscle atrophy and weakness seen in ALS	(Chen et al., 2015)
SOD1^{G93A} mouse spinal cord	↓ VGF peptides, similar findings in ALS plasma	Selective depletion of VGF fragments may be involved in disease etiology	(Brancia et al., 2016)
SOD1^{G93A} mouse spinal cord	67 ↑/↓ lipid raft proteins, involved in vesicular transport, neurotransmitter synthesis/release, cytoskeletal organisation and metabolism	Lipid raft protein changes in ALS may affect vesicular trafficking, neurotransmitter signaling and cytoskeleton	(Zhu et al., 2009)
SOD1^{G93A} mouse ventral horn spinal cord	IP-MS of interactors of misfolded SOD1 (3 timepoints), primarily chaperones, transporters and hydrolases (notably HSPA8, Na^+/K^+ATPase-α3)	Na^+/K^+ATPase-α3 levels are high in vulnerable MNs, and expression may modulate disease pathology and phenotype	(Ruegsegger et al., 2016)
SOD1^{G93A} rat spinal cord mitochondria	↑ 33 proteins & ↓ 21 proteins, mostly involved in complex I and mitochondrial protein import	Mitochondrial protein alterations and ↓ protein import may contribute to mutant SOD1-associated mitochondrial deficits	(Li et al., 2010)
SOD1$^{WT\ or\ G93A\ or\ G85R}$ mouse spinal cord	Enriched detergent-insoluble proteins, including VILIP-1	VILIP-1 may affect oxidation status and calcium levels in ALS	(Liebl et al., 2014)
Squid axoplasm combined with SOD1^{G85R} protein	Addition of HSP110 to mutant SOD1 affected axoplasm rescued the transport defect and phosphorylation of p38 seen in pathology	Highlights potential of HSP110 in association with HSC70 as a mediator of protein disaggregation for mutant SOD1 in ALS	(Song et al., 2013)
Synaptoneurosomes from rat brain	IP-MS of Chmp2b complexes, identifying association with ESCRT-III and postsynaptic proteins	Chmp2b is part of a stable complex that regulates synaptic plasticity, potentially relevant to FTD mechanisms	(Chassefeyre et al., 2015)
Znf179$^{-/-}$ mouse hippocampus	IP-MS of Znf179/RNF112 identifies interaction with TDP-43, TDP-43 is polyubiquitinated by E3 ligase function of RNF112	↑ ubiquitination of TDP-43 → ↑ degradation, loss of RNF112 in ALS may cause TDP-43 aggregation and pathology	(Lee et al., 2018b)

↑ denotes increase; ↓ denotes decrease; ALS, amyotrophic lateral sclerosis; BiP, Endoplasmic reticulum chaperone BiP; CacyBP, calcyclin-binding protein; Chmp2b, charged multivesicular body protein 2b; CHOP, DNA-damage-inducible transcript/CCAAT/enhancer-binding protein; ER, endoplasmic reticulum; FTD, frontotemporal dementia; FTLD, frontotemporal lobar degeneration; HSC70, heat shock cognate 71kDa; HSP110, heat shock protein 110; KO, knockout; MFN2, mitofusin 2; PERK, PKR-like endoplasmic reticulum kinase; PGRN, progranulin; PHB2, prohibitin 2; ssPMPCA, mitochondrial-processing peptidase subunit alpha; RNF112/ZNF179, RING finger protein 112; SOD1, superoxide dismutase 1; TDP-43, TAR DNA binding protein of 43kDa; TMEM106B, transmembrane protein 106B; VGF, neurosecretory protein VGF; VILIP-1, Visinin-like protein 1

Table 3. Cell and in vitro model proteomics studies using label-free techniques for mechanistic insight into ALS and FTD.

Sample	Summary	Remarks	Reference
Differentiated C2C12 mouse myoblasts	Detected muscle specific kinase activation via phosphorylation, which preserves innervation of neuromuscular junctions	Innervation of neuromuscular junctions insufficient however could potentially be used as an adjuvant therapy	(Sengupta-Ghosh et al., 2019)
HEK239T cells and rat primary cortical neurons infected with GR_{149} or PR_{175}	Poly-GR/PR interactome identified RNA-binding proteins (many low-complexity domains), cytoplasmic/mitochondrial ribosomes components, stress granules and splicing factors	Sequestration of ribosomes via interactions with poly-GR/PRs would potentially impair protein translation in FTD pathology	(Hartmann et al., 2018)
HEK293 and N2A cells transfected with cyclin F^{WT} or S621G	Identified 7 phosphorylation sites on cyclin F	Cyclin F S621 phosphorylation by CK2 regulates Lys48-specific E3 ligase activity.	(Lee et al., 2017a)
HEK293 cells expressing RBM45	Identified 132 protein-protein interactors of RBM45	RBM45 associates with enriched proteins involved in nuclear RNA processing: TDP-43, Matrin-3, hnRNP-A1 and FUS	(Li et al., 2016)
HEK293A cells expressing TDP-$43^{\Delta NLS}$ and 2KQ and CBP	Identified TDP-43 acetylation sites K145/192	TDP-43 modulation via acetylation could potentially be used therapeutically	(Cohen et al., 2015)
HEK293E cells expressing TDP-$43^{1\text{-}414}$ or ΔNLS or WT	Removal of 4 lysine ubiquitination sites in CTF TDP-43 = ubiquitination suppression	Indicates interplay between ubiquitination and phosphorylation of TDP-43 in ALS and FTD pathology	(Hans et al., 2018)
HEK293T and H4 cells treated with various drugs	Identified 28 phosphorylation sites within FUS's prion-like domain, following DNA-damaging stress	Multiphosphorylation of these sites does not cause cytoplasmic localisation	(Rhoads et al., 2018)
HEK293T cells expressing DPRs	Interactome of DPRs: RNA-binding proteins and proteins with low complexity sequence domains	DPRs altered phase separation of low complexity domain proteins, suggesting possible mechanism involved in pathogenesis	(Lee et al., 2016)
HEK293T cells expressing FUS^{P525L}	Mutant FUS ↓ interactions with many metabolic enzymes. Novel interactions between FUS and VCP, PSF, UBA1 and PSMD12. FUS accumulation = ↓ ATP levels & ↑ poly-ubiquitinated proteins	Defective energy metabolism and protein degradation arise as a result of FUS accumulating and interacting with key regulators	(Wang et al., 2015)
HEK293T cells expressing FUS^{R521G} or $R521L$	FUS interacting proteins = fALS implicated proteins hnRNPA1 and Matrin-3	Potential common pathogenic roles between FUS-ALS and fALS. FUS present in exosomes suggesting contribution to cell-to-cell transmission/spread. Interactors also sequestered into inclusions	(Kamelgarn et al., 2016)
HEK293T cells expressing mPGRN-HA	PGRN interacts with a network of ER chaperones such as BiP, calreticulin, GRP94 and PDI family proteins	PGRN is a substrate of several PDI proteins and ER chaperone network control could be a therapeutic target	(Almeida et al., 2011)
HEK293T cells transfected with Zfp106	Zfp106 interacts with hexanucleotide repeat (GGGGCC) RNA-binding protein, other RNA-binding proteins: TDP-43 and FUS. Zfp106 KO mice develop motor neuron degeneration. Zfp106 suppresses neurotoxicity in *Drosophila* C9orf72 ALS mode	Importance and role of Zfp106 in ALS pathology	(Celona et al., 2017)
HEK293T cells treated with various drugs	Identified 17 phosphorylation sites within FUS low-complexity domain	Phosphorylated/phosphomimetic FUS reduces aggregation, propensity to aggregate, ameliorates cytotoxicity and disrupt phase separation	(Monahan et al., 2017)
HEL293FT cells expressing poly-DPR sequences	Co-aggregators of poly-GA = Unc119, soluble Unc119 ↓ in poly-GA expressing neurons	Loss of function of Unc119 in neurons with DPR-type pathology as seen in C9orf72 ALS/FTD	(May et al., 2014)
HeLa cells	Arginine-rich DPRs undergo liquid-liquid phase separation and induce this effect on proteins involved in RNA and stress granule metabolism	Arginine-rich DPRs derived from C9ORF72 repeat expansions play an important role in the pathogenesis of ALS/FTD	(Boeynaems et al., 2017)
HeLa cells expressing FUS	FUS forms liquid-like compartments under stress that are crucial for its role	Propensity for aggregation vs functionality of FUS action in liquid-compartments found in disease	(Patel et al., 2015)

In vitro	Cathepsin L cleaves intracellular PGRN into poly-granulin and granulin fragments	Cathepsin L identified as a key intracellular lysosomal protease, therefore demonstrating link between lysosomal dysfunction and FTLD	(Lee et al., 2017b)
In vitro	$SOD1^{G37R}$ did not have the same propensity to aggregate as $SOD1^{G93A}$ and $SOD1^{G93C}$ however still formed oligomeric aggregates	Slow disease progression in $SOD1^{G37R}$ patients is due to structural limitations associated with the arginine substitution at residue 37	(McAlary et al., 2016)
In vitro	Naringin is a strong native interactor of SOD1, demonstrated to stabilise SOD1 dimers and inhibit aggregation	Analytical method for studying interactions between proteins and drug-like molecules, identifying role of naringin	(Zhuang et al., 2016)
In vitro	K225,240,257,311,383 residues in tau involved in crosslinking to K336,338 to α-tubulin	Identified how tau stabilises microtubules through identifying sites of interfacing	(Kadavath et al., 2015)
iPSC-derived motor neurons expressing DPRs and *Drosophila* brain	Arginine DPRs interact with ribosomal proteins, expression of eIF_1A rescued DPR-induced toxicity	Repression of protein translation is involved in C9orf72 hexanucleotide-repeat induced neurodegeneration	(Moens et al., 2019)
Mouse primary hippocampal neurons expressing scrambled shRNA FUS	Identified PSD-95 interacting proteins: ↓ SynGAP with FUS depletion. FUS, ELAV1 and ELAV4 exert a level of control on SynGAP mRNA stability	FUS depleted dendritic spines associated with internalisation of PSD-95	(Yokoi et al., 2017)
N2a cells	Interactors of C9ORF72 = UBQLN2, hnRNPA2/B1, hnRNPA1 & actin. Colocalisation with RAB7 and RAB11 suggests dysregulation of trafficking	Demonstrates the role of C9ORF72 in RAB-mediated trafficking	(Farg et al., 2014)
N2a cells expressing TDP-43 and CTF	Interactome of TDP-43 using BioID identified 254 proteins vs 389 in CTF, many involved in mRNA processing	TDP-43 aggregate associates were involved in nuclear pore complex and transport machinery	(Chou et al., 2018)
NSC-34 cells expressing dipeptide repeat poly-$(PR)_{50}$	Poly-PR peptides interact with mRNA-binding proteins, ribosomal proteins, translation initiation and elongation factors	Alterations via DPRs are potential therapeutic targets and are involved in neurotoxicity	(Kanekura et al., 2016)
PC12 $SOD1^{G93A}$ cells	PSMC1, PSMC4 and TCP-1 activated by pyrazolones in the absence of exogenous proteasome inhibitor	In the absence of the heat shock response, pyrazolones enhance proteasomal activation and could be a potential therapeutic target	(Trippier et al., 2014)
S2 cells expressing $Xrp1^{Short\ or\ Long}$ and actin5C-GAL4	↑ Xrp1 expression in caz mutants, interactors are involved in gene expression regulation	Caz is the orthologue of human FET proteins FUS, EWSR1 and TAF15, all of which implicated in ALS and FTD, dysregulation of gene repair implicated	(Mallik et al., 2018)
SH-SY5Y cells knockdown TDP-43	↓ RanBP1, Dnmt3a and CgB in TDP-43 knockdown. ↓ RanBP1 = ↑ transportin 1	TDP-43 mediates RNA metabolism and intracellular transport	(Stalekar et al., 2015)
SKNBE2 cells expressing tau	AnxA2 interacts with tau^{WT} but not mutant tau^{K369I}	Tau^{K369I} mechanism involves impaired membrane binding due to functional interaction with AnxA2	(Gauthier-Kemper et al., 2011)
SOD1 isolated from yeast	Low molecular weight fractionated SOD1 does not appear to be post-translationally modified compared to high molecular weight SOD1, which is oxidized at residues C146 and H71	Crucial for SOD1 structure, suggesting a role of oxidative damage for protein misfolding	(Martins & English, 2014)
$SOD1^{WT\ or\ G37R\ or\ L38V\ or\ G41D\ or\ G85A\ or\ G93S\ or\ D90N}$ isolated from yeast	Structure of SOD1 amyloid fibrils and mutants demonstrated that fibrils protected the N-terminus from digestion via proteases	SOD1 and mutants fibrillate through the N-terminal fragment, highlighting potential ALS implications	(Chan et al., 2013)

↑ denotes increase; ↓ denotes decrease. AnxA2, Annexin A2; caz, RNA-binding protein cabeza; CgB, chorionic gonadotropin beta; CK2, casein kinase II subunit alpha; CTF, C-terminal fragment; Dnmt3a, DNA (cytosine-5)-methyltransferase 3A; DPR, dipeptide repeat; EIF1A, eukaryotic translation initiation factor 1A; ELAV1/4, embryonic lethal abnormal vision protein 1/4; EWSR1, RNA-binding protein EWS; FUS, fused-in-sarcoma; GFAP, glial fibrillary acidic protein; GR, glycine arginine; GRP94, 94kDa glucose regulated protein; hnRNPA1, heterogeneous nuclear ribonucleoprotein A1; iPSC, induced pluripotent stem cell; MTO, methanethiol oxidase; PDI, protein disulphide-isomerase; PIN1, peptidyl-prolyl cis-trans isomerase NIMA-interacting 1; PR, proline arginine; PSD-95, postsynaptic density protein 95; PSF, polypyrimidine tract-binding protein-associated-splicing factor; PSMC1/4, 26S proteasome regulatory subunit 1/4; PSMD12, 26S proteasome non-ATPase regulatory subunit 12; RAB7/11, Ras-related protein Rab-7/11; RanBP1, Ran-binding protein 1; RBM45, RNA binding motif protein 45; ROCK2, rho-associated protein kinase 2; SOD1, superoxide dismutase 1; SynGAP, Ras/Rap GTPase-activating protein SynGAP; TAG15, TATA binding associated factor 15; TCP-1, T-complex protein 1; TDP-43, TAR DNA-binding protein 43; UBA1, ubiquitin-like modifier-activating enzyme 1; UBQLN2, ubiquilin-2; Unc119, protein unc-119 homolog A; VCP, vasolin-containing protein; Zfp106, zinc finger protein 106

Table 4. MALDI-MS proteomics studies for mechanistic insight into ALS and FTD.

Sample	Summary	Remarks	Reference
Human samples			
ALS spinal cord	CA-I is biotinylated alongside SOD1 + immunoreactive to a SOD1 antibody	Suggests altered CO_2 transport and cellular pH homeostasis	(Liu et al., 2010)
sALS spinal cord	18 proteins ↑/↓, GFAP = most abundant	Proteins involved in apoptosis and cytoskeleton stabilisation	(Ekegren et al., 2006)
FTLD frontal cortex	24 proteins ↑/↓ = UCHL1 and oxidative stress proteins	Ubiquitin-mediated degradation and oxidative stress response altered	(Schweitzer et al., 2006)
FTLD-tau (Pick disease) brain	↑ GFAP with glycoxidation and lipoxidation	GFAP=target of oxidative damage	(Muntane et al., 2006)
FTD temporal lobe	N-terminal fragment ProSAAS enriched in tauopathies	ProSAAS is an inhibitor of neuroendocrine peptide processing - enrichment may cause functional perturbation	(Kikuchi et al., 2003)
FTD CSF	↑/↓ ProSAAS, PEDF, RBP, apoE, HP and ALB	Comparative proteomics to establish pathophysiological mechanisms	(Davidson et al., 2002)
sALS spinal cord	↑ Detergent-insoluble proteins (ACO2, HSC70, PPIase A) + intermediate filaments, chaperones and mitochondrial proteins, some tyrosine-nitration	Aggregation-prone proteins and nitrative stress contribution to inclusion pathology	(Basso et al., 2009)
Animal models			
$SOD1^{G93A}$ mouse synaptic fractions	STAU1+dynein interactions via PP1B	STAU1 regulates mRNA localisation in axons and synapses. Disrupted=toxicity	(Gershoni-Emek et al., 2016)
$SOD1^{G93A}$ mouse facial and trigeminal nuclei	↑/↓ various proteins, ↑RPS19	Proteins contributing to pathology via comparative brain region proteomics	(Acquadro et al., 2014)
$SOD1^{H46R/H48Q}$ mouse spinal cord	Association between SOD1 surface hydrophobicity SOD1 and conformations	HSF1 activation may mitigate ALS pathology	(Lin et al., 2013)
$SOD1^{G93A}$ and $G127X$ mouse spinal cord	Mutant SOD1 interactors = chaperones, HSC70 abundant	Chaperone depletion is not involved in SOD1 mutations of ALS	(Zetterstrom et al., 2011)
$SOD1^{G85R}$ and $G93A$ mouse eMNs	↑ CRMP4a = axonal degeneration and MN cell death ↓ CRMP4a protective	CRMP4a pathologically involved in ALS	(Duplan et al., 2010)
$SOD1^{G127X}$ mouse spinal cord	54 proteins ↑/↓ = oxidative stress, mitochondrial, cellular assembly/organisation and protein degradation	Altered pathways may contribute to disease	(Bergemalm et al., 2009)
$SOD1^{G93A}$ mice spinal cord	↑/↓ proteins = mitochondrial dysfunction, aggregation and stress response	Potential presymptomatic targets	(Massignan et al., 2007)
$SOD1^{G93A}$ mouse spinal cord	↑ Carbonylation of SOD1, TCTP, UCHL1, CRYAB	Oxidative modification contributing factor to ALS	(Poon et al., 2005)
$SOD1^{G93A}$ mouse spinal cord	Peroxidation of DRP-2, HSP70, ENO1	Supports oxidative stress as a major pathological mechanism	(Perluigi et al., 2005)
$hTau40^{P301L}$ mouse brain	↓ Complex I activity, ↑ antioxidant enzymes, altered lipid peroxidation	Tau pathology involves mitochondrial and oxidative stress	(David et al., 2005)
Cell models and in-vitro studies			
N2A cells expressing ATXN2, FUS, C9ORF72, OPTN, TDP-43, UBLQN2 WT/mutants	Interactome of ATXN2, C9ORF72, FUS, OPTN, TDP-43 and UBQLN2 (hundreds of proteins)	Strong interactome overlap for ATXN2, FUS and TDP-43 distinct from OPTN and UBQLN2	(Blokhuis et al., 2016)
C4F6 hybridoma cells + SOD1 mutants	D92/D96 important for SOD1-C4F6 antibody interaction	C4F6 antibody epitope in SOD1 is a potential therapeutic target	(Rotunno et al., 2014)
COS7 cells expressing PGRN	4 N-glycosylation sites of PGRN	PGRN glycosylation may contribute to disease	(Songsrirote et al., 2010)
N2A cells treated with cadmium	Cadmium = ↑/↓ proteins = cellular structure, stress, chaperones, cell death/survival and ROS	Heavy metals suppress function of SOD1	(Huang et al., 2006)
NSC-34 cells expressing $SOD1^{G93A}$	170 proteins, ↑/↓ = mitochondrial, membrane transport, apoptosis, respiratory chain & chaperones	Mitochondrial protein changes = evidence for mitochondrial dysfunction	(Fukada et al., 2004)
$SOD1^{WT}$ or $N26D/N131D/N139D$ isolated from yeast	Deamidation mimic mutant SOD1 aggregated into amyloid fibrils faster than WT	Deamidation may be involved in SOD1 pathology	(Shi et al., 2013b)
In vitro	Acetylated tau prevents degradation of phosphorylated tau	Tau acetylation may be a therapeutic target	(Min et al., 2010)

↑ denotes increase, ↓ denotes decrease; ACO2, aconitase; ALB, albumin; apoE, apolipoprotein E; ATXN2, ataxin-2; C4F6; CA-I, carbonic anhydrase I; CRMP4a, collapsin response mediator protein 4a; CRYAB, alpha-crystallin B chain; CSF, cerebrospinal fluid; DRP-2, dystrophin-related protein 2; eMNs, embryonic motor neurons; ENO1, alpha-enolase; FTD, frontotemporal dementia; FTLD, frontotemporal lobar degeneration; FUS, fused-in sarcoma; GFAP, glial fibrillary acidic protein; HP, haptoglobin; HSC70, heat shock cognate 71kDA; HSP70, heat shock 70kDa; OPTN, optineurin; PEDF, pigment epithelium-derived factor; PGRN, progranulin; PP1B, protein phosphatase 1-beta; PPIase A, peptidyl-prolyl cis-trans isomerase A; ProSAAS, proprotein convertase 1 inhibitor; RBP, retinol binding protein; ROS, reactive oxygen species; RPS19, 40S ribosomal protein S19; sALS, sporadic amyotrophic lateral sclerosis; STAU1, Staufen1; TCTP, translationally-controlled tumour protein; TDP-43, TAR DNA-binding protein of 43kDa; UBQLN2, ubiquilin-2; UCHL1, ubiquitin carboxy-terminal hydrolase L1

Table 5. Labelled-MS proteomics studies for mechanistic insight into ALS and FTD.

Technique	Model	Summary	Remarks	Reference
iTRAQ	$SOD1^{G93A}$ mouse spinal cord	↑ 676 proteins, ↓ 480 proteins	Preliminary insight into altered proteins	(Zhang et al., 2018a)
iTRAQ	Rat neonate spinal cord injected with ALS CSF	↓ 35 mitochondrial & 4 lysosomal proteins and ↑ BNIP3L	Mitochondrial and lysosomal defects involved in pathogenesis	(Sharma et al., 2016)
SILAC	HeLa cells expressing FUS/TLS	↑ FUS/TLS mutant interaction with SMN & ↓ interaction with U1-snRNP	Demonstrates a gain and loss of function in FUS-ALS	(Sun et al., 2015)
SILAC	Primary mouse astrocyte cultures	60 astrocyte proteins regulate secretion with Ang stimulation	Ang taken up by astrocytes = potential neuroprotection	(Skorupa et al., 2013)
SILAC	HEK-293 cells expressing TDP-43 or splice variant	35 proteins co-aggregate with TDP-43 (G3BP, PABPC1 and eIF4A1) 4 ubiquitinated sites on TDP-43 splice variant	TDP-43 aggregation partners + ubiquitination affects oligomerisation	(Dammer et al., 2012)
SILAC and label-free	H1299 cells and HEK293T cells expressing UBXD1 or ERGIC-53	UBXD1 interacts with vesicle, ERGIC and VCP + involved in ERGIC-53 vesicle trafficking	UBXD1-VCP interaction perturbed in VCP mutants of ALS and FTD	(Hanes et al., 2012)
SILAC and label-free	HeLa cells expressing TDP-43	TDP-43 interacts with hnRNP, Drosha and FUS/TLS complexes. mutant TDP-43 ↑ FUS/TLS interactions	TDP-43 involved in mRNA processing & miRNA biogenesis, function overlap with FUS	(Ling et al., 2010)
TMT	C9ALS and sALS iPSCs	RNA stability/binding targets: ↑/↓ 170 altered in C9ALS & 121 in sALS	Destabilization of RNA transcripts involved in oxidative phosphorylation and ribosomal machinery	(Task et al., 2018)
TMT	hESC and hESC MN cells expressing C9ORF72, immunoprecipitated	C9ORF72 stabilizes SMCR8, enables interaction with WDR41	C9ORF72+SMCR8 involved in autoimmunity and lysosomal exocytosis	(Zhang et al., 2018b)
TMT	HeLa cells expressing C9ORF72 DPR proteins	C9ORF72 PR and GR DPRs block spliceosome assembly	DPR-mediated dysfunction = Mis-spliced exons in C9ORF72	(Yin et al., 2017)
TMT	C57BL/6 WT mouse brain	Interactome of tau and isoforms – 101 proteins identified	Selective binding of proteins with specific isoforms of tau	(Liu et al., 2016)
TMT and iTRAQ	HEK293T and SH-SY5Y expressing various tau proteins	Tau^{P301L} disrupts interactions with heat shock, proteasome and microtubule-associated proteins	Mutant tau^{P301L} ↓ interactions with chaperones and proteasome	(Gunawardana et al., 2015)

↑ denotes increase, ↓ denotes decrease; Ang, angiogenin; BNIP3L, BCL2 interacting protein 3-like; CSF, cerebrospinal fluid; DPR, dipeptide repeat; eIF4A1, eukaryotic translation initiation factor 4A1; ERGIC-53, ER-Golgi intermediate compartment 53kDa protein; FTD, frontotemporal dementia; FUS, fused-in-sarcoma; G3BP, ras GTPase-activating protein; GR, glycine arginine; hESC, human embryonic stem cell; iTRAQ, isobaric tags for relative and absolute quantitation; MN, motor neuron; PABPC1, polyadenylate-binding protein 1; PR, proline arginine; sALS, sporadic amyotrophic lateral sclerosis; SILAC, stable isotope labelling by amino acids in cell culture; SMCR8, guanine nucleotide exchange protein; SMN, survival motor neuron protein; TDP-43, TAR DNA binding protein of 43kDa; TMT, tandem mass tag; UBXD1, UBX domain-containing protein 1; VCP, valosin-containing protein; WDR41, WD repeat-containing protein 41

Table 6. Biomarker discovery studies using proteomics for ALS and FTD.

Technique	Sample	Summary	Remarks	Reference
iTRAQ	ALS CSF	↓ IGF-2, ↑ GRIA4 (levels correlate with ALS severity)	Potential biomarker for disease severity (gender differences)	(Chen et al., 2016)
iTRAQ	sALS CSF	31 proteins ↑ in ALS CSF, ↑ CHIT1 10x	CHIT1 expression = ↑ microglial activity (potential CSF biomarker)	(Varghese et al., 2013)
Label free	TDP-43/Tau FTD CSF and blood	56 proteins ↑/↓ in FTD subtypes (notably CHI3L-1 and CAT)	Requires validation in FTD pathology cohorts	(Teunissen et al., 2016)
Label-free	ALS CSF and plasma	27 proteins ↑/↓ in ALS CSF, 20 proteins ↑/↓ in ALS plasma (Validated CHI3L-1 & ACT)	New and previously identified potential biomarkers	(Bereman et al., 2018)
Label-free	ALS CSF	↑ CHIT1, CHI3L-1 and CHI3L-2	Neuroinflammatory mechanisms implicated through microglial activation	(Thompson et al., 2018)
Label-free	sALS plasma	Serum proteome characterisation	Lipid homeostasis proteins implicated	(De Benedetti et al., 2017)
Label-free	sALS CSF	WDR63, APLP2, SPARCL1 and CADM3 = potential biomarkers	Panel of CSF proteins for biomarkers	(Collins et al., 2015)
Label-free	sALS and other neural diseases	↑ MyBP-H potential ALS biomarker compared to other motor neuropathies	↑ MyBP-H = attempted regeneration	(Conti et al., 2014)
Label-free	$SOD1^{G93A}$ mouse spinal cord, ALS spinal cord/CSF	14 proteins ↑/↓, ↑ Gal-3 in ALS	Comparative study of mouse and human ALS	(Zhou et al., 2010)
Label-free (MRM)	ALS and FTD blood, CSF and brain	TDP-43 in CSF appears to originate from the blood	TDP-43 in blood and CSF not a viable biomarker	(Feneberg et al., 2014)
Label-free (SRM)	$SOD1^{G93A}$ mouse muscles	Shift in fiber-type composition of hindlimb muscles	Diagnostic-prognostic tool for neuromuscular diseases via myosin heavy chain isoform?	(Peggion et al., 2017)
MALDI	ALS blood	↑/↓blood coagulation proteins	SVM-based model with >97% recognition capability and >90% specificity and sensitivity	(Courtney et al., 2013)
MALDI	$SOD1^{G93A}$ mouse muscle	↑/↓ muscle albumin, complex I, complex II, citrate synthase, FAS, PI3K, PGC1α, SEMA-3A semaphorin-3A, ROCK1	Potential dysmetabolism molecular signatures in ALS	(Capitanio et al., 2012)
MALDI	sALS and $SOD1^{G93A}$ rat blood	↑/↓ ER stress, nitrative stress, redox, RNA metabolism proteins	Related to pathogenic mechanisms in ALS	(Nardo et al., 2011)
MALDI	sALS and $SOD1^{G93A}$ rat blood	↑ protein nitration early in disease	Nitrated proteins = presymptomatic biomarker for ALS	(Nardo et al., 2009)
MALDI and label-free	sALS and fALS (nonSOD1) plasma	GC2 allele of DBP = potential risk factor for fALS	Small cohort, requires validation	(Palma et al., 2008)
SILAC	ALS fibroblasts	33 proteins ↑/↓ (↓ ApoB48 & HSP20, ↑ FIBL-1)	Potential biomarkers/therapeutic targets	(Narayan et al., 2016)
Stable isotope dimethyl-labelling	ALS tibialis anterior muscle	↑/↓ KBTBD10, MYL3, AGL, VCP	Potential muscle biopsy biomarkers and therapeutic targets	(Elf et al., 2014)
SWATH	ALS plasma	↑/↓ GSN, APOJ, CDL5, FCN3	↓ coagulation pathway proteins and ↑complement pathway proteins	(Xu et al., 2018)
TMT	$SOD1^{G93A}$ mouse and sALS plasma	↑/↓ApoE in human and Gal-3, CD61 and TGF-β1 in $SOD1^{G93A}$ mice	Altered immunosenescence and metabolic markers	(Zubiri et al., 2018)

↑ denotes increase; ↓ denotes decrease; ACT, alpha-1-antichymotrypsin; AGL, glycogen debranching enzyme; APLP2, amyloid-like protein 1; ApoE, apolipoprotein E; CADM3, cell adhesion molecule 3; CAT, catalase; CD5L, CD5 antigen-like; CD61, integrin beta 3; CHI3L-1, chitinase 3-like protein 1; CHI3L-2, chitinase 3-like protein 2; CHIT1, chitotriosidase-1; CSF, cerebrospinal fluid; DBP, vitamin D-binding protein; fALS, familial amyotrophic lateral sclerosis; FAS, tumor necrosis factor receptor superfamily member 6; FCN3, ficolin 3; FIBL-1, fibulin-1; FTD, frontotemporal dementia; Gal-3, galectin-3; GRIA4, glutamate receptor 4; GSN, gelsolin; APOJ, clusterin; IGF-2, insulin growth factor II; iTRAQ, isobaric tags for relative and absolute quantitation; KBTBD10, BTB and kelch domain-containing protein 10; MALDI, matrix-assisted laser desorption ionisation; MRM, multiplex reaction monitoring; MYL3, myosin light chain 3; PGC1α, peroxisome proliferator-activated receptor gamma coactivator 1-alpha; PI3K, phosphoinositide 3-kinase; ROCK1, rho-associated protein kinase 1; sALS, sporadic amyotrophic lateral sclerosis; SEMA-3A, semaphorin-3A; SILAC, stable isotope labelling by amino acids in cell culture; SOD1, superoxide dismutase 1; SPARCL1, SPARC-like protein 1; SRM, selected reaction monitoring; SWATH, sequential window acquisition of all theoretical mass spectra; TDP-43, TAR DNA binding protein of 43kDa; TGF-β1, transforming growth factor beta-1; TMT, tandem mass tag; VCP, transitional ER ATPase; WDR63, WD repeat-containing protein 63

Figure Legends

Figure 1. Proteomics workflow for label-free and labelling quantitation of proteins from complex mixtures relevant to understanding ALS and FTD. Protein samples derived from models/human tissue can either be labelled for targeted proteomics or analysed label-free for broader detection.

DDA, data-dependent acquisition; DIA, data-independent acquisition; SILAC, stable isotope labelling by amino acids in cell culture

Figure 1.TIF